Aspects of Divalent Rare-Earth-Metal Alkyl and Amide Chemistry

Dissertation

der Mathematisch-Naturwissenschaftlichen Fakultät
der Eberhard Karls Universität Tübingen
zur Erlangung des Grades eines
Doktors der Naturwissenschaften
(Dr. rer. nat.)

vorgelegt von
M. Sc. Markus Katzenmayer
aus Reutlingen

Tübingen
2023

Gedruckt mit Genehmigung der Mathematisch-Naturwissenschaftlichen Fakultät der Eberhard Karls Universität Tübingen.

Tag der mündlichen Qualifikation	06.07.2023
Dekan:	Prof. Dr. Thilo Stehle
1. Berichterstatter:	Prof. Dr. Reiner Anwander
2. Berichterstatter:	Prof. Dr. Michael Seitz

Aspects of Divalent Rare-Earth-Metal Alkyl and Amide Chemistry

Markus Katzenmayer

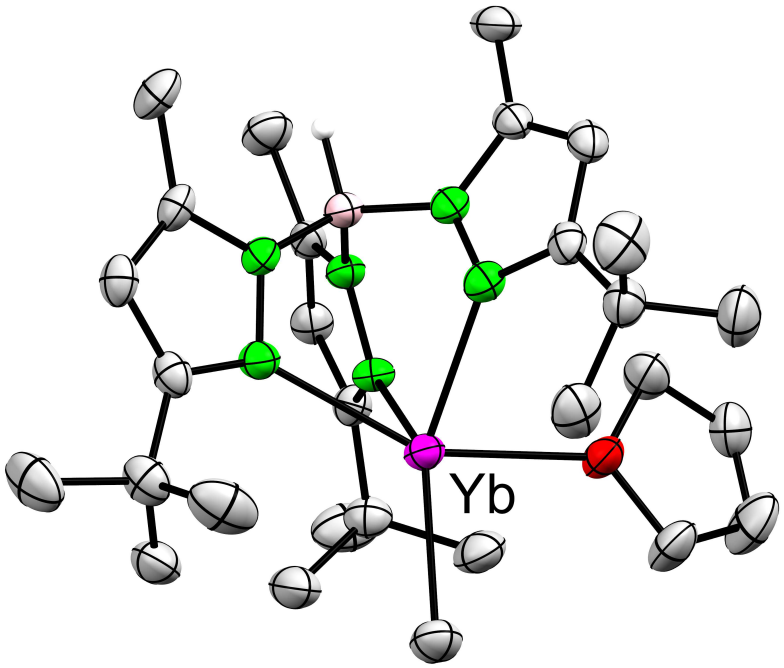

Preface

The following PhD thesis consists of a survey of related works, a summary of the main results, and original scientific papers. The work was carried out at the Institut für Anorganische Chemie of the Eberhard Karls Universität Tübingen, Germany, over the period from October 2018 to October 2022 under the supervision of Prof. Dr. Reiner Anwander. Funding was gratefully received from the Deutsche Forschungsgemeinschaft (DFG). Parts of this thesis were presented at two international conferences as a poster.

Acknowledgements

First of all, I wish to thank my supervisor, Prof. Reiner Anwander for giving me the opportunity to join his group and work on this challenging and interesting topic and for offering support in all cases.

I am especially grateful to Dr. Cäcilia Maichle-Mössmer for the insights into the very unique world of crystallography, teaching me how to operate a diffractometer and for her patience in handling hopeless crystal samples finding the needle in the haysack. And further for managing lots of administrative work for the working group.

This work could not have been realized without the work of many others. First I want to thank Dr. Klaus Eichele and Kristina Heß for taking care of the NMR and providing help in solving many mysteries, Dr. Jochen Glaser for ICP-OES measurements, Wolfgang Bock and Mohammad Ghani for elemental analysis measurements. I want to thank the technical and administrative staff of the Anwander Group Tobias Wolf, Heinz-Jürgen Kolb, Elke Niquet and Sabine Ehrlich for keeping things running smoothly and preventing that things descend into chaos. In case of Sabine, her uncountable fights with administration and in case of Elke the many nice conversations and all the support she provided earn special mentioning.

Thanks to all former and current coworkers of the Anwander Group, namely: Dennis, Damir, Benni, Renita, Jochen, Holli, Doro, Uwe, Verena, Lars, Simon, Lorenz, Dominic, Stuhl, Yali, Jitpisut, Manfred, Tassilo, Jakob, Eric, Felix, Jonas, Indi, Gernot, Cindy, Alex and especially Theresa, Viktoriia and Gogo who have become good friends of mine. Without you, the last years would have been way more difficult, discussions not as fun, jokes would have been too serious and the time nowhere near fun! I am very grateful to Holli for always having good advice and providing an open ear whenever needed and, last but not least, introducing me to the Holy Ground. Thank you all!

I am very grateful to Josi. Your unconditional support, your patience, understanding and your love, even when times were rough, helped me through. Thanks for going the way together.

Zum Abschluss möchte ich mich noch bei meiner Familie bedanken. Danke Mama, Papa und danke Kerstin, dass ihr immer für mich da seid und ich immer auf euch zählen kann. Nicht nur für die finanzielle Unterstützung, sondern auch für aufbauenden Worte und guten Rat. Danke, dass ihr mich durch mein Studium und die Promotion begleitet und unterstützt habt!

Contents

Preface I

Acknowledgements II

Abbreviations V

Summary VII

Zusammenfassung VIII

Publications IX

Objective of the Thesis XII

A Aspects of Divalent Ytterbium Chemistry 1

1 The Rare-Earth Metals 3

1.1 Milestones in Organometallic Chemistry 3

1.2 General Properties of Rare-Earth Metals 5

1.3 Alkaline-Earth Metals and Divalent Rare-Earth Metals 6

2 Rare-Earth-Metal Alkyl Complexes 8

2.1 Rare-Earth-Metal Methyl Complexes 8

2.2 Rare-Earth-Metal Aluminates 11

2.3 Rare-Earth-Metal Benzyl Complexes 12

3 Rare-Earth-Metal Imide Chemistry 15

B Summary of the Main Results 23

1 Divalent Rare-Earth-Metal Alkyl Complexes 25

2 Synthesis of new Rare-Earth-Metal Amide Complexes 28

C Unpublished Results 31

D Bibliography 39

E Publications 47

F Appendix **135**

Abbreviations

°	Degree	**Hz**	Hertz
°C	Degree Celsius	δ	Chemical shift
Å	Ångstrøm (10^{-10} m)	$\tilde{\nu}$	Wave number
AE	Alkaline-Earth metals	***i. e.***	*id est* (that is)
AN	Atomic Number	**ICP**	Inductively Coupled Plasma
Ar	Aryl group	**iPr**	iso propyl ($CHMe_2$)
Bn	CH_2Ph^-	^nJ	Coupling constant over *n* bonds
cf.	*confer* (compare)	**Ln**	Rare-earth metal (Sc, Y, La–Lu)
CN	Coordination Number	**Me**	Methyl (CH_3)
Cp*	C_5Me_5	**Me_3TACN**	1,4,7-Trimethyl-1,4,7-triazacyclononane
CP/MAS	Cross Polarization/Magic Angle Spinning	**MS**	Molecular Sieves
Dipp	2,6-Diisopropylphenyl	**NMR**	Nuclear Magnetic Resonance
DMAP	4-Dimethylaminopyridine	**OTf**	$F_3CSO_3^-$, triflato
do	Donor	**Ph**	Phenyl (C_6H_5)
DRIFT	Diffuse Reflectance Infrared Fourier Transformation	**ppm**	parts per million
EA	Elemental Analysis	**pz**	Pyrazolyl
e.g.	*exempli gratia* (for example)	**R**	alkyl group
Et	Ethyl (C_2H_5)	**rt**	ambient temperature
et al.	*et alii* (and others)	**SC-XRD**	Single Crystal X-Ray Diffraction
HSQC	Heteronuclear Single Quantum Coherence	***t*Bu**	*tert*-butyl (CMe_3)

THF	Tetrahydrofuran
TMEDA	Tetramethylethylenediamine
Tp^{tBu,Me}	Tris(3-*tert*-butyl-5-methyl-pyrazolyl)borato
vide infra	see above
vide supra	see below
VT	Variable Temperature
X	Halide (F, Cl, Br, I)
$\tilde{\nu}$	Wave number

Summary

Defined metalmethyl compounds were first reported in the middle of the 19th century and the interest in metal alkyls is still growing. So far 26 out of 60 non-radioactive metals have been found to form homoleptic isolable methyl componds [$M(CH_3)_x$] (x = 1–6). The report on the successful synthesis of dimethylcalcium [$CaMe_2$]$_n$ triggered further research on the often discussed parallels of alkaline-earth metals and the divalent rare-earth-metals Sm^{2+}, Eu^{2+} and Yb^{2+}. Dimethylytterbium [$YbMe_2$]$_n$ could be accessed via the reaction of the donor-free precursor [$Yb\{N(SiMe_3)_2\}_2$]$_2$ with methyllithium. [$YbMe_2$]$_n$ was fully characterized and follow–up chemistry was investigated. Noteworthily, the protonolysis reaction of [$YbMe_2$]$_n$ with protic hydrotris(3–*t*Bu–5–Me–pyrazolyl)borate $HTp^{tBu,Me}$ gave the first terminal Yb^{2+} methyl complex [$Tp^{tBu,Me}Yb(CH_3)(thf)$] providing direct evidence of the existence of the methyl precursor. Further, the synthesis of the divalent dimethyl compounds of samarium and europium was attempted.

The focus of the second part of this work was the synthesis of new rare-earth-metal imide complexes. Through a one-pot salt-metathesis reaction ($LnI_2(thf)_2$ + $KTp^{tBu,Me}$ + KNHR with Ln = Sm, Eu, Yb and R = 2,6-*i*Pr-C_6H_3, 2,6-Me-C_6H_3, 3,5-CF_3-C_6H_3, $SiPh_3$) or a protonolysis approach ($Tp^{tBu,Me}Yb(N(SiMe_3)_2)$ + H_2NR, R = R = 2,6-*i*Pr-C_6H_3, 3,5-CF_3-C_6H_3, $SiPh_3$) efficient access to amide complexes [$Tp^{tBu,Me}YbNH(R)(thf)_x$] (R = 2,6-*i*Pr-$C_6H_3$, 2,6-Me-$C_6H_3$, 3,5-$CF_3$-$C_6H_3$, $SiPh_3$) could be gained. All synthesized complexes were fully characterized and their reactivity toward Lewis acids and bases as well as their redox chemistry was further investigated. The obtained compounds are potential precursor complexes for the synthesis of rare-earth-metal imide complexes.

Zusammenfassung

Erste Berichte über wohldefinierte Metallmethyl–Verbindungen gab es seit Mitte des 19. Jahrhunderts und das Interesse an Metallalkylen lässt nicht nach. So wurden bisher für 26 der 60 nicht radioaktiven Metalle homoleptische Metallalkyle $[M(CH_3)_x]$ (x =1–6) isoliert. Der Bericht über die erfolgreiche Synthese des einfachen Calciumalkyls Dimethylcalcium $[CaMe_2]_n$ bot Anlass, die häufig diskutierten Ähnlichkeiten zwischen Erdalkalimetallen und den zweiwertigen Seltenerdmetallen Sm^{2+}, Eu^{2+} und Yb^{2+} auch in diesem Bereich genauer zu untersuchen. So konnte durch die Reaktion der donor–freien Vorstufe $[Yb\{N(SiMe_3)_2\}_2]_2$ mit Methyllithium Dimethylytterbium $[YbMe_2]_n$ erhalten werden. $[YbMe_2]_n$ wurde vollständig charakterisiert und die Folgechemie wurde genauer untersucht. Besonders hervorzuheben ist die Protonolysereaktion mit dem protischen Hydro tris(3–*t*Bu–5–Me–pyrazolyl)borat $HTp^{tBu,Me}$, die den terminalen Methylkomplex $[Tp^{tBu,Me}Yb(CH_3)(thf)]$ ergab und somit das Vorhandensein der Methylgruppen in $[YbMe_2]_n$ bestätigte. Es wurden erste Versuche zur Darstellung zweiertiger Methylverbindungen des Samariums und Europiums durchgeführt.

Im zweiten Teil dieser Arbeit stand die Synthese neuer Seltenerdmetall–Imidkomplexe im Fokus. Durch effiziente one–pot Salzmetathese ($LnI_2(thf)_2$ + $KTp^{tBu,Me}$ + KNHR with Ln = Sm, Eu, Yb and R = 2,6-*i*Pr-C_6H_3, 2,6-Me-C_6H_3, 3,5-CF_3-C_6H_3, $SiPh_3$) oder Protonolyseprotokolle ($Tp^{tBu,Me}Yb(N(SiMe_3)_2)$ + H_2NR, R = R = 2,6-*i*Pr-C_6H_3, 3,5-CF_3-C_6H_3, $SiPh_3$) konnten zweiwertige Ytterbium–Amidprecursorkomplexe der Form $[Tp^{tBu,Me}YbNH(R)(thf)_x]$ (R = 2,6-*i*Pr-C_6H_3, 2,6-Me-C_6H_3, 3,5-CF_3-C_6H_3, $SiPh_3$) erhalten werden. Alle erhaltenen Komplexe wurden vollständig charakterisiert und ihre Folgechemie gegenüber Lewissäuren und Basen sowie ihre Redoxchemie genauer untersucht. Die erhaltenen Verbindungen sind potente Vorstufen für die Synthese von Seltenerdmetall–Imidkomplexen.

Publications

Publications incorporated into this thesis

Paper I Polymeric Dimethylytterbium and the Terminal Methyl Complex ($Tp^{tBu,Me}$)Yb(CH_3)(thf)

Markus M. Katzenmayer, Benjamin M. Wolf, Alexandros Mortis, Cäcilia Maichle-Mössmer and Reiner Anwander

Chem. Commun. **2021**, *57*, 243 - 146.

https://doi.org/10.1039/D0CC06981G

Paper II Potential precursors for terminal ytterbium(II) imide complexes bearing the tris(3-tert-butyl-5-methylpyrazolyl)hydroborato ligand

Markus M. Katzenmayer, Felix Kracht, Cäcilia Maichle-Mössmer and Reiner Anwander

Dalton Trans. **2023**, *52*, 6273

https://doi.org/10.1039/D3DT00861D

Publications with minor contributions

Paper III Donor–stabilized molecular Mg/Al–bimetallic hydrides

Christoph Stuhl, Markus M. Katzenmayer, Cäcilia Maichle-Mössmer and Reiner Anwander

Dalton Trans. **2018**, *47*, 15173 - 15180.

https://doi.org/10.1039/C8DT03343A

Poster presentations

Poster I Synthesis and reactivities of divalent Dimethyleuropium and Dimethylytterbium

Markus M. Katzenmayer, Cäcilia Maichle-Mössmer, Reiner Anwander

XXX. Terrae Rarae, Montpellier, France, *September 22 - 24*, **2021**.

Poster II Synthesis and reactivities of divalent Dimethyleuropium and Dimethylytterbium

Markus M. Katzenmayer, Cäcilia Maichle-Mössmer, Reiner Anwander

Rahmenprogramm zur 71. Lindauer Nobelpreisträgertagung, Tübingen, Germany, *Juni*, **2022**.

Personal Contribution

Paper I. All reactions and analyses described were planned and conducted by myself. Research of Dr. Benjamin M. Wolf laid the foundation for this work. Analysis consists of one dimensional (^{1}H, ^{11}B, ^{13}C{^{1}H}, ^{13}C and ^{171}Yb CP/MAS) and two dimensional (^{1}H–^{171}Yb–HSQC) NMR spectroscopic methods, single–crystal X–ray diffraction, DRIFT spectroscopy, ICP–AES and elemental analysis. Sample preparations were done by myself. Writing of the publication was also performed by me.

Alexandros Mortis executed the ^{1}H–^{171}Yb–HSQC NMR measurements and supported me with the evaluation of some NMR spectra. All structure refinements and partly the sample preparation of single–crystal X–Ray diffraction analysis where executed by Dr. Cäcilia Maichle-Mössmer. Dr. Klaus Eichele performed the solid state ^{13}C and ^{171}Yb CP/MAS NMR spectra. Dr. Jochen Glaser performed the ICP–AES and Wolfgang Bock performed the measurements of all C, H, N microanalyses.

Paper II. All reactions and analyses described were planned and conducted by myself. Analysis consists of one dimensional (^{1}H, ^{11}B, ^{13}C{^{1}H}, ^{13}C UDEFT) and two dimensional (^{1}H–^{13}C–HSQC and ^{1}H–^{171}Yb–HSQC) NMR spectroscopic methods, single–crystal X–ray diffraction, DRIFT spectroscopy and elemental analysis. Sample preparations were done by myself. Writing of the publication was also performed by me.

Felix Kracht executed the ^{1}H–^{171}Yb–HSQC NMR measurements and supported me with the evaluation of some NMR spectra. Gernot Zug executed one variable temperature ^{1}H NMR experiment. All structure refinements of single–crystal X–Ray diffraction analysis where executed by Dr. Cäcilia Maichle-Mössmer. Mohammad Ghani performed the measurements of all C, H, N microanalyses.

Paper III. For Paper III I executed the synthesis of several compounds as part of a mandatory laboratory course during my master studies.

Objective of the Thesis

The main emphasis of this thesis is to investigate the synthesis and reactivity of divalent rare-earth-metal alkyl and imide complexes.

Part A contains a brief overview across achieved milestones in the organometallic chemistry of the rare-earth metals, general properties of rare-earth metals and the relation between divalent rare-earth metals and alkaline-earth metals. Furthermore, an overview of rare-earth-metal alkyl complexes and rare-earth metal imide complexes is given.

Part B contains a summary of the main results of this thesis:

- Synthesis and characterization of $[Yb(Me)_2]_n$
- Synthesis and characterization of divalent rare-earth-metal amide complexes

Part C is a summary of findings which are not part of a publication.

Part E is a compilation of publications.

Part F is a compilation of compounds that were structurally characterized and all structurally characterized compounds from the papers.

A

Aspects of Divalent Ytterbium Chemistry

1 The Rare-Earth Metals

1.1 Milestones in Organometallic Chemistry

In 1760, the French pharmacist and chemist Louis Claude Cadet de Gassicourt came across a nauseatingly smelling and fuming oil during his studies on invisible inks. The reaction of potassium acetate KOAc with arsenic trioxide As_2O_3 yields the socalled "Cadet's fuming liquid" or tetramethyldiarsane As_2Me_4 (see Scheme A.1, **1**). Cadet had found, unintentionally, the first organometallic compound in history. Despite the fact that arsenic itself is a metalloid, organoarsenic compounds as well as other organo–metalloid compounds are classified as organometallic compounds.[1] During the peroid of 1837–1843 Robert Wilhelm Bunsen continued the work on Cadet's fuming liquid. The weak As–As bond in As_2Me_4 and its alkyl analogoues As_2R_4 (R = alkyl) allowed Bunsen to synthesize numerous derivatives and enlarge the family of organo–metal complexes.[2,3]
Edward Frankland, a student of Bunsen, fundamentally influenced chemistry with his groundbreaking discovery of dimethylzinc $Zn(CH_3)_2$ and diethylzinc $Zn(CH_2CH_3)_2$ by reacting elemental zinc with methyl iodide or ethyl iodide, respectively (see Scheme A.1, **2**).[4–6]

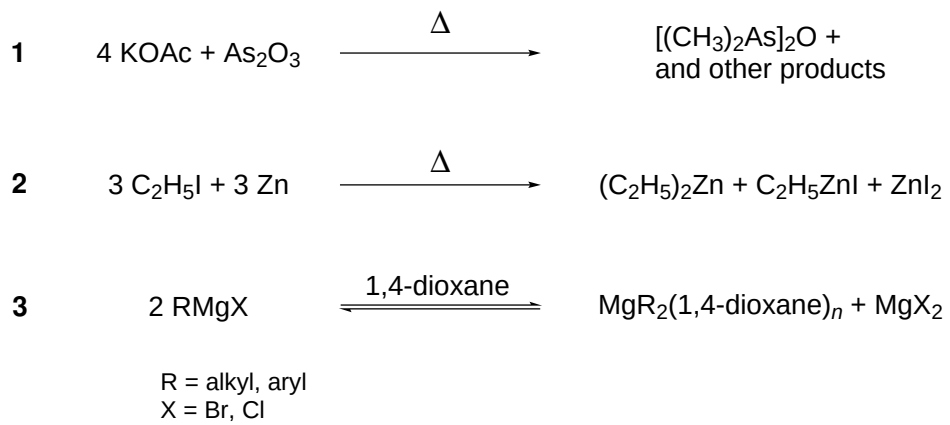

Scheme A.1: Historic procedures first executed and reported by L. C. Cadet de Gassicourt (**1**) and E. Frankland (**2**). Generic representation of the Schlenk equilibrium and the influence of the solvent (**3**).

Since Frankland's discovery in 1849, scientists have found metal-methyl compounds $[M(CH_3)_x]$ (x = 1–6) for 26 out of the 60 metals across the periodic table. Important representatives are alkaline metal alkyls, *e.g.* methyllithium (CH_3Li), *n*-butyllithium (C_4H_9Li), *tert*-butyllithium

(C_4H_9Li) which are widely applied in inorganic and organic syntheses. Organometallic compounds of the heavier alkaline metals are less important except $NaCp^*$ [$Na(C_5Me_5)$] as the most widely used heavier alkaline-metal reagent.[1] Organometallic compounds of group 2 and 12 elements, especially magnesium alkyl compounds, are often utilized in organic and inorganic synthesis. High reactivity and easy accessibility make organomagnesium compounds ideal reagents for diverse syntheses. Utilization of the Schlenk equilibrium (see Scheme A.1, **3**) allows a cheap and easy way to access magnesium alkyls MgR_2, starting from Grignard reagents RMgX (R = alkyl; X = halide).[7] Victor Grignard created the basis for this and future work with his groundbreaking research results and was awarded the Nobel Prize for his discovery in 1912.[8,9] Following Grignard, many efforts were put on the synthesis of Grignard reagent analogue compounds bearing heavier alkaline-earth metals like calcium, strontium or barium. Those so called heavy Grignard reagents were elusive a long time. In 1958, Sanderson and Payne reported on the synthesis of dimethyl compounds of calcium [$Ca(CH_3)_2$], barium [$Ba(CH_3)_2$] and strontium [$Sr(CH_3)_2$].[10] Their results are questionable because their procedures were not successfully reproduced by any others. 60 years later, in 2018, the group of Anwander reported on the successful synthesis of polymeric, pyrophoric dimethyl calcium, $[Ca(CH_3)_2]_n$ (see Scheme A.2).[11]

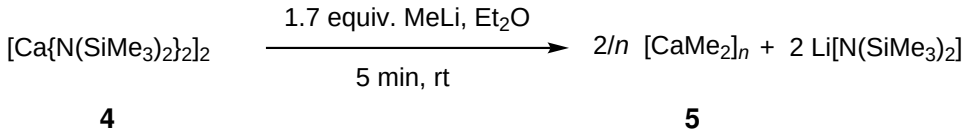

Scheme A.2: Simplified synthesis procedure for the synthesis of dimethylcalcium, $[Ca(CH_3)_2]_n$.[11]

The key step was utilizing a modified Lochmann procedure,[12] using calcium bis(trimethylsilyl)amide $[Ca(N(SiMe_3)_2)_2]_2$ as precursor complex in the reaction with chloride-free methyl lithium.

1.2 General Properties of Rare-Earth Metals

The elements scandium (AN 21), yttrium (AN 39), and lanthanum (AN 57) to lutetium (AN 71) form the family of heavily related lanthanides (Ln). Elements from cerium to lutetium possess 4f orbitals, which are successively filled with electrons. The existence of those 4f orbitals provide the rare-earth metals with unique chemical and physical properties delimiting them from transition metals. Combining a weaker electronic shielding from the atom core with the energetic levels of the inert 4f shell subsequently leads to a higher effective nuclear charge causing a shrinkage of the atom radii with increasing number of electrons. This phenomenon is known as the lanthanide contraction.[1,13] Having very similar atomic radii (compare Table A.1) aggravates the separation of these metals, making them expensive materials. Liquid–liquid extraction came out on top as the separation method in industrial scales.[14]

Within the rare-earth metals, the most frequently found oxidation state is the stable +III (Ln^{3+}). This fact is reflected in the amount of reports on trivalent rare-earth metal complexes that can found in literature.[15–18] The oxidation states +II or +IV are rarely observed and are relatively stable for elements which can achieve filled or half-filled orbitals. Europium Eu^{2+} ($4f^7$, half filled) and ytterbium Yb^{2+} ($4f^{14}$, filled) form the most stable divalent compounds. Moreover, complexes of samarium Sm^{2+} ($4f^6$, nearly half-filled) and thulium Tm^{2+} ($4f^{13}$, nearly filled) with nearly or half-filled orbitals are known. Divalent samarium is comparatively less stable due to its reduction potential (Sm^{3+}–Sm^{2+}: $E^\circ = -1.5V$).[15] The most delicate divalent species are thulium Tm^{2+} complexes.[19,20] Interest in divalent rare-earth-metal compounds is still rising, indicated by the increasing number of reports on preparations of stable complexes of samarium, europium, thulium and ytterbium in literature.[21–23] Stable molecular complexes containing metals in the tetravalent oxidation state +IV can be found for the elements cerium Ce^{4+} ($4f^0$),[24,25] praseodymium Pr^{4+} ($4f^1$)[26,27] and terbium Tb^{4+} ($4f^7$).[28,29] Due to its high stability and vivid redox behavior, cerium is the best investigated representative of the tetravalent rare-earth metals. The large ionic radii and the high charge density of the trivalent rare-earth-metal ions make them the relatively hard Lewis acids, according to the HSAB concept, striving for coordination numbers in the range of 6–12.[30,31] The metal-ligand bonding situation is determined by electrostatic and steric aspects.[15]

Rare-earth metals are an essential part of strategic materials like modern ceramics or magnets.[13] Regarding the luminescence properties, the sharp transition bands caused by electronic rearrangement within the 4f orbitals (f–f transitions) make the rare-earth metals indispensable in

modern phosphors for light emitting diodes (LED).[1,32,33] The rare-earth metals also made their way to organic synthesis, providing several well established reagents. For example, cerium ammonium nitrate (CAN) is used as an oxidant whereas divalent samarium iodide SmI_2 is a popular reducing agent in manifold organic syntheses.[13,34]

Table A.1: General properties of the lanthanides.[1,13,31,35,36]

	Electronic configuration				Redox potential [V]			Ionic
	Atom	M^{2+}	M^{3+}	M^{4+}	Ln/Ln^{3+}	Ln^{2+}/Ln^{3+}	Ln^{3+}/Ln^{4+}	radii [Å] Ln^{3+}
La	$5d^16s^2$	$5d^1$	[Xe]	-	+2.52	+3.74[a]	-	1.172
Ce	$4f^15d^16s^2$	$4f^2$	$4f^1$	[Xe]	+2.48	+3.76[a]	−1.74	1.15
Pr	$4f^36s^2$	$4f^3$	$4f^2$	$4f^1$	+2.46	+3.03[a]	−3.2	1.13
Nd	$4f^46s^2$	$4f^4$	$4f^4$	$4f^2$	+2.43	+2.6	-	1.123
Pm	$4f^56s^2$	$4f^5$	$4f^4$	-	+2.42	+2.67[a]	-	-
Sm	$4f^66s^2$	$4f^6$	$4f^5$	-	+2.41	+1.55	-	1.098
Eu	$4f^76s^2$	$4f^7$	$4f^6$	-	+2.41	+0.35	-	1.087
Gd	$4f^75d^16s^1$	$4f^75d^1$	$4f^7$	-	+2.40	+3.82[a]	-	1.078
Tb	$4f^96s^2$	$4f^9$	$4f^8$	$4f^7$	+2.39	+3.47[a]	−3.1	1.063
Dy	$4f^{10}6s^2$	$4f^{10}$	$4f^9$	$4f^8$	+2.35	+2.5	-	1.052
Ho	$4f^{11}6s^2$	$4f^{11}$	$4f^{10}$	-	+2.32	+2.80[a]	-	1.041
Er	$4f^{12}6s^2$	$4f^{12}$	$4f^{11}$	-	+2.30	+2.96[a]	-	1.033
Tm	$4f^{13}6s^2$	$4f^{13}$	$4f^{12}$	-	+2.28	+2.3	-	1.020
Yb	$4f^{14}6s^2$	$4f^{14}$	$4f^{13}$	-	+2.27	+1.15	-	1.008
Lu	$4f^{15}5d^16s^1$	-	$4f^{14}$	-	+2.25	-	-	1.001

[a]: direct experimentally derived values. Using $\Delta G_f{}^0(M^{2+}, aq)$ and $\Delta G_f{}^0(M^{3+}, aq)$[37]

1.3 Alkaline-Earth Metals and Divalent Rare-Earth Metals

A comparison of divalent rare-earth-metal complexes with complexes of the alkaline-earth metals (AE) shows remarkable similarities in their structural chemistry. Following Shannon *et al.*, the ionic radii of the divalent rare-earth metals and of the alkaline-earth metals are very similar (see Table A.2).[31] Especially the radii of Ca^{2+} and Yb^{2+} differ just slightly (0.02 Å for coordination number: 6). The electronic situation of Ln^{2+} (d^0 species) and limited radial expansion of the f-orbitals leave electrostatics and sterical factors as the only driving forces for complex formations.[38]

The metallocenes $Cp^*{}_2M$ ($Cp^* = C_5Me_5^-$, M = Ca, Ba, Sr, Sm, Eu, Yb) show very similar centroid-metal-centroid angles in the gas phase as well as in the solid state.[39,40] Isomorphous structures

Table A.2: Effective ionic radii of selected Ln^{2+} and Ae^{2+} (coordination number: 6).[31]

Metal ion	Ca^{2+}	Yb^{2+}	Eu^{2+}	Sr^{2+}	Sm^{2+}	Ba^{2+}
Radius [Å]	1.00	1.02	1.17	1.18	1.22	1.35

are pervasive. The β-diketiminate complexes (**6**) as well as complexes of bidentate benzyls (**7**) (named exemplarily) have isomorphous geometries and very similar cell parameters (see scheme A.3).[41,42] Harder *et al.* reported on the similar IR spectra obtained for complexes $\mathbf{7}^{Yb}$ and $\mathbf{7}^{Ca}$, indicating very similar bonding conditions.[41] Further, they observed similar stabilizing C–H$\cdots\pi$ interaction of the β-diketiminato ligands in both complexes ($\mathbf{7}^{Yb}$ and $\mathbf{7}^{Ca}$). In addition, theoretical studies revealed an identical activation barrier for the puckering inversion in both complexes.[42]

Utilization of well-established synthesis procedures for either metal center can be easily used for the other metal center delivering good results.

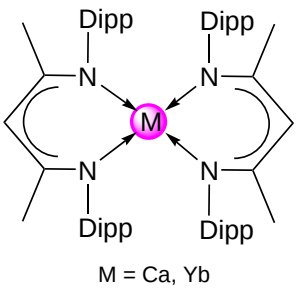

6

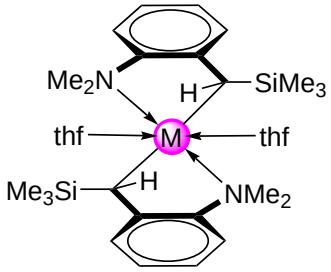

7

Scheme A.3: Selected complexes with isomorphous geometry for Yb^{2+} and Ca^{2+}.[38]

2 Rare-Earth-Metal Alkyl Complexes

Since Frankland's report on dimethylzinc,[4–6] homoleptic metal methyl compounds [$M(CH_3)_x$], the most simple alkyl derivatives of metals, have stayed in the focus of interest (see Section 1.1). Transition metals have been the most commonly used metals in organometallic chemistry due to easy handling and wide range of applications. Until the 1960s for most of the main group elements homoleptic σ-bond alkyl compounds, primarily for higher oxidation states were described.[43] When Lappert and Wilkinson independently introduced bulky alkyl groups (CH_2SiMe_3, $CH(SiMe_3)_2$, or CH_2Ph), the isolation of stable transition-metal-alkyl complexes became viable and the understanding of M–C σ-bonds in alkyls like $TiMe_4$, $HgMe_2$, or $ZrMe_4$ changed.[44–50]

The +III oxidation state dominates the solution chemistry of the lanthanides. Solely Ce^{4+} [Xe], Sm^{2+} [Xe]$4f^6$, Eu^{2+} [Xe]$4f^7$ and Yb^{2+} [Xe]$4f^{14}$ offer a second oxidation state with decent stability, but no Ln offers both stable $Ln^{2+/4+}$ states in addition to their trivalent oxidation state in solution (compare Section 1.1). Studies on simple cyclopentadienyl rare-earth metal complexes $(C_5H_5)_3Ln$ (Ln = Sc, Y, La, Ce, Pr, Nd, Sm, Gd, Dy, Er, Yb) revealed the ionic character of these compounds[51] and at the time made scientists conclude that lanthanide chemistry is limited and rare-earth metal complexes were seen as a trivalent versions of group I and II elements.[15,52,53] Despite drawbacks, scientists kept looking for ways to get their hands on rare-earth-metal alkyl compounds. Their lack of thermodynamic/kinetic stability comes with a high reactivity accompanied by large catalytic potential. Following their *d*-transition metal chemistry, Eaborn and Lappert introduced ligands of the "neopentyl"-type to the lanthanides, paving the way for a fast-growing field of science.[50,54–57] It took another decade until Hitchcock *et al.* reported on the first structural characterization of rare-earth metal σ-bonded hydrocarbyl complexes, namely [$Ln\{CH(SiMe_3)_2\}_3$] (Ln=La, Sm).[58]

2.1 Rare-Earth-Metal Methyl Complexes

In the time span from 1978–1984 the Schumann group reported on the synthesis of series of rare-earth-metal hexamethyl ate-complexes [$Ln(\mu\text{-}Me)_6Li_3(TMEDA)_3$] (Ln=Y, La, Pr, Nd, Sm, Gd, Tb, Dy, Ho, Er, Tm, Lu) by reacting $LnCl_3$ with six equivalents MeLi and TMEDA (schematic procedure see Scheme A.4, **8**).[59–62] In these anionic ate-complexes, the rare-earth-

metal centers are coordinated in a distorted octahedral fashion by six methyl moieties. The lithium counter ions are coordinated by two bridging methyl groups and two donor atoms, thus laying in the center of a tetrahedron. These compounds are soluble in THF and diethyl ether and insoluble in aliphatic solvents. By increasing the effective radii of the metal centers, their thermal stability decreases. High sensitivity towards oxygen and water was observed for all hexamethyl ate-complexes. Further studies on the reactivity and stability of these complexes were made by the group of Okuda in 2008. As part of their studies they found complexes of the type $[Ln_2(\mu\text{-}Me)_6Li_3(Et_2O)_n(thf)_m]$ (Ln = Sc, n = 3, m = 2; Ln = Y, Tb, n = 2, m = 3).[63] The group of Bercaw followed a different approach, reacting rare-earth-metal chlorides stabilized by the neutral N_3 donor ligand 1,4,7-Trimethyl-1,4,7-triazacyclononane, $[(Me_3TACN)LnCl_3]$, with three equivalents of methyllithium, which afforded trimethyl rare-earth metal complexes $[(Me_3TACN)LnMe_3]$ (Ln = Sc, Y) (see Scheme A.4, **9**).[64]

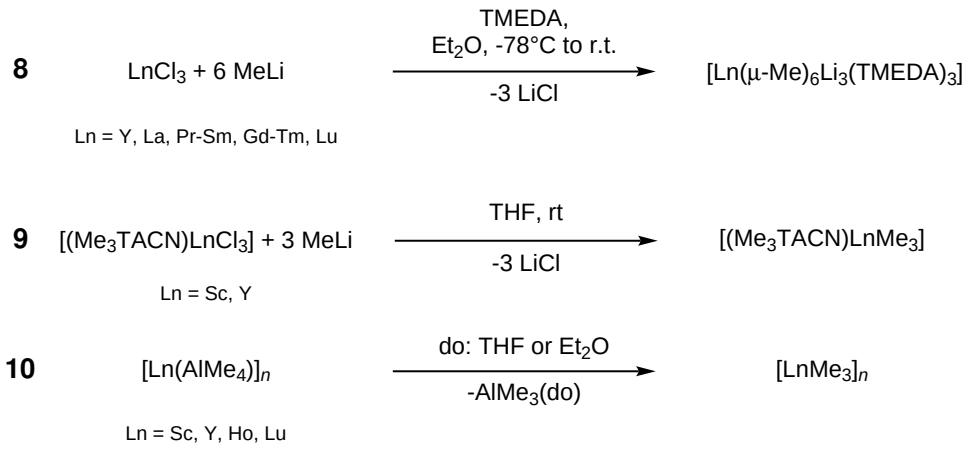

Scheme A.4: Different synthesis approaches towards rare-earth-metal methyl complexes.

Two decades after the reports of Schumann, Anwander *et al.* applied the donor-induced aluminate cleavage of the rare-earth-metal aluminates $[Ln(AlMe_4)_3]_n$ to access homoleptic methyl complexes $[LnMe_3]_n$ (Ln=Sc, Y, Ho, Lu) (see Scheme A.4, **10**).[57,65,66] These compounds were obtained as polymeric amorphous powders with a (M-μ-CH_3) network. The insolubility in aliphatic and aromatic solvents prevented the characterization via solution NMR and single-crystal X-Ray diffraction analysis. The polymeric character could be confirmed via solid-state NMR (MAS) and DRIFTS experiments. The compounds decompose slowly in the presence of donor solvents.[57,67] Trimethylscandium is thermally labile, soluble in THF and it decomposes at temperatures above $-40\,°C$ under the loss of methane and polymerization of THF. $[ScMe_3]_n$ was

characterized via solution NMR spectroscopy (^{1}H and ^{13}C, ^{45}Sc) in THF-d_8 at $-40\,°C$ revealing singlets in the proton NMR spectrum at -0.79 ppm and carbon NMR spectrum at 20.1 ppm. The shift found in the ^{13}C NMR is in good accordance with the signals found for $[YMe_3]_n$ (^{13}C CP/MAS: 28.3 ppm) and $[LuMe_3]_n$ (^{13}C CP/MAS: 31.4 ppm)[68] and also fits to the alkaline-earth metal analogue $[CaMe_2]_n$ (^{13}C CP/MAS: 12.6 ppm[11]).[69]

Reports on rare-earth-metal methyl complexes of the divalent lanthanides Sm^{2+}, Eu^{2+} and Yb^{2+} are rarely found in comparison to the trivalent representatives.[57,67] Solely heterobimetallic rare-earth-metal methyl complexes bearing μ-bridging methyl groups between unsaturated metal centers Ln^{2+} and M (M = Be,[70] Al,[71] Ti(III),[72] Yb(III),[72] Pt(II)[73]) or containing $[AlR_4]^-$ entities (R = Me, Et) are known.[65,74,75] Selected examples are depicted in figure A.1.

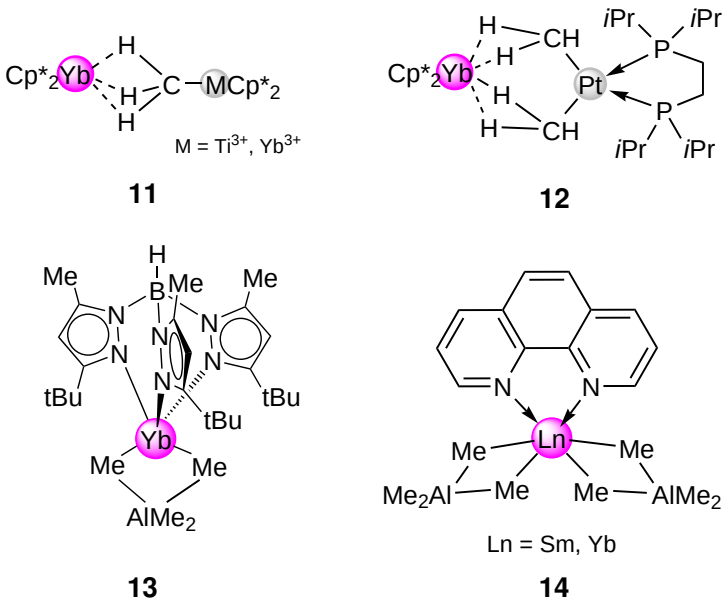

Figure A.1: Selected examples of divalent rare-earth-metal methyl complexes reported in literature.

The group around Andersen applied an oxidative methylation approach. The reaction of $[Cp^*_2Yb]$ with methyl transfer reagents (MeCu, Cp^*_2VMe, Cp^*_2TiMe) gave divalent heterobimetallic ytterbium complexes containing bridging methyl groups $[Cp^*_2Yb](\mu\text{-Me})[Cp^*_2M]$ (M = Yb, Ti) (the structural motive is depicted in figure A.1, **11**).[72] Furthermore, they described the reaction of $[(L)Pt(Me)_2]$ (L = $(^iPr)_2P(CH_2)_2P(^iPr)_2$) with $[Cp^*_2Yb]$ forming $[(L)Pt(\mu\text{-}CH_3)_2YbCp^*_2]$ (see figure A.1, **12**) in previous reports.[73]

Divalent heterobimetallic rare-earth-metal methyl complexes containing stable $[AlMe_4]^-$ enti-

ties are counted to a second branch of alkyl complexes, the so called "alkyls in disguise".[76] (*vide infra*, section 2.2) Anwander and Takats *et al.* reported on the reaction of a simple bis(trimethylsilyl)amide Yb precursor stabilized by the very bulky scorpionate ligand hydrotris(3-*t*Bu-5-Me-pyrazolyl) borato $Tp^{tBu,Me}$, $[Tp^{tBu,Me}YbN(SiMe_3)_2]$, with an excess of the Lewis acid $AlMe_3$ forming the $[Tp^{tBu,Me}Yb^{II}(AlMe_4)]$ (see figure A.1, **13**).[75] Another member of this group, $[(Phen)Yb(AlMe_4)_2]$ (Phen = 1,10-phenanthroline), was found within the scope of the investigations on rare-earth metal aluminates. Anwander *et al.* could show that the reaction of polymeric divalent ytterbium aluminate $[Yb(AlMe_4)_2]_n$ with 1,10-phenanthroline leads to the formation of the adduct $[Ln(AlMe_4)_2(Phen)]$ (Ln = Sm, Yb) (see Figure A.1, **14**).[74]
Despite all efforts, homoleptic divalent rare-earth-metal methyls have remained elusive. This conjuncture paired with recent groundbreaking reports by Anwander *et al.* on the synthesis of dimethyl calcium $[Ca(Me)_2]_n$[11] are the motivation to keep up the research in this field.

2.2 Rare-Earth-Metal Aluminates

Rare-earth metal tetraalkylaluminates $Ln(AlMe_4)_n$ (n = 3, Ln = Y, Sc, La–Eu, Gd–Lu, R = Me, Et; n = 2, Ln = Sm, Yb, R = Me, Et) are offering twofold applicability as precursor compounds. Due to the coordination of AlR_3 they can be seen as Lewis acid stabilized alkyls, easily undergoing protonolysis reactions. On the other hand, seeing the aluminates as ionic complexes, the $\{AlMe_4\}$ moiety can be displaced in salt metathesis.[57,67,77]
Evans *et al.* reported in 1995 on the synthesis of the first rare-earth-metal tetramethylaluminates $[Ln(AlMe_4)_3]$ (Ln=Y, Nd).[78] Treatment of the Ln(III) dimethylamide precursors with six equivalents of trimethylaluminium $AlMe_3$ in *n*-hexane accomplished a series of rare-earth-metal aluminates $[Ln(AlMe_4)_3]$ (Ln = Y, La–Sm, Gd–Lu) (compare Scheme A.5).[17,77,79,80] The amide-methyl exchange approach was unsuccessful for scandium. Instead, the treatment of the hexamethyl scandium ate-complex $[Sc(\mu\text{-}Me)_6Li_3(thf)_{1.2}]$ with an excess of $AlMe_3$ gave, after recrystallization, the desired product $[Sc(AlMe_4)_3(Al_2Me_6)_{0.5}]$.[17,69,78] Trivalent aluminates are often referred to as "alkyls in disguise" because of their ability to cleaving $AlMe_3$ moieties in the presence of donors or polar solvents (THF, diethyl ether, pyridine). This allowed the synthesis of the most simple rare-earth-metal alkyl compounds, homoleptic trivalent rare-earth metal methyl complexes $LnMe_3$ (Ln=Sc,[69] Y,[68] Ho,[81] Lu[68]) (see Scheme A.4, **10**).

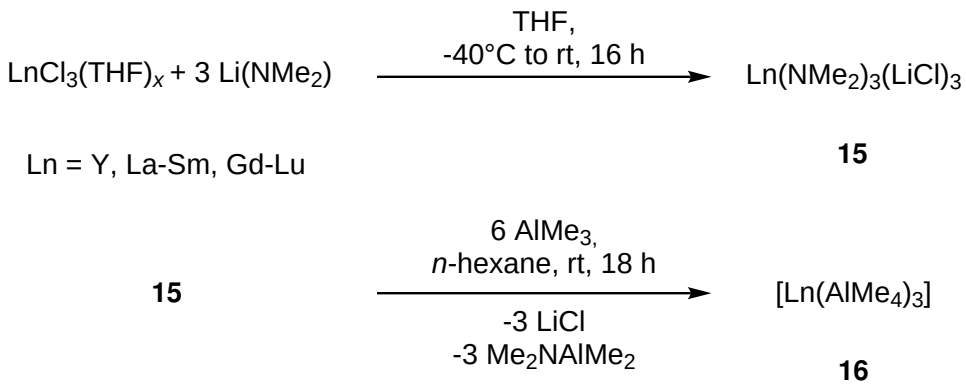

Scheme A.5: Synthesis procedure toward lanthanide tetramethylaluminates $[Ln(AlMe_4)_3]$ (Ln=Y, La-Sm, Gd-Lu).

Tetraalkylaluminates of the divalent rare-earth metals $[Ln^{II}(AlR_4)_2]$ (Ln = Sm, Eu, Yb; R = Me, Et) can be accessed via amide-alkyl or alkoxide-alkyl exchange reactions utilizing *bis*-silylamide complexes $[Ln(N(SiMe_3)_2)_2(thf)_2]$ (Ln=Sm, Yb) or *bis*-alkoxides $Ln(ODipp)_2(thf)_x$ (Ln=Sm, Yb) as precursors.[66,74,82] Alternatively, $[Yb(AlMe_4)_2]_n$ can be obtained by thermally induced self-reduction of the trivalent $[Yb(AlMe_4)_3]$ to the divalent aluminate, Al_2Me_6 and C_2H_6. To successfully obtain aluminates of divalent europium, trivalent $[Eu\{N(SiHMe_2)_2\}_3(thf)_2]$ was employed as a precursor and reacted with an excess of AlR_3 (R = Me, Et).[77] In contrast to the trivalent representatives, divalent aluminates tolerate the presence of donors and polar solvents, forming adducts instead of the already discussed donor-induced aluminate cleavage.[66]

2.3 Rare-Earth-Metal Benzyl Complexes

Benzyl (Bn = $\{CH_2Ar\}^-$) entities offer the advantage of acting as multihapto ligands, stabilizing rare-earth-metal alkyl complexes via π-donor interactions while maintaining the basicity/nucleophilicity of the compound. Benzyl ligands are found in three different variants: unsubstituted, alkyl/silyl substituted and as bidentate donor-functionalized ligands. The group around Manzer reported in 1978 on the first synthesis of a *tris*-benzyl scandium complex $[Sc(Bn^{NMe_2})]$ by reacting $ScCl_3$ with three equivalents of the amino-functionalized $Li(Bn^{NMe_2})$ ($Bn^{NMe_2} = CH_2\{2\text{-}(NMe_2)\text{-}C_6H_4\}$).[83] The metathesis salt LiCl complicated the workup process.[23] A more convenient synthesis can be realized by using potassium benzyl salts. The groups of Harder[84–86] and Hou[87] synthesized a series of trivalent rare-earth-metal benzyl complexes

[Ln(Bn^{NMe_2})$_3$] by employing $LnCl_3$ and $LnBr_3(thf)_4$ precursors, respectively. The metal centers are coordinated by three bidentate benzyl ligands fully saturating the coordination sphere (see Figure A.2, **17**).[84–87] The first monodentate benzyl complexes [La(Bn)$_3$(thf)$_3$] **18**^{La} and [La(Bn^{Me})$_3$(thf)$_3$] (Bn^{Me} = CH_2{4-Me-C_6H_4}$^-$) were obtained in the reaction of [$LaBr_3(thf)_3$] with the respective potassium salts.[88] The groups of Harder,[84] Roesky[89] and Diaconescu[90] completed the series by synthesizing benzyl complexes for Sc, Y, Nd, Gd, Tb–Lu. The group of Liddle used rare-earth-metal iodides [Ln(I)$_3$(thf)$_3$] (Ln = Y, La–Sm, Gd, Dy, Er) and benzyl potassium as starting compounds at 0 °C.[91]

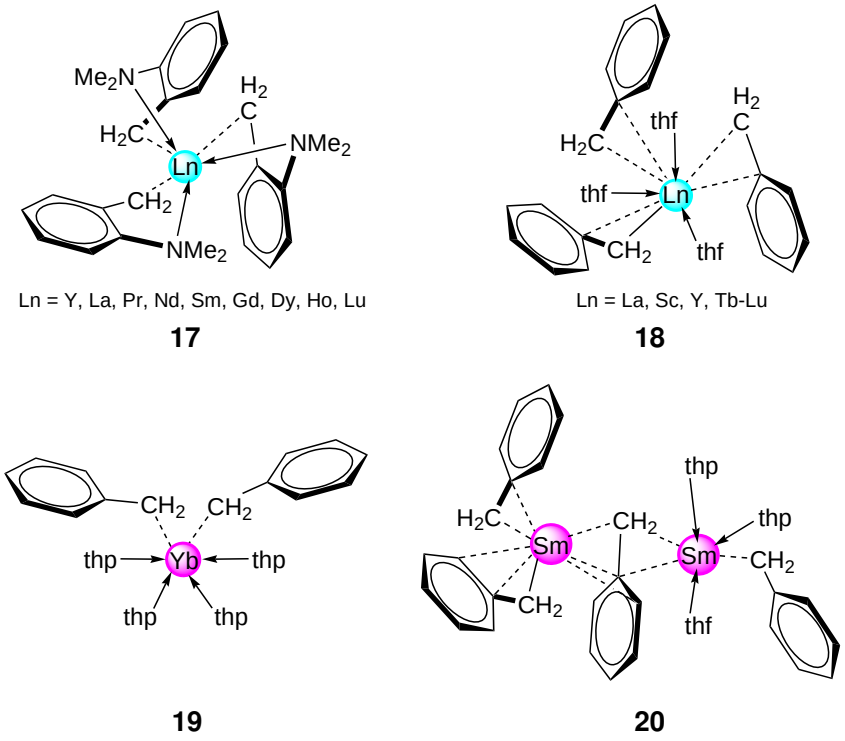

Figure A.2: Selected examples of rare-earth-metal benzyl complexes. The asymmetric unit of the polymeric arrangement of complex **20** is depicted.

The first divalent benzyl complexes were reported by the group of Harder in 2004 utilizing a derivative of Bn^{NMe_2} to further stabilize the metal center with an additional α-silyl group. Complexes [Ln{$CH_2(C_6H_4NMe_2(SiMe_3)\}_2(thf)_2$] (Ln = Sm, Eu, Yb) were obtained in a simple salt metathesis reaction protocol.[38] Monodentate divalent benzyl complexes [Ln^{II}(Bn)$_2$]$_n$ were reported by Anwander *et al.* in 2018. The reaction of $LnI_2(thf)_2$ with KBn led to the formation of amorphous powders [Ln(Bn)$_2$] (**21**). Recrystalization in donor solvents gave discrete donor stabilized species [$Eu_4(Bn)_8(thf)_2$], [Yb(Bn)$_2$(thp)$_4$] (**19**), [$Sm_2(Bn)_4(thf)(thp)_2$]$_n$ (**20**), and

$[Yb(Bn)_2(dme)_2]$.[92] Benzyl complexes are potent precursors for protonolysis reactions toward new organometallic compounds (see Section 3, Scheme A.9, bottom).[57,67,85,88,92,93]

3 Rare-Earth-Metal Imide Chemistry

During the last decades, rare-earth-metal imide chemistry has become a fast growing field of research. Especially after the reports of Chen *et al.* on their terminal scandium imide complex in 2010 the topic got a boost of attention.[94] Early reports of Bochkarev and Schumann in 1991 mark the beginning of this field for the rare-earth metals.[95] They described the successful utilization of the redox active rare-earth-metal precursor complex ytterbium naphthalide $[Yb(C_{10}H_8)(thf)_3]$ in the reductive cleavage of azobenzene N_2Ph_2, obtaining the first rare-earth-metal imide complex $[Yb_4(\mu\text{-}\eta^2\text{:}\eta^2\text{-}Ph_2N_2)_4(\mu_3\text{-}NPh)_2(thf)_4]$. Complex **22** contains four trivalent Yb^{3+} metal centers, coordinated by two bridging PhN^{2-} groups with Yb–N(imido) distances found in the range of 2.21(2)–2.29(1) Å.[95] A structural analogue of complex **22** was obtained by reacting the analogous samarium complex following the reported procedure.[96] The reaction of $[Ph_2Si(NAr^{iPr})_2]_2Sm[K(Et_2O)_2]_2$, a samarium complex containing bulky bis(amido) moieties, with N_2Ph_2 yielded the tetranuclear samarium imide $[Ph_2Si(NAr^{iPr})_2]Sm_4(NPh)_2(N_2Ph_2)(thf)_3$ (see Figure A.3, **23**).[97] The PhN^{2-} moieties are bridging between two samarium atoms forming an inner core similar to complex **22**.

Table A.3: Different synthesis approaches toward rare-earth metal imide complexes Ln=NR.[18]

Approach	Precursors	Reagents
Reductive cleavage[95]	Redox-active compounds Ln^0/Ln^{2+}	Ph–N=N–Ph
Salt metathesis[18]	Rare-earth halides LnX_3	Alkaline metal amides AMNHR
Imide transfer[98]	Rare-earth halides LnX_3	Mg-NPh
Deprotonation[99,100]	$Ln(NHR)_3$	$AlMe_3/n$-BuLi
Organoaluminium assisted deprotonation[92,101,102]	$(L)Ln(AlMe_4)/(L)Ln(HAlMe_3)_2$	$MNHAr/H_2NAr$
Intramolecular deprotonation[94]	(L)Ln(alkyl)(NHAr)	Lewis Base
1,2-addition[103]	$(L)LnH_2/Ln(alkyl)_2$	RNC (nitriles)
Utilization of Ln-methylidene complexes[104]	$(L)Ln(CH_2)$	H_2NAr

The reaction of the samarium complex $[(Me_2Si\{NC(Ph)N(2,6\text{-}iPr_2Ph)\}_2)SmI_2Li_2(thf)(Et_2O)_2]$ with azobenzene gave a rare silyl-bridged bis(amidinate) cluster $[(Me_2Si\{NC(Ph)N(2,6\text{-}iPr_2Ph)\}_2)_2Sm_4(\mu\text{-}NPh)_4]$ (**24**). Complex **24** consists of a cubane-like core with samarium metals and bridging PhN^{2-} groups located on the edges. The cube is encapsulated and stabilized by two silyl-bridged bis(amidinate) ligands (see Figure A.3, **24**).[105] The reductive cleavage of azobenzene has become a successful way to rare-earth-metal imide complexes. Hence, the limitation to redox active rare-earth metals and the commonly observed mulitnuclearity of product complexes containing only bridging imido groups made scientists search for alternative synthesis routes

(see Table A.3 for different synthesis approaches).

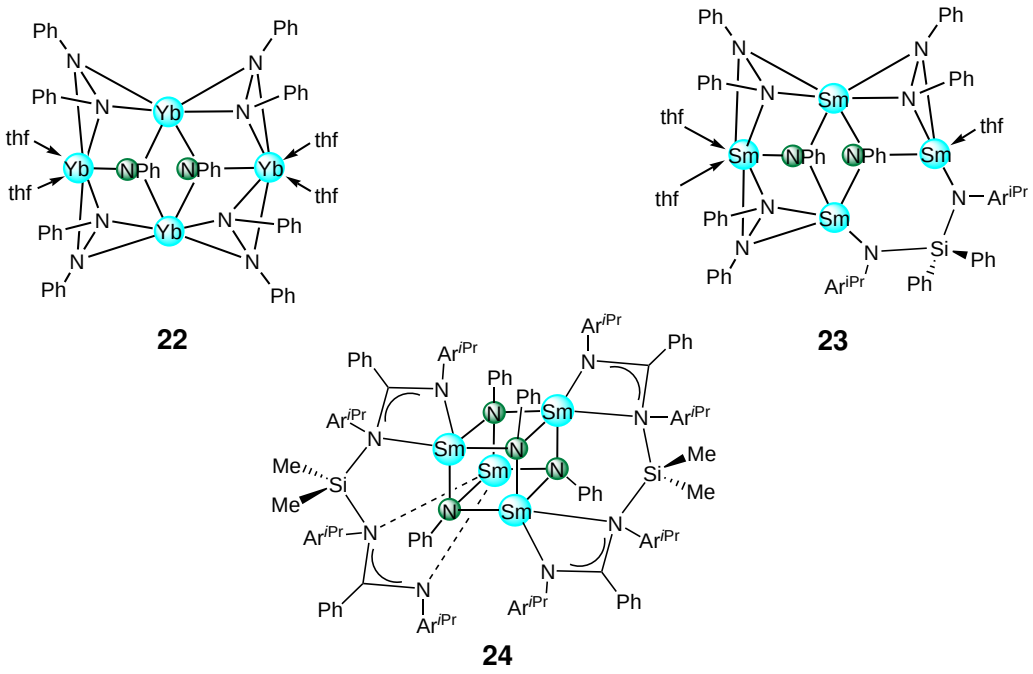

Figure A.3: Selection of structurally characterized rare-earth-metal imide complexes obtained via reductive cleavage of azobenzene.

In 1996, five years after the reports of Bochkarev and Schumann, the group around Evans used another approach, treating the neodymium precursor complex $Nd(NHPh)_3(KCl)_3$ with an excess of the organoaluminium reagent $AlMe_3$.[99] Blue crystals of $[(Me_2Al(\mu\text{-}Me)_2Nd\ (\mu_3\text{-}NC_6H_5)(\mu\text{-}Me)AlMe)]_{22}$ were isolated. The dimeric neodymium imido complex contains two phenylimido moieties bridging two aluminium and one neodymium center (see Figure A.4, **25**).

The reaction of $AlMe_3$ as a Lewis acid with the homoleptic samarium amide complex $[Sm(NHAr^{iPr})_3]_2$ led the group of Gordon to the trivalent samarium imide complex $[Sm(NAr^{iPr})(NHAr^{iPr})(AlMe_3)_2]$. The imido moiety $Ar^{iPr}N^{2-}$ bridges between two samarium metal centers.[106] Changing from $AlMe_3$ to *n*-butyllithium, the partially deprotonated ytterbium anilide/imide complex $[Yb_2(NAr^{iPr})_4(NHAr^{iPr})_2Na_2Li_2(thf)_4]$ and the fully deprotonated complex $[Yb_2(NAr^{iPr})_6Na_2Li_4(thf)_4]$ were obtained by adjusting the used amount of base, as reported by the group of *Xie* in 2002.[100] Both complexes consist of two ytterbium metal centers bridged by two $Ar^{iPr}N^{2-}$ entities and terminal $Ar^{iPr}N^{2-}$, respectively. Incorporated alkali-metal ions and the bulky aryl ligands stabilize both complexes.

A different approach, avoiding the incorporation of alkali metals, is displayed by the reaction of the yttrium alkyl precursor [N(Ar)(NC_5H_3)N(Ar)C(Me)N($C_5H_3CH_2$-2,6-Me)]Y(CH_2SiMe_3)(thf) (Ar = 2,6-Me-C_6H_3) with borazane $NH_3{\cdot}BH_3$. The dimeric yttrium imido complex [{N(Ar)(NC_5H_3)N(Ar)C(Me)N($C_5H_3CH_2$-2,6-Me)}Y{N(H)BH_3}]$_2$ is Lewis acid stabilized, featuring two bridging $[NH{\cdot}BH_3]^{2-}$ moieties (see Figure A.4, **26**).[107]

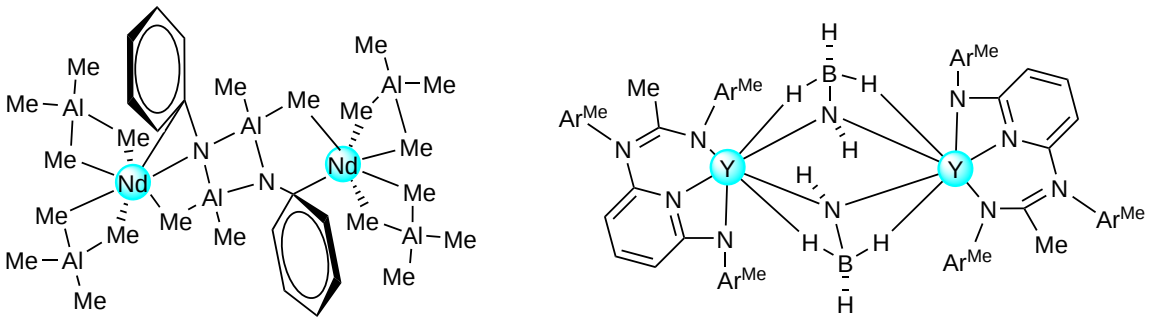

25 **26**

Figure A.4: Selection of structurally characterized rare-earth-metal imide complexes.[99,107]

Ever since Lu *et al.* reported on their synthesis of a terminal rare-earth-metal imide complex, the bane of elusive terminal imides has been broken. They showed that the Ln=N(imide) bond, in theory stable, is isolable by applying steric pressure to the complex, inducing an alkane elimination from their β-diketiminate precursor complex [(Ar^{iPr}NC(Me)(CH)C(Me)N(CH_2)$_2$ NMe_2)Sc(Me)($NHAr^{iPr}$)] (see Scheme A.6).

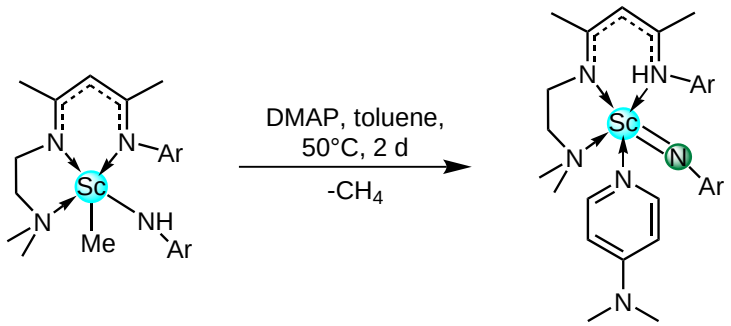

27 **28**

Scheme A.6: Synthesis procedure reported by Lu *et al.*[94]

Introducing the Lewis base 4-(dimethylamino)-pyridine (DMAP) to the precursor complex **27** provides the steric pressure needed to enforce the elimination of methane. Complex **28** [(Ar^{iPr}NC(Me)(CH)C(Me)N(CH_2)$_2$NMe_2)Sc(NAr^{iPr})(dmap)] featured not only the first terminal rare-earth-metal imide complex, but also exhibited the shortest Sc–N(imido) distance (1.881(5) Å) and the most linear Sc–N(imide)–C bonding angle of 169.6(5)° reported in literature.[94,108] In a later publication they showed that the steric pressure does not necessarily need to come from an introduced Lewis base, but can be achieved intramolecularly by an extended ligand system.[109] The route developed by the group of Chen was taken as stencil by other groups, successfully reporting on the synthesis of other new terminal rare-earth-metal imide complexes. The group around Piers started with scandium arylamid-methyl precursor complexes stabilized by a β-diketiminato ligand (see Scheme A.7, **29**). Thermolysis in the presence of DMAP led to the formation of the terminal scandium imide complex **30**. Further kinetic studies found activation parameters of $\Delta H^{\ddagger}$=73.5(2) kJ·mol^{-1} and $\Delta S^{\ddagger}$=−70.4(5) J·K^{-1}·mol^{-1}.[110]

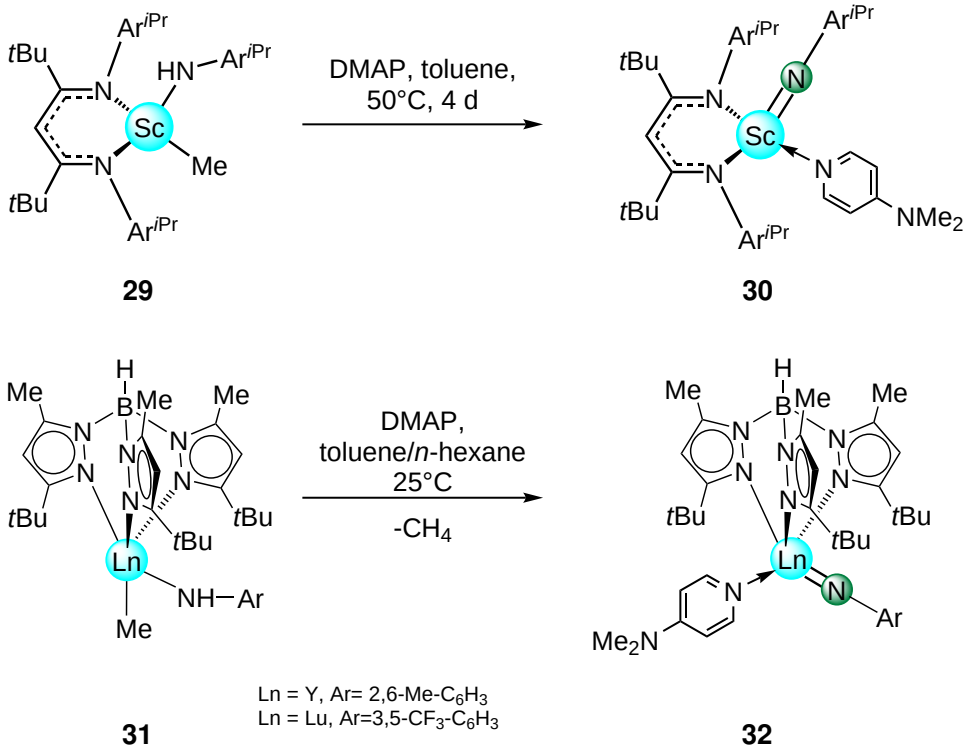

29 **30**

31 **32**

Scheme A.7: Synthesis of terminal rare-earth-metal imide complexes utilizing a Lewis base induced alkane elimination.[110,111]

In 2015 Anwander *et al.* reported on terminal imide complexes of yttrium and lutetium stabilized by a very bulky hydrotris(3-Me-5-*t*Bu-pyrazolyl)borato ($Tp^{tBu,Me}$)$^-$ ligand. The precursor arylamido methyl complexes [$Tp^{tBu,Me}$Ln(Me)(NHAr)] (Ln = Y, Ar = 2,6-Me-C_6H_3; Ln = Lu, Ar = 3,5-CF_3-C_6H_3) were treated with DMAP at ambient temperature, yielding the terminal imide complexes [$Tp^{tBu,Me}$Ln(NAr)(dmap)] (see Scheme A.7, **32**). Both complexes were obtained in good yields and were fully characterized. The single-crystal X-ray analysis revealed Ln = N_{imide} distances of 2.024(4) Å(Ln = Y); 1.993(5) Å (Ln = Lu) (both CN = 5). Nearly linear Y–N_{imide}–C_{aryl} angles with 173.6(4)° and Lu–N_{imide}–C_{aryl} 175.8(5)° were observed in the solid state.[111] Just recently Anwander *et al.* reported that stabilized methylidene gallate complexes [$Tp^{tBu,Me}$Ln(μ_3-CH_2)[(μ_2-Me)$GaMe_2$]$_2$] (Ln = Ce, Nd, Sm) when reacted with H_2NAr^{iPr} in a mixture of THF/toluene readily form terminal imide complexes [$Tp^{tBu,Me}$Ln($NC_6H_3iPr_2$-2,6)(thf)$_2$] (see Scheme A.8). Changing the solvent to solely toluene led to Lewis acid stabilized imide complexes [$Tp^{tBu,Me}$Ln($NC_6H_3iPr_2$-2,6)($GaMe_3$)] (Ln = Ce, Nd, Sm). Further studies revealed that by adding THF and removing the solvents subsequently, complexes **34** were obtainable. In the presence of the Lewis acid $GaMe_3$ in *n*-hexane compound **34** yielded the Lewis acid stabilized complex [$Tp^{tBu,Me}$ Ln(NAr^{iPr})($GaMe_3$)] (Ln = Nd, Sm).[112]

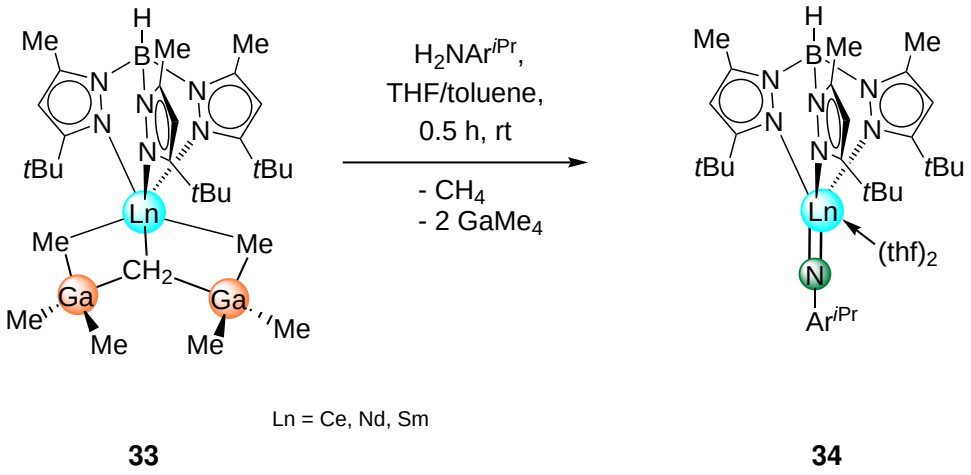

Scheme A.8: Synthesis of terminal rare-earth-metal imide complexes utilizing Lewis-acid stabilized methylidene complexes in protonolysis reactions.[112]

The field of trivalent rare-earth-metal imide complexes is rapidly growing both for bridging or terminal imides, respectively. In contrast, non-trivalent rare-earth-metal imide complexes are still scarce. In 2016 the Schelter group reported on the synthesis of a tetravalent cerium imide

Ce^{IV+} complex. The use of potassium bis(trimethylsilylamide) as base to deprotonate the TriNOx (= $N(CH_2C_6H_4NO(tBu))_3$) ligand-supported Ce^{IV+} precursor complex **35** led, after the addition of dimethoxyethane (DME) as donor, to the formation of the alkali-metal capped terminal cerium imide complex **36** (depicted in Scheme A.9). The highly polarized $Ce–N^{imide}$ bond shows multiple bond character in DFT calculations. The atom distance $Ce–N_{imide}$ (2.119(3 Å)) is among the shortest Ce–N atom distances found in literature.[18] The bond angle found for complex **36** differs significantly from an ideal angle ($Ce–N_{imide}–C$: 144.0(3)°). By using different silylamides a series of tetravalent cerium imides of the type [(TriNOx)Ce($NArCF_3$)M(do)$_x$] (M = Li, do = TMEDA; M = K, Rb, Cs do = DME) were obtained.[113,114]

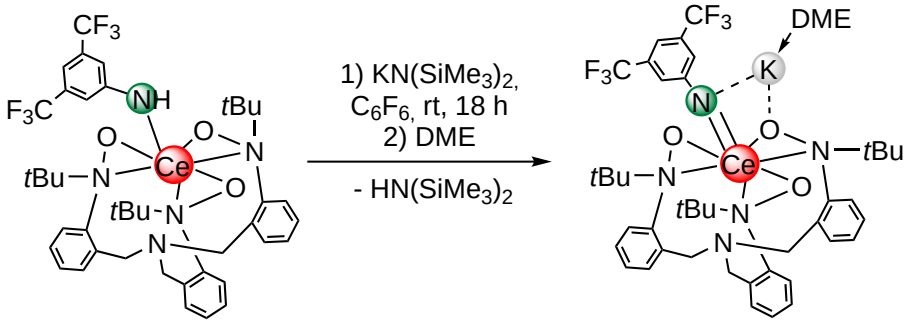

35 **36**

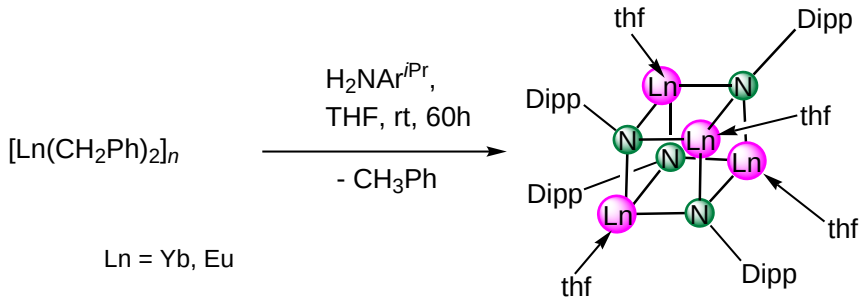

21 **37**

Scheme A.9: Synthesis procedures of non-trivalent rare-earth-metal imide complexes.[92,113,114]

Anwander *et al.* utilized a deprotonation approach of viable precursor compounds to access divalent rare-earth-metal imide complexes. Treatment of divalent rare-earth-metal benzyl complexes $[Ln(Ch_2Ph)_2]_n$ (**21**), acting as base, with commercially available aromatic arylamines NH_2Ar^{iPr} led to the formation of tetrameric imide complexes $[Ln(NAr^{iPr})(thf)]_4$ (Ln = Eu, Yb)

(see Scheme A.9, **37**). The complexes are isostructural, containing four metal centers bridged by $Ar^{iPr}N^{2-}$ entities forming cubane-like geometries.[92]

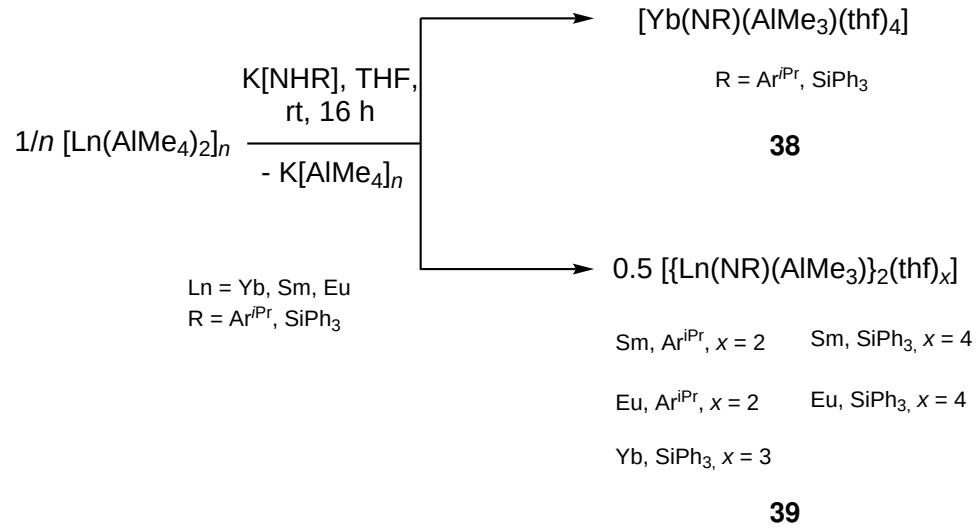

Scheme A.10: Tandem salt-metathesis protonolysis procedure for the synthesis of divalent rare-earth-metal imides stabilized by the Lewis acid $AlMe_3$.[102]

Apart from the procedures described above, Anwander *et al.* established a tandem salt-metathesis protonolysis procedure via treatment of divalent bis(tetramethylaluminate) precursors $[Ln(AlMe_4)_2]_n$ with potassium salts KNHR (R = Ar^{iPr}, $SiPh_3$), generating Lewis acid stabilized imide complexes (see Scheme A.10).[102] In the solid state, mono- and dilanthanide complexes were found, depending on the ionic radii of the metal center and the steric demand of the imido entity. Reactions of $[Yb(AlMe_4)_2]_n$ with $KNHAr^{iPr}$ yielded the Lewis acid stabilized ytterbium imide complexes $[Yb(NSiPh_3)(AlMe_3)(thf)_4]$/ $[\{Yb(NSiPh_3)(AlMe_3)\}_2(thf)_x]$ depending on the crystallization temperature. Use of divalent samarium and europium with bigger ionic radii gave dimeric complexes independently of the used amide reagent only (compare Scheme A.10). As part of these studies, it was shown that redox chemistry of those complexes is feasible. Accordingly, reactions with Cp^*_2Pb were executed leading to half-sandwich complexes of the type $[Cp^*Ln(NR)(AlMe_3)(thf)_2]$ (Ln = Sm, R = $SiPh_3$; Ln = Yb, R = Ar^{iPr}, $SiPh_3$).[102]

B

Summary of the Main Results

1 Divalent Rare-Earth-Metal Alkyl Complexes

The chemistry of divalent rare-earth metals Sm^{2+}, Eu^{2+} and Yb^{2+} is often compared to that of the alkaline-earth metals Ca^{2+}, Ba^{2+}, and Sr^{2+}. Especially the parallels of $Yb^{2+} \leftrightarrow Ca^{2+}$ and $Sm^{2+}/Eu^{2+} \leftrightarrow Sr^{2+}$ are often discussed.[38,115] These parallels can be explained through their very similar ionic radii (see Table A.2, Subsection 1.3), the ionic character of the metal–ligand bonds and the insignificant metal–ligand orbital interactions. The bonding interaction of ligand molecules with the large divalent metal ions Ln^{2+} /Ae^{2+} is mainly controlled by electrostatics and steric factors. Triggered by the reports on dimethylcalcium $[Ca(CH_3)_2]_n$[11] the question arose whether there exists a corresponding divalent rare-earth-metal chemistry. While these simple alkyl compounds are well established for magnesium[7,8] and trivalent rare-earth metals,[57] compounds $[Ln(CH_3)_2]$ were unknown.

Reacting $[Yb\{N(SiMe_3)_2\}_2(thf)_2]$ as precursor in a modified Lochmann protocol with methyllithium (MeLi) in diethylether gave orange, amorphous, pyrophoric, water and oxygen sensitive $[YbMe_2]_n$ (**D**). Elemental analysis revealed impurities which were traced back to the synthesis of the precursor complexes. Changing to donor-free ytterbium bis(trimethyl)silylamide $[Yb\{N(SiMe_3)_2\}_2]_2$ (**C**) increased the number of reaction steps, but an analytically pure product could be obtained (see Scheme B.1).

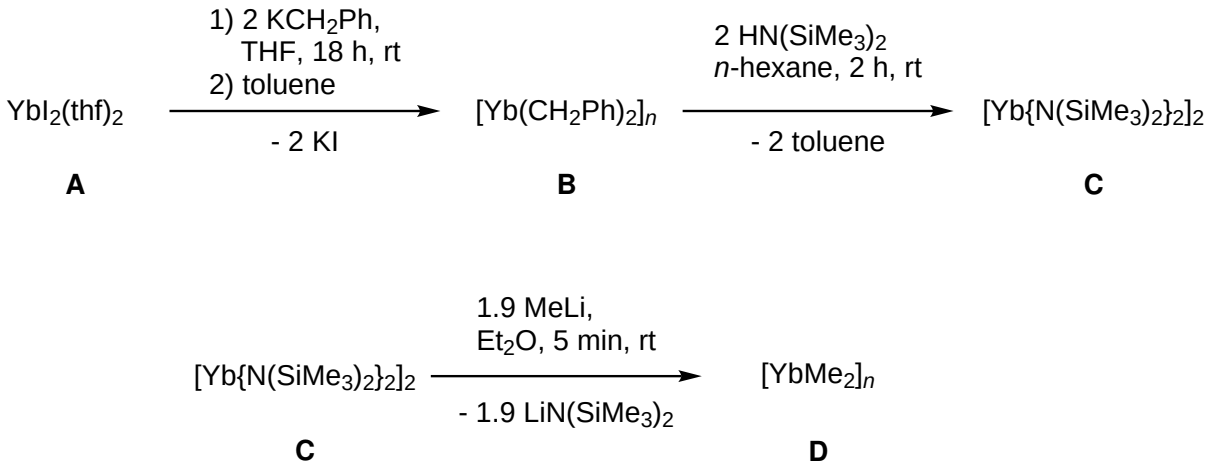

Scheme B.1: Schematic synthesis protocol for $[YbMe_2]_n$.

Due to the poor solubility of $[YbMe_2]_n$ the analytics were limited. Solid-state CP/MAS NMR spectroscopy revealed chemical shifts for ^{171}Yb and ^{13}C ($\delta(^{171}Yb)$: 947 ppm,

$\delta(^{13}C)$: 25 ppm). Infrared spectroscopy of **D** showed vibrational bands identical to those in the calcium analogue $[CaMe_2]_n$. The micro-scale reaction of **D** with the protic proligand $HTp^{tBu,Me}$and the reaction of **D** with $Tp^{tBu,Me}{}_2Yb$ led to the formation of $[Tp^{tBu,Me}Yb(CH_3)(thf)]$ (**E**). $[Tp^{tBu,Me}Yb(CH_3)(thf)]$ features the first divalent terminal methyl ytterbium complex, stabilized by a $Tp^{tBu,Me}$ ligand. The solid-state structure of compound **E** is depicted in Figure B.1.

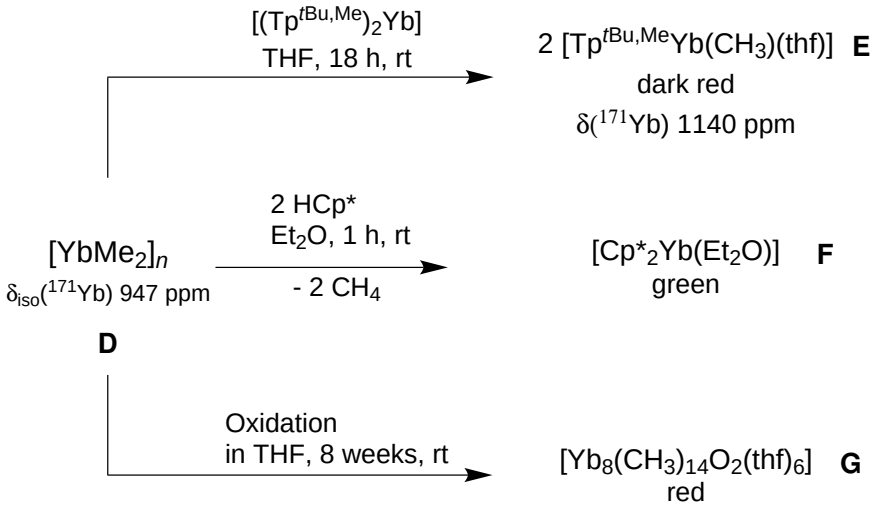

Scheme B.2: Derivatization reactions of $[Yb(Me)_2]_n$.

Furthermore, the protonolysis of **D** with HCp* gave $[Cp^*{}_2Yb(Et_2O)]$ (**F**). Evolution of methane verified the existence of methyl moieties in **D**. For $[Ca(Me)_2]_n$ a solid-state structure of the heptametallic donor adduct $[(thf)_{10}Ca_7Me_{14}]$ was obtained from THF solutions at low temperatures.[11] In contrast to these reports, analogous attempts storing $[Yb(Me)_2]_n$ in THF at low temperatures turned out differently. This can be explained by the enhanced insolubility of $[Yb(Me)_2]_n$. Storing a mixture at ambient temperature over several weeks afforded single crystals of $[Yb_8(CH_3)_{14}O_2(thf)_6]$ (**G**). Complex **G** can be considered as a snapshot from the degradation process of compound **D** in THF. This unusual octametallic methyl ytterboxane features the first ytterbium oxocluster without stabilizing, sterically demanding ligands.[116] The mixed-valence complex **G** revealed two Yb^{3+} centers bridged by two oxygen atoms, building the central plane of the complex. Around each oxygen atom four Yb^{2+} centers adopt a butterfly arrangement. Two μ_2- and two μ_3-bridging methyl groups connect the Yb^{2+} centers. The ladder motif found in the center is noteworthy and can be compared to the ladder motif proposed for the elusive methylalumoxane (MAO).[117]

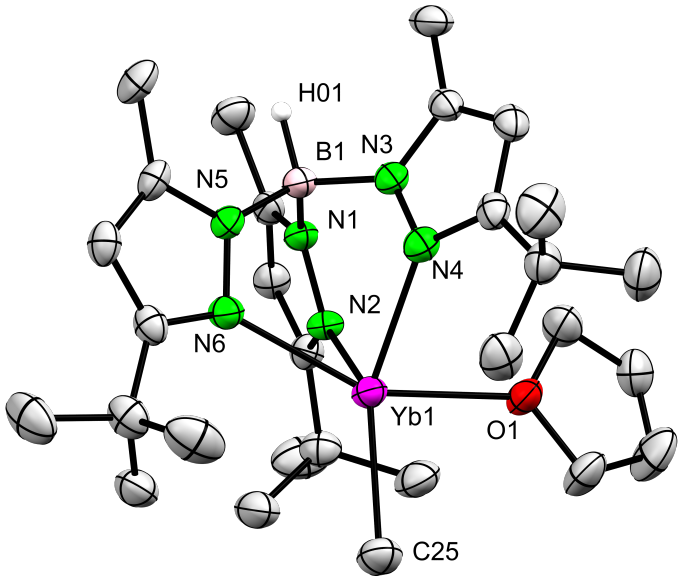

Figure B.1: Crystal structure of [Tp^{tBu,Me}Yb(CH$_3$)(thf)] (**E**). Compound **E** crystallizes with two molecules and one molecule lattice solvent per unit cell. All atoms are represented by atomic displacement ellipsoids set at 50% probability. Hydrogen atoms except B–H and one molecule lattice solvent are omitted for clarity.

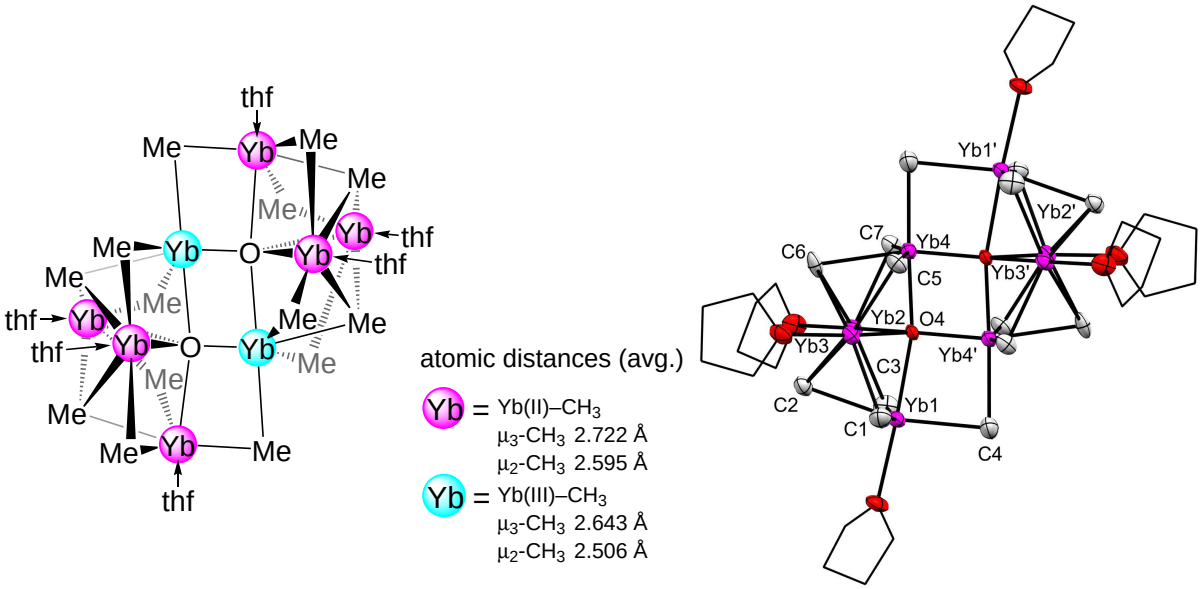

Figure B.2: Crystal structure of [Yb$_8$(CH$_3$)$_{14}$O$_2$(thf)$_6$] (**G**). All atoms are represented by atomic displacement ellipsoids set at 50% probability. Hydrogen atoms are omitted and donor THF molecules are displayed as wireframe for clarity.

2 Synthesis of new Rare-Earth-Metal Amide Complexes

The synthesis of rare-earth-metal imide complexes draws on a broad variety of different approaches.[18] The protonolysis of rare-earth-metal anilide complexes by suitable bases like metal alkyls is commonly used. Evans *et al.* reported on the synthesis of $[(AlMe_4)_2Nd(NPh)(AlMe_4)]_2$ by treating $Nd[NH(Ph)]_3(KCl)_3$ with an excess of organoaluminium reagents.[17,78] Tandem salt-metathesis-protonolysis reactions are an alternative synthesis approach. Anwander *et al.* reported in 2018 on the successful synthesis of divalent imide complexes by reacting permethylated complexes $[Ln(AlMe_4)_2]_n$ with aniline derivatives or triphenylsilylamine.[102] Furthermore, applying a simple double deprotonation of Ln^{2+} benzyl complexes (Ln = Eu, Yb) with 2,6-di*iso*propylaninline (NH_2Ar^{iPr}) provided cubane-like imide complexes.[92] In search for terminal imide complexes, utilization of the very bulky, monoanionic $Tp^{tBu,Me}$ scorpionat ligand provides a promising platform for preventing bridging imido moieties.[111,112,118]

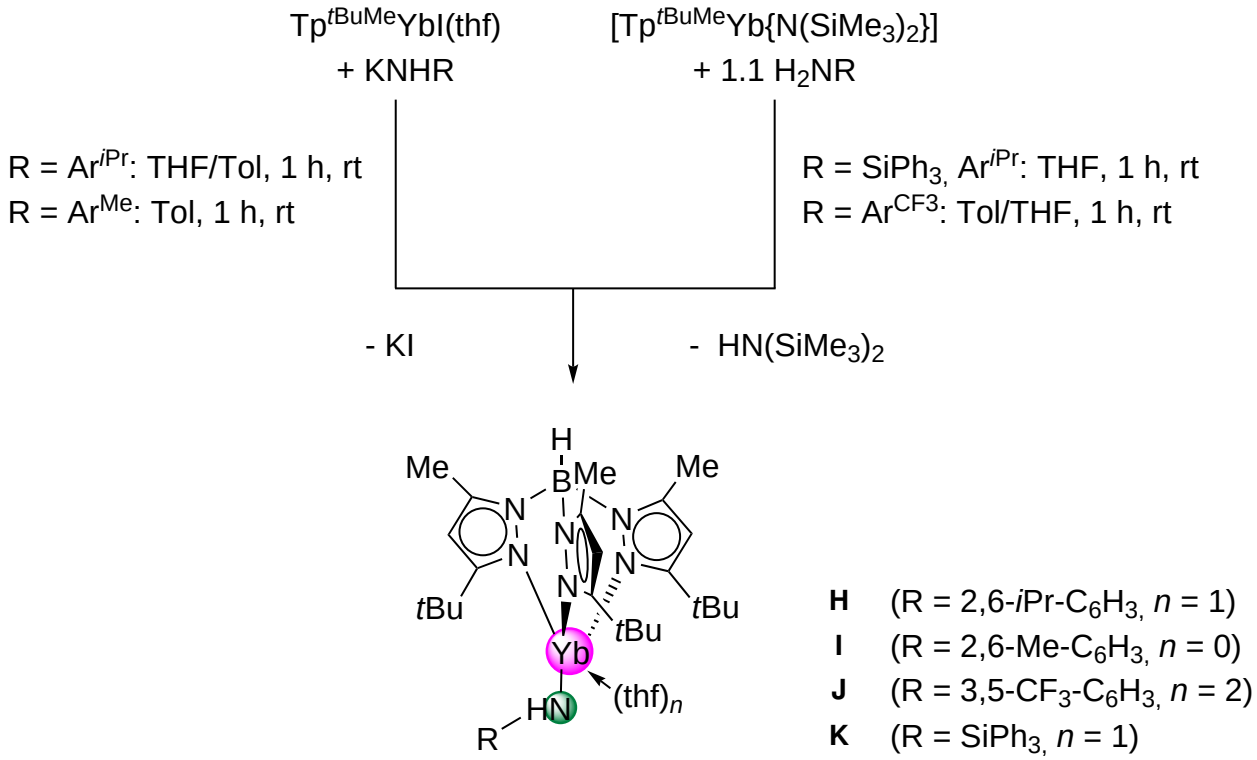

Scheme B.3: Synthesis protocols for different divalent ytterbium amides coordinated by a very bulky $Tp^{tBu,Me}$ ligand.

Divalent ytterbium amide complexes [Tp^{tBu,Me}Yb(NHR)(thf)$_n$] were synthesized by either applying a salt-metathesis reaction protocol or via protonolysis of [Tp^{tBu,Me}Yb{N(SiMe$_3$)$_2$}] with different aniline derivatives H$_2$NR (R = 2,6-di*iso*propyl-C$_6$H$_5$ (**H**), 2,6-methyl-C$_6$H$_5$ (**I**), 3,5-CF$_3$-C$_6$H$_5$ (**J**), SiPh$_3$ (**K**)) (see Scheme B.3). Performing the salt-metathesis reaction in toluene afforded the solvent-free complex [Tp^{tBu,Me}Yb(NHAr^{iPr})] (**L**).

Table B.1: ^{171}Yb chemical shifts determined by ^{1}H-^{171}Yb HSQC NMR spectroscopy (C$_6$D$_6$, r.t.) for divalent ytterbium complexes **H** - **O** and **Q**.

Complex		δ^{171}Yb/ppm
[Tp^{tBu,Me}Yb(NHAr^{iPr})(thf)]	**H**	718
[Tp^{tBu,Me}Yb(NHAr^{iPr})]	**L**	750
[Tp^{tBu,Me}Yb(NHAr^{Me})]	**I**	778
[Tp^{tBu,Me}Yb(NHAr^{CF_3})(thf)$_2$]	**J**	763
[Tp^{tBu,Me}Yb(NHSiPh$_2$)(thf)]	**K**	863
[Tp^{tBu,Me}Yb(NHAr^{iPr})(dmap)]	**M**	776
[Tp^{tBu,Me}Yb(NHAr^{CF_2})(dmap)]	**N**	862
[Tp^{tBu,Me}Yb(NHSiPh$_3$)(dmap)]	**O**	955
[Tp^{tBu,Me}Yb(NHAr^{CF_3})(GaMe$_3$)]	**Q**	582

In protonolysis experiments of **J** and **L** with simple metal alkyls like methyllithium and benzyl potassium no abstraction of the amido proton was observed. Neither did the use of silylamides M[N(SiMe$_3$)$_2$] (M = K, Cs, Na) yield the desired outcome. The addition of crownethers 18-crown-6, Me$_3$TACN or 1,4,7,10-tetramethyl-1,4,7,10-tetraazacyclododecane had no detectable effect. No defined products could be identified . The exchange of donor THF with the N-donor 4-dimethylaminopyridine (DMAP) gave complexes [Tp^{tBu,Me}Yb(NHR)(dmap)] (R = 2,6-di*iso*propyl-C$_6$H$_5$ (**M**), 3,5-CF$_3$-C$_6$H$_5$ (**N**), SiPh$_3$ (**O**)). The product of the reaction of **J** with the Lewis acid trimethylaluminium (TMA) revealed a cocrystallization of [Tp^{tBu,Me}Yb(NHAr^{CF3})(AlMe$_3$)] (**P**) beside the tetramethylaluminate [Tp^{tBu,Me}Yb(AlMe$_4$)]. In contrast, changing the Lewis acid to trimethylgallium GaMe$_3$, the adduct complex [Tp^{tBu,Me}Yb(NHAr^{CF3})(GaMe$_3$)] (**Q**) was obtained in quantitative yield. Heating compound **Q** to 120 °C for 2 h did not result in any activation of the complex or observable decomposition by ^{1}H NMR spectroscopy.

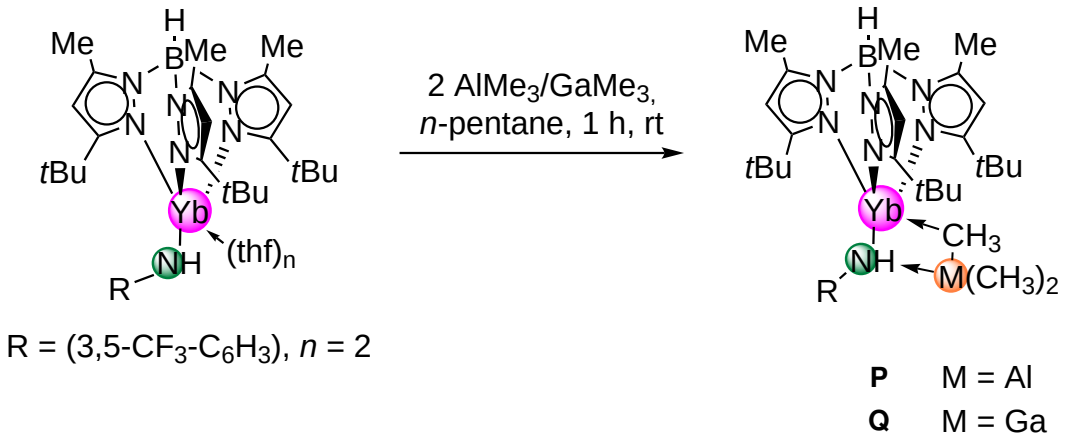

Scheme B.4: Synthesis protocol for complexes [Tp$^{t\mathrm{Bu,Me}}$Yb(NHAr$^{\mathrm{CF3}}$)(MMe$_3$)] (M = Al, Ga).

The oxidation reactions of **H** and **J** with C_2Cl_6 led to the trivalent complexes [Tp$^{t\mathrm{Bu,Me}}$Yb(NHAr$^{\mathrm{R}}$)(Cl)] (R = 2,6-*i*Pr (**R**); 3,5-CF_3 (**T**)). Using $TeBr_4$ as an oxidation agent gave the bromide analogues [Tp$^{t\mathrm{Bu,Me}}$(YbNHAr$^{\mathrm{R}}$)(Br)] (R = 2,6-*i*Pr (**S**); 3,5-CF_3 (**U**)). Elemental iodine as oxidation agent gave divalent Tp$^{t\mathrm{Bu,Me}}$YbI(THF). Silver triflate AgOTf as oxidation agent resulted in complex decomposition. Initial alkylation experiments of **R**, **S**, **T**, and **U** with methyllithium and benzylpotassium at ambient and at low temperatures (−40 °C) did not yield any defined products.

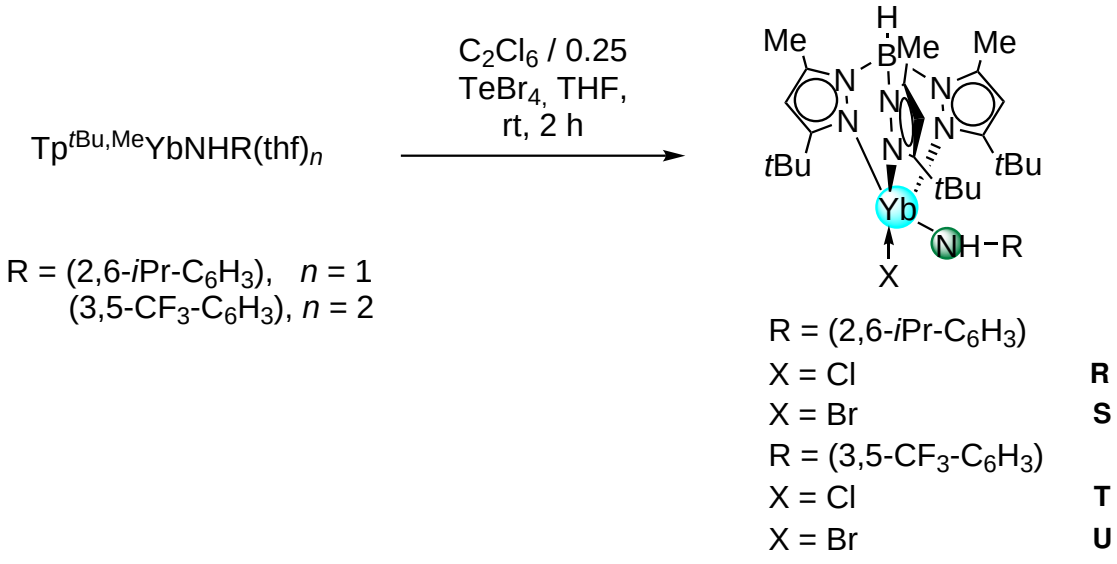

Scheme B.5: Synthesis protocols for the trivalent complexes [Tp$^{t\mathrm{Bu,Me}}$Yb(NHAr$^{\mathrm{R}}$)(X)] (R = 2,6-*i*Pr, 3,5-CF_3; X = Cl, Br).

C

Unpublished Results

Unpublished Results

Chapter C contains all experimental and analytical data for complexes that are not part of the attached papers/manuscripts. Compounds listed in Chapter C were obtained as crude product mixtures, in very low yields or nothing but a crystal structure/connectivity was obtainable. Therefore analytical data are incomplete.

Divalent Rare-Earth-Metal Alkyls

In the scope of the investigations on $[YbMe_2]_n$, experiments targeting alternative synthesis pathways and further reactivities of $[YbMe_2]_n$ were performed. The reaction of the precursor $Yb[N(SiMe_3)_2]_2(thf)_2$ with Me_3TACN as stabilizing neutral ligand gave $[(Me_3TACN)Yb\{N(SiMe_3)_2\}_2]$ (**V**). Changing from Me_3TACN to the bigger Me_4-tetraazacyclododecane (Me_4cyclam) complex $[(Me_4cyclam)Yb\{N(SiMe_3)_2\}_2]$ (**W**) was obtainable. In compound **W** the (Me_4cyclam) ligand coordinates with only two nitrogen atoms to the metal center, indicating a non-perfect fit or a weak coordination to the Yb^{2+}. Both complexes **V** and **W** could act as precursors for the synthesis of terminal dimethyl ytterbium complexes

.

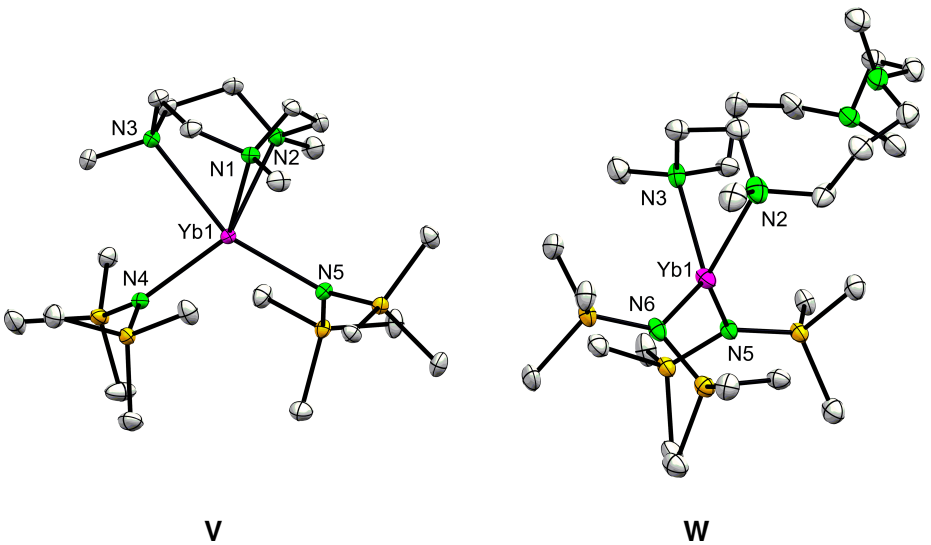

V **W**

Figure C.1: Crystal structure of $[(Me_3TACN)Yb\{N(SiMe_3)_2\}_2]$ (**V**) and $[(Me_4cyclam)Yb\{N(SiMe_3)_2\}_2]$ (**W**). All atoms are represented by atomic displacement ellipsoids set at 50% probability. Hydrogen atoms are omitted for clarity.

After the successful adaption of the synthesis protocol for dimethyl calcium to divalent ytterbium first approaches towards the other divalent rare-earth metals Eu^{2+} and Sm^{2+} where carried out. The solvent THF of the reaction mixture of $EuI_2(thf)_2$ with benzyl potassium was removed. Excess of bis(trimethylsilyl)amine $HN(SiMe_3)_2$ in *n*-hexane was added to the residual solid. After work-up, yellow crystals of donor-free $[Eu\{N(SiMe_3)_2\}_2]_2$ (**X**) were obtained (see Scheme C.1). Complex **X** is isostructural to the ytterbium complex.

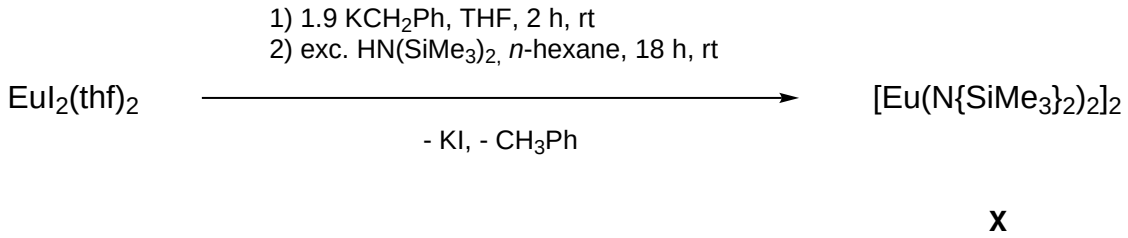

Scheme C.1: Synthesis procedure for the synthesis of $[Eu\{N(SiMe_3)_2\}_2]_2$.

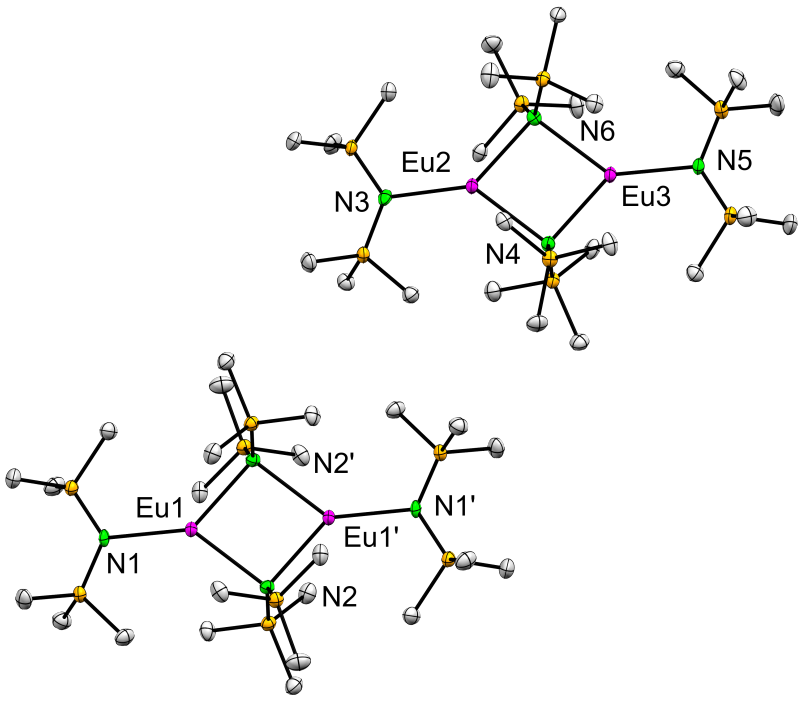

Figure C.2: Crystal structure of donor-free $[Eu\{N(SiMe_3)_2\}_2]$ (**X**). All atoms are represented by atomic displacement ellipsoids set at 50% probability. Hydrogen atoms are omitted for clarity.

Reacting **X** with methyl lithium gave of a bright yellow, amorphous, pyrophoric powder with orange fluorescence **Y**. The reaction behavior and the DRIFT spectrum of **Y** are in conformity to the behavior of **D** leading to the assumption that a divalent europium methyl species, presumably $[Eu(CH_3)_2]_n$, was successful synthesized. Reacting $Sm[N(SiMe_3)_2]_2(thf)_2$ with methyllithium led to the formation of a dark green, amorphous powder, presumably $[Sm(CH_3)_2]_n$ (**Z**). Storing the powder at ambient temperature overnight resulted in a color change to black, indicating decomposition of the complex. Complexes **Y** and **Z** were not further investigated.

Experimental Details

If not otherwise specified all reactions were carried out under inert atmosphere (Argon) in a glovebox (MBraun MB200B <0,1 ppm O_2, <0,1 ppm H_2O). The syntheses of the organic ligands were carried out under standard Schlenk techniques in oven-dried glassware. The solvents were purified using Grubbs-type columns (MBraun SPS solvent purification system). Tetrahydrofuran was stored over activated molecular sieves (3 Å). Deuterated solvents were purchased from Sigma Aldrich or Eurisotop and were stored over Na/K alloy in a glovebox. Potassium bis(trimethylsilyl)amide K[N(SiMe$_3$)$_2$] (95 %, Sigma Aldrich) was sublimed before use and stored in a glovebox. The chloride content of MeLi (1.6 M in Et_2O, Aldrich) was determined via potentiometric titration as described previously.[11] The newly synthesized complexes are stored at ambient temperature or at -40 °C under inert atmospheres, respectively. The proligand hydrotris(3-tert-butyl-5-methylpyrazolyl)borate (HTp$^{t\mathrm{Bu,Me}}$)[119] and the ytterbium(II) precursors Yb(CH$_2$Ph)$_2$[92] and Yb(Tp$^{t\mathrm{Bu,Me}}{}_2$)[120] were synthesized according to slight modifications of the literature procedures. The NMR spectra of air- and moisture-sensitive compounds were recorded by using J. Young-valved NMR tubes on a BRUKER AVIII+300 (^{1}H: 300.13 MHz, ^{11}B: 96.29 MHz, ^{13}C: 59.63 MHz), a BRUKER AVII+400 instrument (^{1}H: 400.13 MHz, ^{13}C: 100.61 MHz) or a Bruker AVII+500 (^{1}H: 500.13 MHz, ^{13}C: 125.76 MHz, ^{171}Yb: 87.52 MHz). The residual solvent signals are referenced to TMS.[121] Solid-state NMR spectra were recorded on a Bruker ASX 300 instrument (^{13}C: 75.47 MHz, ^{171}Yb: 52.52 MHz) equipped with MAS (magic angle spinning) hardware and using a ZrO_2 rotor with an outer diameter of 4 mm. Infrared spectra were recorded on a Nicolet 6700 FT-IR spectrometer with a DRIFTS cell (KBr window), and the samples were prepared in a glovebox and mixed with KBr powder. UV/Vis measurements were carried out in tetrahydrofuran or *n*-hexane on a PG Instruments T60 UV-Vis spectrophotometer. Elemental analysis (C, H, N) were performed with an Elementar Vario Micro Cube.

[(Me$_3$TACN)Yb{N(SiMe$_3$)$_2$}$_2$] (**V**): To a solution of Yb[N(SiMe$_3$)$_2$]$_2$(thf)$_2$ (181 mg, 0.284 mmol) in *n*-hexane (5ml) a solution of Me$_3$TACN (48.7 mg, 0.284 mmol) in 2 ml *n*-hexane was added and stirred for 1 h at ambient temperature. All volatiles were removed under reduced pressure and the residual solids were dissolved in *n*-hexane and stored at -40 °C. (Me$_3$TACN)Yb{N(SiMe$_3$)$_2$}$_2$ was obtained as red crystals. Analysis: X-ray crystallography.

[(Me$_4$cyclam)Yb{N(SiMe$_3$)$_2$}$_2$] (**W**): To a solution of $YbI_2(thf)_2$ (180 mg, 0.315 mmol) in THF (3 ml) solutions of Me_4cyclam (71.3 mg, 0.278 mmol) in 3 ml THF and $KN(SiMe_3)_2$ (122.6 mg, 0.615 mmol) in 3 ml THF were added and stirred over night at ambient temperature. After filtration, all volatiles were removed under reduced pressure and the residual solids were dissolved in *n*-hexane and stored at -40 °C. [(Me_4cyclam)Yb{$N(SiMe_3)_2$}$_2$] was obtained as violet crystals in 41% (86 mg) crystalline yield. Analysis: X-ray crystallography.

[Eu{N(SiMe$_3$)$_2$}$_2$]$_2$ (**X**): To $EuI_2(thf)_2$ (450 mg, 0.830 mmol) in 3 ml THF a solution of KCH_2Ph (211 mg, 1.62 mmol) in 3 ml THF was slowly added. The solution was stirred at ambient temperature for 2 h. After filtration, all volatiles were removed under reduced pressure. The residual solids were dissolved in *n*-hexane (5 ml) and an excess of bis(trimethylsilyl)amine in 3 ml *n*-hexane was added. The mixture was stirred overnight. After filtration of the bright yellow solution all volatiles were removed under reduced pressure. The solids were dissolved in *n*-hexane and the solution was stored at -40 °C. [Eu{$N(SiMe_3)_2$}$_2$]$_2$ was obtained as yellow crystals in 57 % (156 mg, 0.428 mmol) crystalline yield. Elemental analysis calcd. (%) for $C_{12}H_{36}EuN_2Si_4$: C 30.49, H 7.68, N 5.93; found C 30.52, H 7.76, N 6.00. Further analysis: X-ray crystallography.

[K(Tp$^{t\mathrm{Bu,Me}}$)$_2$(K{18-crown-6}·Et$_2$O)]: To a solution of $Tp^{t\mathrm{Bu,Me}}Yb(NHAr^{i\mathrm{Pr}})(thf)$ (41 mg, 0.05 mmol) in 0.3 ml thf-*d8* solutions of KCH_2Ph and 18-crown-6 in 0.2 ml THF-*d8* were added. After 30 min all volatiles were removed under reduced pressure and the residual solids were dissolved in *n*-hexane and stored at -40 °C. The product was obtained as colorless needles. Analyses: X-ray crystallography.

D

Bibliography

References

[1] C. Elschenbroich in *Organometallchemie*, Springer, **2008**, pp. 15–18.

[2] D. Seyferth, *Organometallics* **2001**, *20*, 1488–1498.

[3] R. Bunsen, *Annalen der Pharmacie* **1839**, *31*, 175–180.

[4] E. von Frankland, *Justus Liebigs Ann. Chem.* **1849**, *71*, 213–216.

[5] E. von Frankland, *Justus Liebigs Ann. Chem.* **1849**, *71*, 171–213.

[6] E. Frankland, *Quarterly Journal of the Chemical Society of London* **1850**, *2*, 263–296.

[7] W. Schlenk, W. Schlenk jun., *Ber. Dtsch. Chem. Ges. (A and B Series)* **1929**, *62*, 920–924.

[8] V. Grignard, *Acad. Sci.* **1900**, *130*, 1322–1325.

[9] W. Schlenk, J. Holtz, *Ber. Dtsch. Chem. Ges.* **1917**, *50*, 262–274.

[10] D. A. Payne, R. T. Sanderson, *J. Am. Chem. Soc.* **1958**, *80*, 5324–5324.

[11] B. M. Wolf, C. Stuhl, C. Maichle-Mössmer, R. Anwander, *J. Am. Chem. Soc.* **2018**, *140*, 2373–2383.

[12] L. Lochmann, J. Pospíšil, D. Lím, *Tetrahedron Lett.* **1966**, *7*, 257–262.

[13] T. Imamoto, *Lanthanides in Organic Synthesis*, Academic Press, **1994**.

[14] J. Lucas, P. Lucas, T. Le Mercier, A. Rollat, W. G. Davenport, *Rare Earths: Science, Technology, Production and Use*, 1st ed., Elsevier, **2014**.

[15] W. J. Evans, *Polyhedron* **1987**, *6*, 803–835.

[16] F. T. Edelmann, D. M. M. Freckmann, H. Schumann, *Chem. Rev.* **2002**, *102*, 1851–1896.

[17] M. Zimmermann, N. Å. Frøystein, A. Fischbach, P. Sirsch, H. M. Dietrich, K. W. Törnroos, E. Herdtweck, R. Anwander, *Chem. Eur. J.* **2007**, *13*, 8784–8800.

[18] D. Schädle, R. Anwander, *Chem. Soc. Rev.* **2019**, *48*, 5752–5805.

[19] F. Jaroschik, F. Nief, X.-F. Le Goff, L. Ricard, *Organometallics* **2007**, *26*, 3552–3558.

[20] I. L. Fedushkin, F. Girgsdies, H. Schumann, M. N. Bochkarev, *Eur. J. Inorg. Chem.* **2001**, 2405–2410.

[21] P. Girard, J. L. Namy, H. B. Kagan, *J. Am. Chem. Soc.* **1980**, *102*, 2693–2698.

[22] J. Gottfriedsen, F. T. Edelmann, *Coord. Chem. Rev.* **2007**, *251*, 142–202.

[23] J. H. Farnaby, T. Chowdhury, S. J. Horsewill, B. Wilson, F. Jaroschik, *Coord. Chem. Rev.* **2021**, *437*, 213830.

[24] R. Anwander, M. Dolg, F. T. Edelmann, *Chem. Soc. Rev.* **2017**, *46*, 6697–6709.

[25] Y.-M. So, W.-H. Leung, *Coordination Chemistry Reviews* **2017**, *340*, 172–197.

[26] D. E. Hobart, K. Samhoun, J. P. Young, V. E. Norvell, G. Mamantov, J. R. Peterson, *Inorganic and Nuclear Chemistry Letters* **1980**, *16*, 321–328.

[27] A. R. Willauer, C. T. Palumbo, F. Fadaei-Tirani, I. Zivkovic, I. Douair, L. Maron, M. Mazzanti, *J. Am. Chem. Soc.* **2020**, *142*, 5538–5542.

[28] C. T. Palumbo, I. Zivkovic, R. Scopelliti, M. Mazzanti, *J. Am. Chem. Soc.* **2019**, *141*, 9827–9831.

[29] N. Rice, I. A. Popov, D. R. Russo, J. Bacsa, E. R. Batista, P. Yang, J. Telser, H. S. La Pierre, *J. Am. Chem. Soc.* **2019**, *141*, 13222–13233.
[30] R. G. Pearson, *J. Am. Chem. Soc.* **1963**, *85*, 3533–3539.
[31] R. D. Shannon, *Acta Crystallogr. A* **1976**, *32*, 751–767.
[32] G. A. Crosby, *Mol. Cryst.* **1966**, *1*, 37–81.
[33] J.-C. G. Bunzli, V. K. Pecharsky, *Handbook on the Physics and Chemistry of Rare Earths: Including Actinides*, Elsevier, **2016**.
[34] H. B. Kagan, J. L. Namy, *Tetrahedron* **1986**, *42*, 6573–6614.
[35] K. Mikami, M. Terada, H. Matsuzawa, *Angew. Chem. Int. Ed.* **2002**, *41*, 3554–3572.
[36] W. J. Evans, G. Zucchi, J. W. Ziller, *J. Am. Chem. Soc.* **2003**, *125*, 10–11.
[37] L. R. Morss, *Chem. Rev.* **1976**, *76*, 827–841.
[38] S. Harder, *Angew. Chem. Int. Ed.* **2004**, *43*, 2714–2718.
[39] R. A. Andersen, J. M. Boncella, C. J. Burns, R. Blom, A. Haaland, H. V. Volden, *J. Organomet. Chem.* **1986**, *312*, C49–C52.
[40] M. Kaupp, P. v. R. Schleyer, M. Dolg, H. Stoll, *J. Am. Chem. Soc.* **1992**, *114*, 8202–8208.
[41] S. Harder, F. Feil, A. Weeber, *Organometallics* **2001**, *20*, 1044–1046.
[42] S. Harder, *Organometallics* **2002**, *21*, 3782–3787.
[43] M. Zimmermann, D. Rauschmaier, K. Eichele, K. Törnroos, R. Anwander, *Chem. Commun.* **2010**, *46*, 5346.
[44] H. J. Berthold, G. Groh, *Z. Anorg. Allg. Chem.* **1963**, *319*, 230–235.
[45] K. C. C. Beermann, *Angew. Chem.* **1959**, *71*, 627.
[46] H. J. Berthold, G. Groh, *Angew. Chem. Int. Ed.* **1966**, *5*, 516–516.
[47] W. Mowat, A. Shortland, G. Yagupsky, N. J. Hill, M. Yagupsky, G. Wilkinson, *J. Chem. Soc., Dalton Trans.* **1972**, 533–542.
[48] G. Yagupsky, W. Mowat, A. Shortland, G. Wilkinson, *J. Chem. Soc. D* **1970**, 1369–1370.
[49] M. R. Collier, M. F. Lappert, M. M. Truelock, *J. Organomet. Chem.* **1970**, *25*, C36–C38.
[50] M. R. Collier, M. F. Lappert, R. Pearce, *J. Chem. Soc., Dalton Trans.* **1973**, 445–451.
[51] J. M. Birmingham, G. Wilkinson, *J. Am. Chem. Soc.* **1956**, *78*, 42–44.
[52] A. v. Grosse, *Z. Anorg. Allg. Chem.* **1926**, *152*, 133–148.
[53] F. A. Cotton, *Chem. Rev.* **1955**, *55*, 551–594.
[54] M. F. Lappert, R. Pearce, *J. Chem. Soc., Chem. Commun.* **1973**, 126–126.
[55] G. Barker, M. Lappert, *J. Organomet. Chem.* **1974**, *76*, C45–C46.
[56] C. Eaborn, P. B. Hitchcock, K. Izod, J. D. Smith, *J. Am. Chem. Soc.* **1994**, *116*, 12071–12072.
[57] M. Zimmermann, R. Anwander, *Chem. Rev.* **2010**, *110*, 6194–6259.
[58] P. B. Hitchcock, M. F. Lappert, R. G. Smith, R. A. Bartlett, P. P. Power, *J. Chem. Soc., Chem. Commun.* **1988**, 1007–1009.
[59] H. Schumann, J. Müller, *Angew. Chem. Int. Ed.* **1978**, *17*, 276–276.
[60] H. Schumann, J. Pickardt, N. Bruncks, *Angew. Chem. Int. Ed.* **1981**, *20*, 120–121.

[61] H. Schumann, J. Mueller, N. Bruncks, H. Lauke, J. Pickardt, H. Schwarz, K. Eckart, *Organometallics* **1984**, *3*, 69–74.

[62] H. Schumann, H. Lauke, E. Hahn, J. Pickardt, *J. Organomet. Chem.* **1984**, *263*, 29–35.

[63] M. U. Kramer, D. Robert, S. Arndt, P. M. Zeimentz, T. P. Spaniol, A. Yahia, L. Maron, O. Eisenstein, J. Okuda, *Inorg. Chem.* **2008**, *47*, 9265–9278.

[64] S. Hajela, W. P. Schaefer, J. E. Bercaw, *J. Organomet. Chem.* **1997**, *532*, 45–53.

[65] M. G. Klimpel, R. Anwander, M. Tafipolsky, W. Scherer, *Organometallics* **2001**, *20*, 3983–3992.

[66] M. G. Schrems, H. M. Dietrich, K. W. Törnroos, R. Anwander, *Chem. Commun.* **2005**, 5922–5924.

[67] F. Ortu, *Chem. Rev.* **2022**, *122*, 6040–6116.

[68] H. M. Dietrich, G. Raudaschl-Sieber, R. Anwander, *Angew. Chem. Int. Ed.* **2005**, *44*, 5303–5306.

[69] D. Barisic, D. Diether, C. Maichle-Mössmer, R. Anwander, *J. Am. Chem. Soc.* **2019**, *141*, 13931–13940.

[70] C. J. Burns, R. A. Andersen, *J. Am. Chem. Soc.* **1987**, *109*, 5853–5855.

[71] H. Yamamoto, H. Yasuda, K. Yokota, A. Nakamura, Y. Kai, N. Kasai, *Chem. Lett.* **1988**, *17*, 1963–1966.

[72] M. D. Walter, P. T. Matsunaga, C. J. Burns, L. Maron, R. A. Andersen, *Organometallics* **2017**, *36*, 4564–4578.

[73] D. J. Schwartz, G. E. Ball, R. A. Andersen, *J. Am. Chem. Soc.* **1995**, *117*, 6027–6040.

[74] H.-M. Sommerfeldt, C. Meermann, M. G. Schrems, K. W. Törnroos, N. Å. Frøystein, R. J. Miller, E.-W. Scheidt, W. Scherer, R. Anwander, *Dalton Trans.* **2008**, 1899–1907.

[75] R. Litlabø, K. Saliu, M. J. Ferguson, R. McDonald, J. Takats, R. Anwander, *Organometallics* **2009**, *28*, 6750–6754.

[76] W. T. Klooster, R. S. Lu, R. Anwander, W. J. Evans, T. F. Koetzle, R. Bau, *Angew. Chem. Int. Ed.* **1998**, *37*, 1268–1270.

[77] G. Occhipinti, C. Meermann, H. M. Dietrich, R. Litlabø, F. Auras, K. W. Törnroos, C. Maichle-Mössmer, V. R. Jensen, R. Anwander, *J. Am. Chem. Soc.* **2011**, *133*, 6323–6337.

[78] W. J. Evans, R. Anwander, J. W. Ziller, *Organometallics* **1995**, *14*, 1107–1109.

[79] A. Nieland, A. Mix, B. Neumann, H.-G. Stammler, N. W. Mitzel, *Eur. J. Inorg. Chem.* **2014**, 51–57.

[80] C. O. Hollfelder, L. N. Jende, D. Diether, T. Zelger, R. Stauder, C. Maichle-Mössmer, R. Anwander, *Catalysts* **2018**, *8*.

[81] M. Zimmermann, K. W. Törnroos, R. M. Waymouth, R. Anwander, *Organometallics* **2008**, *27*, 4310–4317.

[82] A. Fischbach, E. Herdtweck, R. Anwander, G. Eickerling, W. Scherer, *Organometallics* **2003**, *22*, 499–509.

[83] L. E. Manzer, *J. Am. Chem. Soc.* **1978**, *100*, 8068–8073.

[84] S. Harder, C. Ruspic, N. N. Bhriain, F. Berkermann, M. Schürmann, *Z. Naturforsch. B* **2008**, *63*, 267–274.
[85] C. Ruspic, J. R. Moss, M. Schürmann, S. Harder, *Angew. Chem. Int. Ed.* **2008**, *47*, 2121–2126.
[86] S. Harder, *Organometallics* **2005**, *24*, 373–379.
[87] W.-X. Zhang, M. Nishiura, T. Mashiko, Z. Hou, *Chem. Eur. J.* **2008**, *14*, 2167–2179.
[88] S. Bambirra, A. Meetsma, B. Hessen, *Organometallics* **2006**, *25*, 3454–3462.
[89] N. Meyer, P. W. Roesky, S. Bambirra, A. Meetsma, B. Hessen, K. Saliu, J. Takats, *Organometallics* **2008**, *27*, 1501–1505.
[90] W. Huang, B. M. Upton, S. I. Khan, P. L. Diaconescu, *Organometallics* **2013**, *32*, 1379–1386.
[91] A. J. Wooles, D. P. Mills, W. Lewis, A. J. Blake, S. T. Liddle, *Dalton Trans.* **2010**, *39*, 500–510.
[92] B. M. Wolf, C. Stuhl, R. Anwander, *Chem. Commun.* **2018**, *54*, 8826–8829.
[93] S. Harder, D. Naglav, C. Ruspic, C. Wickleder, M. Adlung, W. Hermes, M. Eul, R. Pöttgen, D. B. Rego, F. Poineau, K. R. Czerwinski, R. H. Herber, I. Nowik, *Chem. Eur. J.* **2013**, *19*, 12272–12280.
[94] E. Lu, Y. Li, Y. Chen, *Chem. Commun.* **2010**, *46*, 4469–4471.
[95] A. A. Trifonov, M. N. Bochkarev, H. Schumann, J. Loebel, *Angew. Chem. Int. Ed.* **1991**, *30*, 1149–1151.
[96] N. S. Emel'yanova, M. N. Bochkarev, H. Schuman, J. Loebel, L. Esser, *Russ. J. Coord. Chem.* **1994**, *20*, 789–793.
[97] C.-L. Pan, W. Chen, J. Song, *Organometallics* **2011**, *30*, 2252–2260.
[98] J.-C. Berthet, P. Thuéry, M. Ephritikhine, *Eur. J. Inorg. Chem.* **2008**, 5455–5459.
[99] W. J. Evans, M. A. Ansari, J. W. Ziller, S. I. Khan, *Inorg. Chem.* **1996**, *35*, 5435–5444.
[100] H.-S. Chan, H.-W. Li, Z. Xie, *Chem. Commun.* **2002**, 652–653.
[101] D. Schädle, C. Schädle, K. W. Törnroos, R. Anwander, *Organometallics* **2012**, *31*, 5101–5107.
[102] B. M. Wolf, C. Stuhl, C. Maichle-Mössmer, R. Anwander, *Chem. Eur. J.* **2018**, *24*, 15921–15929.
[103] D. J. Beetstra, A. Meetsma, B. Hessen, J. H. Teuben, *Organometallics* **2003**, *22*, 4372–4374.
[104] J. Hong, L. Zhang, K. Wang, Y. Zhang, L. Weng, X. Zhou, *Chem. Eur. J.* **2013**, *19*, 7865–7873.
[105] C.-L. Pan, W. Chen, S. Song, H. Zhang, X. Li, *Inorg. Chem.* **2009**, *48*, 6344–6346.
[106] J. C. Gordon, G. R. Giesbrecht, D. L. Clark, P. J. Hay, D. W. Keogh, R. Poli, B. L. Scott, J. G. Watkin, *Organometallics* **2002**, *21*, 4726–4734.
[107] V. Rad'kov, V. Dorcet, J.-F. Carpentier, A. Trifonov, E. Kirillov, *Organometallics* **2013**, *32*, 1517–1527.
[108] E. Lu, J. Chu, Y. Chen, *Acc. Chem. Res.* **2018**, *51*, 557–566.
[109] E. Lu, J. Chu, Y. Chen, M. V. Borzov, G. Li, *Chem. Commun.* **2011**, *47*, 743–745.
[110] T. Chu, W. E. Piers, J. L. Dutton, M. Parvez, *Organometallics* **2013**, *32*, 1159–1165.
[111] D. Schädle, M. Meermann-Zimmermann, C. Schädle, C. Maichle-Mössmer, R. Anwander, *Eur. J. Inorg. Chem.* **2015**, 1334–1339.

[112] T. E. Rieser, R. Thim-Spöring, D. Schädle, P. Sirsch, R. Litlabø, K. W. Törnroos, C. Maichle-Mössmer, R. Anwander, *J. Am. Chem. Soc.* **2022**, *144*, 4102–4113.

[113] L. A. Solola, A. V. Zabula, W. L. Dorfner, B. C. Manor, P. J. Carroll, E. J. Schelter, *J. Am. Chem. Soc.* **2016**, *138*, 6928–6931.

[114] L. A. Solola, A. V. Zabula, W. L. Dorfner, B. C. Manor, P. J. Carroll, E. J. Schelter, *J. Am. Chem. Soc.* **2017**, *139*, 2435–2442.

[115] K. Izod, W. Clegg, S. T. Liddle, *Organometallics* **2000**, *19*, 3640–3643.

[116] R. Anwander, *Angew. Chem. Int. Ed.* **1998**, *37*, 599–602.

[117] H. S. Zijlstra, S. Harder, *Eur. J. Inorg. Chem.* **2015**, 19–43.

[118] D. Schädle, C. Maichle-Mössmer, C. Schädle, R. Anwander, *Chem. Eur. J.* **2015**, *21*, 662–670.

[119] S. Trofimenko, *Chem. Rev.* **1993**, *93*, 943–980.

[120] X. Zhang, R. McDonald, J. Takats, *New. J. Chem.* **1995**, *19*, 573–585.

[121] G. R. Fulmer, A. J. M. Miller, N. H. Sherden, H. E. Gottlieb, A. Nudelman, B. M. Stoltz, J. E. Bercaw, K. I. Goldberg, *Organometallics* **2010**, *29*, 2176–2179.

E

Publications

Paper I

Polymeric dimethylytterbium and the terminal methyl complex $(Tp^{tBu,Me})Yb(CH_3)(thf)$

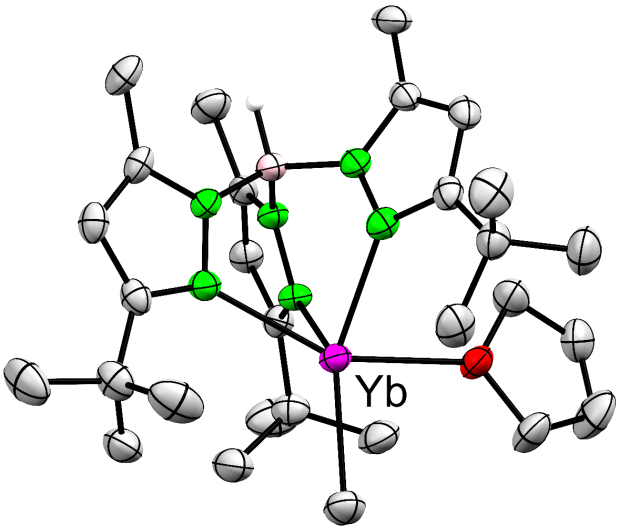

https://doi.org/10.1039/D0CC06981G
reprinted with the permission from
Chem. Commun. **2021**, *57*, 243-246.

ChemComm

ROYAL SOCIETY OF CHEMISTRY

COMMUNICATION

View Article Online
View Journal | View Issue

Cite this: *Chem. Commun.*, 2021, **57**, 243

Received 20th October 2020,
Accepted 24th November 2020

DOI: 10.1039/d0cc06981g

rsc.li/chemcomm

Polymeric dimethylytterbium and the terminal methyl complex $(Tp^{tBu,Me})Yb(CH_3)(thf)$†

Markus M. Katzenmayer, Benjamin M. Wolf, Alexandros Mortis, Cäcilia Maichle-Mössmer and Reiner Anwander *

Divalent ytterbium bis(trimethylsilyl)amides $[Yb\{N(SiMe_3)_2\}_2]_2$ and $Yb[N(SiMe_3)_2]_2(thf)_2$ react with purified methyllithium to amorphous dimethylytterbium $[YbMe_2]_n$. The characterisation was performed by ^{171}Yb and ^{13}C CP/MAS NMR spectroscopy as well as by conducting protonolysis reactions with HC_5Me_5 and $HTp^{tBu,Me}$, affording known $(C_5Me_5)_2Yb(OEt_2)$ and new $(Tp^{tBu,Me})Yb(CH_3)(thf)$.

Edward Frankland's groundbreaking discoveries of diethylzinc, $Zn(C_2H_5)_2$, and dimethylzinc ("Zinkmethyl"), $Zn(CH_3)_2$, clearly marked the start of organometallic chemistry.[1] In the meantime 26 out of the 60 non-radioactive metals across the periodic table have been shown to form isolable homoleptic methyl complexes $[M(CH_3)_x]$ (x = 1–6).[2] Well-defined dimethyl compounds $[M(CH_3)_2]$ were reported for the alkaline-earth metals (Ae) beryllium, magnesium and calcium,[3–5] as well as the d-"transition" metals zinc, cadmium and mercury.[6] Although polymeric dimethylmagnesium, $[MgMe_2]_n$, can be straightforwardly obtained by exploiting the Schlenk equilibrium,[7] a single-crystal X-ray diffraction (XRD) study was reported not until 2018. Shortly before, we also described the preparation of polymeric dimethylcalcium, $[CaMe_2]_n$, and performed an XRD analysis on the "short-lived" THF-adduct $Ca_7(CH_3)_{14}(thf)_{10}$.[5] Crucial for the successful synthesis of $[CaMe_2]_n$ was the application of a modified Lochmann protocol,[8] employing bis(trimethylsilyl)amide $[Ca\{N(SiMe_3)_2\}_2]_2$[9] and purified methyllithium as vital precursors. Since the similarity of Ae^{2+} and divalent lanthanide (Ln^{2+}) (structural) chemistry has been stressed quite often,[10] on the basis of their ionic radii (see Table 1) and closed-shell character (low-lying 4f orbitals for Ln^{2+}), we wondered about the feasibility of permethylated compounds $[LnMe_2]_n$.[11] Previous related examples of the Yb/Ca similarity include the metallocenes $[M(C_5Me_5)_2]$,[12,13] benzyls $[M(CH_2Ph)_2]$,[14,15] silylalkyls $M[C(SiMe_3)_3]_2$[16,17] and tetraalkylaluminates $[M(AlR_4)_2]$ (R = Me, Et).[18,19] Herein we report on the synthesis, characterisation and derivatisation of the first homoleptic f-element dimethyl complex, dimethylytterbium $[YbMe_2]_n$ ($[Xe]4f^{14}$).

Adopting the synthesis scheme developed for dimethylcalcium, we initially chose the bis(trimethylsilyl)amide complex $Yb[N(SiMe_3)_2]_2(thf)_2$ ($\mathbf{2^{thf}}$, red-orange colour; for UV-visible spectrum, see ESI†)[20] as an easily accessible component of the Lochmann protocol (route I, Scheme 1). Unfortunately, the synthesis of $\mathbf{2^{thf}}$ from bright yellow $YbI_2(thf)_2$ and 1.95 equivalents of $K[N(SiMe_3)_2]$ in tetrahydrofuran (THF) repeatedly indicated the presence of residual iodine (ICP-OES analysis and potentiometric titration, see ESI†), despite several recrystallisation steps. In order to avoid the implementation of additional impurities into the next reaction step, a commercially available methyllithium solution was further purified by treatment with $K[N(SiMe_3)_2]$ (removal of residual chloride).[5]

The reaction of such a purified MeLi solution with $\mathbf{2^{thf}}$ led to the precipitation of an amorphous orange powder denoted by $[YbMe_2]_n(thf)_x$ ($\mathbf{3^{thf}}$) in approximate quantitative yields. Compound $\mathbf{3^{thf}}$ is highly sensitive towards oxygen and water and insoluble in aliphatic and aromatic solvents. Not unexpectedly, ICP-OES analysis of $\mathbf{3^{thf}}$ revealed a residual iodine content of 2.03%. Pursuing the more elaborate synthesis route II with the detour *via* the benzyl complex $[Yb(CH_2Ph)_2]_n$ (**1**)[13] gave access to a cleaner product. The protonolysis of **1** with bis(trimethylsilyl)amine $HN(SiMe_3)_2$ in diethyl ether afforded red-orange dimeric $[Yb\{N(SiMe_3)_2\}_2]_2$ (**2**; for an XRD analysis and a UV-visible spectrum, see ESI†)[22] with toluene as the only side-product being easily removable *in vacuo*. The subsequent

Institut für Anorganische Chemie, Eberhard Karls Universität Tübingen, Auf der Morgenstelle 18, 72076 Tübingen, Germany.
E-mail: reiner.anwander@uni-tuebingen.de

† Electronic supplementary information (ESI) available. CCDC 2039518–2039521. For ESI and crystallographic data in CIF or other electronic format see DOI: 10.1039/d0cc06981g

Table 1 Effective ionic radii of selected Ln^{2+} and Ae^{2+} (coordination number: 6)[21]

Metal ion	Ca^{2+}	Yb^{2+}	Eu^{2+}	Sr^{2+}	Sm^{2+}	Ba^{2+}
Radius [Å]	1.00	1.02	1.17	1.18	1.22	1.35

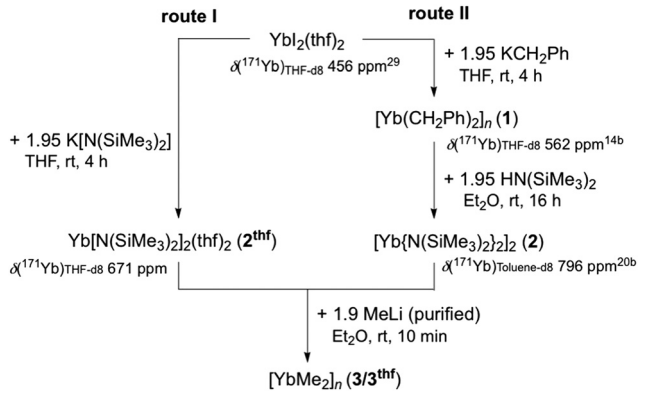

Scheme 1 Synthesis of dimethyl ytterbium $[Yb(CH_3)_2]_n$ according to a modified Lochmann protocol, employing ytterbium(II) bis(trimethylsilyl)amides and MeLi.

reaction of pre-isolated **2** with purified MeLi gave orange $[YbMe_2]_n$ (**3**) with a minor iodine impurity of 0.39% (see ESI†).

The ^{13}C CP/MAS NMR spectrum of $\mathbf{3}^{thf}$ shows one signal at 25.0 ppm (Fig. 1) comparable to $[CaMe_2]_n$ (δ 12.6 ppm),[12] $[YMe_3]_n$ (δ 28.3 ppm) and $[LuMe_3]_n$ (δ 31.4 ppm),[23] or $[Yb(AlMe_4)_2]_n$ (δ 13.4 and 4.1 ppm).[18a] Moreover, one single resonance was observed by ^{171}Yb CP/MAS NMR spectroscopy.[24] The extreme downfield ^{171}Yb chemical shift of 947 ppm clearly reflects the deshielding effect of the σ-bonded alkyl ligands (here methyl).[25,26] For further comparison, complexes $Yb[CH(SiMe_3)_2]_2(OEt_2)_2$,[27] $Yb(CH_2Ph)_2(thf)_4$,[14b] $Yb(C_6F_5)_2(thf)_4$,[28] $YbI_2(thf)_2$[29] and $[Yb(AlEt_4)_2]_n$[17] displayed ^{171}Yb resonances in solution at δ = 1035, 562, 463 and 363 ppm, respectively. The DRIFT spectrum of **3** matches that of $[CaMe_2]_n$ very well, while the small deviations of the absorption bands might reflect the slightly different ionic radii of the metal centres (see ESI†).[21]

Compound **3** is poorly soluble in THF while decomposition was indicated by a colour change from red to brown. Despite substantial efforts, neither crystalline $[YbMe_2]_n$ nor a crystalline donor (THF) adduct of it could be obtained. However, on one occasion, we succeeded in the isolation of the single-crystalline mixed-valent octametallic ytterbium oxo cluster $[Yb_8(CH_3)_{14}O_2(thf)_6]$ (**4**, orange colour). The solid-state structure of this unusual methyl ytterboxane is depicted in Fig. 2. Ytterbium oxo clusters (*e.g.*, $(C_5H_4CH_3)_3Yb_4(\mu_2\text{-}Cl)(\mu_3\text{-}Cl)(\mu_4\text{-}O)(thf)_3$)[30] and mixed-valent ytterbium complexes (*e.g.*, $(C_5Me_5)_6Yb_4F_4$, *via* partial oxidation of $(C_5Me_5)_2Yb$ with AgF)[31] have been reported previously, but complex **4** features the first organoytterbium cluster devoid of sterically demanding ancillary ligands.[32] Considering the asymmetric unit of **4**, four ytterbium atoms adopt a butterfly arrangement around the central oxygen, and are connected by two μ_2- and two μ_3-bridging methyl groups. Considering **4** as a whole, each two of the ytterbium centres of one asymmetric unit engage in the bridging to the other one *via* the two oxy and two methyl moieties. As a result, the interconnecting atoms "$Yb_4O_2C_2$" form a ladder motif with the oxy ligands now residing in the centre of trigonal bipyramidally arranged ytterbium atoms. It is noteworthy that a similar ladder motif has been proposed for the illustrious but structurally elusive methylalumoxane (MAO).[33]

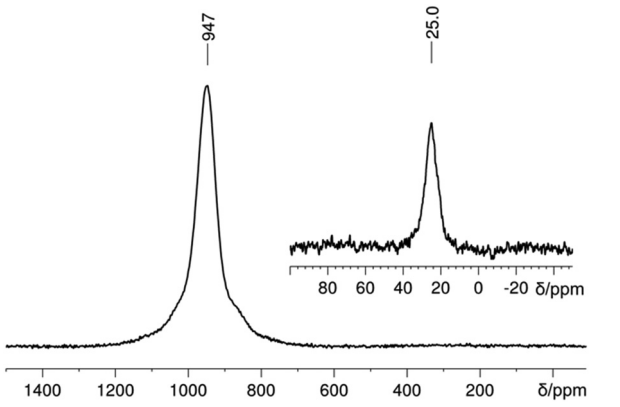

Fig. 1 ^{171}Yb CP/MAS NMR spectrum and ^{13}C CP/MAS NMR spectrum (top right) of dimethyl ytterbium ($\mathbf{3}^{thf}$).

A prominent example of a μ_5-O-centred ytterbium(III) complex features $[Yb_5(\mu_5\text{-}O)(\mu_3\text{-}OiPr)_4(\mu_2\text{-}OiPr)_4(OiPr)_5]$[34] with 6-coordinate metal centres showing Yb–O(oxy) distances of 2.285(23)–2.339(24) Å. Of all 6-coordinate metal centres in **4** (4 C, 2 O) the Yb_2O_2 ladder core exhibits the shortest Yb–O(oxy) distances of 2.152(4) and 2.268(4) Å, evidencing the trivalence of the Yb(4) centres. The Yb(II)–O(oxy) distances amount to 2.386(5), 2.416(5) and 2.467(4) Å. Accordingly, the metal–carbon distances are shorter for Yb(III) (=Yb(4); μ_3-CH_3 2.643(8) Å, μ_2-CH_3 av. 2.506 Å) than those involving the Yb(II) centres (μ_3-CH_3 av. 2.722 Å, μ_2-CH_3 av. 2.595 Å). The latter Yb–C distances match those in $Yb(AlMe_4)_2(phen)$ (2.600(5)–2.621(6) Å, phen = 1,10-phenathroline).[18a] The coordination sphere of the six "outer" Yb(II) centres is completed by each one thf molecule. The formation of the ytterbium oxocluster **4** indicates slow decomposition of $[YbMe_2]_n$ in THF solution *via* partial oxidation, a decomposition pathway, infeasible for $[CaMe_2]_n$. Any degradation of THF *via* formation of vinyl alcoholates[19] could not be observed in micro-scale NMR experiments.

Initial investigations into the targeted derivatisation of $[YbMe_2]_n$ (**3**) *via* protonolysis in diethyl ether showed the release of methane and the formation of $\mathbf{2}^{OEt_2}$ and $Yb(C_5Me_5)_2(OEt_2)$ (**5**, green colour; for UV-visible spectrum, see ESI†)[12] in the presence of a slight excess of bis(trimethylsilyl)amine and HC_5Me_5, respectively. Complex **5** was also characterised by XRD analysis (see ESI†). Given the capability of superbulky scorpionate ligands $Tp^{R,R'}$ (= tris(3-R-5-R′-pyrazolyl)borato) to stabilise monomeric terminal alkyl complexes of both divalent rare-earth metals[35] and alkaline-earth metals,[36] we wondered about the feasibility of a terminal Yb(II)-methyl complex. Adopting the synthesis protocol of the calcium complexes $(Tp^{tBu,Me})Ca(CH_3)(Do)$ (Do = thf, thp), $[YbMe_2]_n$ (**3**) was treated with 0.5 equivalents of proligand $HTp^{tBu,Me}$ in THF, yielding a red solution (Scheme 2). The formation of complex $(Tp^{tBu,Me})Yb(CH_3)(thf)$ (**6**, orange colour; for UV-visible spectrum, see ESI†) in analogy to the corresponding calcium complex[12] was indicated by ^1H and ^{13}C NMR spectroscopy at ambient temperature; the appearance of one set of signals for the $Tp^{tBu,Me}$ ligand indicated a dynamic behaviour in solution.

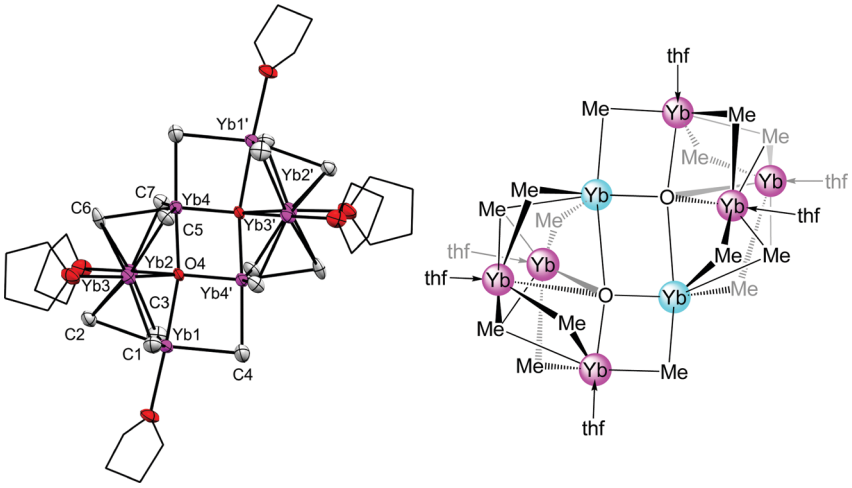

Fig. 2 Crystal structure of $[Yb_8(CH_3)_{14}O_2(thf)_6]$ (**4**). All atoms except for thf carbon atoms are represented by atomic displacement ellipsoids set at 50% probability. Hydrogen atoms are omitted for clarity. For interatomic distances and angles, see ESI.†

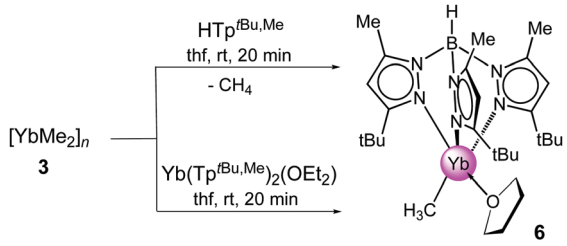

Scheme 2 Synthesis of terminal Yb(II)-methyl complex **6**.

In previous studies on similar complexes we found that at low temperatures the signals of the pyrazolyl rings split into two sets with a 2 : 1 ratio, in line with distinct scorpionate pincers and sting.[37] The coupling pattern in the ^{1}H–^{13}C HSQC spectrum implies the overlapping of the Yb–CH_3 and the pz–CH_3 methyl groups in the $^{13}C\{^{1}H\}$ NMR spectrum.

The ^{1}H–^{171}Yb HSQC NMR spectrum shows one ^{171}Yb resonance at 1140 ppm, which is considerably shifted to lower field than those detected for the related complexes $(Tp^{tBu,Me})Yb(CH_2SiMe_3)(thf)$ (δ = 985 ppm) and $(Tp^{tBu,Me})Yb[CH(SiMe_3)_2]$ (δ = 865 ppm).[35e] For further comparison donor-free complexes $Yb(Tp^{tBu,Me})_2$ and $(Tp^{tBu,Me})Yb(AlMe_4)$ displayed ^{171}Yb signals at 329 ppm[36a] and 505 ppm, respectively.[35d] The reaction of $[YbMe_2]_n$ with more than 0.5 equivalents of $HTp^{tBu,Me}$ results in a partial formation of the homoleptic ytterbium(II) complex $Yb(Tp^{tBu,Me})_2$ (yellow colour; for UV-visible spectrum, see ESI†)[38] which is hard to separate from **6**. This protonolysis protocol seems more suitable for $[CaMe_2]_n$, which displays better solubility in THF.[5] On the other hand, terminal methyl complex **6** can be obtained in good yield *via* the equimolar reaction of **3** with $Yb(Tp^{tBu,Me})_2(OEt_2)$ (Scheme 2), consistent with the calcium chemistry.[5] However, decomposition of compound **6** prevails when kept too long under reduced pressure or when stored at ambient temperatures, as indicated by NMR spectroscopy and elemental analysis (see ESI†).

The solid-state structure of **6** is isostructural with the calcium congener $(Tp^{tBu,Me})Ca(CH_3)(thf)$ (Fig. 3 and Tables S2 and S3, ESI†).[5] Accordingly, the ytterbium(II) centre in **6** is five-coordinate by the $Tp^{tBu,Me}$ ligand (κ^3 fashion), one methyl moiety and one thf molecule, accomplishing a heavily distorted square pyramidal coordination geometry (τ_5 = 0.22). It is striking that the Yb–C(methyl) distance in compound **6** (2.521(3)/2.503(4) Å) is comparatively longer than in the calcium complex (2.482(2)/2.477(2) Å), however, it matches those in closely related σ-alkyl-bonded $(Tp^{tBu,Me})Yb[CH(SiMe_3)_2]$ (2.552(5) Å) and $(Tp^{tBu,Me})Yb(CH_2SiMe_3)(thf)$ (2.526(4) Å).[35e] On the other hand, the terminal Yb(II)–C(methyl) distance is markedly shorter than the bridging ones in bimetallic complexes $[(C_5Me_5)_2Yb]_2(\mu\text{-}Me)$ (Yb(II)–C 2.755(5) Å), $[(C_5Me_5)_2Yb](\mu\text{-}Me)[Ti(C_5Me_5)_2]$ (Yb–C 2.792(7) Å)[39] and **4**.

In conclusion, like $[CaMe_2]_n$ the ytterbium congener $[YbMe_2]_n$ is accessible *via* the modified Lochmann protocol

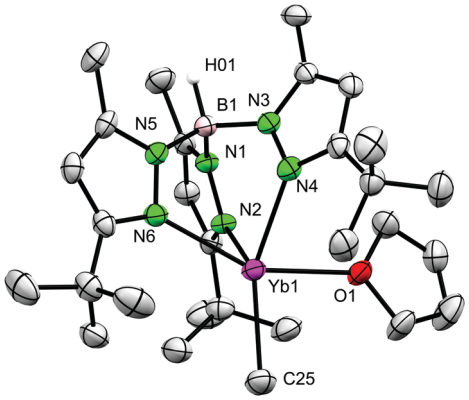

Fig. 3 Crystal structure of the ytterbium(II)-methyl complex $(Tp^{tBu,Me})Yb(CH_3)(thf)$ (**6**). All atoms are represented by atomic displacement ellipsoids set at 50% probability. Compound **6** crystallises with two molecules and one molecule lattice solvent per unit cell (see ESI†). Hydrogen atoms except B–H and one molecule lattice solvent are omitted for clarity. For detailed metrics, see ESI.†

employing donor-free $[Yb\{N(SiMe_3)_2\}_2]_2$ and purified methyllithium. Polymeric $[YbMe_2]_n$ is a pyrophoric, moisture-sensitive, amorphous powder. In contrast to $[CaMe_2]_n$ it is also increasingly sensitive to metal oxidation as evidenced by the isolation and structural characterisation of the methyl ytterboxane complex $[Yb_8(CH_3)_{14}O_2(thf)_6]$. Although featuring only a structural snapshot, the octametallic cluster provides unprecedented insights into the molecular connectivity of such methyl metaloxane oligomers. Notwithstanding, $[YbMe_2]_n$ proved a useful precursor for the first terminal Yb(II) methyl complex, $(Tp^{tBu,Me})Yb(CH_3)(thf)]$.

Conflicts of interest

There are no conflicts to declare.

Notes and references

1 (*a*) E. Frankland, *Liebigs Ann. Chem.*, 1849, **71**, 171–213; (*b*) E. Frankland, *Liebigs Ann. Chem.*, 1849, **71**, 213–216; (*c*) E. Frankland, *Q. J. Chem. Soc.*, 1850, **2**, 263–296.
2 C. Stuhl and R. Anwander, *Dalton Trans.*, 2018, **47**, 12546–12552.
3 A. I. Snow and R. E. Rundle, *Acta Crystallogr.*, 1951, **4**, 348–352.
4 (*a*) E. Weiss, *J. Organomet. Chem.*, 1964, **2**, 314–321; (*b*) G. E. Coates, J. A. Heslop, M. E. Redwood and D. Ridley, *J. Chem. Soc. A*, 1968, 1118–1125.
5 B. M. Wolf, C. Stuhl, C. Maichle-Mössmer and R. Anwander, *J. Am. Chem. Soc.*, 2018, **140**, 2373–2383.
6 (*a*) J. Bacsa, F. Hanke, S. Hindley, R. Odedra, G. R. Darling, A. C. Jones and A. Steiner, *Angew. Chem., Int. Ed.*, 2011, **50**, 11685–11687; (*b*) F. Hanke, S. Hindley, A. C. Jones and A. Steiner, *Chem. Commun.*, 2016, **52**, 10144–10146; (*c*) F. Hanke, S. Hindley, A. C. Jones and A. Steiner, *Chem. Commun.*, 2016, **52**, 10144–10146.
7 W. Schlenk and W. Schlenk Jr., *Ber. Dtsch. Chem. Ges. B*, 1929, **62**, 920–924.
8 L. Lochmann, *Eur. J. Inorg. Chem.*, 2000, 1115–1126.
9 (*a*) M. Westerhausen, *Inorg. Chem.*, 1991, **30**, 96–101; (*b*) M. Westerhausen and W. Schwarz, *Z. Anorg. Allg. Chem.*, 1991, **604**, 127–140.
10 For examples, see: (*a*) R. A. Andersen, J. M. Boncella, C. J. Burns, R. Blom, A. Haaland and H. V. Volden, *J. Organomet. Chem.*, 1986, **312**, C49–C52; (*b*) T. K. Hollis, J. K. Burdett and N. Bosnich, *Organometallics*, 1993, **12**, 3385–3386; (*c*) C. Eaborn, P. B. Hitchcock, K. Izod, Z.-R. Lu and J. D. Smith, *Organometallics*, 1996, **15**, 4783–4790; (*d*) K. Izod, W. Clegg and S. T. Liddle, *Organometallics*, 2000, **19**, 3640–3643; (*e*) F. Weber, H. Sitzmann, M. Schultz, C. D. Sofield and R. A. Andersen, *Organometallics*, 2002, **21**, 3139–3146; (*f*) S. Harder, *Angew. Chem., Int. Ed.*, 2004, **43**, 2714–2718.
11 M. Zimmermann and R. Anwander, *Chem. Rev.*, 2010, **110**, 6194–6259.
12 (*a*) T. D. Tilley, R. A. Andersen, B. Spencer, H. Ruben, A. Zalkin and D. H. Templeton, *Inorg. Chem.*, 1980, **19**, 2999–3003; (*b*) T. D. Tilley, J. M. Boncella, D. J. Berg and R. A. Andersen, *Inorg. Synth.*, 1990, **27**, 146–150; (*c*) M. Schulz, C. J. Burns, D. J. Schwartz and R. A. Andersen, *Organometallics*, 2000, **19**, 781–789.
13 (*a*) P. Jutzi, W. Leffers, G. Müller and B. Huber, *Chem. Ber.*, 1989, **122**, 879–884; (*b*) R. A. Williams, T. P. Hanusa and J. C. Huffman, *Organometallics*, 1990, **9**, 1128–1134.
14 (*a*) B. M. Wolf, C. Stuhl and R. Anwander, *Chem. Commun.*, 2018, **54**, 8826–8829; (*b*) D. Schuhknecht, K.-N. Truong, T. P. Spaniol, L. Maron and J. Okuda, *Chem. Commun.*, 2018, **54**, 11280–11283.
15 (*a*) S. Harder, S. Müller and E. Hübner, *Organometallics*, 2004, **23**, 178–183; (*b*) K. Izod and P. G. Waddell, *Organometallics*, 2015, **34**, 2726–2730.
16 C. Eaborn, P. B. Hitchcock, K. Izod and J. D. Smith, *J. Am. Chem. Soc.*, 1994, **116**, 12071–12072.
17 C. Eaborn and P. B. Hitchcock, *Chem. Commun.*, 1997, 1961–1962.
18 (*a*) H.-M. Sommerfeldt, C. Meermann, M. G. Schrems, K. W. Törnroos, N. Å. Frøystein, R. J. Miller, E.-W. Scheidt, W. Scherer and R. Anwander, *Dalton Trans.*, 2008, 1899–1907; (*b*) G. Occhipinti, C. Meermann, H. M. Dietrich, R. Litlabø, F. Auras, K. W. Törnroos, C. Maichle-Mössmer, V. R. Jensen and R. Anwander, *J. Am. Chem. Soc.*, 2011, **133**, 6323–6337.
19 O. Michel, C. Meermann, K. W. Törnroos and R. Anwander, *Organometallics*, 2009, **28**, 4783–4790.
20 (*a*) T. D. Tilley, R. A. Andersen and A. Zalkin, *J. Am. Chem. Soc.*, 1982, **104**, 3725–3727; (*b*) A. G. Avent, M. A. Edelman, M. F. Lappert and G. A. Lawless, *J. Am. Chem. Soc.*, 1989, **111**, 3423–3425.
21 R. Shannon, *Acta Crystallogr., Sect. A: Cryst. Phys., Diffr., Theor. Gen. Crystallogr.*, 1976, **32**, 751–767.
22 J. M. Boncella, PhD thesis, University of California, Berkeley, 1982.
23 H. M. Dietrich, G. Raudaschl-Sieber and R. Anwander, *Angew. Chem., Int. Ed.*, 2005, **44**, 5303–5306.
24 For early examples on ^{171}Yb CP/MAS NMR spectroscopy, see: (*a*) X. Mao, X. Zhao, C. Ye and S. Wang, *Solid State Nucl. Magn. Reson.*, 1994, **3**, 107–110; (*b*) G. W. Rabe and A. Sebald, *Solid State Nucl. Magn. Reson.*, 1996, **6**, 197–200; (*c*) J. M. Keates, G. A. Lawless and M. P. Waugh, *Chem. Commun.*, 1996, 1527–1628; (*d*) M. Keates and G. A. Lawless, *Organometallics*, 1997, **16**, 2842–2846.
25 (*a*) D. Barisic, D. Diether, C. Maichle-Mössmer and R. Anwander, *J. Am. Chem. Soc.*, 2019, **141**, 13931–13940; (*b*) A. Mortis, D. Barisic, K. Eichele, C. Maichle-Mössmer and R. Anwander, *Dalton Trans.*, 2020, **49**, 7829–7841.
26 R. E. White and T. P. Hanusa, *Organometallics*, 2006, **25**, 5621–5630.
27 (*a*) P. B. Hitchcock, S. A. Holmes, M. F. Lappert and S. Tan, *J. Chem. Soc., Chem. Commun.*, 1994, 2691–2692; (*b*) J. R. van der Hende, P. B. Hitchcock, S. A. Holmes, M. F. Lappert and S. Tan, *Dalton Trans.*, 1995, 3933–3939.
28 G. B. Deacon and C. M. Forsyth, *Organometallics*, 2003, **22**, 1349–1352.
29 S. P. Constantine, G. M. De Lima, P. B. Hitchcock, M. Keates and G. A. Lawless, *Chem. Commun.*, 1996, 2421–2422.
30 X. Zhou, H. Ma, Z. Wu, X. You, Z. Xu and X. Huang, *J. Organomet. Chem.*, 1995, **503**, 11–13.
31 C. J. Burns, D. J. Berg and R. A. Andersen, *J. Chem. Soc., Chem. Commun.*, 1987, 272–273.
32 R. Anwander, *Angew. Chem., Int. Ed.*, 1998, **37**, 599–602.
33 H. S. Zijlstra and S. Harder, *Eur. J. Inorg. Chem.*, 2015, 19–43.
34 D. C. Bradley, H. Chudzynska, D. M. Frigo, M. E. Hammond, M. B. Hursthouse and M. A. Mazid, *Polyhedron*, 1990, **9**, 719–726.
35 (*a*) L. Hasinoff, J. Takats, X. W. Zhang, A. H. Bond and R. D. Rogers, *J. Am. Chem. Soc.*, 1994, **116**, 8833–8834; (*b*) G. M. Ferrence, A. J. Arduengo, A. Jockisch, H.-J. Kim, R. McDonald and J. Takats, *J. Alloys Compd.*, 2006, **418**, 184–188; (*c*) J. Cheng, J. Takats, M. J. Ferguson and R. McDonald, *J. Am. Chem. Soc.*, 2008, **130**, 1544–1545; (*d*) R. Litlabø, K. Saliu, M. J. Ferguson, R. MacDonald, J. Takats and R. Anwander, *Organometallics*, 2009, **28**, 6750–6754; (*e*) X. W. Zhang, G. H. Maunder, S. Gießmann, R. MacDonald, M. J. Ferguson, A. H. Bond, R. D. Rogers, A. Sella and J. Takats, *Dalton Trans.*, 2011, **40**, 195–210.
36 (*a*) X. Shi, C. Hou, C. Zhou, Y. Song and J. Cheng, *Angew. Chem., Int. Ed.*, 2017, **56**, 16650–16653; (*b*) B. M. Wolf, C. Stuhl, C. Maichle-Mössmer and R. Anwander, *Organometallics*, 2019, **38**, 1614–1621.
37 M. Zimmermann, J. Takats, G. Kiel, K. W. Törnroos and R. Anwander, *Chem. Commun.*, 2008, 612–614.
38 (*a*) X. Zhang, R. McDonald and J. Takats, *New J. Chem.*, 1995, **19**, 573–585; (*b*) K. O. Saliu, J. Takats and M. J. Ferguson, *Acta Crystallogr., Sect. E: Struct. Rep. Online*, 2009, **65**, m643–m644.
39 M. D. Walter, P. T. Matsunaga, C. J. Burns, L. Maron and R. A. Andersen, *Organometallics*, 2017, **36**, 4564–4578.

Electronic Supplementary Material (ESI) for Chemical Communications.

Supporting Information

Polymeric dimethylytterbium and the terminal methyl complex $(Tp^{tBu,Me})Yb(CH_3)(thf)$

Markus M. Katzenmayer, Benjamin M. Wolf, Alexandros Mortis, Cäcilia Maichle-Mössmer and Reiner Anwander*

Institut für Anorganische Chemie, Eberhard Karls Universität Tübingen, Auf der Morgenstelle 18, 72076 Tübingen, Germany

*E-mail for R.A.: reiner.anwander@uni-tuebingen.de.

Table of Contents

Experimental Section	S3
Crystal Structures and Crystallographic Data	S5
NMR Spectra	S11
IR Spectra	S17
UV/Vis Spectra	S20
Potentiometric Titrations	S21
References	S22

Experimental Section

General considerations

If not otherwise specified all reactions were carried out under inert atmosphere (Argon) in a glovebox (MBraun MB200B <0,1 ppm O_2, <0,1 ppm H_2O). The syntheses of the organic ligands were carried out under standard Schlenk techniques in oven-dried glassware. The solvents were purified using Grubbs-type columns (MBraun SPS solvent purification system). Tetrahydrofuran was stored over activated molecular sieves (3 Å). Deuterated solvents were purchased from Aldrich or Eurisotop and were stored over Na/K alloy in a glovebox. Potassium bis(trimethylsilyl)amide K[$N(SiMe_3)_2$] (95 %, Sigma Aldrich) was sublimed before use and stored in a glovebox. The chloride content of MeLi (~1.6 M in Et_2O, Aldrich) was determined via potentiometric titration as described previously.[1] The newly synthesized complexes are stored at ambient temperature or at -40 °C under inert atmospheres, respectively. The proligand hydrotris(3-*tert*-butyl-5-methylpyrazolyl)borate ($HTp^{tBu,Me}$)[2] and the ytterbium(II) precursors $Yb(CH_2Ph)_2$ (**1**)[3] and $Yb(Tp^{tBu,Me})_2$[4] were synthesized according to slight modifications of the literature procedures. The NMR spectra of air- and moisture-sensitive compounds were recorded by using J. Young valve NMR tubes on a BRUKER AVIII+300 (^{1}H: 300.13 MHz, ^{11}B: 96.29 MHz, ^{13}C: 59.63 MHz), a BRUKER AVII+400 instrument (^{1}H: 400.13 MHz, ^{13}C: 100.61 MHz) or a Bruker AVII+500 (^{1}H: 500.13 MHz, ^{13}C: 125.76 MHz, ^{171}Yb: 87.52 MHz). The residual solvent signals are referenced to TMS.[5] Solid-state NMR spectra were recorded on a Bruker ASX 300 instrument (^{13}C: 75.47 MHz, ^{171}Yb: 52.52 MHz) equipped with MAS (magic angle spinning) hardware and using a ZrO_2 rotor with an outer diameter of 4 mm. Infrared spectra were recorded on a Nicolet 6700 FT-IR spectrometer with a DRIFT cell (KBr window), and the samples were prepared in a glovebox and mixed with KBr powder. UV/Vis measurements were carried out in tetrahydrofuran or n-hexane on a PG Instruments T60 UV-Vis spectrophotometer. Elemental analysis (C, H, N) were performed with an Elementar Vario Micro Cube.

Synthesis Procedures

$[Yb\{N(SiMe_3)_2\}_2]_2$ (2): To a suspension of $[Yb(CH_2Ph)_2]_n$ (**1**, 514 mg, 1.4 mmol) in Et_2O (8 mL) a solution of $HN(SiMe_3)_2$ (467 mg, 2.8 mmol, 0.6 mL in Et_2O (2 mL) was slowly added and stirred overnight at ambient temperature. After filtration, the solvent was removed under reduced pressure. Recrystallization from *n*-hexane gave $[Yb\{N(SiMe_3)_2\}_2]_2$ (**2**) as red crystals. Crystalline yield: 411 mg, 58 %. ^{1}H NMR (400 MHz, [D_6]benzene, 26°C): δ 0.35 ppm. Elemental analysis calcd. (%) for $C_{12}H_{36}N_2Si_4Yb$ (987.66 g/mol): C 29.19, H 7.35, N 5.67; found C 29.64, H 7.44, N 5.73. ICP-OES (%): found: I 0.04. This compound was synthesized previously from YbI_2 and Na[$N(SiMe_3)_2$] in diethyl ether at 0 °C and subsequent desolvation of pre-isolated $Yb[N(SiMe_3)_2]_2(OEt_2)_2$ in toluene at 80 °C.[6]

$[YbMe_2]_n$ ($3/3^{thf}$): Method a. According to a slightly modified procedure, previously described for synthesis of $[CaMe_2]_n$.[1] To a solution of $Yb[N(SiMe_3)_2]_2(thf)_2$ (490 mg, 768 mmol) in 8 ml Et_2O a solution of chloride-free methyl lithium (3.23 ml, 0.45 M, 1.46 mol) was slowly added under vigorous stirring. After adding approximately 2/3 of the MeLi solution, the product precipitated as an orange powder. The solvent was removed via filter cannula and the orange powder was washed with Et_2O (3 x 2 ml) and dried under vacuum. The product was obtained in quantitative yields as orange amorphous powder, denoted $\mathbf{3^{thf}}$. Elemental analysis calcd. (%) for C_2H_6Yb (203.12 g/mol): C 11.83, H 2.98, N 0; found C 11.03, H 3.01, N 0.23. ICP-OES (%): found: I 2.03.

Method b. Following the procedure described in method a, THF-free $[Yb\{N(SiMe_3)_2\}_2]_2$ (400 mg, 0.42 mmol) in 8 ml Et_2O and methyllithium in Et_2O (5.2 ml, 0.31 M 1.6 mmol) afforded $[YbMe_2]_n$ as orange powder in quantitative yields. The powder was dried at high vacuum for 3 h. ^{13}C CP-MAS NMR (75 MHz, 26 °C): δ_{iso} 24.9 (s, br, Yb–*C*H$_3$) ppm. ^{171}Yb CP-MAS NMR (52 MHz, 26 °C): δ_{iso} 947.3 (s, br, *Yb*–CH$_3$) ppm. Elemental analysis calcd. (%) for C_2H_6Yb (203.12 g/mol): C 11.83, H 2.98, N 0; found C 11.85, H 2.95, N 0. ICP-OES (%): found: I 0.39.

$(C_5Me_5)_2Yb(Et_2O)$ (5): To a suspension of $[YbMe_2]_n$ (15 mg, 0.07 mmol) in 1 ml Et_2O a solution of HC_5Me_5 (20 mg, 0.15 mmol) in 3 ml Et_2O was slowly added under vigorous stirring. After stirring for 18 h at 40 °C the mixture was filtered and the bright green solution was reduced to 1 ml and stored at -40 °C. Crystalline yield: 23 mg, 60 %. ^{1}H NMR (400 MHz, [D_6]benzene, 26°C): δ 2.90 (q, 4 H, O(C*H*$_2$CH$_3$)), 2.07 (s, 30 H, (C*H*$_3$)$_5$-Cp), 0.85 (t, 6 H, O(CH$_2$C*H*$_3$)). Elemental analysis calcd. (%) for $C_{24}H_{40}OYb$ (517.60 g/mol): C 55.69, H 7.79, N 0; found C 55.13, H 6.81, N 0.1. This compound was synthesized previously from YbI_2 and Na[C_5Me_5] 20 °C in diethyl ether at 20 °C, but not analyzed by XRD.[7]

$(Tp^{tBu,Me})Yb(CH_3)(thf)$ (6): In a micro-scaled reaction, hydrotris(3-*tert*-butyl-5-methylpyrazolyl)borate $HTp^{tBu,Me}$ (10.5 mg, 0.025 mmol) in 2 ml tetrahydrofuran was added dropwise to a suspension of $[YbMe_2]_n$ (10 mg, 0.05 mmol) in tetrahydrofuran (1 ml). The mixture was stirred for 20 minutes at ambient temperature until a clear red solution formed. The solution was filtered, and the volume was reduced in vacuo. Single crystals of **6** suitable for XRD analysis could be obtained from a saturated THF solution at –40°C. Alternatively, $Yb(Tp^{tBu,Me})_2$ (60 mg, 0.06 mmol) in 0.4 ml THF was slowly added to a stirred suspension of $[YbMe_2]_n$ (12 mg, 0.06 mmol) in 0.2 ml THF. After 15 minutes a clear red solution was obtained. The solvent was evaporated under reduced pressure, yielding 67 mg of a red solid (84% of **6**). According to NMR-scale experiments, complex **6** was produced immediately in the $Yb(Tp^{tBu,Me})_2$/$[YbMe_2]_n$ reaction, indicating that the heteroleptic complex is the preferred species in donor solvents. The red color of solid **6** turned dark (decomposition) at ambient temperatures. ^{1}H NMR (500 MHz, [D8] thf, 26 °C): δ 5.80 (s, 3 H, pz-C*H*), 2.35 (s, 9 H, pz-C*H*$_3$). 1.35 (s, 27 H, pz-C(C*H*$_3$)$_3$), –1.29 (s, 3 H, Yb–C*H*$_3$) ppm. ^{11}B{^{1}H} NMR (160 MHz, [D_8]thf, 26 °C): δ –8.4 (s, br) ppm. ^{13}C{^{1}H} NMR (125 MHz, [D_8]thf, 26 °C): δ 162.8 (3-pz-*C*), 145.2 (5-pz-*C*), 102.5 (4-pz-*C*), 32.6 (pz-*C*(CH$_3$)$_3$), 31.2 (pz-C(*C*H$_3$)$_3$), 13.4 (pz-*C*H$_3$, Yb–*C*H$_3$) ppm. ^{171}Yb from ^{1}H-^{171}Yb HSCQ (500.13 MHz, 87.52 MHz, [D_8]thf, 26 °C): 1140 ppm. Elemental analysis calcd. (%) for $C_{29}H_{51}BN_6OYb$ (683.63 g/mol): C 50.95, H 7.52, N 12.29; found C 50.63, H 7.56, N 10.97.

Micro-scale reaction $Yb[N(SiMe_3)_2]_2(thf)_2$: In a J. Young NMR tube bis(trimethylsilyl)amine (8.3 mg, 0.052 mmol) in 0.5 ml deuterated tetrahydrofuran was added to $[YbMe_2]_n$ (5 mg, 0.025 mmol). Slow formation of methane was observed. The solvent was removed under reduced pressure. The residual crude product was dissolved in 1 ml *n*-hexane and the solution was filtrated. The volume was reduced under reduced pressure and stored at -40 °C. Crystalline yield: 95 %, 15 mg. ^{1}H NMR (400 MHz, [D8] thf, 26 °C): δ 0.18 (C*H*$_4$), 0.02 (N{SiC*H*$_3$}$_2$) ppm. ^{171}Yb from ^{1}H-^{171}Yb HSCQ (500.13 MHz, 87.52 MHz, [D_8]thf, 26 °C): 671 ppm.

Crystal Structures and Crystallographic Data

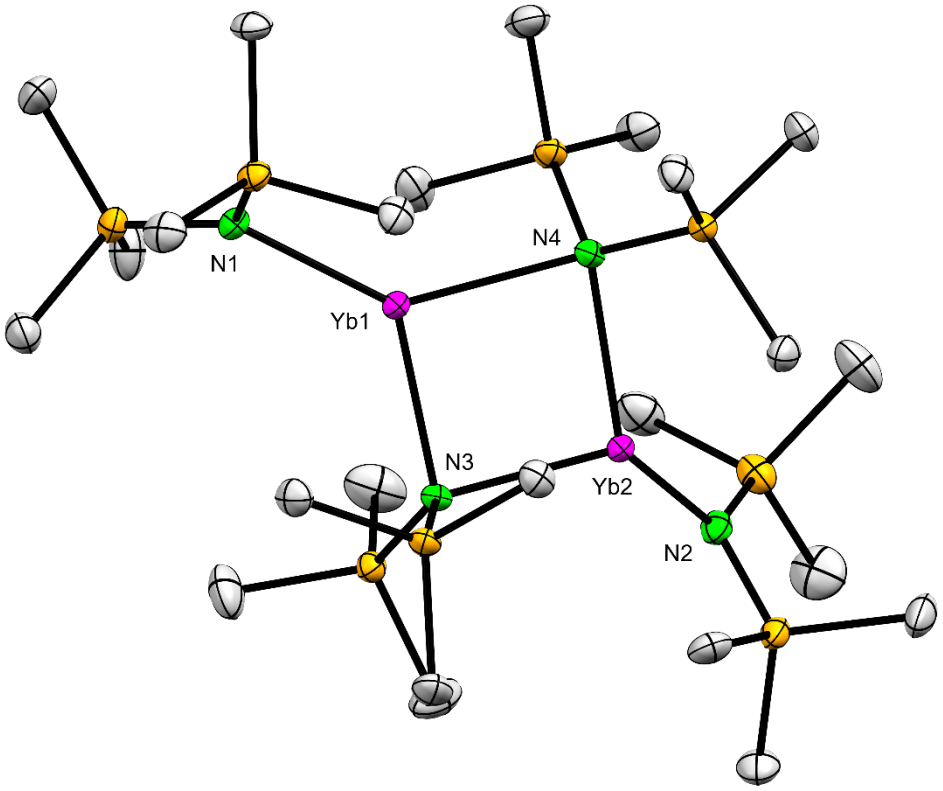

Figure S1. Crystal structure of $[Yb\{N(SiMe_3)_2\}_2]_2$ (**2**). All atoms are represented by atomic displacement ellipsoids set at 50 % probability. Hydrogen atoms are omitted for clarity. Selected bond lengths [*Å*] and angles [°]: Yb1-N1 2.3222(18), Yb1-N3 2.4885(17), Yb1-N4 2.5728(18), Yb2-N2 2.3039(19), Yb2-N3 2.4471(18), Yb2-N4 2.4908(18), Yb1-N3-Yb2 89.18(6), Yb1-N4-Yb2 86.35(6), N1-Yb1-N3 129.44(6), N1-Yb1-N4 139.54(6), N3-Yb1-N4 90.76(6), N2-Yb2-N3 123.53(6), N2-Yb2-N4 127.72(7), N3-Yb2-N4 93.71(6). The crystal structure of complex **2** was previously reported in a PhD thesis.[6]

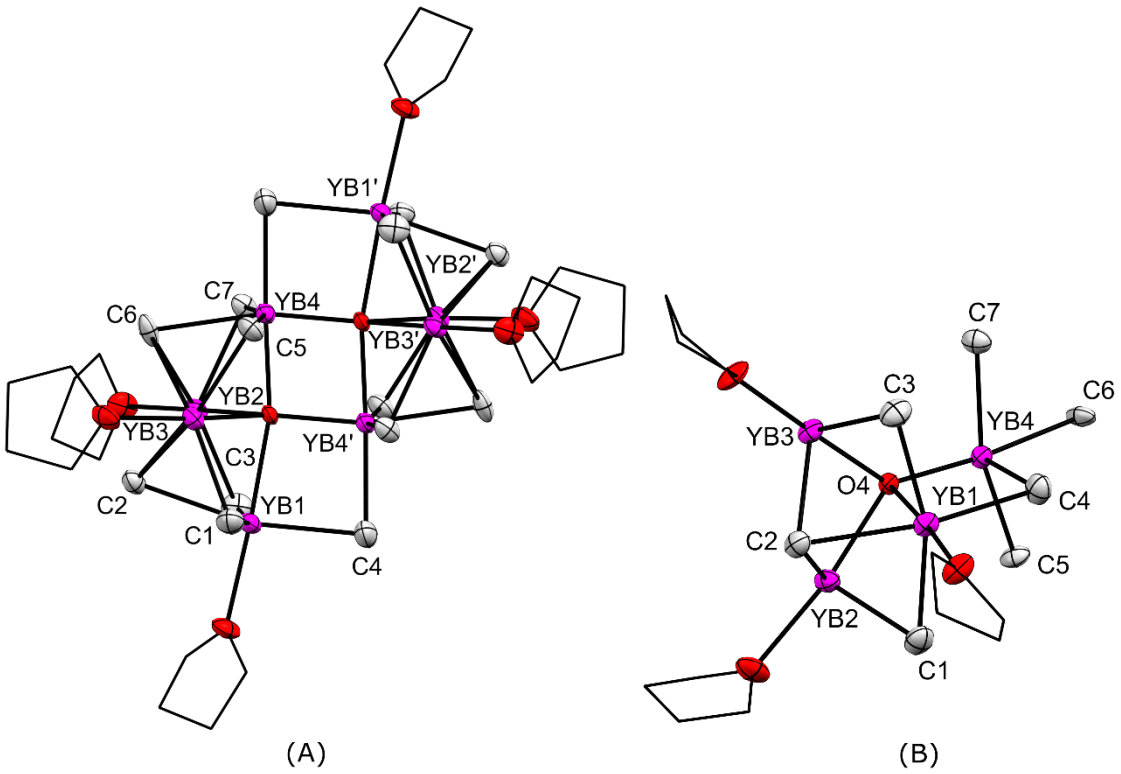

Figure S2. Crystal structure of $[Yb(II)_6Yb(III)_2(CH_3)_{14}O_2(thf)_6]$ **(4) (A)** and its asymmetric unit **(B)**. All atoms except thf carbon atoms are represented by atomic displacement ellipsoids set at 50 % probability. Hydrogen atoms are omitted for clarity. Selected bond lengths [Å] and angles [°]: Yb1-C1 2.645(10), Yb1-C2 2.753(9), Yb1-C3 2.616(10), Yb1-C4 2.598(8), Yb1-O4 2.467(4), Yb2-C1 2.575(9), Yb2-C2 2.676(9), Yb2-O4 2.416(5), Yb3-C2 2.676(9), Yb3-C3 2.652(9), Yb3-O4 2.386(5), Yb4-C4 2.495(8), Yb4-C5 2.500(8), Yb4-C6 2.643(8), Yb4-C7 2.524(8), Yb4-O4 2.152(4). Yb1-C1-Yb2 76.6(3), Yb1-C3-Yb3 76.8(3), Yb1-C4-Yb4 84.4(3), Yb1-O4-Yb4 95.36(17), Yb2-C2-Yb3 80.3(2), Yb2-O4-Yb4 135.0(2), O4-Yb4-C4 94.9(2), O4-Yb4-C5 100.9(3), O4-Yb4-C6 166.9(2), O4-Yb4-C7 97.3(2),C4-Yb4-C5 91.4(3), C4-Yb4-C6 98.2(3), C4-Yb4-C7 93.1(3), C5-Yb4-C6 78.8(3), C5-Yb4-C7 160.8(3), C6-Yb4-C7 82.1(3)

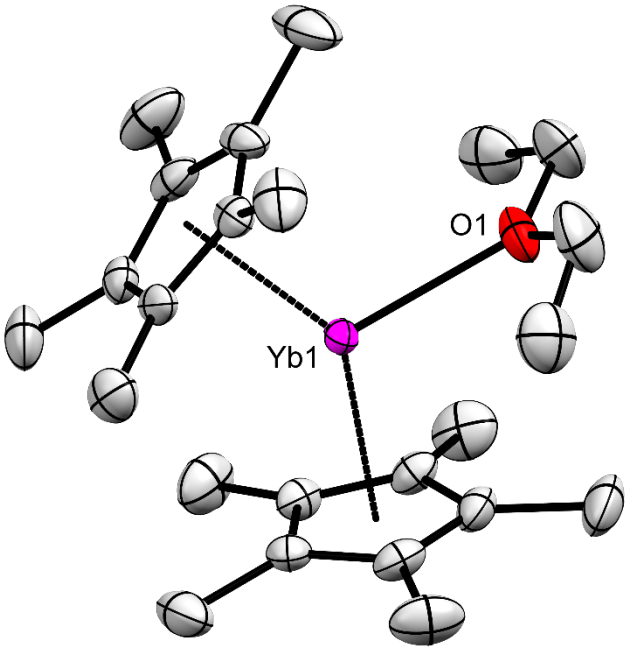

Figure S3. Crystal structure of $(C_5Me_5)_2Yb(Et_2O)$ (**5**). All atoms are represented by atomic displacement ellipsoids set at 50% probability. Hydrogen atoms are omitted for clarity.

Table S1. Selected structural parameters [Å, °] for complex **5** and $(C_5Me_5)_2Yb(thf)$[8]

	$(C_5Me_5)_2Yb(Et_2O)$ (**5**)	$(C_5Me_5)_2Yb(thf)$
Yb1-O1	2.454(4)	2.412(5)
Yb1-Cp*1 (ring centroid)	2.4171(9)	-
Yb1-Cp*2 (ring centroid)	2.4079(8)	-
Yb1-C(Cp*1), range	2.678(6)-2.702(5)	2.654(7)-2.694(8)
Yb1-C(Cp*1), av.	2.691	2.672
Yb1-C(Cp*2), range	2.674(5)-2.728(5)	2.643(7)-2.664(7)
Yb1-C(Cp*2), av.	2.701	2.654
Cp*1-Yb1-Cp*2	140.25	143.5(3)
Cp*1-Yb1-O1	111.45	108.8(3)
Cp*2-Yb1-O1	108.19	107.7(3)

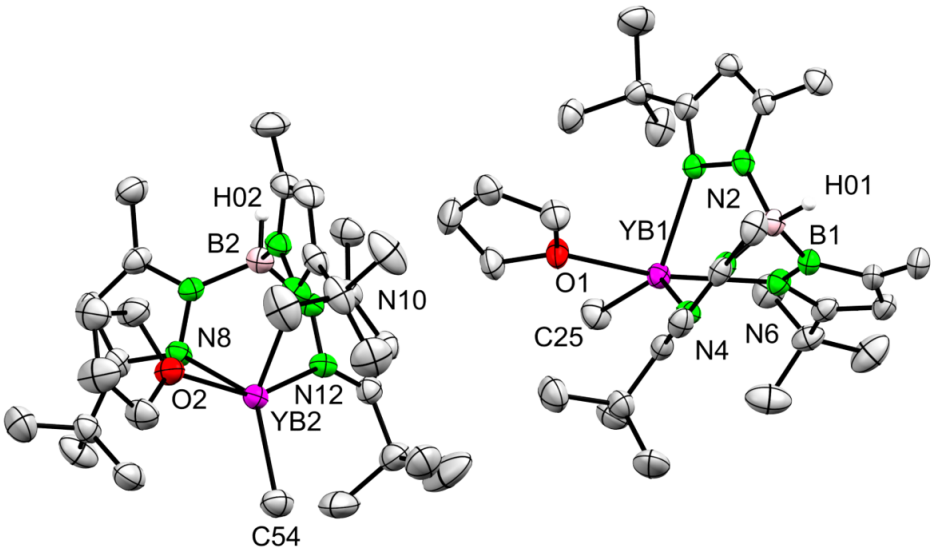

Figure S4. Crystal structure of ($Tp^{tBu,Me}$)Yb(CH_3)(thf) (**6**). All atoms are represented by atomic displacement ellipsoids set at 50 % probability. Hydrogen atoms expect B-H and disorder in the solvent thf are omitted for clarity.

Table S2. Selected structural parameters [Å, °] for complex **6**

molecule 1		molecule 2	
Yb1-C25	2.521(4)	Yb2-C54	2.503(4)
Yb1-B1	3.371(4)	Yb2-B2	3.366(4)
Yb1-N	2.467(3)-2.491(3)	Yb2-N	2.469(3)-2.474(3)
Yb1-O1	2.441(2)	Yb2-O2	2.440(3)
C25-Yb1-N2	128.32(12)	C54-Yb2-N8	136.20(12)
C25-Yb1-N4	139.39(12)	C54-Yb2-N10	129.87(12)
C25-Yb1-N6	117.48(12)	C54-Yb2-N12	117.34(13)
C25-Yb1-O1	89.79(12)	C54-Yb2-O2	93.25(12)
B1-Yb1-C25	165.48(13)	B2-Yb2-C54	166.27(14)

Table S3. Selected structural parameters [Å, °] for complex ($Tp^{tBu,Me}$)Ca(CH_3)(thf)[1]

molecule 1		molecule 2	
Ca1-C29	2.4822(16)	Ca2-C58	2.4772(16)
Ca1-B1	3.3616(16)	Ca2-B2	3.3515(17)
Ca1-N	2.4461(12)-2.4777(12)	Ca2-N	2.4494(12)-2.4608(13)
Ca1-O1	2.4026(10)	Ca2-O2	2.4006(11)
C29-Ca1-N2	128.32(5)	C58-Ca2-N8	129.42(5)
C29-Ca1-N4	116.46(5)	C58-Ca2-N10	116.30(5)
C29-Ca1-N6	139.52(5)	C58-Ca2-N12	136.82(5)
C29-Ca1-O1	89.36(5)	C58-Ca2-O2	92.62(5)
B1-Ca1-C29	164.81(5)	B2-Ca2- C58	165.58(5)

X-ray Crystallography and Crystal Structure Determinations.

Crystals of **2, 4, 5** and **6** were grown by standard techniques from saturated solutions using *n*-hexane (**2**), diethyl ether (**5**), thf (**4**) and a mixture of d8-thf and *n*-hexane for **6** at -40 °C. Suitable crystals for X-ray structure analyses were selected in a glovebox and coated with Parabar 10312 (previously known as Paratone N, Hampton Research) and fixed on a nylon loop/glass fiber.

X-ray data for above mentioned compounds were collected on a Bruker APEX II DUO instrument, equipped with an IμS microfocus sealed tube and QUAZAR optics for MoKα (λ = 0.71073 Å) radiation. The data collection strategy was determined using COSMO[9] employing ω-scans. Raw data were processed using APEX[10] and SAINT,[11] corrections for absorption effects were applied using SADABS.[12] The structures were solved by direct methods and refined against all data by full-matrix least-squares methods on F^2 using SHELXTL[13] and SHELXLE.[14] All graphics were produced employing MERCURY[15] and POV-Ray.[16] Disorder models for THF are calculated using DSR,[17] a program included in ShelXle, for refining disorder.

Further details of the refinement and crystallographic data are listed in Table S3, and in the CIF files. CCDC depositions 2039518-2039521 contain all the supplementary crystallographic data for this paper. These data can be obtained free of charge from The Cambridge Crystallographic Data Centre via www.ccdc.cam.ac.uk/structures/.

Crystallographic data

Table S4. Crystallographic data

Compound[a]	$[Yb\{N(SiMe_3)_2\}_2]_2$ (**2**)	$Yb_8(CH_3)_{14}O_2(thf)_6$ (**4**)	$(C_5Me_5)_2Yb(Et_2O)$ (**5**)	$(Tp^{tBu,Me})Yb(CH_3)(thf)$ (**6**)
Molecular formula	$C_{24}H_{72}N_4Si_8Yb_2$	$C_{38}H_{90}O_8Yb_8$	$C_{24}H_{40}OYb$	$C_{31}H_{55}BN_6O_{1.5}Yb$
CCDC	2039521	2039518	2039519	2039520
M [g/mol]	987.65	2059.41	517.60	719.66
Temperature [K]	100	100	150	100
Wavelength [Å]	0.71073	0.71073	0.71073	0.71073
Crystal dimensions [mm]	0.106x0.132x0.409	0.90x0.020x0.018	0.224x0.176x0.105	0.108x0.079x0.064
Crystal description	Orange needle	Orange needle	Green plate	Orange needle
Crystal system	Triclinic	Triclinic	Orthorhombic	Triclinic
Space group	$P\bar{1}$	$P\bar{1}$	$P2_12_12_1$	$P\bar{1}$
a [Å]	8.8586(4)	11.0309(12)	8.521(3)	11.6943(12)
b [Å]	12.4947(6)	12.0062(13)	15.070(4)	15.8997(16)
c [Å]	21.8119(9)	12.2428(14)	18.244(5)	19.6227(19)
α [°]	73.7690(10)	109.5700(10)	90	79.970(3)
β [°]	86.7190(10)	111.8730(10)	90	80.792(3)
γ [°]	71.3230(10)	97.5130(10)	90	81.066(3)
V [^{3}]	2194.58(17)	1355.9(3)	2343.9(4)	3515.9(3)
Z	2	1	4	4
ρ [mg/m^3]	1.495	2.522	1.467	1.380
μ [mm^{-1}]	4.473	13.685	4.001	2.692
F (000)	992	942	1048	1480
θ range [°]	0.973 to 30.546	2.701 to 28.782	1.753 to 32.046	1.811 to 28.696
Indices	-12 ≤ h ≤ 12	-14 ≤ h ≤ 14	-11 ≤ h ≤ 11	-15 ≤ h ≤ 15
	-17 ≤ k ≤ 17	-16 ≤ k ≤ 16	-22 ≤ k ≤ 22	-21 ≤ k ≤ 21
	-31 ≤ l ≤ 31	-16 ≤ l ≤ 16	-27 ≤ l ≤ 27	-26 ≤ l ≤ 26
Number of reflexes	108603	36789	35504	169173
Unique reflexes	13408	7010	8160	18045
R_1/wR_2 (I>2σ)[a]	0.0225/0.0472	0.0383/0.0812	0.0294/0.0553	0.0356/0.0719
R_1/wR_2 (all data)[b]	0.0294/0.0501	0.0599/0.0910	0.0437/0.0605	0.0664/0.0837
GOF (in F^2)[c]	1.028	1.022	1.034	1.038

[a] $R_1 = \Sigma(||F_0|-|F_c||)/\Sigma|F_0|$, $F_0 > 4\sigma(F_0)$. [b] $wR_2 = \{\Sigma[w(F_0^2-F_c^2)^2/\Sigma[w(F_0^2)^2]\}^{1/2}$. [c]: $GOF = [\frac{(\sum W(F_0 - F_c)^2}{(no-np)}]^{0.5}$

NMR Spectra

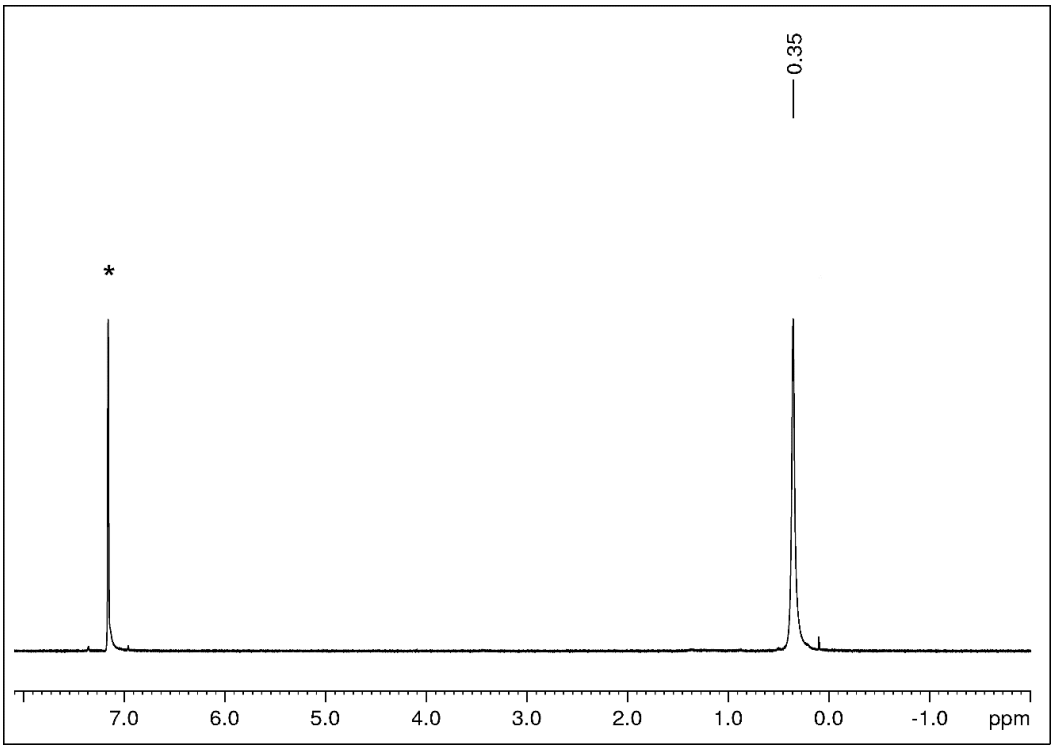

Figure S5. ^{1}H NMR spectrum (400 MHz) of $[Yb\{N(SiMe_3)_2\}_2]_2$ in D_6[benzene] at 26 °C. Residual solvent signal is marked with *.

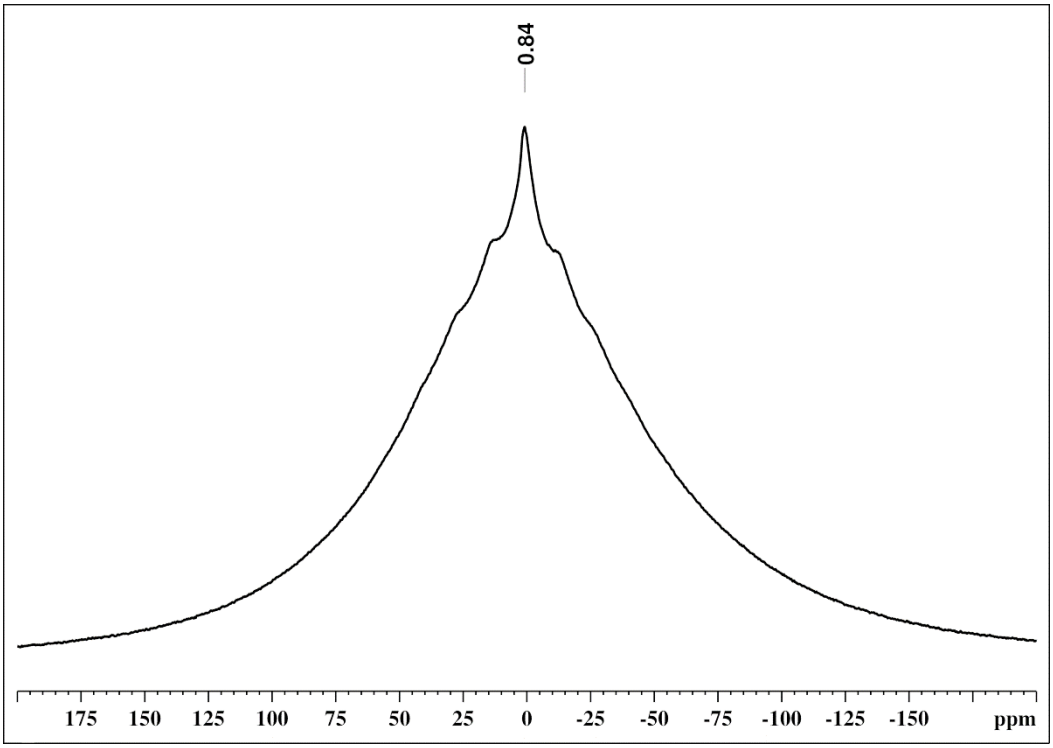

Figure S6. ^{1}H MAS NMR spectrum (300 MHz, spinning frequency 4000 Hz) of $[YbMe_2]_n$.

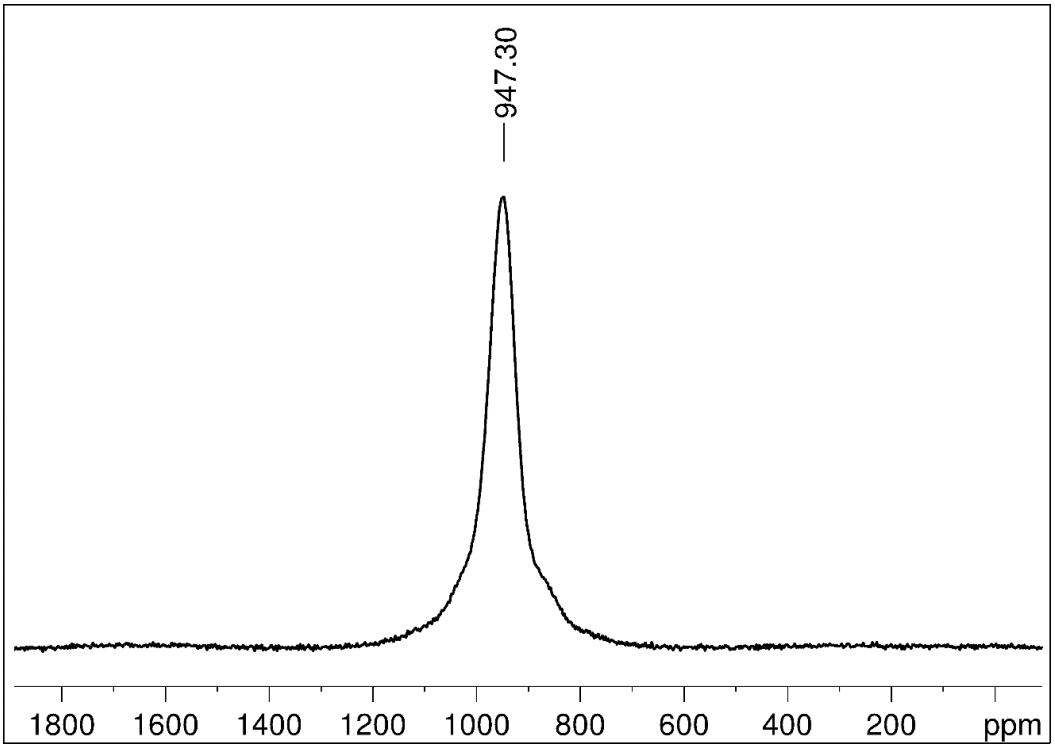

Figure S7. ^{171}Yb CP/MAS NMR spectrum (52 MHz, spinning frequency 4000 Hz) of $[YbMe_2]_n$.

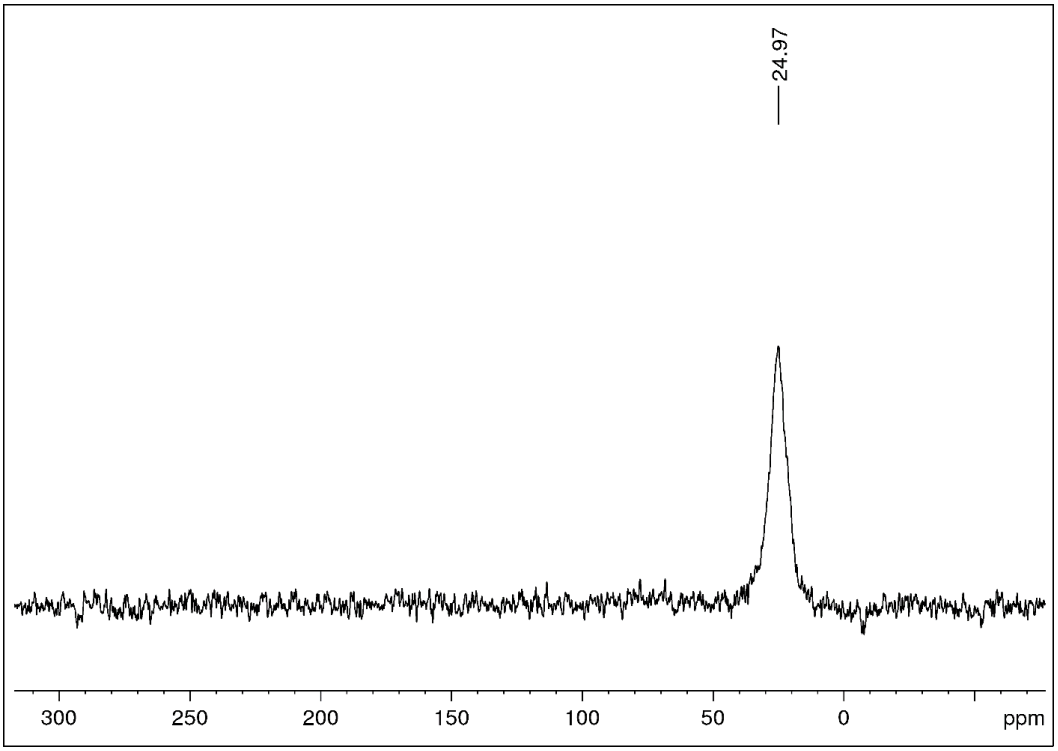

Figure S8. ^{13}C CP/MAS NMR spectrum (75 MHz, spinning frequency 4000 Hz) of $[YbMe_2]_n$.

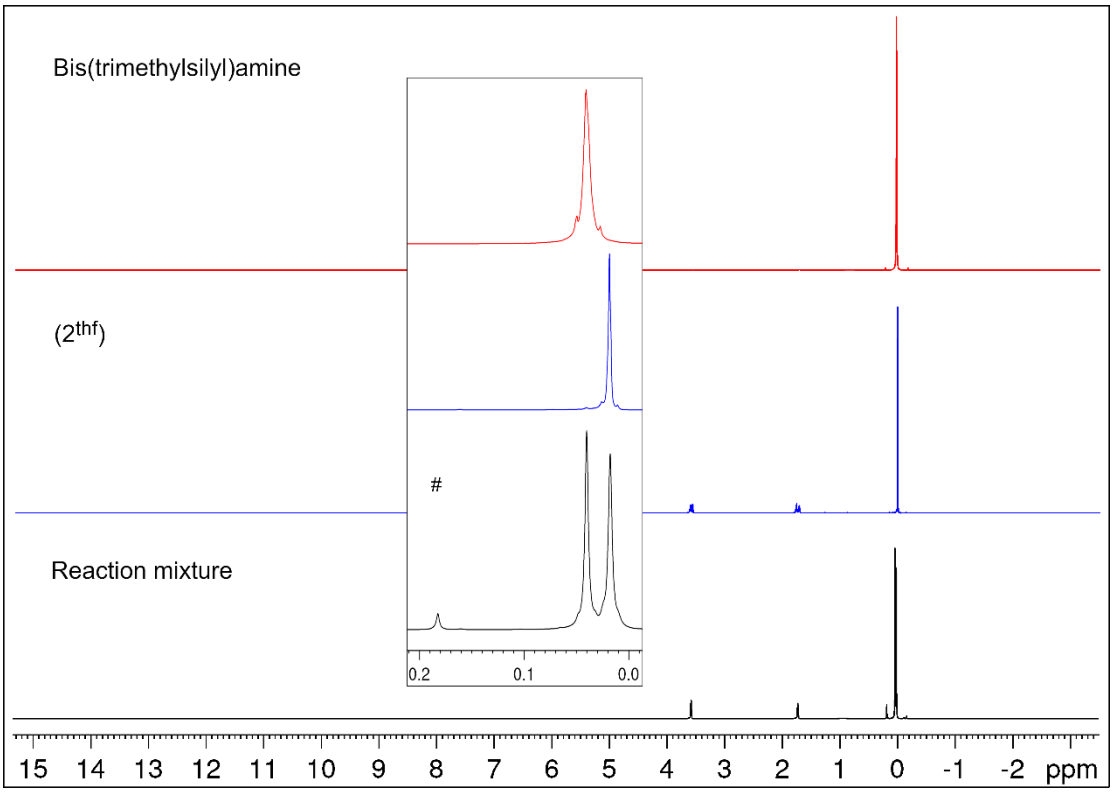

Figure S9. ^{1}H NMR spectra (400 MHz) of a micro-scale reaction of $[YbMe_2]_n$ with bis(trimethylsilyl)amine, performed in a J. Young NMR tube in $[D_8]$thf at 26 °C. Both the comparison with the spectra of **2**^{thf} and bis(trimethylsilyl)amine and the formation of CH_4 (marked with #) indicated a successful reaction.

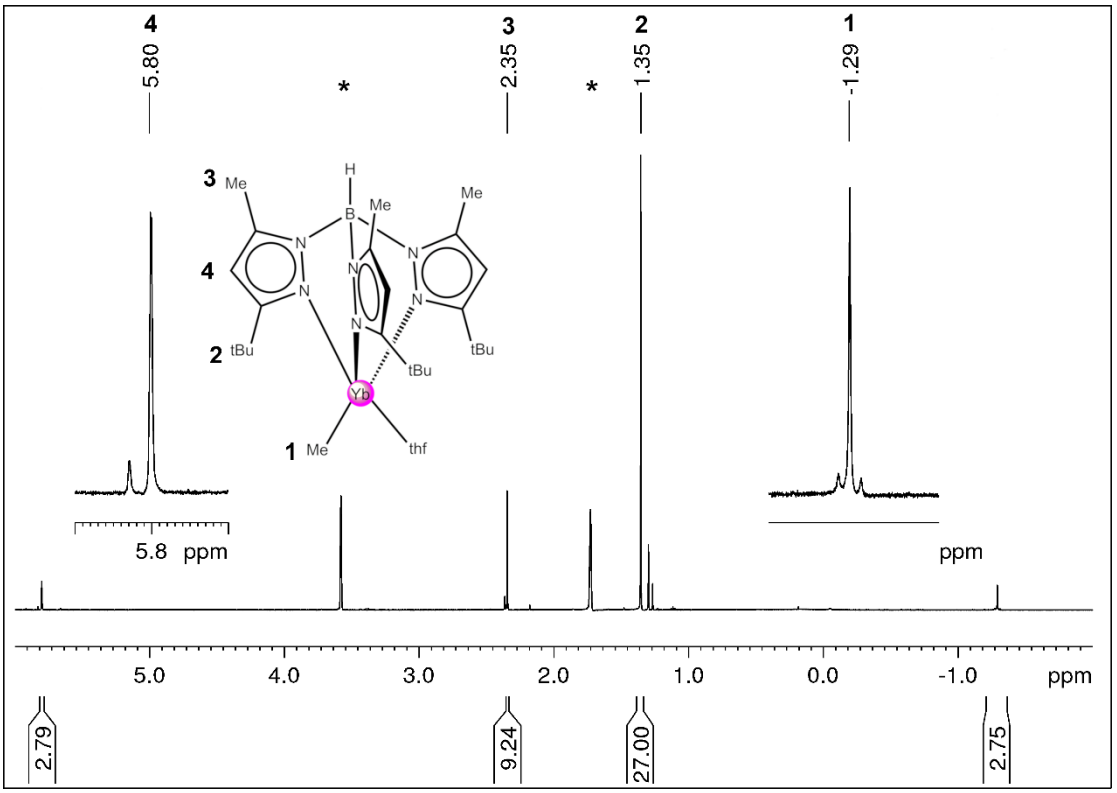

Figure S10. ^{1}H NMR spectrum (500 MHz) of a micro-scale reaction of $[YbMe_2]_n$ with hydro tris(3-tert-butyl-5-methylpyrazolyl)borate $HTp^{tBu,Me}$, performed in a J. Young NMR tube in $[D_8]$thf at 26 °C. Residual solvent signal is marked with *.

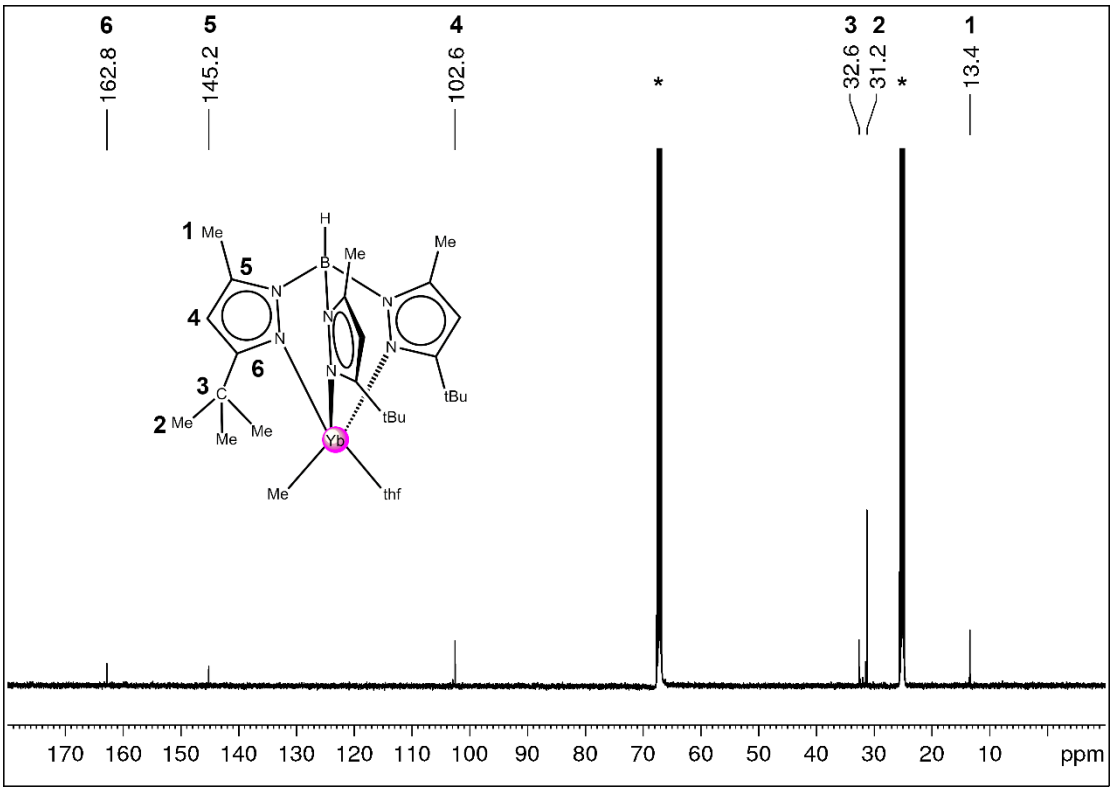

Figure S11. $^{13}C\{^{1}H\}$ NMR spectrum (125 MHz) of a micro-scale reaction of $[YbMe_2]_n$ with hydrotris(3-tert-butyl-5-methylpyrazolyl) borate $HTp^{tBu,Me}$, performed in a J. Young NMR tube in $[D_8]$thf at 26 °C. Residual solvent signal are marked with *.

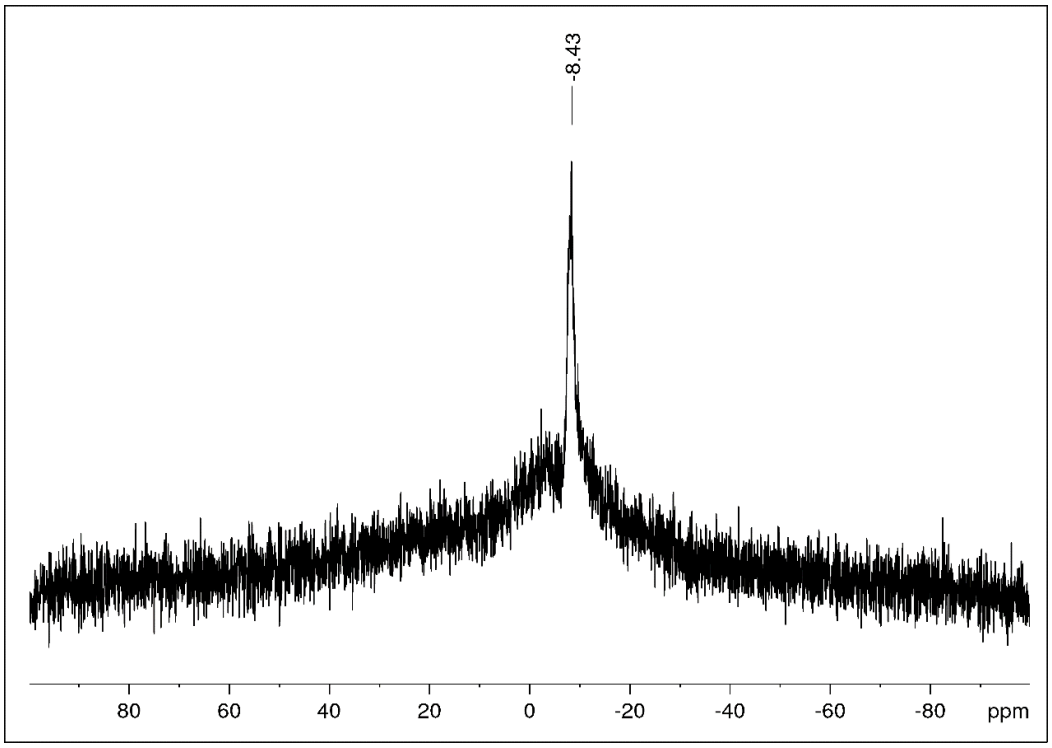

Figure S12. ^{11}B NMR spectrum (160 MHz) of a micro-scale reaction of $[YbMe_2]_n$ with hydrotris(3-tert-butyl-5-methylpyrazolyl) borate $HTp^{tBu,Me}$, performed in a J. Young NMR tube in $[D_8]$thf at 26 °C.

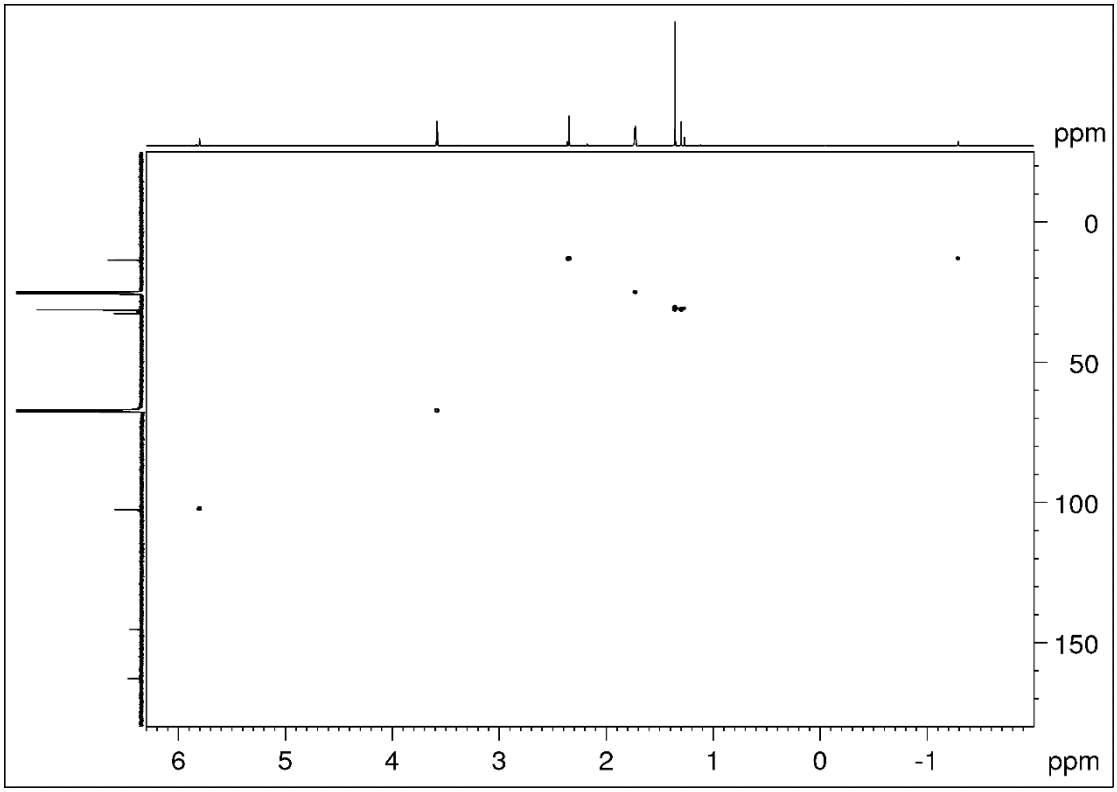

Figure S13. $^{1}H–^{13}C$ HSQC NMR spectrum (500 MHz, 125 MHz) of a micro-scale reaction of $[YbMe_2]_n$ with hydrotris(3-tert-butyl-5-methylpyrazolyl) borate $HTp^{tBu,Me}$, performed in a J. Young NMR tube in $[D_8]$thf at 26 °C.

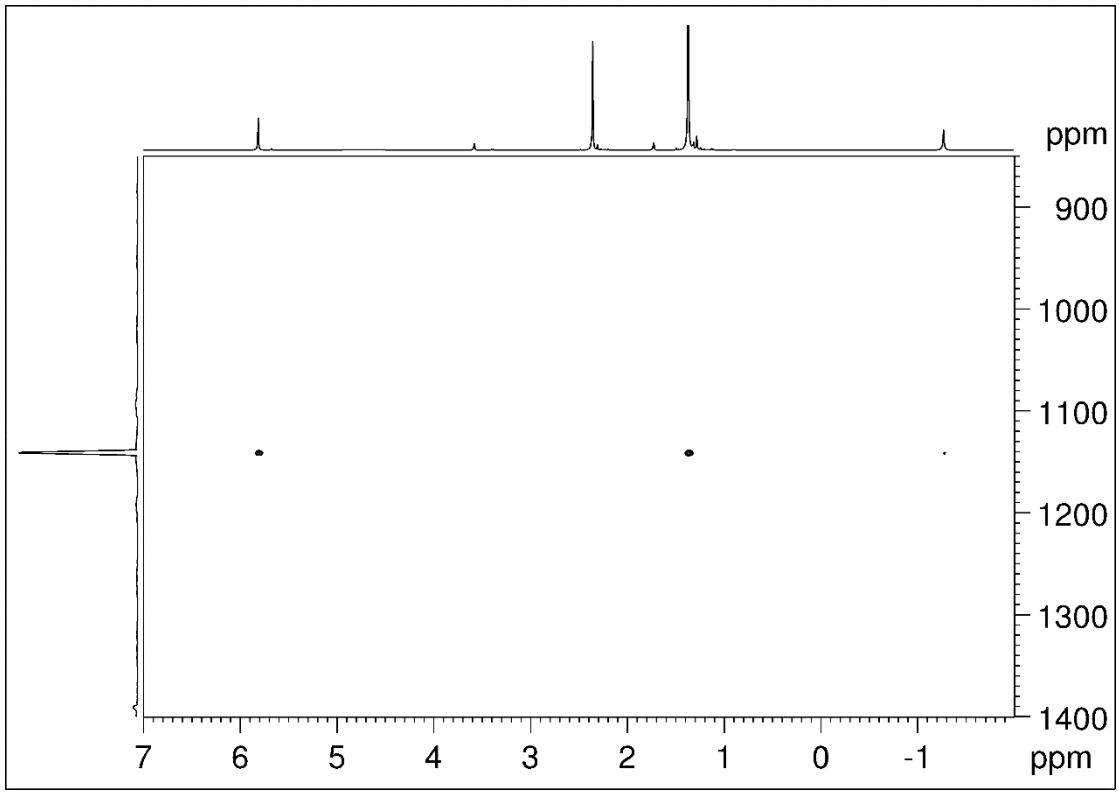

Figure S14. $^{1}H–^{171}Yb$ HSQC NMR spectrum (500 MHz, 87.52 MHz) of complex **6** in $[D_8]$thf at 26 °C.

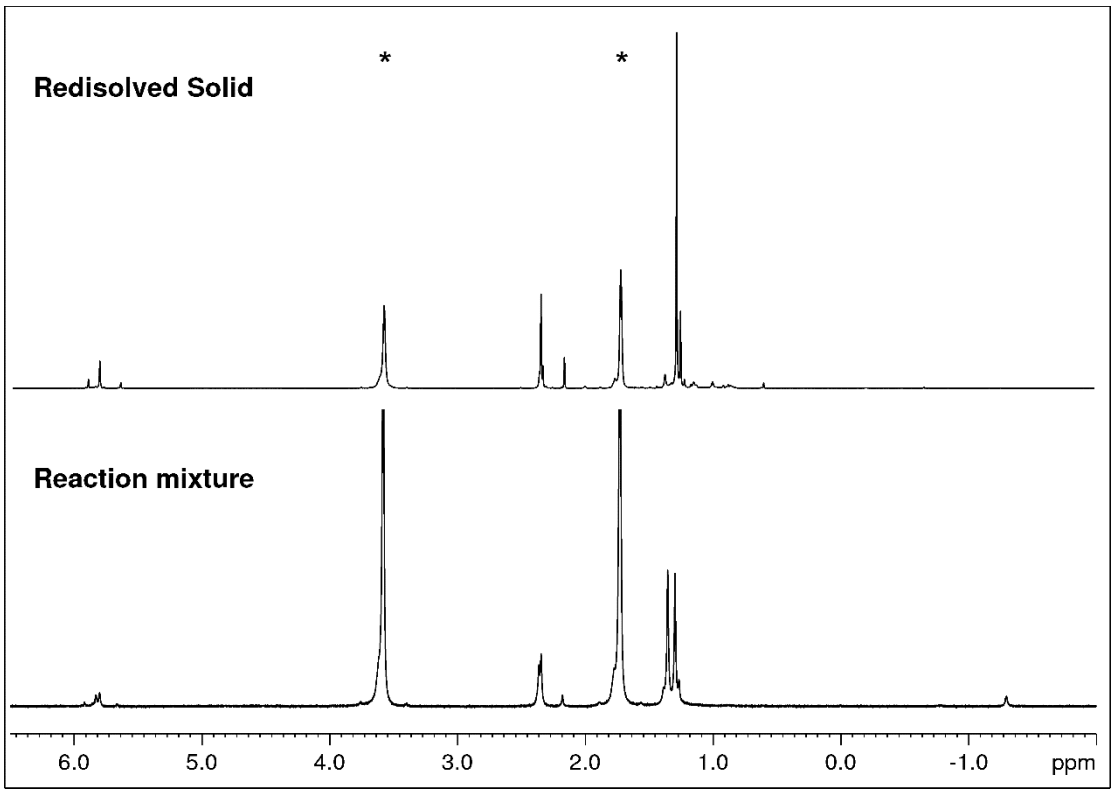

Figure S15. ^{1}H NMR spectra (400 MHz) of a reaction of $[YbMe_2]_n$ with hydrotris(3-tert-butyl-5-methylpyrazolyl)borate $HTp^{tBu,Me}$ (bottom) and the dried solids (top) in $[D_8]$thf at 26 °C. Residual solvent signal is marked with *. The missing methyl signal at -1.3 ppm in the spectrum of the dried and the resolved solids indicated decomposition.

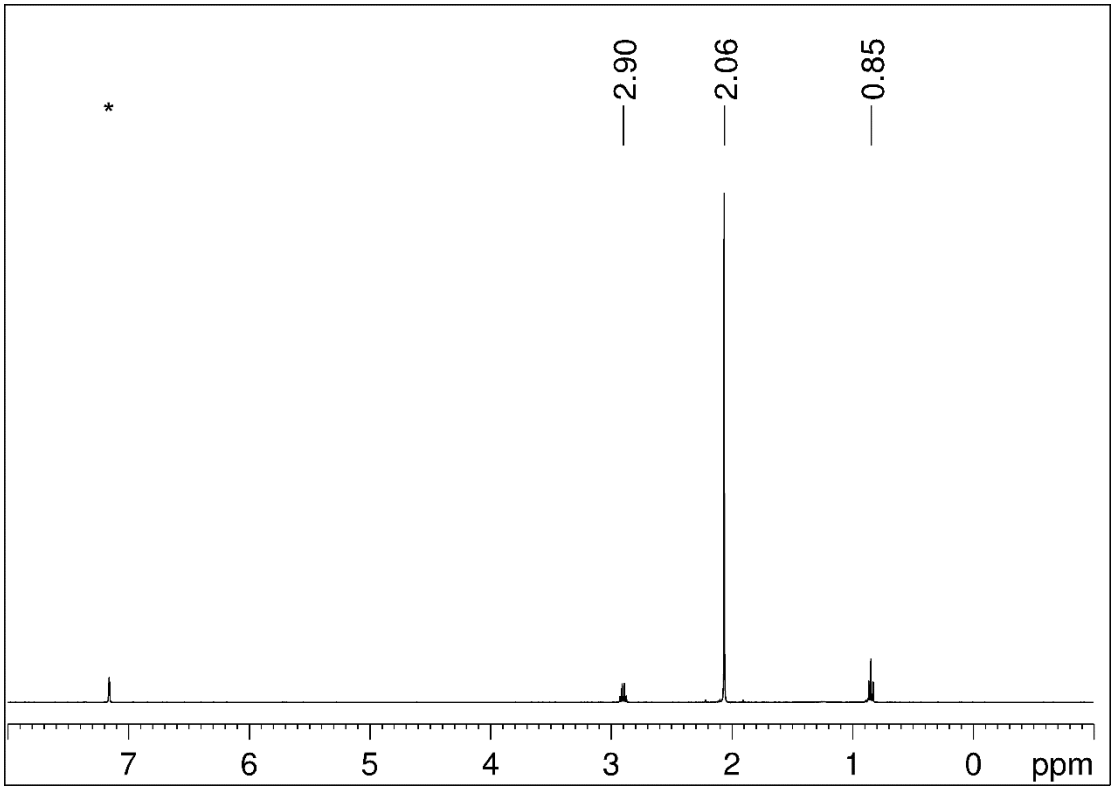

Figure S16. ^{1}H NMR spectrum (400 MHz) of $(C_5Me_5)_2Yb(Et_2O)$ in D_6[benzene] at 26 °C. Residual solvent signal is marked with *.

DRIFT Spectra

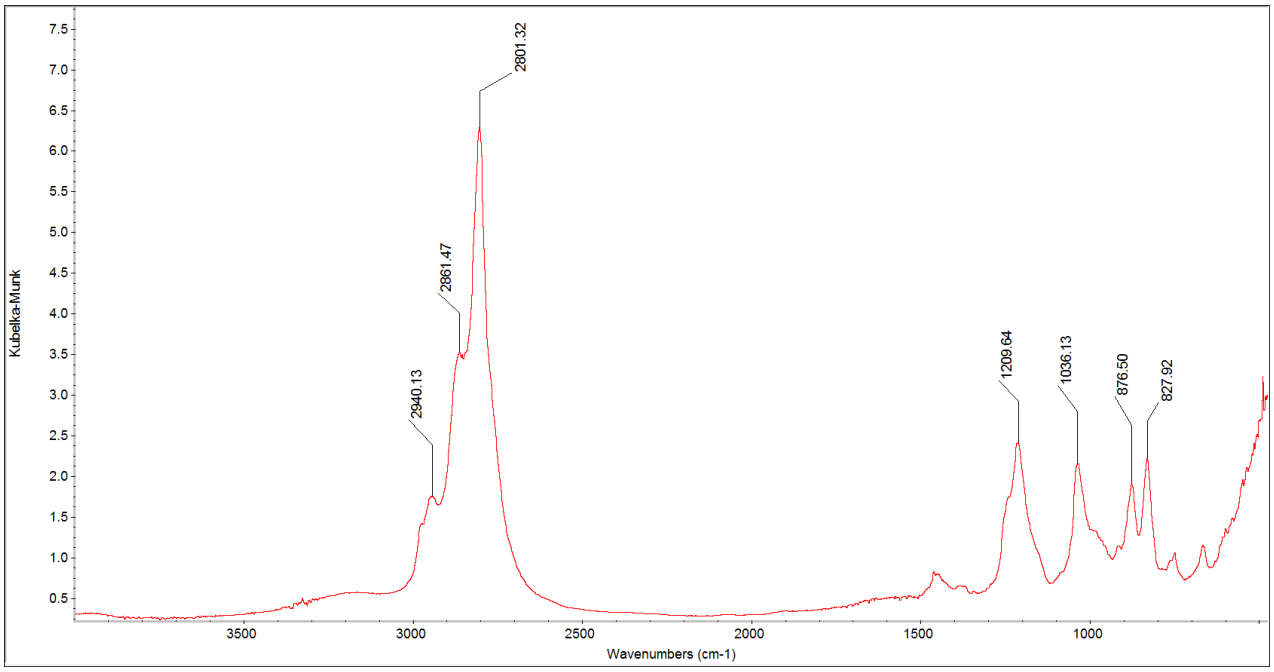

Figure S17. DRIFT spectrum of $[YbMe_2]_n$ via route **I**.

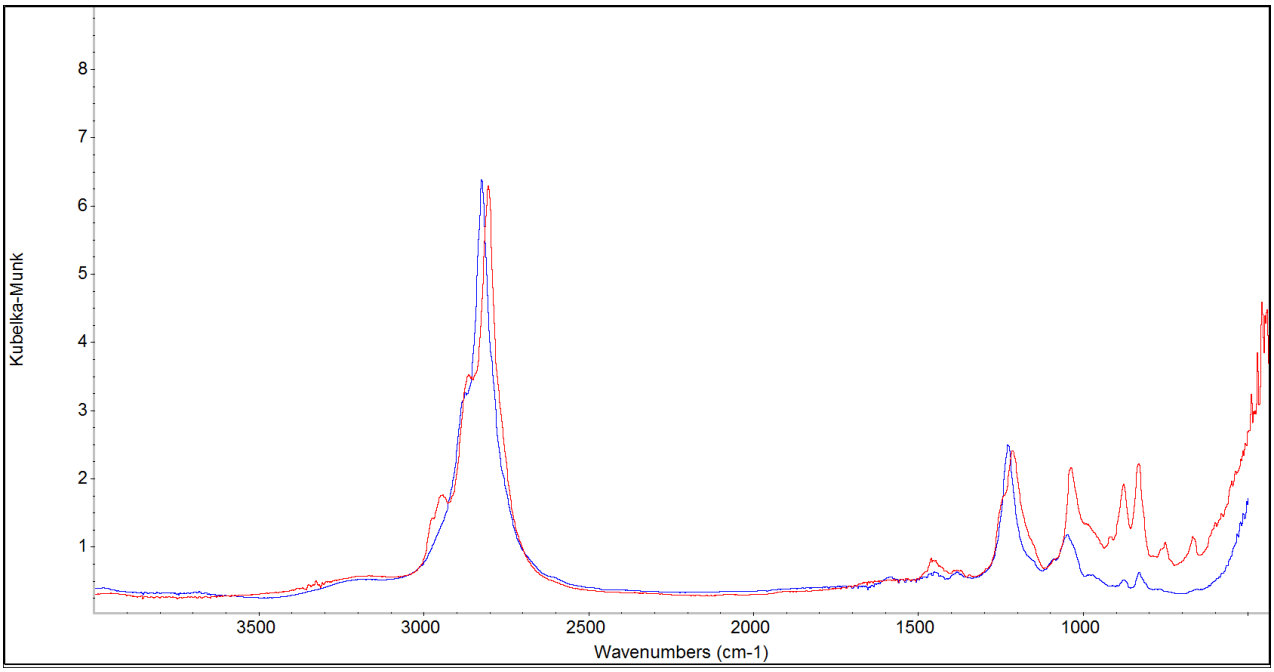

Figure S18. Overlain DRIFT spectra of $[YbMe_2]_n$ (**3**^{thf}, red) and $[CaMe_2]_n$ (blue).[1]

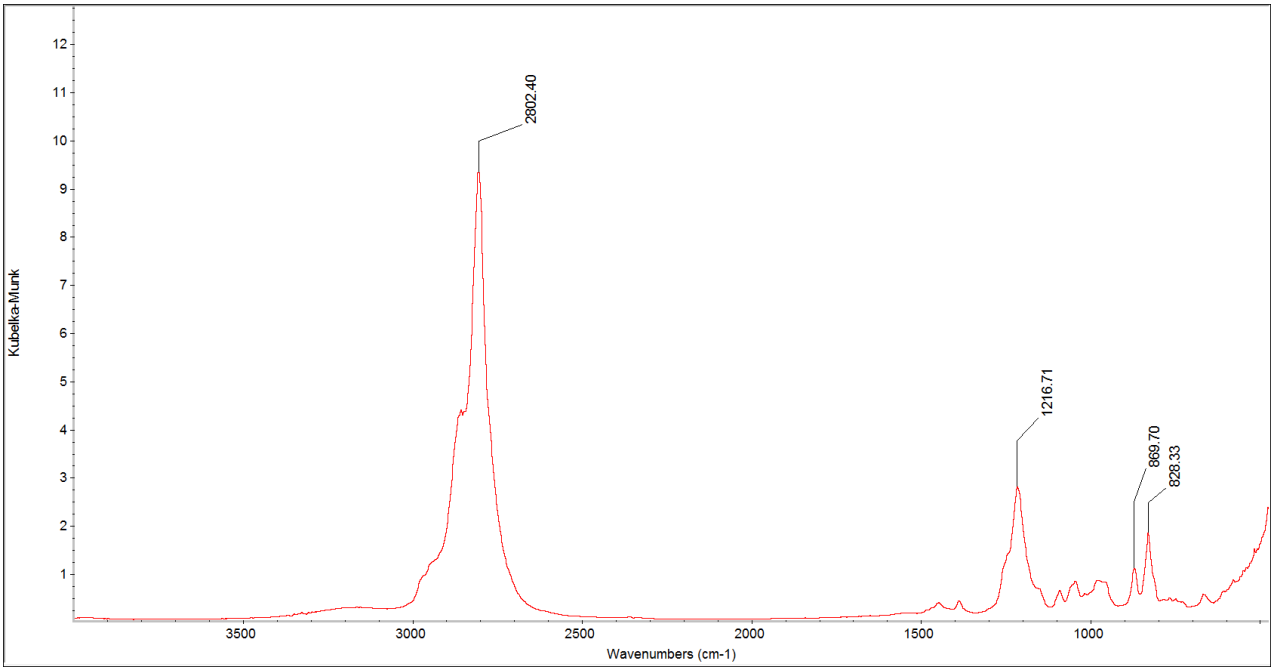

Figure S19. DRIFT spectrum of $[YbMe_2]_n$ via route **II**.

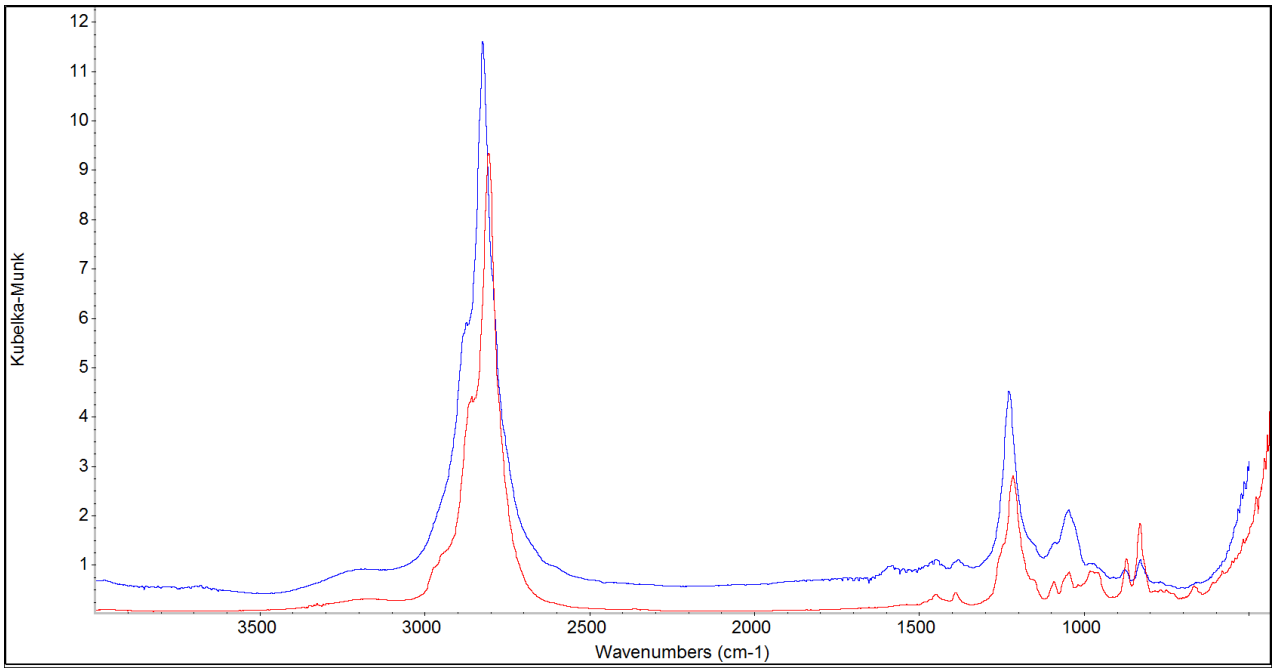

Figure S20. Overlain DRIFT spectra of $[YbMe_2]_n$ (**3**, red) and $[CaMe_2]_n$ (blue).[1]

UV/Vis Spectra

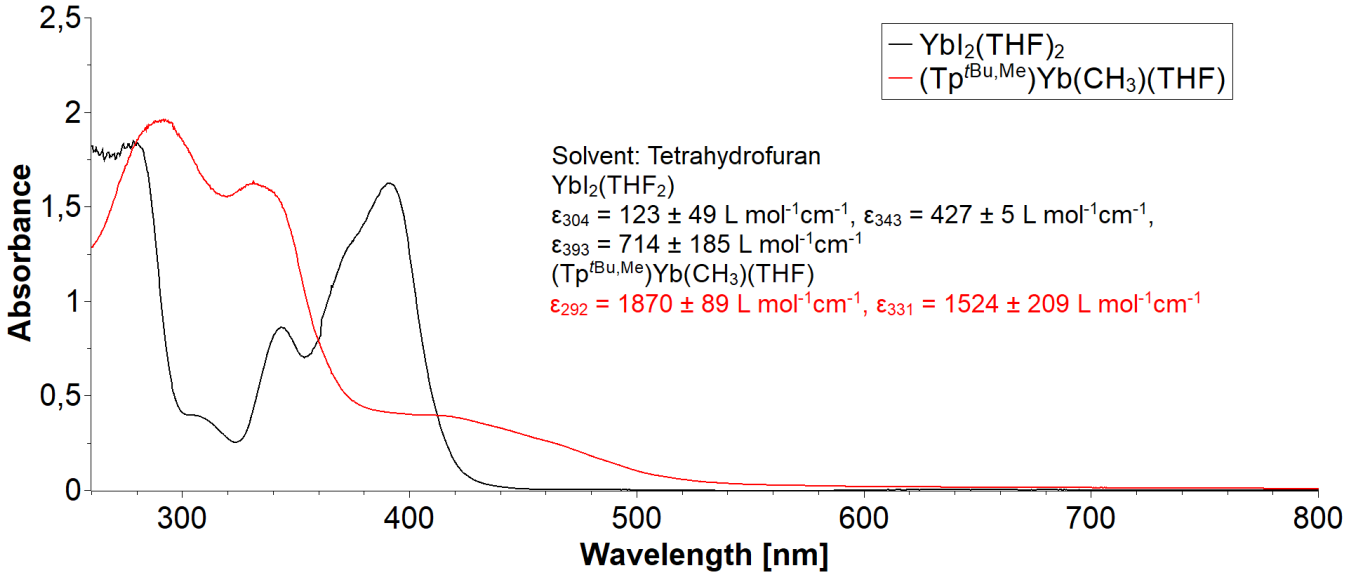

Figure S21. UV/Vis spectra of $YbI_2(THF)_2$ and $(Tp^{tBu,Me})Yb(CH_3)(THF)$ in tetrahydrofuran.

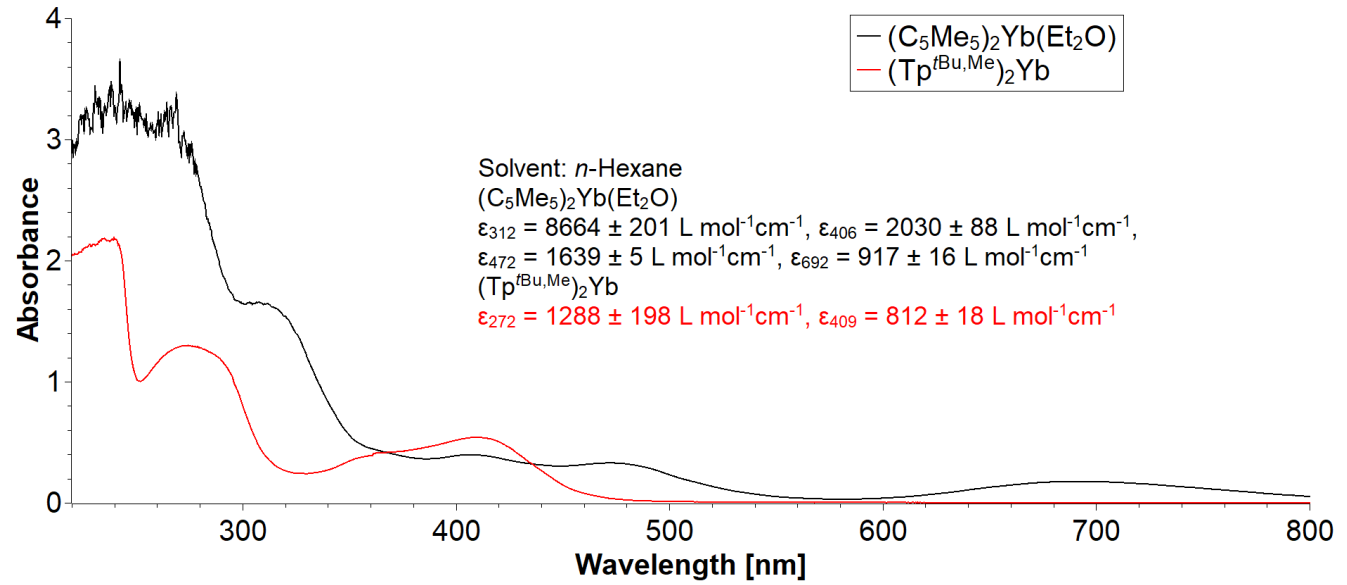

Figure S22. UV/Vis spectra of $(C_5Me_5)_2Yb(Et_2O)$ and $(Tp^{tBu,Me})_2Yb$ in *n*-hexane.

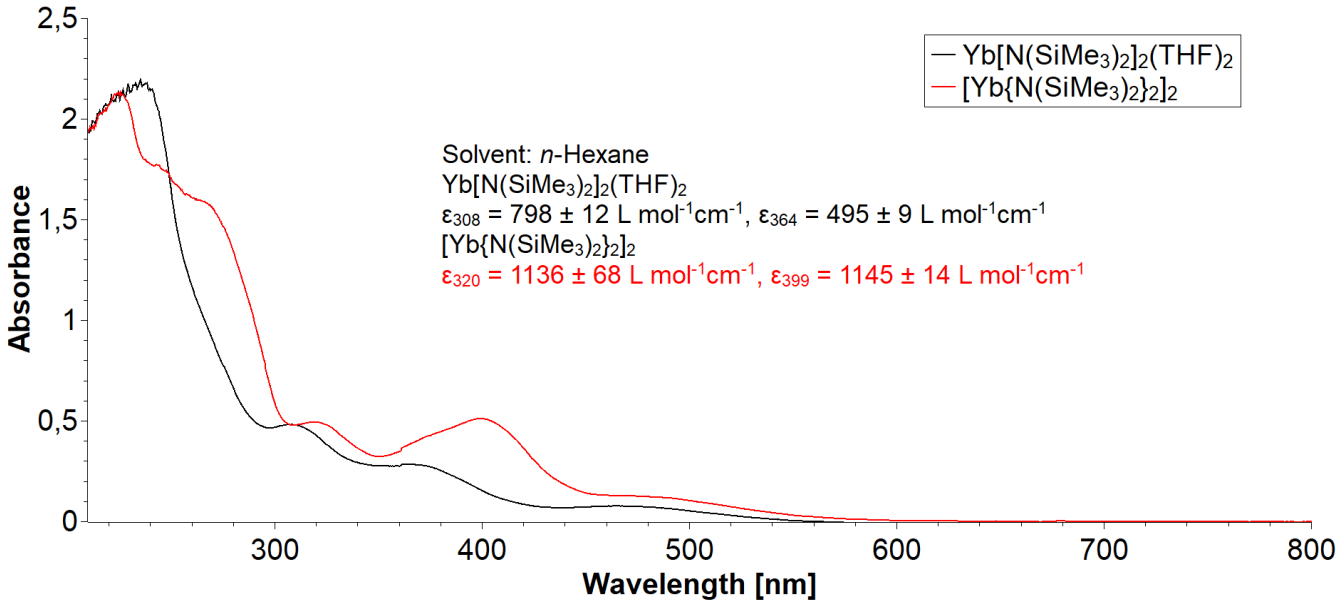

Figure S23. UV/Vis spectra of $Yb[N(SiMe_3)_2]_2(THF)_2$ and $[Yb\{N(SiMe_3)_2\}_2]_2$ in *n*-hexane.

Potentiometric determination of iodine in different precursor complexes

Samples of $Yb[N(SiMe_3)_2]_2(THF)_2$ (21 mg) and $[Yb\{N(SiMe_3)_2\}_2]_2$ (16 mg) were quenched with methanol (2 ml) and deionized water (2 ml). The solvents were removed completely under reduced pressure. The residual solids where dissolved with diluted nitric acid and titrated with 0.001 M $AgNO_3$.

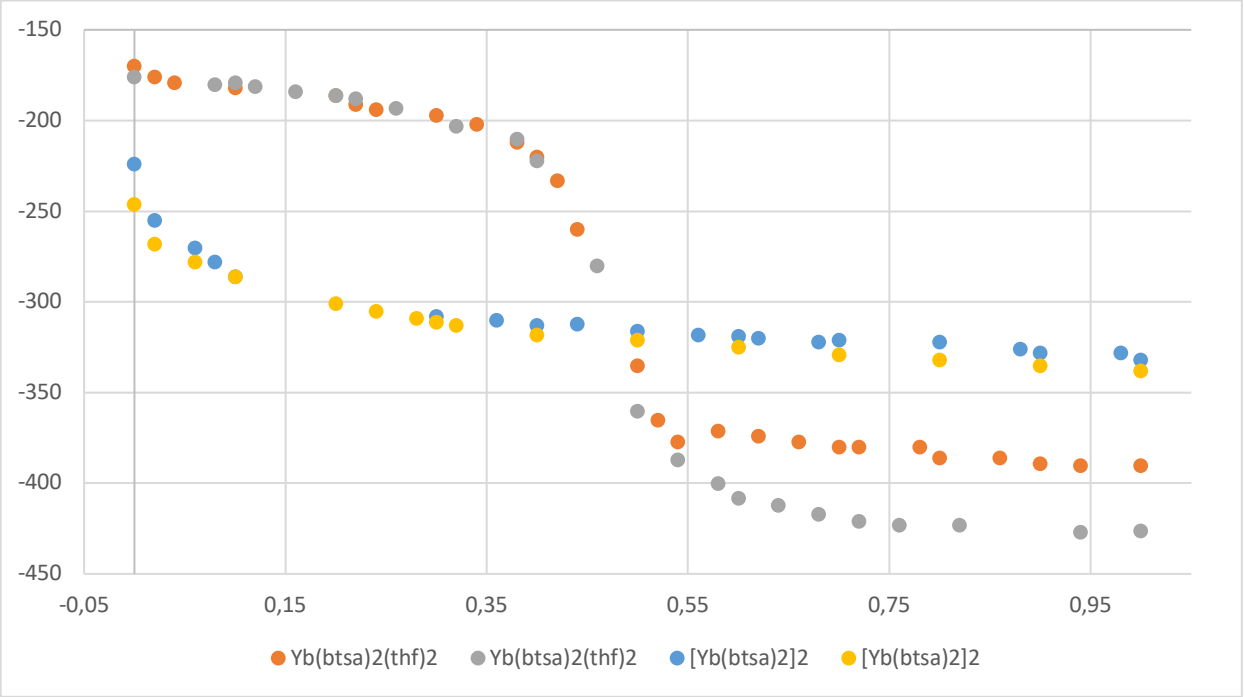

Figure S24. Potentiometric titrations of $Yb[N(SiMe_3)_2]_2(THF)_2$ (**2 do**) (orange and grey) and $[Yb\{N(SiMe_3)_2\}_2]_2$ (**2**) (blue and yellow) (3 aliquots) with 0.001 M $AgNO_3$.

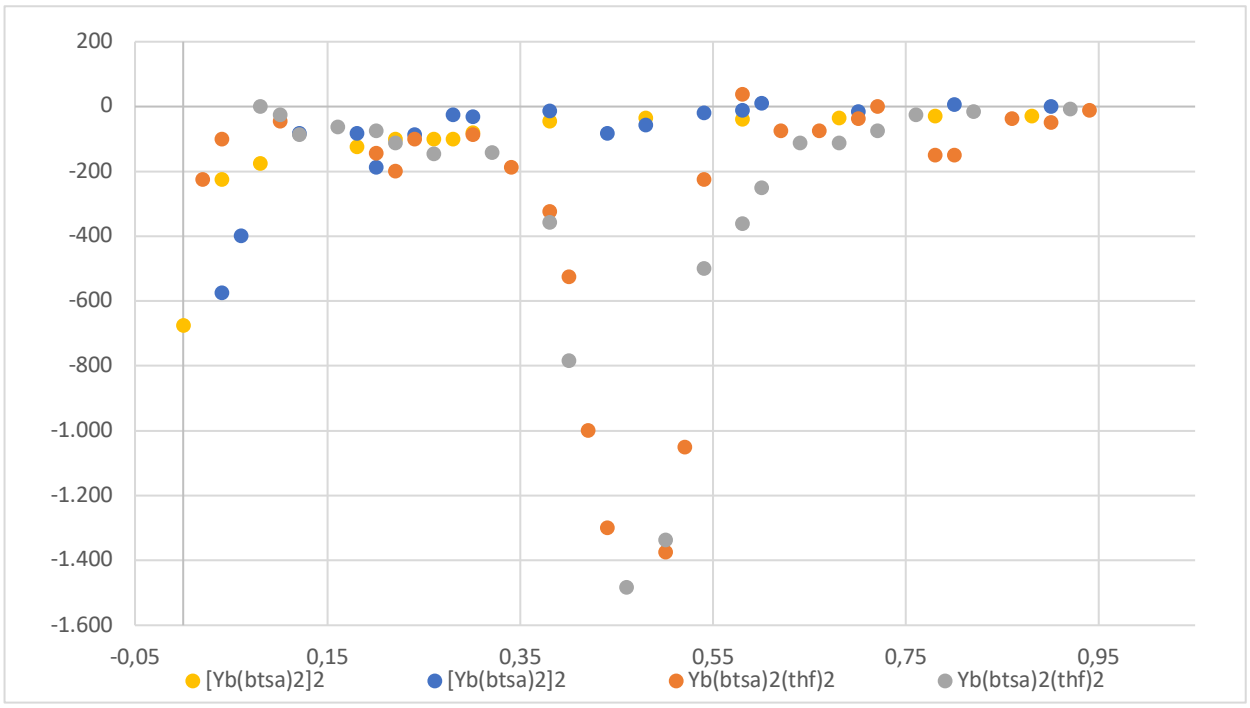

Figure S25. Numerical derivation of the curves shown in Figure S10. For $[Yb\{N(SiMe_3)_2\}_2]_2$ (**2**) (blue and yellow) no definite minima is observable. For $Yb[N(SiMe_3)_2]_2(THF)_2$ (**2 do**) (orange and grey).

References

1. B. M. Wolf, C. Stuhl, C. Maichle-Mössmer and R. Anwander, *J. Am. Chem. Soc.,* 2018, **140**, 2373-2383.
2. S. Trofimenko, *Chem. Rev.*, 1993, **93**, 943-980
3. B. M. Wolf, C. Stuhl and R. Anwander, *Chem. Commun.*, 2018, **54**, 8826-8829.
4. X. Zhang, R. McDonald and J. Takats, *New J. Chem.*, 1995, **19**, 573-585.
5. G. R. Fulmer, A. J. M. Miller, N. H. Sherden, H. E. Gottlieb, A. Nudelman, B. M. Stoltz, J. E. Bercaw and K. I. Goldberg, *Organometallics*, 2010, **29**, 2176-2179.
6. J. M. Boncella, PhD Thesis, University of California, Berkeley, 1982.
7. T. D. Tilley, J. M. Boncella, D. J. Berg and R. A. Andersen, *Inorg. Synth.*, 1990, **27**, 165-150.
8.
9. *COSMO v. 1.61*, Bruker AXS Inc., Madison, WI, 2012.
10. APEX 3 V. 2017.3-0, Bruker AXS Inc., Madison, WI, 2017.
11. *SAINT v. 8.38A*, Bruker AXS Inc., Madison, WI, 2017.
12. *SADABS,* L. Krause, R. Herbst-Irmer, G. M. Sheldrick and D. Stalke, *J. Appl. Cryst.*, 2015, **48,** 3-10.
13. *SHELXT, Acta Cryst.,* 2015, **A71**, 3-8.
14. SHELXLE, C. B. Huebschle, G. M. Sheldrick, B. Dittrich, *J. Appl. Crystallogr* , 2011, **44**, 1281-1284.
15. Mercury CSD 2.0 - New Features for the Visualization and Investigation of Cryst. Structures, C. F. Macrae, I. J. Bruno, J. A. Chisholm, P. R. Edgington, P. McCabe, E. Pidcock, L. Rodriguez-Monge, R. Taylor, J. van de Streek and P. A. Wood, *J. Appl. Cryst.,* 2008, **41**, 466-470.
16. v. 3.6, P. o. V. P. L., POV-Ray Williamstown, Victoria, Australia, 2004, *http://www.povray.org*.
17. D. Kratzert, J. J. Holstein and I.Krossing, DSR: enhanced modelling and refinement of disordered structures with SHELXL. *J. Appl. Cryst* , 2015, **48**, 933-938.

Paper II

Potential precursors for terminal ytterbium(II) imide complexes bearing the tris(3-*tert*-butyl-5-methylpyrazolyl)hydroborato ligand

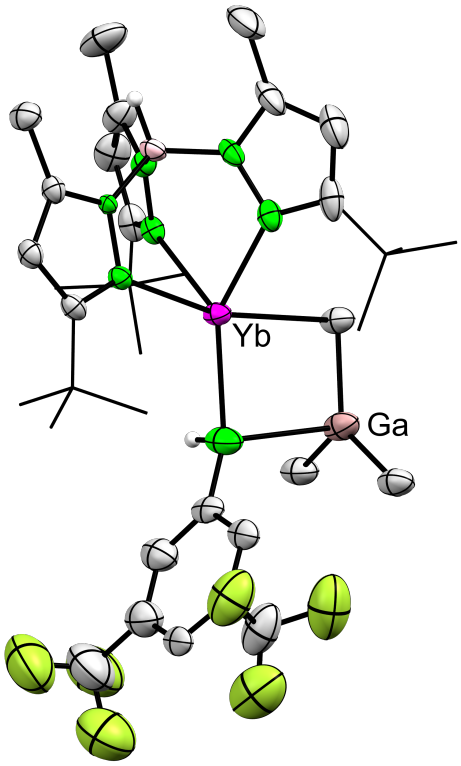

https://doi.org/10.1039/d3dt00861d
reprinted with the permission from
Dalton Trans., **2023**, **52**, 6273

Dalton Transactions

ROYAL SOCIETY OF CHEMISTRY

PAPER

View Article Online
View Journal | View Issue

Cite this: *Dalton Trans.*, 2023, **52**, 6273

Potential precursors for terminal ytterbium(II) imide complexes bearing the hydrotris(3-*tert*-butyl-5-methylpyrazolyl)borato ligand†

Markus M. Katzenmayer, Felix Kracht, Cäcilia Maichle-Mössmer and Reiner Anwander *

Received 21st March 2023,
Accepted 17th April 2023

DOI: 10.1039/d3dt00861d

rsc.li/dalton

Monomeric, divalent ytterbium primary amides $Tp^{tBu,Me}Yb(NHR)(thf)_x$ (R = $C_6H_3iPr_2$-2,6 = Ar^{iPr} = Dipp, $C_6H_3(CF_3)_2$-3,5 = Ar^{CF3}, $SiPh_3$) supported by the bulky hydrotris(3-*t*Bu-5-Me-pyrazolyl)borato scorpionate ligand are synthesized acccording to salt metathesis and protonolysis protocols, respectively. Yb(II) precursors comprise $YbI_2(thf)_2$, $Yb[N(SiMe_3)_2]_2(thf)_2$ and $Tp^{tBu,Me}Yb[N(SiMe_3)_2]$. Complexes $Tp^{tBu,Me}Yb(NHR)(thf)_x$ readily engage in donor (thf) exchange with nitrogen donors like DMAP (4-dimethylaminopyridine) and pyridine. Treatment of $Tp^{tBu,Me}Yb(NHAr^{CF3})(thf)_2$ with the Lewis acids $AlMe_3$ and $GaMe_3$ results in the heterobimetallic complexes $Tp^{tBu,Me}Yb(NHAr^{CF3})(MMe_3)$ (M = Al, Ga). Reactions of $Tp^{tBu,Me}Yb(NHR)(thf)_x$ (R = Ar^{iPr}, Ar^{CF3}) with the halogenating agents C_2Cl_6 and $TeBr_4$ give access to trivalent complexes $[Tp^{tBu,Me}Yb(NHR)(X)]$ (X = Cl, Br). The ytterbium(II) complexes under study display ^{171}Yb NMR chemical shifts in the range 582 ppm for $Tp^{tBu,Me}Yb(NHAr^{CF3})(GaMe_3)$ to 954 ppm for $Tp^{tBu,Me}Yb(NHSiPh_3)$(dmap). The salt-metathesis route is also applicable for the synthesis of complexes $Tp^{tBu,Me}Ln(NHAr^{iPr})(thf)$ (Ln = Sm, Eu) and $Tp^{tBu,Me}Yb(NHAr^{Me})$ (Ar^{Me} = $C_6H_3Me_2$-2,6).

Introduction

In 1991, Schumann and Bochkarev reported on the synthesis and structural characterization of the first molecular rare-earth-metal organoimide complex.[1] Applying a redox protocol *via* reductive cleavage of azobenzene with ytterbium naphthalide $Yb(C_{10}H_8)(thf)_3$ gave access to trivalent tetranuclear ytterbium imide $Yb_4(N_2Ph_2)_4(NPh)_2(thf)_4$ (**I**, Fig. 1).[1] Surprisingly, the field of rare-earth-metal imide chemistry has witnessed considerable progress only 20 years later, triggered by Chen's terminal scandium imide $[MeC(NAr^{iPr})CHC(Me)(NCH_2CH_2NMe_2)]Sc(=NAr^{iPr})(dmap)$.[2] In particular, the synthesis and structural characterization of terminal imide complexes [Ln=NR] poses a major challenge.[3–10] Primary amido moieties of the type [Ln(NHR)], more specifically anilides [Ln(NHAr)], display crucial imide precursors since they are prone to ultimate deprotonation. Basic reagents MB employed for intermolecular deprotonations comprise *n*-BuLi, $M[N(SiMe_3)_2]$ (M = Li, K, Rb, Cs) and trimethylaluminium (Fig. 1).[3] For example, early reports described the synthesis of $Yb_2(NAr^{iPr})_6Na_2Li_4(thf)_4$ from $Yb(NHAr^{iPr})_4Na(thf)$ and *n*-BuLi,[11] or of $[(AlMe_4)_2Nd(NPh)(AlMe_2)]_2$ from $Nd(NHPh)_3(KCl)_3$ and $AlMe_3$,[12,13] *via* alkane elimination. This approach also paved the way for the first terminal cerium(IV) imide complexes, (TriNOx)Ce[=N{$C_6H_3(CF_3)_2$-3,5}]M(do)$_x$ *via* treatment of anilide (TriNOx)Ce[NH{$C_6H_3(CF_3)_2$-3,5}] ($TriNOx^{3-}$ = N{$CH_2C_6H_4NO(tBu)$}$_3$) with alkali–metal bis(trimethylsilyl)amides.[14] Despite the breakthrough successes in Ln(III) and Ce(IV) terminal imide chemistry, corresponding Ln(II) complexes have remained elusive. In fact, the first divalent rare-earth-metal organoimide complexes $[Ln(NAr^{iPr})(thf)]_4$ (Ln = Sm, Eu, Yb) were reported only in 2018 (**II**, Fig. 1),

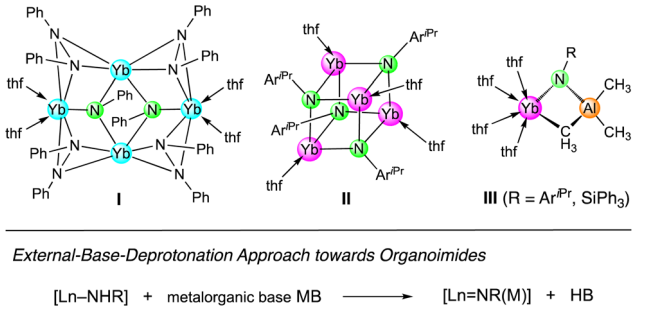

Fig. 1 Top: Selected examples of ytterbium imide complexes. Bottom: External base approach towards rare-earth-metal imide complexes.

Institut für Anorganische Chemie, Eberhard Karls Universität Tübingen, Auf der Morgenstelle 18, 72076 Tübingen, Germany.
E-mail: reiner.anwander@uni-tuebingen.de

† Electronic supplementary information (ESI) available. CCDC 2248520–2248541. For ESI and crystallographic data in CIF or other electronic format see DOI: https://doi.org/10.1039/d3dt00861d

according to the protonolysis of $[Ln(CH_2Ph)_2]_n$ with the respective aniline.[15] Moreover, treatment of $[Ln(AlMe_4)_2]_n$ (Ln = Sm, Eu, Yb) with potassium primary amides KNHR (R = $C_6H_3iPr_2$-2,6, $SiPh_3$) gave Lewis-acid-stabilized monolanthanide imides such as $Yb(NAr^{iPr})(AlMe_3)(thf)_4$ (**III**, Fig. 1).[16]

Here, we report on the synthesis and characterization of divalent primary amide complexes of ytterbium, $Tp^{tBu,Me}Yb(NHR)(thf)_x$ (R = $Ar^{R'}$, $SiPh_3$), bearing the superbulky scorpionate ligand hydrotris(3-*t*Bu-5-Me-pyrazolyl)borato. Such discrete complexes can be obtained according to one-pot salt metatheses [protocol: $YbI_2(thf)_2$/$KTp^{tBu,Me}$/K(NHR)] or protonolysis [protocol: $Yb[N(SiMe_3)_2]_2(thf)_2$/$HTp^{tBu,Me}$/H_2NR]. The reactivity of $Tp^{tBu,Me}Yb(NHR)(thf)_x$ was probed towards alkali–metal bases, Lewis acids, different donors and oxidants.

Results and discussion

Synthesis of primary amides $Tp^{tBu,Me}Yb(NHR)(thf)_x$

As depicted in Scheme 1, two protocols were applied for the synthesis of the ytterbium(II) primary amides **1–4**. Approach **A** follows a one-pot salt-metathesis reaction with equimolar amounts of $YbI_2(thf)_2$, $KTp^{tBu,Me}$ and KNHR. Route **B** utilizes Takat's compound $Tp^{tBu,Me}Yb[N(SiMe_3)_2]$[17] in protonolysis reactions with primary amines. The heteroleptic silylamide precursor was synthesized smoothly by reacting $Yb[N(SiMe_3)_2]_2(thf)_2$ (ref. 18) with the proligand hydrotris(3-*t*Bu-5-Me-pyrazolyl)borate $HTp^{tBu,Me}$ in THF. Protonolysis protocol **B** offers the advantage of choosing from a broad variety of amines and avoiding extensive metathesis-salt impurities. The primary amines H_2NR (R = $C_6H_3iPr_2$-2,6 = Ar^{iPr} = Dipp, $C_6H_3Me_2$-2,6 = Ar^{Me}, $C_6H_3(CF_3)_2$-3,5 = Ar^{CF3}, $SiPh_3$) were chosen according to their steric bulk and Brønsted acidity as the main criteria.

Since amine H_2NAr^{iPr} has proven useful in previous syntheses of rare-earth-metal imides, it was also the starting point for assessing the feasibility of approaches **A** and **B**. Complex $Tp^{tBu,Me}Yb(NHAr^{iPr})(thf)$ (**1^{thf}**) could be accessed *via* both methods in good to very good yields. Crystals suitable for X-ray diffraction (XRD) analysis were grown from saturated *n*-hexane solutions at −40 °C as orange needles (space group *C*2/*c*). The ytterbium metal in **1^{thf}** is coordinated by the $Tp^{tBu,Me}$ ligand in

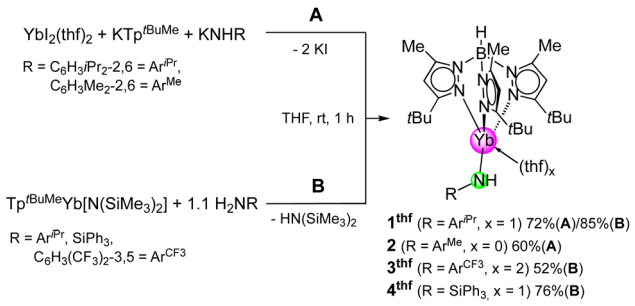

Scheme 1 Salt-metathesis (**A**) and protonolysis approaches (**B**) towards primary amides $Tp^{tBu,Me}Yb(NHR)(thf)_x$.

Table 1 Selected interatomic distances of amide complexes under study

Complex	Ln–N_{amido} [Å]	Ln–pz(N2/4/6)$_{avg.}$ [Å]	Ln–N–C(Ar) [°]
1^{thf}	2.353(4)	2.519	147.8(3)
1	2.345(5)	2.427	139.1(4)
2	2.30(3)/2.29(3)	2.423	150(2)
3^{thf}	2.411(12)/2.411(12)	2.511	143.2(19)/145.4(10)
4^{thf}	2.341(3)/2.287(10)	2.480	Yb–N–Si: 154.0(2)
$1^{thf,Sm}$	2.483(2)	2.636	157.46(18)
$1^{thf,Eu}$	2.474(17)/2.48(3)	2.618	158.4(16)/159(2)
1^{py}	2.358(4)	2.493	147.6(3)
1^{dmap}	2.3443(16)	2.499	138.03(12)
3^{dmap}	2.372(6)	2.474	144.6(6)
4^{dmap}	2.337(3)	2.500	Yb–N–Si: 149.92(18)
6	2.513(9)/2.510(9)	2.402	136.0(10)/126.3(10)
7	2.471(14)/2.477(12)	2.433	140.0(13)/131.6(14)
9a	2.160(2)	2.369	156.08(19)
10a	2.2131(14)	2.357	137.42(11)
9b	2.162(2)	2.374	155.52(16)
10b	2.253(3)	2.349	136.6(2)
11	2.233(3)	2.396	136.0(2)

κ³-fashion with a Yb–pz(N2/4/6) distances averaging 2.519 Å (Table 1, Fig. 2), hence being slightly longer than the respective ones in $Tp^{tBu,Me}YbI(thf)$ (av. 2.453 Å),[17] $Tp^{tBu,Me}Yb[N(SiMe_3)_2]$ (av. 2.462 Å)[17] or $Tp^{tBu,Me}Yb(CH_3)(thf)$ (av. 2.476 Å).[19] The coordination sphere is completed by the amido ligand (Yb–$N7_{amido}$, 2.353(4) Å; Yb–N_{amido}–Ar(C), 147.8(3)°) and one thf molecule (O1). The complex geometry is best described as distorted trigonal bipyramidal where N2, N6 and N7 form the basis of the bipyramid and O1 and N4 occupy the apical positions. Performing approach **A** in toluene as a solvent (not shown in Scheme 1) afforded the donor-free complex $Tp^{tBu,Me}Yb(NHAr^{iPr})$ (**1**) as red needles in moderate crystalline yield (72%, space group $P2_1/n$). Four-coordinate complex **1** features also a κ³-coordinated $Tp^{tBu,Me}$ ligand (Fig. 2). Overall, the pyrazole nitrogen atoms N2, N4 and N6 form the base of a distorted trigonal pyramid with the apical amido nitrogen atom N7. The Yb–$pz(N)_{avg}$ distances of av. 2.427 Å are considerably shorter than those in **1^{thf}**, while the Yb–$N7_{amido}$ distance of 2.345(5) Å is in the same range (Table 1). The absence of the thf donor implies a more acute Yb–N7–C25 angle of 139.1(4)°. The ^{1}H-NMR spectrum of crystalline **1^{thf}** shows the expected signal set (Fig. S1†) with a very broad signal at 4.81 ppm for the BH moiety, which is typical for complexes bearing Tp ligands.[10,17,19]

The resonance of the amido proton was detected at 3.78 ppm as a singlet with low intensity. The absence of coordinating thf in complex **1** only marginally affects the chemical shifts in the ^{1}H NMR spectrum, measured in C_6D_6 (see ESI†). Approach **A** is also viable for the synthesis of complexes $Tp^{tBu,Me}Ln(NHAr^{iPr})(thf)$ (**$1^{thf,Ln}$**) of the larger metals samarium and europium. Since these complexes are less stable and more prone to ligand redistribution, they have not been further considered for derivatization reactions. Complexes **$1^{thf,Sm}$** and **$1^{thf,Eu}$** are isostructural to **1^{thf}** (Fig. S51 and S52†). Interestingly, the elongated Ln–N distances entail significantly more obtuse Yb–N7–C25 angles (*ca.* 158°, Table 1).

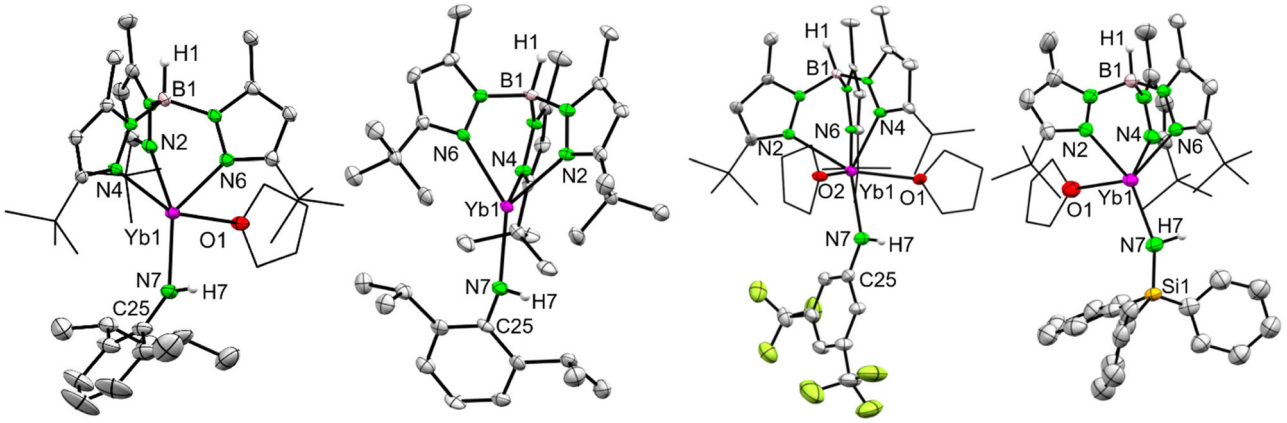

Fig. 2 Crystal structures of complexes $\mathbf{1}^{thf}$ (leftmost), **1** (left), $\mathbf{3}^{thf}$ (right) and $\mathbf{4}^{thf}$ (rightmost) with atomic displacement parameters set at 50% probability. For selected interatomic distances and angles, see Table 1 and ESI.† For complex $\mathbf{4}^{thf}$, only one molecule of the asymmetric unit is shown (see Fig. S48†).

Following a slightly modified salt-metathesis protocol **A** (Scheme 1), pre-isolated $Tp^{tBu,Me}YbI(thf)$ was treated with $KNHAr^{Me}$ to afford $Tp^{tBu,Me}Yb(NHAr^{Me})$ (**2**). Crystals of **2** could be grown from a saturated diethyl ether solution at −40 °C as yellow needles (space group $Pca2_1$). However, due the poor crystallization behaviour of **2**, XRD analysis resulted only in low-quality crystallographic data. Significant inseparable impurities are also indicated in the ^{1}H NMR spectrum of crystalline **2** (see ESI†). The molecular structure of **2** revealed the same connectivity as donor-free complex **1**. Surprisingly, despite carrying out the synthesis in THF, ytterbium complex **2** bearing the less sterically demanding amido ligand does not accommodate a thf donor molecule in the solid state as found for $\mathbf{1}^{thf}$. As for complex **1**, the pyrazole nitrogen atoms N2, N4 and N6 form the base of a distorted trigonal pyramid, revealing overall Yb–N distances in the range of complex **1** (Table 1, Yb–$pz(N2/4/6)_{avg}$ 2.423 Å, Yb–$N7_{amide}$ 2.30(3) Å), but a significantly obtuse Yb–N7–C25 angle (150(2)°). The equimolar reaction mixture $EuI_2(thf)_2$, $KTp^{tBu,Me}$ and $KNHAr^{Me}$ led to the isolation of homoleptic complex $Eu(Tp^{tBu,Me})_2$ (**5**), corroborating the preferred ligand redistribution in the presence of larger rare-earth metals. The crystal structure of **5** is isostructural with the samarium and ytterbium congeners, exhibiting europium centres with differently coordinated $Tp^{tBu,Me}$ ligands (κ^3- and κ^2-fashion, Fig. S57†).[20]

Complexes $Tp^{tBu,Me}Yb(NHAr^{CF3})(thf)_2$ ($\mathbf{3}^{thf}$) and $Tp^{tBu,Me}Yb(NHSiPh_3)(thf)$ ($\mathbf{4}^{thf}$), derived from the stronger Brønsted-acidic amine H_2NAr^{CF3} and H_2NSiPh_3, were obtained *via* aminolysis of $Tp^{tBu,Me}Yb[N(SiMe_3)_2]$ in THF (route **B**, Scheme 1). Both complexes readily crystallized from saturated *n*-hexane solutions at −40 °C as red needles (52%, space group *C*2/*c*) and red blocks (76%, space group *C*2/*c*), respectively. Complex $\mathbf{4}^{thf}$ is isostructural with $\mathbf{1}^{thf}$, but showing slightly shorter Yb–N distances (Table 1, Fig. 2). The Yb1–N7–Si1 angle of 154.0(2)° is larger than the previously discussed Yb–N–C_{ipso} angles and the silicon-bonded phenyl groups display a propeller-like arrangement. In contrast to the other primary amide complexes, the amido proton signal of crystalline complex $\mathbf{4}^{thf}$ was not observed in the ^{1}H NMR spectrum. Complex $\mathbf{3}^{thf}$ exhibits a coordination number of six, and thus, the highest found in this series. This is mainly attributed to the least direct steric shielding of the metal centre provided by this amido ligand. The Yb–N–C(Ar) angles in $\mathbf{3}^{thf}$ (143.2(10)°/145.4(10)°) are similar to those found in complex $\mathbf{1}^{thf}$. The ytterbium centre in $\mathbf{3}^{thf}$ adopts a very distorted octahedral coordination geometry with the pyrazole atoms N2/N6 and the thf atoms O1/O2 building the equatorial plane and the pyrazole and amido atoms N4 and N7, respectively, in the axial positions. The ^{1}H-NMR spectrum of complex $\mathbf{3}^{thf}$ shows very broadened thf signals, while the amido proton signal resonates at 4.13 ppm, significantly shifted to lower field compared to the signals found for complexes $\mathbf{1}^{thf}$/**1** (3.78 ppm/3.83 ppm).

Derivatization of primary amides $Tp^{tBu,Me}Yb(NHR)(thf)_x$

Initial derivatization reactions addressed the possibility of deprotonating the primary amido ligand in divalent complexes $Tp^{tBu,Me}Yb(NHR)(thf)_x$ ($\mathbf{1}^{thf}$, $\mathbf{3}^{thf}$, $\mathbf{4}^{thf}$). Unfortunately, all reactions with bases like $LiCH_3$, $LiCH_2SiMe_3$, $MN(SiMe_3)_2$ (M = Li, K, Cs), KCH_2Ph or phosphazene P_4-*t*Bu towards putative $[Tp^{tBu,Me}Yb(NR)M][HBase]$ (*cf.*, Fig. 1) were inconclusive (according to NMR spectroscopy) and did not result in any isolable product, even when the reaction was conducted at −40 °C. Also, prior exchange of the thf donor ligands in complexes $Tp^{tBu,Me}Yb(NHR)(thf)_x$ ($\mathbf{1}^{thf}$, $\mathbf{3}^{thf}$, $\mathbf{4}^{thf}$) for stronger *N*-donor ligands did not lead to isolable imide complexes. Most of the attempted deprotonation reactions resulted in a gradual darkening of the reaction mixture. Pyridine readily engaged in donor exchange with $\mathbf{1}^{thf}$ to afford $Tp^{tBu,Me}Yb(NHAr^{iPr})(py)$ ($\mathbf{1}^{py}$, not shown in Scheme 2),[21] as indicated by a colour change from red to black, but $\mathbf{1}^{py}$ displayed only poor crystallization behaviour (space group $P2_1/c$, crystal structure shown in the ESI†). In contrast, thf/4-dimethylaminopyridine (DMAP) exchange afforded better crystallizing products. Adducts $Tp^{tBu,Me}Yb(NHAr^{iPr})(dmap)$ ($\mathbf{1}^{dmap}$), $Tp^{tBu,Me}Yb$

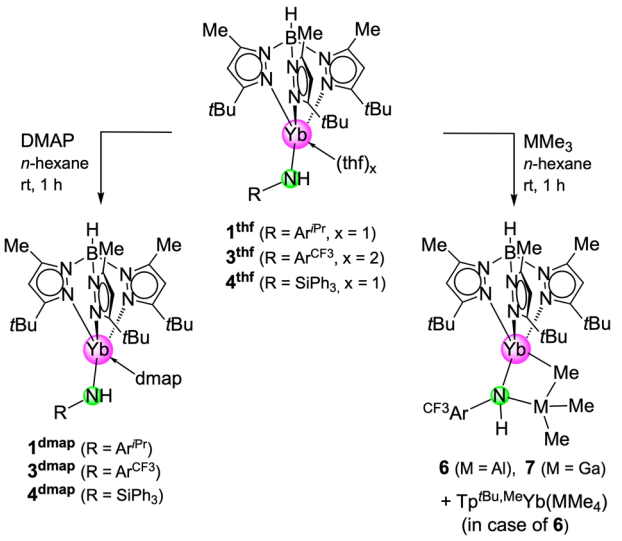

Scheme 2 Derivatization of complexes $Tp^{tBu,Me}Yb(NHR)(thf)_x$ with DMAP (donor exchange) and Lewis acids $AlMe_3$ and $GaMe_3$.

$(NHAr^{CF3})(dmap)$ ($\mathbf{3}^{\mathbf{dmap}}$) and $Tp^{tBu,Me}Yb(NHSiPh_3)(dmap)$ ($\mathbf{4}^{\mathbf{dmap}}$) were obtained by treatment of *n*-hexane solutions of $\mathbf{1}^{\mathbf{thf}}$, $\mathbf{3}^{\mathbf{thf}}$ and $\mathbf{4}^{\mathbf{thf}}$ with equimolar amounts of DMAP at ambient temperature (Scheme 2).

Red and yellow single-crystalline dmap adducts were obtained from *n*-hexane solutions at −40 °C in good to moderate yields ($\mathbf{1}^{\mathbf{dmap}}$, space group $P2_1/n$, 65%, red blocks; $\mathbf{3}^{\mathbf{dmap}}$, $P\bar{1}$, 58%, red plates; $\mathbf{4}^{\mathbf{dmap}}$, $P2_1/c$, 56%, yellow blocks) (Fig. 3). Donor exchange in mono(thf) adducts $\mathbf{1}^{\mathbf{thf}}$ and $\mathbf{4}^{\mathbf{thf}}$ led to an enhanced bending of the angle Yb1–N7–Ar(C_{ipso}) in $\mathbf{1}^{\mathbf{dmap}}$ and $\mathbf{4}^{\mathbf{dmap}}$ (147.8(3)° *versus* 138.03(12)°, 154.0(2)° *versus* 149.92 (18)°, Table 1), while only a marginal change was observed for the exchange of two thf molecules in $\mathbf{3}^{\mathbf{thf}}$ to yield $\mathbf{3}^{\mathbf{dmap}}$ (143.2 (19)°/145.4(10)° *versus* 144.6(6)°).

Since trimethylaluminium was shown to promote amido → imido conversion *via* deprotonation,[3,13,14] complex $\mathbf{3}^{\mathbf{thf}}$ with the sterically least demanding and most Brønsted-acidic anilido ligand, was probed in reactions with such group 13 alkyls. Accordingly, $\mathbf{3}^{\mathbf{thf}}$ was treated with 2 equivalents of $AlMe_3$ in *n*-pentane at ambient temperature. However, instead of the anticipated deprotonation towards putative imide $[Tp^{tBu,Me}Yb(NAr^{CF3})(AlMe_2)]$, competitive reactions towards adduct $Tp^{tBu,Me}Yb(NHAr^{CF3})(AlMe_3)$ (**6**) and known tetramethylaluminate complex $Tp^{tBu,Me}Yb(AlMe_4)$ took place.[22] Both complexes co-crystallized. Reducing the amount of $AlMe_3$ gave a mixture of the same reaction products in the solid-state. Surprisingly, $Tp^{tBu,Me}Yb(AlMe_4)$ could not be observed in the ^{1}H-NMR spectrum, which was also supported by only one signal in the ^{11}B-NMR spectrum (see ESI Fig. S33 and S34†). Compound **6** results from simple Lewis base/acid exchange. Similar rare-earth-metal-centred $AlMe_3$ adducts of primary amides have been described previously, *e.g.*, for $Cp^QYMe[NH(Ad)](AlMe_3)$ (Cp^Q = 2,3,4,5-tetramethyl-1-(8-quinolyl)cyclopentadienyl).[23] Crystals of **6** (yellow needles, space group $P2_1/c$) and $Tp^{tBu,Me}Yb(AlMe_4)$ (yellow prisms, $P1$) suitable for XRD analysis co-crystallized from saturated *n*-pentane solutions and were selected by handpicking. Due to the co-crystallization issue, complex **6** was further analysed only by ^{1}H-NMR spectroscopy (see ESI Fig. S33†). The 4-membered metallacycle featured by complex **6** involves ytterbium and aluminium and the bridging methyl and anilido ligands (Fig. 3). The Yb–N_{amido} distance of 2.513(9)/2.510(9) Å is elongated compared to precursor $\mathbf{3}^{\mathbf{thf}}$, while the Yb–C distance is longer than those in $Tp^{tBu,Me}Yb(AlMe_4)$ (2.702(3)/2.698(2) *versus* 2.810(6) Å (**6**)). Once more, the respective treatment of $\mathbf{3}^{\mathbf{thf}}$ with trimethylgallium revealed a distinct reactivity of the higher group 13 homologue.[10] Other than for the $\mathbf{3}^{\mathbf{thf}}/AlMe_3$ reaction, adduct $Tp^{tBu,Me}Yb(NHAr^{CF3})(GaMe_3)$ (**7**) was the only product and could be readily crystallized as yellow needles in 90% yield (space group $P2_1/c$, the formation of putative $[Tp^{tBu,Me}Yb(GaMe_4)]$ as a co-product was not observed).

Complex **7** is isotypical with the aluminium congener **6**. The 4-membered metallacycle in **7** displays Yb–N and Yb–C distances of 2.471(14)/2.477(12) Å and 2.868(8) Å, respectively. The switch from $AlMe_3$ to $GaMe_3$ bears also on the Yb1–N7–Ar(C_{ipso}) angles, indicating a widening for the gallium adduct (139.7(13)/131.8(12)° *versus* 135.9(8)/126.4(9)°). Noteworthy, on

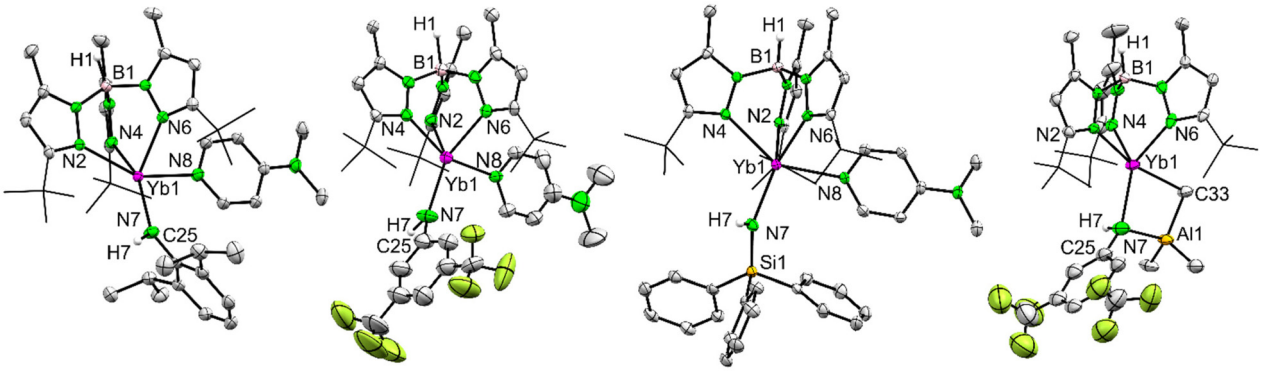

Fig. 3 Crystal structures of complexes $\mathbf{1}^{\mathbf{dmap}}$ (leftmost), $\mathbf{2}^{\mathbf{dmap}}$ (left), $\mathbf{4}^{\mathbf{dmap}}$ (right) and **6** (rightmost) with atomic displacement parameters set at 50% probability. For selected interatomic distances and angles, see ESI.†

one occasion, when treating $Tp^{tBu,Me}Yb(NHAr^{iPr})(thf)$ ($\mathbf{1}^{thf}$, contaminated with $Tp^{tBu,Me}YbI(thf)$) with $GaMe_3$, the separated ion pair $[(Tp^{tBu,Me})_2Yb_2I][NHAr^{iPr}(GaMe_3)_2]$ (**8**) could be crystallized. The crystal structure of **8** is shown in the ESI† and features the same anion as previously found in $[Tp^{tBu,Me}Nd(NHAr^{iPr})(thf)_2][NHAr^{iPr}(GaMe_3)_2]$.[10]

The ^{1}H-NMR signal of the amido proton of compound **7** was detected at 3.40 ppm, only slightly shifted to lower field compared to the free aniline H_2NAr^{iPr} (3.21 ppm). Complexes $\mathbf{1}^{thf}$ (3.78 ppm), **1** (3.83 ppm), and $\mathbf{3}^{thf}$ (4.13 ppm) display a more pronounced low-field shift of the amido proton, clearly indicating increased negative charge on the amido nitrogen atom. The $Ga(CH_3)_3$ moiety appeared as a sole, prominent singlet at 0.03 ppm, indicating a rapid exchange of the methyl groups at ambient temperature. Performing low temperature NMR experiments showed a splitting of this signal into two signals with an integral ratio of 2 : 1 matching the situation in the solid-state (Fig. 4). Heating solutions of complex **7** at 120 °C for 2 h did not result in any visible change of colour or change of the ^{1}H-NMR spectrum (see ESI Fig. S40†).

An alternative route to ytterbium imide complexes might involve oxidation/halogenation of divalent $Tp^{tBu,Me}Yb(NHR)(thf)_x$ to trivalent $[Tp^{tBu,Me}Yb(NHR)X(thf)_y]$ (X = halogenido), and subsequent alkylation, forcing alkali–metal salt elimination and amido deprotonation.[3] According to Scheme 3, complexes $\mathbf{1}^{thf}$ and $\mathbf{3}^{thf}$ were applied in halogenation protocols. The use of a slight excess of hexachloroethane C_2Cl_6 in THF solutions led to a slow colour change over 2 h from intensely red to turquoise (for complex $\mathbf{1}^{thf}$) and from red to purple (for complex $\mathbf{3}^{thf}$) indicating an oxidation reaction. After removing all volatiles and re-dissolving the residual solids in *n*-pentane, donor-free complexes $Tp^{tBu,Me}Yb(NHA^{iPr})(Cl)$ (**9a**, 77%) (intensely blue needles) and $Tp^{tBu,Me}Yb(NHAr^{CF3})(Cl)$ (**10a**, 72%) (purple needles) could be crystallized. The corresponding bromides $Tp^{tBu,Me}Yb(NHA^{iPr})(Br)$ (**9b**) (turquoise needles) and $Tp^{tBu,Me}Yb(NHAr^{CF3})(Br)$ (**10b**) (deep blue needles) were

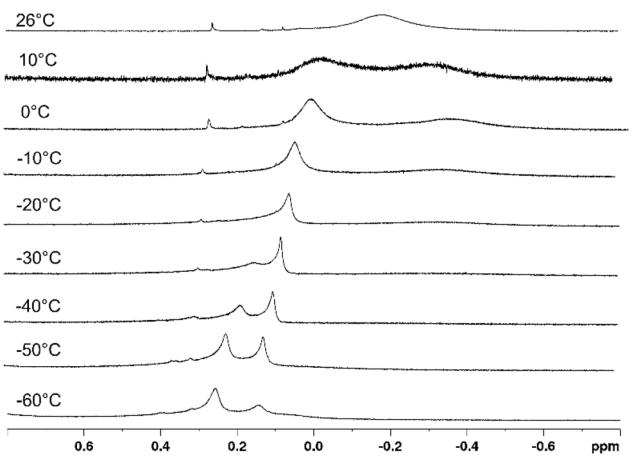

Fig. 4 Variable temperature ^{1}H NMR spectra of complex **7** in toluene-d_8, showing the metal alkyl region.

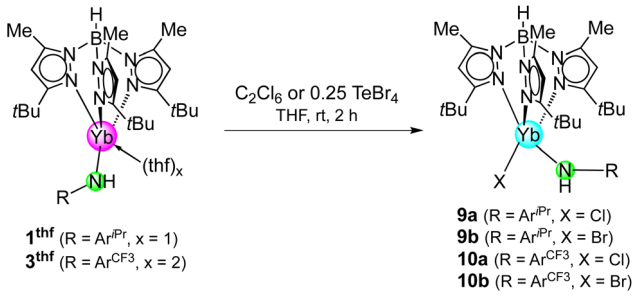

Scheme 3 Oxidative halogenation of complexes $\mathbf{1}^{thf}$ and $\mathbf{3}^{thf}$.

obtained by treatment of $\mathbf{1}^{thf}$ and $\mathbf{3}^{thf}$, respectively, with 0.25 equivalents $TeBr_4$.

The ytterbium(III) halide complexes **9** and **10** are isostructural (Fig. 5). The Yb^{III}–N(pz) distances range from 2.303(2) to 2.485(2) Å, and match those of other Yb^{III}–Tp complexes,[24] and more specifically those reported for $Tp^{Me,Me}YbCl_2(thf)$ (2.30(2) to 2.39(2) Å).[25] Striking are the distinct Yb1–N7–C25 angles which are much more obtuse for the $NHAr^{iPr}$ ligand (**9a**: 156.08(19)°; **9b**: 155.52(16)°; **10a**: 137.42(11)°, **10b**: 136.6 (2)°). A likely reason might be the reduced steric hindrance imparted by the *meta*-substituted ligand $NHAr^{CF3}$, resulting in a better fit into the gap between two pyrazole rings. The Cl/Br switch does not have a significant impact on the Yb^{III}–N (amido) distances (**9a**: 2.160(2) Å **9b**: 2.162(2) Å; **10a**: 2.2131 (14) Å **10b**: 2.253(3) Å). A similar connectivity has been observed for yttrium complex $Tp^{Me,Me}Y[N(SiMe_3)_2](Cl)(thf)$.[26]

Elemental iodine, azobenzene and silver triflate have been probed as alternative oxidants. The use of elemental iodine did not lead to putative $[Tp^{tBu,Me}Yb(NHR)(I)]$ but literature

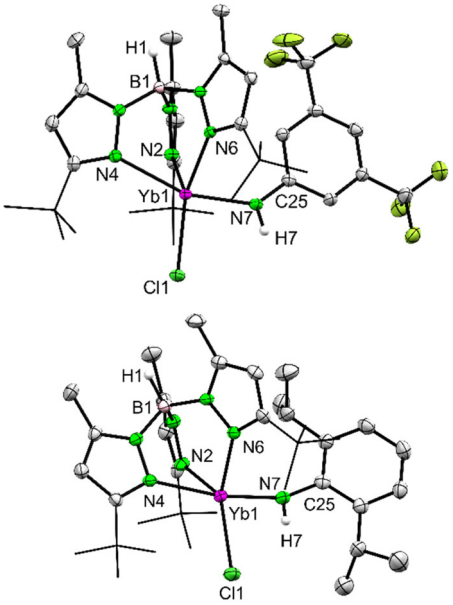

Fig. 5 Crystal structures of complexes **9a** (top) and **10a** (bottom) with atomic displacement parameters set at 50% probability. For selected interatomic distances and angles, see ESI.†

known divalent complex $Tp^{tBu,Me}YbI(thf)$[17] was the only isolable product. The equimolar reaction of $Tp^{tBu,Me}Yb(NHAr^{CF3})(thf)_2$ (**3^{thf}**) with azobenzene resulted simply in donor exchange and formation of divalent $Tp^{tBu,Me}Yb(NHAr^{CF3})(N_2Ph_2)$ (**11**) in high yield. Neither oxidation of the metal centre[27] nor degradation of PhN=NPh, *e.g.*, into an imido moiety, occurred.[1,28] The crystal structure of **11** is shown in the ESI† (Yb–N(amido) 2.233(3) Å, Yb(N_2Ph_2) 2.274(2) and 2.229(2) Å). Treatment of $Tp^{tBu,Me}Yb(NHAr^{iPr})(thf)$ (**1^{thf}**) with AgOTf in THF afforded oxidation of the ytterbium centre but was accompanied by partial degradation of the $Tp^{tBu,Me}$ ligand.[29] Crystallization of the *n*-hexane soluble fraction gave compound $Tp^{tBu,Me}Yb(pz^{tBu,Me})(OTf)$ (**12**) in low crystalline yield. The Yb–O(triflato) distance in 6-coordinate **12** amounts to 2.216(3) Å (for the crystal structure, see ESI†). Noteworthy, in complex $[(Tp^{Me,Me})_2Yb][OTf]$ the ytterbium centre maintains 6-coordination by forming a separated ion pair.[30]

Finally, alkylation of complex $Tp^{tBu,Me}Yb(NHAr^{CF3})(Cl)$ (**10a**) with MeLi (THF, −40 °C) and KCH_2Ph (*n*-hexane, −40 °C) has been attempted, but led only to $LiTp^{tBu,Me}$ and $(Tp^{tBu,Me})_2Yb$ as isolable products. Also, treatment of $Tp^{tBu,Me}Yb(NHA^{iPr})(Cl)$ (**9a**) with trimethylaluminium led to the reduction of the Yb(III) centre and formation of compound $Tp^{tBu,Me}{}_4Yb_5Cl_6$ (**13**). The $\{Yb_5\}$ cluster **13** features a central ytterbium atom coordinated by chlorido anions exclusively. Four peripheral ytterbium atoms are 5-coordinated by κ^3-$Tp^{tBu,Me}$ ligands and two bridging chloridos each (for a connectivity structure, see ESI†).

^{171}Yb-NMR spectroscopic studies

Ytterbium(II) ([Xe] $4f^{14}$) complexes are amenable to ^{171}Yb NMR spectroscopy (14.3% natural abundance, nuclear spin I = $\frac{1}{2}$, sensitivity relative to ^{1}H = 5.46×10^{-3}, positive gyromagnetic ratio (4.712×10^7 rad T^{-1} s^{-1})).[31] In the past decades, the number of reports on complexes characterized by ^{171}Yb NMR spectroscopy in the solid-state as well as in solution showed a steady increase.[32,33] The ^{171}Yb chemical shifts can be found in a broad range from +2500 to −500 ppm.[31] Representative examples are $[Yb(AlEt_4)_2]_n$ (363 ppm, C_6D_6),[34] $YbI_2(thf)_4$ (456 ppm, THF-d_8),[35] $Tp^{tBu,Me}Yb(AlMe_4)$ (505 ppm, C_6D_6),[22] $Yb(CH_2Ph)_2(thf)_4$ (562 ppm, THF-d_8),[36] $Yb[N(SiMe_3)_2]_2$ (796 ppm, toluene-d_8),[32a] $Tp^{tBu,Me}Yb[CH(SiMe_3)_2]$ (865 ppm, toluene-d_8),[37] $[YbMe_2]_n$ (954 ppm, δ_{iso}) and $Tp^{tBu,Me}Yb(CH_3)(thf)$ (1140 ppm, THF-d_8).[19] The ytterbium(II) anilide complexes $Tp^{tBu,Me}Yb(NHR)(donor)_x$ under study display ^{171}Yb chemical shifts in the range +863 to +718 ppm. The silylamide complexes $Tp^{tBu,Me}Yb(NHSiPh_3)(thf)$ (**4^{thf}**, $\delta(^{171}Yb)$ 863 ppm) and $Tp^{tBu,Me}Yb(NHSiPh_3)(dmap)$ (**4^{dmap}**, 954 ppm) show the furthest down-field shifted signals (Table 2). This is tantamount to an enhanced deshielding effect compared to the anilide complexes derived from ligands H_2NAr^{iPr} and H_2NAr^{CF3}. The ^{171}Yb chemical shift of complex $Tp^{tBu,Me}Yb[N(SiMe_3)_2]$ was detected at 711 ppm.[37] Striking is the significant down-field shift upon thf/dmap donor exchange. Displacement of the donor THF with a Lewis acid like $GaMe_3$ in complex $Tp^{tBu,Me}Yb(NHAr^{CF3})(GaMe_3)$ (**7**) leads to a high-field shift of the ^{171}Yb signal (582 ppm), in analogy to the tetramethylaluminate complex $Tp^{tBu,Me}Yb(AlMe_4)$ (505 ppm).[22]

Table 2 ^{171}Yb-NMR chemical shifts of amide complexes under study[a]

Complex	**1**	**1^{thf}**	**3^{thf}**	**4^{thf}**
$\delta(^{171}Yb)$ [ppm]	750	718	763	863
Complex	**1^{dmap}**	**3^{dmap}**	**4^{dmap}**	**8**
$\delta(^{171}Yb)$ [ppm]	776	862	954	582

[a] Determined by ^{1}H–^{171}Yb HSQC spectroscopy (500 MHz, 87.52 MHz) in C_6D_6 at ambient temperature.

Conclusions

Divalent heteroleptic ytterbium amides $[Tp^{tBu,Me}Yb(NHR)(thf)_x]$ (R = Ar^{iPr}, Ar^{Me}, Ar^{CF3}, $SiPh_3$) are accessible either by one-pot salt-metathesis reactions involving intermediate $Tp^{tBu,Me}YbI(thf)$ and potassium amides or following a protonolysis protocol starting from $Tp^{tBu,Me}Yb[N(SiMe_3)_2]$ with the corresponding aniline/amine. Like shown for trivalent rare-earth-metal chemistry, DMAP acts as a stronger donor than THF, giving readily access to complexes $Tp^{tBu,Me}Yb(NHR)(dmap)$ (R = Ar^{iPr}, Ar^{CF3}, $SiPh_3$). The THF donor ligand is also easily displaced by Lewis acids MMe_3 (M = Al, Ga) as revealed for the isolation of thermally stable $Tp^{tBu,Me}Yb(NHAr^{CF3})(MMe_3)$. Moreover, divalent $[Tp^{tBu,Me}Yb(NHR)(thf)_x]$ (R = Ar^{iPr}, Ar^{CF3}) are readily oxidised by halogenating reagents to yield ytterbium(III) complexes $[Tp^{tBu,Me}Yb(NHR)(X)]$ (R = Ar^{iPr}, Ar^{CF3}; X = Cl, Br). Unfortunately, both divalent $[Tp^{tBu,Me}Yb(NHR)(thf)_x]$ and trivalent $[Tp^{tBu,Me}Yb(NHR)(X)]$ did not engage in any conclusive deprotonation reactions towards the putative ytterbium(II) imide ate complexes $[Tp^{tBu,Me}Yb(=NR)M][HBase]$ aimed for.

Experimental

General considerations

All operations were performed under exclusion of oxygen and water, using standard Schlenk procedures and glovebox techniques (MBraun MB200B <0.1 ppm O_2, <0.1 ppm H_2O) in oven-dried glassware. Solvents were purified using Grubbs-type columns (MBraun SPS solvent purification system). Tetrahydrofuran was stored over activated molecular sieves (3 Å). Deuterated solvents were purchased from Aldrich or Eurisotop and were stored over Na/K alloy in a glovebox. Potassium bis(trimethylsilyl)amide $K[N(SiMe_3)_2]$ (95%, Sigma Aldrich) was sublimed before use and stored in a glovebox. The newly synthesized complexes are stored at ambient temperature or at −40 °C under inert atmospheres, respectively. The proligand hydrotris(3-*tert*-butyl-5-methylpyrazolyl)borate ($HTp^{tBu,Me}$)[38] and the ytterbium(II) precursors $YbI_2(thf)_2$[1] and $Tp^{tBu,Me}Yb[N(SiMe_3)_2]$[37] were synthesized according to slight

modifications of the literature procedures. The NMR spectra of air- and moisture-sensitive compounds were recorded by using J. Young-valved NMR tubes on a BRUKER AVIII+300 (^{1}H: 300.13 MHz, ^{11}B: 96.29 MHz, ^{13}C: 59.63 MHz), a BRUKER AVII+400 instrument (^{1}H: 400.13 MHz, ^{13}C: 100.61 MHz) or a Bruker AVII+500 (^{1}H: 500.13 MHz, ^{11}B: 160.46 MHz, ^{13}C: 125.76 MHz, ^{171}Yb: 87.52 MHz). The residual solvent signals are referenced to TMS.[39] Elemental analyses (C, H, N) were performed with an Elementar Vario Micro Cube.

Synthesis of [Tp^{tBu,Me}Yb(NHAr^R)(thf)$_x$]. In a standard procedure, $YbI_2(thf)_2$ (300 mg, 0.53 mmol) was dissolved in 6 ml THF. KTp^{tBu,Me} (242.5 mg, 0.53 mmol) in 2 ml THF was added slowly under stirring. After 10 min KNHAr^R (R = 2,6-iPr: 113.1 mg, 0.53 mmol; R = 2,6-Me: 83.7 mg, 0.53 mmol) in 2 ml THF was added dropwise and the stirring continued for 1 h at ambient temperature. After removal of all volatiles under reduced pressure, the residual solids were extracted with *n*-hexane (3 × 2 ml). The volume of the combined phases was reduced under vacuum and the solution stored at −40 °C.
Alternative route: In a standard procedure, to a solution of Tp^{tBu,Me}Yb[N(SiMe$_3$)$_2$] (500 mg, 0.660 mmol) in 5 ml THF a solution of NH_2R (R = Ar^{iPr}: 128 mg, 0.721 mmol, R = Ar^{CF3}: 226 mg, 0.990 mmol; R = $SiPh_3$: 181.9 mg, 0.660 mmol) in 2 ml THF was added dropwise and the stirring continued for 1 h at ambient temperature. After removal of all volatiles under reduced pressure, the residual solids were extracted with *n*-hexane (3 × 2 ml). The volume of the combined phases was reduced under vacuum and the solution stored at −40 °C.

Tp^{tBu,Me}Yb(NHAr^{iPr})(thf) (1^{thf}). The product was obtained as orange needles in 85% yield. ^{1}H NMR (500 MHz, C_6D_6, 26 °C): δ 7.32 (d, 2 H, Ar–H_{meta}), 6.86 (t, 1 H, Ar–H_{para}), 5.70 (s, 3 H, pz-*H*), 4.81 (br, 1 H, B*H*), 3.78 (s, 1 H, N*H*), 3.52 (sept., 2 H, C*H*Me$_2$), 2.17 (s, 9 H, pz-CH_3), 1.49 (d, 12 H, CH(CH_3)$_2$), 1.38 (s, 27 H, pz-C(CH_3)$_3$) ppm. ^{11}B{^{1}H} NMR (160 MHz, [D$_8$]thf, 26 °C): δ −7.96 (s, br) ppm. ^{13}C{^{1}H} NMR (125 MHz, [D$_8$]thf, 26 °C): δ 163.4 (3-pz-C), 157.3 (*ipso*-Ar–C), 145.7 (5-pz-C), 132.3 (*o*-Ar–C), 121.9 (*p*-Ar–C), 110.4 (*m*-Ar–C), 103.1 (4-pz-C), 68.0 (O*C*H$_2$–CH$_2$), 32.3 (pz-C(*C*H$_3$)$_3$), 31.3 (pz-*C*(CH$_3$)$_3$), 28.7 (*C*H(CH$_3$)$_2$), 26.2 (OCH$_2$–*C*H$_2$), 24.0 (CH(*C*H$_3$)$_2$), 13.6 (pz-*C*H$_3$) ppm. ^{171}Yb from ^{1}H–^{171}Yb HSQC (500.13 MHz, 87.52 MHz, C_6D_6, 26 °C): 718 ppm. IR Nujol (CsI, cm^{-1}): 2953 (vs, Nujol, C–H), 2924 (vs, Nujol, C–H), 2852 (vs, Nujol, C–H), 2724 (vw), 2688 (vw), 1588 (vw), 1541 (w), 1461 (vs, Nujol), 1377 (vs, Nujol), 1366 (w), 1337 (w), 1305 (vw), 1260 (w), 1241 (vw), 1200 (vw), 1179 (vw), 1068 (vw), 1028 (vw), 1010 (vw), 983 (vw), 921 (vw), 876 (vw), 772 (w), 736 (w), 725 (w), 647 (vw). Elemental analysis calcd (%) for $C_{40}H_{66}BN_7OYb$ (844.88 g mol^{-1}): C 56.86, H 7.87, N 11.61; found C 56.67, H 7.51, N 11.09.

Tp^{tBu,Me}Yb(NHAr^{iPr}) (1). The reaction was performed as described above but the solvent was changed to toluene. The product was obtained as orange crystals in 72% yield. ^{1}H NMR (500 MHz, C_6D_6, 26 °C): δ 7.28 (d, 2 H, Ar–H_{meta}), 6.83 (t, 1 H, Ar–H_{para}), 5.68 (s, 3 H, pz-*H*), 4.78 (br., 1 H, B*H*), 3.83 (s, 1 H, N*H*), 3.43 (sept, 3 H, C*H*(CH$_3$)$_2$, 2.15 (s, 9 H, pz-CH_3), 1.45 (d, 12 H, CH(CH_3)$_2$), 1.36 (s, 27 H, pz-C(CH_3)$_3$) ppm. ^{11}B{^{1}H} NMR (160 MHz, C_6D_6, 26 °C): δ −8.16 (s, br) ppm. ^{13}C{^{1}H} NMR (125 MHz, C_6D_6, 26 °C): δ 163.8 (3-pz-*C*), 156.9 (*ipso*-Ar–C), 145.9 (5-pz-*C*), 132.0 (o-C–Ar), 122.7 (*p*-C–Ar), 111.5 (*m*-C–Ar), 103.1 (4-pz-C), 32.1 (pz-C(*C*H$_3$)$_3$), 31.1 (pz-*C*(CH$_3$)$_3$), 29.6 (Ar–*C*H(CH$_3$)$_2$), 24.0 (Ar–CH(*C*H$_3$)$_2$), 13.6 (pz-*C*H$_3$) ppm. ^{171}Yb from ^{1}H–^{171}Yb HSQC (500.13 MHz, 87.52 MHz, C_6D_6, 26 °C): 750 ppm. IR Nujol (CsI, cm^{-1}): 3175 (vw). 3047 (vw), 2953 (vs, Nujol, C–H), 2923 (vs, Nujol, C–H), 2854 (vs, Nujol, C–H), 2583 (vw), 1815 (vw), 1588 (w), 1539 (s), 1461 (vs, Nujol), 1420 (vs), 1377 (vs, Nujol), 1363 (vs), 1335 (s), 1261 (s), 1241 (m), 1204 (m), 1177 (vs), 1150 (w), 1112 (vw), 1068 (s), 1024 (w), 1012 (w), 983 (w), 925 (vw), 882 (vw), 839 (w), 817 (vw), 782 (s), 770 (s), 731 (s), 679 (w), 646 (m), 623 (vw), 563 (vw), 536 (vw), 514 (w). Elemental analysis calcd (%) for $C_{36}H_{58}BN_7Yb$ (772.77 g mol^{-1}): C 55.95, H 7.57, N 12.69; found C 55.79, H 7.66, N 11.88.

Tp^{tBu,Me}Yb(NHAr^{Me}) (2). (Tp^{tBu,Me})YbI (150.4 mg, 0.189 mmol) was dissolved in 6 ml THF. KNHAr^{Me} (30.1 mg, 0.189 mmol) in 2 ml THF was added dropwise and the mixture was stirred for 1 h at ambient temperature. After removal of all volatiles under reduced pressure, the residual solids were extracted with *n*-hexane (3 × 2 ml). The volume of the combined phases was reduced under vacuum and the solution stored at −40 °C. The product was obtained in 60% (80 mg) crude yield. Crystals suitable for XRD analysis could be obtained from a saturated diethyl ether solutions. ^{1}H NMR (500 MHz, C_6D_6, 26 °C): δ 7.29 (d, 2 H, Ar–H_{meta}), 6.68 (t, 1 H, Ar–H_{para}), 5.71 (s, 3 H, pz-*H*), 4.80 (br, 1 H, B*H*), 3.90 (s, 1 H, N*H*), 2.55 (s, 6 H, Ar–(CH_3)$_2$), 2.16 (s, 9 H, pz-CH_3), 1.35 (s, 27 H, pz-C(CH_3)$_3$) ppm.

Tp^{tBu,Me}Yb(NHAr^{CF3})(thf)$_2$ (3^{thf}). The product was obtained as red crystals in 51% yield. ^{1}H NMR (500 MHz, C_6D_6, 26 °C): δ 7.13 (d, 2 H, Ar–H_{ortho}), 7.09 (s, 1 H, Ar–H_{para}), 5.66 (s, 3 H, pz-*H*), 4.79 (br, 1 H, B*H*), 4.13 (s, 1 H, N*H*), 3.01 (br., 4 H, THF O(CH_2)$_2$(CH$_2$)$_2$), 2.17 (s, 9 H, pz-CH_3), 1.32 (s, 27 H, pz-C(*C*H$_3$)$_3$), 1.07 (br, 4 H, THF O(CH$_2$)$_2$(*C*H$_2$)$_2$) ppm. ^{11}B{^{1}H} NMR (160 MHz, C_6D_6, 26 °C): δ −8.1 (s, br) ppm. ^{13}C{^{1}H} NMR (125 MHz, C_6D_6, 26 °C): δ 163.4 (3-pz-*C*), 163.1 (*ipso*-Ar–*C*), 145.5 (5-pz-*C*), 132.4 (*C*F$_3$), 124.0 (*m*-Ar–*C*), 115.4 (*o*-Ar–*C*), 102.9 (4-pz-*C*), 101.6 (*p*-Ar–*C*), 68.7 (O–*C*H$_2$–CH$_2$), 32.2 (pz-*C*(CH$_3$)$_3$), 31.1 (pz-C(*C*H$_3$)$_3$), 25.4 (O–CH$_2$–*C*H$_2$), 13.5 (pz-*C*H$_3$) ppm. ^{171}Yb from ^{1}H–^{171}Yb HSQC (500.13 MHz, 87.52 MHz, C_6D_6, 26 °C): 763 ppm. IR Nujol (CsI, cm^{-1}): 3275 (vw), 3123 (vw), 2954 (vs, Nujol, C–H), 2924 (vs, Nujol, C–H), 2854 (vs, Nujol, C–H), 2729 (vw), 2666 (vw), 2553 (vw), 1622 (w), 1597 (s), 1541 (s), 1462 (vs, Nujol), 1394 (vs), 1378 (vs, Nujol), 1359 (s), 1337 (m), 1296 (w), 1274 (vs), 1240 (w), 1207 (w), 1170 (vs), 1122 (vs), 1068 (m), 1031 (w), 1011 (w), 986 (s), 945 (m), 921 (vw), 877 (w), 844 (m), 796 (m), 781 (m), 770 (s), 723 (m), 696 (w), 679 (m), 644 (m), 595 (w), 584 (w), 562 (vw), 515 (vw), 509 (vw). Elemental analysis calcd (%) for $C_{43}H_{67}BF_6N_7O_2Yb$ (968.81 g mol^{-1}): C 49.59, H 6.24, N 10.12; found C 48.0, H 7.66, N 10.92.

Tp^{tBu,Me}Yb(NHSiPh$_3$)(thf) (4^{thf}). The product was obtained as red crystals in 76% yield. ^{1}H NMR (400 MHz, C_6D_6, 26 °C): δ 8.09 (d, 6 H, Ph–H_{ortho}), 7.33 (t, 6 H, Ph–H_{meta}), 7.26 (t, 3 H, Ph–H_{para}), 5.68 (s, 3 H, pz-*H*), 4.80 (broad, 1 H, B–*H*), 3.35

(broad, 4 H, THF-*H*), 2.18 (s, 9 H, pz-CH_3), 1.36 (s, 27 H, pz-C(CH_3)$_3$) ppm. The N–H signal as well thf signals (partially) were not detected. ^{11}B{^{1}H} NMR (160 MHz, C_6D_6, 26 °C): δ −7.73 (s, br) ppm. ^{13}C{^{1}H} UDEFT NMR (125 MHz, C_6D_6, 26 °C): δ 163.0 (3-pz-*C*), 145.1 (5-pz-*C*), 136.4 (*o*–PhC), 128.4 (*m*–PhC), 127.5 (*p*–PhC), 102.7 (4-pz-*C*), 68.8 (O–*C*H$_2$–CH$_2$), 32.1 (pz-C(*C*H$_3$)$_3$), 31.4 (pz-*C*(CH$_3$)$_3$), 26.0 (O–CH$_2$–*C*H$_2$), 13.6 (pz-*C*H$_3$) ppm. ^{171}Yb from ^{1}H–^{171}Yb HSQC (500.13 MHz, 87.52 MHz, C_6D_6, 26 °C): 863 ppm. IR Nujol (CsI, cm^{-1}): 3062 (vw), 3042 (vw), 2923 (vs, Nujol, C–H), 2857 (vs, Nujol, C–H), 2728 (vw), 2521 (vw), 1539 (vw), 1461 (vs, Nujol), 1377 (vs, Nujol), 2364 (w), 1338 (vw), 1302 (vw), 1241 (vw), 1198 (vw), 1170 (vw), 1101 (vw), 1063 (vw), 1029 (vw), 1009 (vw), 982 (vw), 911 (w), 848 (vw), 785 (vw), 766 (vw), 739 (vw), 699 (vw), 644 (vw). Elemental analysis calcd (%) for $C_{46}H_{64}BN_7OSiYb$ (943.02 g mol^{-1}): C 58.59, H 6.84, N 10.40; found C 58.26, H 7.15, N 9.97.

Tp^{tBu,Me}Sm(NHAr^{iPr})(thf) (1^{thf,Sm}). To a solution of $SmI_2(thf)_2$ (120 mg, 0.219 mmol) in 3 ml THF solutions of KTp^{tBu,Me} (101 mg, 0.219 mmol) in 3 ml THF and KNHAr^{iPr} (47.1 mg, 0.219 mmol) in 3 ml THF were added slowly. The mixture was stirred for 2 h at ambient temperature. After filtration, the solvent of the filtrate was removed under reduced pressure and the residual solids were dissolved in *n*-hexane and stored at −40 °C. The product was obtained as green blocks in 45% (84 mg) crystalline yield. Elemental analysis calcd (%) for $C_{40}H_{66}BN_7OSm$ (822.19 g mol^{-1}): C 58.43, H 8.09, N 11.93; found C 58.11, H 7.73, N 11.37.

Tp^{tBu,Me}Eu(NHAr^{iPr})(thf) (1^{thf,Eu}). To a solution of $EuI_2(thf)_2$ (25 mg, 0.046 mmol) in 2 ml THF solutions of KTp^{tBu,Me} (20.2 mg, 0.046 mmol) in 2 ml THF and KNHAr^{iPr} (9.9 mg, 0.046 mmol) in 2 ml THF were added slowly. The mixture was stirred for 2 h at ambient temperature. After filtration, the solvent of the filtrate was removed under reduced pressure and the residual solids were dissolved in *n*-hexane and stored at −40 °C. The product was obtained as yellow plates in 32% (12 mg) crystalline yield. Elemental analysis calcd (%) for $C_{40}H_{66}BN_7OEu$ (823.76 g mol^{-1}): C 58.32, H 8.08, N 11.90; found C 58.23, H 7.70, N 12.37.

Tp^{tBu,Me}Yb(NHAr^{iPr})(py) (1^{py}). To a solution of **1^{thf}** (76 mg, 0.09 mmol) in 2 ml THF, pyridine (7.1 mg, 0.09 mmol) in 2 ml THF was added slowly. The mixture was stirred for 2 h at ambient temperature. All volatiles were removed under reduced pressure and the residual solids were dissolved in *n*-hexane and stored at −40 °C. The product was obtained as black needles. Yield 30% (22.8 mg). No further analytics was performed.

[Tp^{tBu,Me}Yb(NHR)(dmap)]. In a standard procedure, to a solution of [Tp^{tBu,Me}Yb(NHR)(thf)$_n$] (R = iPr 50 mg, 0.059 mmol; R = CF_3, 50 mg, 0.052 mmol; R = $SiPh_3$, 50 mg, 0.053 mmol) in 2 ml *n*-hexane a solution of DMAP (2.3 mg, 0.019 mmol) in 1 ml *n*-hexane was added dropwise and stirred for 1 h at ambient temperature. After removal of all volatiles under reduced pressure, the residual solids were extracted with *n*-hexane (3 × 1 ml). The volume of the combined phases was reduced under vacuum and the concentrated solution stored at −40 °C.

Tp^{tBu,Me}Yb(NHAr^{iPr})(dmap) (1^{dmap}). The product was obtained as red crystals in 65% yield. ^{1}H NMR (500 MHz, C_6D_6, 26 °C): δ. 7.80 (s, 2 H, DMAP-H_{ortho}), 7.42 (d, 2 H, Ar-H_{meta}), 6.92 (t, 1 H, Ar-H_{para}), 5.79 (s, 3 H, pz-*H*), 5.68 (DMAP-H_{meta}), 4.97 (br, 1 H, B*H*), 4.04 (s, 1 H, N*H*), 3.83 (sept, 2 H, C*H*(Me)$_2$, 2.32 (s, 9 H, pz-CH_3), 1.90 (s, 6 H, N(CH_3)$_2$), 1.59 (d, 12 H, CH(CH_3)$_2$), 1.36 (s, 27 H, pz-C(CH_3)$_3$) ppm. ^{11}B{^{1}H} NMR (160 MHz, C_6D_6, 26 °C): δ −7.5 (s, br) ppm. ^{13}C UDEFT NMR (125 MHz, C_6D_6, 26 °C): δ 163.6 (3-pz-C), 157.6 (Ar-C$_{ipso}$), 154.3 (DMAP-C$_{para}$), 149.7 (DMAP-C$_{ortho}$), 145.2 (5-pz-*C*), 132.5 (Ar-*C*$_{ortho}$), 122.9 (Ar-*C*$_{para}$), 111.0 (Ary-*C*$_{meta}$), 106.3 (DMAP-*C*$_{meta}$), 103.3 (4-pz-*C*), 37.9 (DMAP-C(*C*H$_3$)$_2$), 32.1 (*C*(CH$_3$)$_3$), 31.2 (C(*C*H$_3$)$_3$), 28.8 (Ary-*C*HMe$_2$), 24.5 (Ar-CH(*C*H$_3$)$_2$), 13.8 (pz-*C*H$_3$) ppm. ^{171}Yb from ^{1}H–^{171}Yb HSQC (500.13 MHz, 87.52 MHz, C_6D_6, 26 °C): 776 ppm. IR Nujol (CsI, cm^{-1}): 3161 (vw), 2954 (vs), 2924 (vs, Nujol, C–H), 2854 (vs, Nujol, C–H), 2725 (vw), 2561 (vw), 1610 (vs), 1589 (m), 1539 (vs), 1461 (vs, Nujol), 1417 (vs), 1378 (vs, Nujol), 1364 (vs), 1335 (s), 1304 (vw), 1261 (s), 1234 (s), 1200 (s), 1176 (s), 1147 (w), 1113 (w), 1065 (s), 982 (w), 949 (w), 883 (vw), 837 (w), 806 (m), 784 (vs), 770 (s), 744 (s), 679 (vw), 645 (m), 532 (w). Elemental analysis calcd (%) for $C_{43}H_{68}BN_9Yb$ (894.93 g mol^{-1}): C 57.71, H 7.66, N 14.09; found C 57.75, H 7.82, N 13.97.

Tp^{tBu,Me}Yb(NHAr^{CF3})(dmap) (3^{dmap}). The product was obtained as red crystals in 58% yield. ^{1}H NMR (500 MHz, C_6D_6, 26 °C): δ 7.57 (br s, 3 H, DMAP-H_{ortho}), 7.30 (s, 2 H, Ar–H_{ortho}), 7.14 (s, 1 H, Ar–H_{para}), 5.71 (s, 2 H, pz-*H*), 5.59 (br s, 2 H, DMAP-H_{meta}), 4.95 (br, 1 H, B–*H*), 4.50 (s, 1 H, N–*H*), 2.31 (s, 9 H, pz-CH_3), 1.87 (s, 6 H, N(CH_3)$_2$), 1.28 (s, 27 H, pz-C(CH_3)$_3$) ppm. ^{11}B{^{1}H} NMR (128 MHz, C_6D_6, 26 °C): δ −7.57 (s, br) ppm. ^{13}C{^{1}H} UDEFT NMR (125 MHz, C_6D_6, 26 °C): δ. 163.8 (3-pz-*C*), 163.2 (Ar-C_{ipso}), 154.3 (DMAP-C_{para}), 149.1 (DMAP-*C*$_{ortho}$), 145.2 (5-pz-*C*), 132.5 (*C*F$_3$), 124.8 (Ar-*C*$_{meta}$), 115.6 (Ar-*C*$_{ortho}$) 106.5 (DMAP-*C*$_{meta}$), 103.0 (4-pz-*C*), 101.4 (Ar-*C*$_{para}$), 37.9 (N(*C*H$_3$)$_2$), 32.2 (*C*(CH$_3$)$_3$), 31.0 (C(*C*H$_3$)$_3$), 13.7 (pz-*C*H$_3$) ppm. ^{171}Yb from ^{1}H–^{171}Yb HSQC (500.13 MHz, 87.52 MHz, C_6D_6, 26 °C): 862 ppm. IR Nujol (CsI, cm^{-1}): 3181 (vw), 2954 (vs), 2924 (vs, Nujol, C–H), 2853 (vs, Nujol, C–H), 2724 (vw), 2667 (w), 1611 (w), 1540 (w), 1462 (vs, Nujol), 1377 (vs, Nujol), 1364 (vs), 1340 (m), 1295 (vw), 1276 (s), 1234 (vw), 1175 (m), 1138 (w), 1111 (w), 1068 (w), 1001 (w), 980 (w), 946 (w), 891 (vw), 807 (vw), 770 (w), 724 (s), 682 (vw), 646 (vw), 590 (vw). Elemental analysis calcd (%) for $C_{39}H_{54}BF_6N_9Yb$ (946.78 g mol^{-1}): C 49.48, H 5.75, N 13.31; found C 48.89, H 6.08, N 12.66.

Tp^{tBu,Me}Yb(NHSiPh$_3$)(dmap) (4^{dmap}). The product was obtained as red crystals in 56% yield.^{1}H NMR (500 MHz, C_6D_6, 26 °C): δ 8.22 (d, 6 H, Ph–*H*$_{ortho}$), 7.63 (d, 2 H, DMAP-*H*$_{ortho}$), 7.38 (t, 6 H, Ph–*H*$_{meta}$), 7.29 (t, 3 H, Ph–*H*$_{para}$), 5.72 (s, 3 H, pz-*H*), 5.70 (d, 2 H, DMAP-*H*$_{meta}$), 4.95 (br, 1 H, B–*H*), 2.33 (s, 9 H, pz-CH_3), 1.89 (s, 6 H, N(CH_3)$_2$), 1.32 (s, 27 H, pz-C(CH_3)$_3$) ppm. ^{11}B{^{1}H} NMR (160 MHz, C_6D_6, 26 °C): δ −7.67 (s, br) ppm. ^{29}Si DEPT45 NMR (60 MHz, C_6D_6, 26 °C): δ −16.5 (s) ppm. ^{13}C{^{1}H} NMR (125 MHz, C_6D_6, 26 °C): δ 163.0 (3-pz-*C*), 154.0 (*ipso*-Ar-C), 149.6 (DMAP-C$_{ortho}$), 145.5 (5-pz-*C*), 144.8 (Ar–C$_{ipso}$), 136.6 (Ar–C$_{ortho}$), 106.1 (DMAP-C$_{meta}$), 102.9 (4-pz-*C*), 37.9 (N(*C*H$_3$)$_2$), 32.2 (*C*(CH$_3$)$_3$), 31.3 (C(*C*H$_3$)$_3$), 13.7 (pz-*C*H$_3$) ppm. ^{171}Yb from

^{1}H–^{171}Yb HSQC (500.13 MHz, 87.52 MHz, C_6D_6, 26 °C): 954 ppm. IR Nujol (CsI, cm^{-1}): 3062 (vw), 3037 (vw), 2953 (vs), 2923 (vs, Nujol, C–H), 2872 (vs), 2853 (vs, Nujol, C–H), 2727 (vw), 2669 (vw), 1620 (w), 1607 (w), 1538 (w), 1461 (vs, Nujol), 1377 (vs, Nujol), 1369 (w), 1337 (w), 1304 (vw), 1230 (w), 1197 (w), 1174 (w), 1103 (w), 1064 (w), 1030 (vw), 1000 (w), 949 (vw), 910 (m), 849 (vw), 806 (w), 786 (w), 768 (w), 739 (w), 725 (w), 702 (m), 644 (w). Elemental analysis calcd (%) for $C_{49}H_{66}BN_9SiYb$ (993.08 g mol^{-1}): C 59.26, H 6.70, N 12.69; found C 59.31, H 7.99, N 12.49.

(Tp^{tBu,Me})$_2$Eu (5). Crystals of **5** were isolated as sole product from the here described reaction. To a solution of $EuI_2(thf)_2$ (300 mg, 0.554 mmol) in 3 ml THF, solutions of KTp^{tBu,Me} (255.5 mg, 0.554 mmol) in 3 ml THF and KNHAr^{Me} (88.2 mg, 0.554 mmol) in 3 ml THF were added slowly and the mixture was stirred for 2 h at ambient temperature. After filtration, all volatiles were removed from the filtrate under reduced pressure. The residual solids were dissolved in *n*-hexane and stored at −40 °C. Complex **5** was obtained as yellow blocks. No yield was determined.

[Tp^{tBu,Me}Yb(NHAr^{CF3})(MMe$_3$)]. In a standard procedure, to a solution of Tp^{tBu,Me}Yb(NH^{CF3})(thf)$_2$ (50 mg, 0.052 mmol) in 3 ml *n*-hexane a solution of M(CH$_3$)$_3$ (M = Al: 7.4 mg, 0.15 mmol; M = Ga: 17.8 mg, 0.15 mmol) in 2 ml *n*-hexane was added dropwise and stirred for 1 h at ambient temperature. After removal of all volatiles under reduced pressure, the residual solids were extracted with *n*-hexane (3 × 1 ml). The volume of the combined phases was reduced under vacuum and the concentrated solution stored at 40 °C.

Tp^{tBu,Me}Yb(NHAr^{CF3})(AlMe$_3$) (6). Due to the co-crystallization of Tp^{tBu,Me}Yb(Al(CH$_3$)$_4$) no further analytics was performed. Solely an XRD analysis was performed by selectively picking single crystals.

Tp^{tBu,Me}Yb(NHAr^{CF3})(GaMe$_3$) (7). The product was obtained as yellow crystals in 90% yield. ^{1}H NMR (500 MHz, C_6D_6, 26 °C): δ 7.38 (s, 3 H, Ar–$H_{ortho/para}$), 5.60 (s, 3 H, pz-*H*), 4.68 (br, 1 H, B*H*), 3.40 (s, 1 H, N*H*), 2.06 (s, 9 H, pz-CH_3), 1.24 (s, 27 H, pz-C(CH_3)$_3$), 0.03 (s, 9 H, Ga(CH_3)$_3$ ppm. ^{11}B{^{1}H} NMR (160 MHz, C_6D_6, 26 °C): δ −8.17 (s, br) ppm. ^{13}C{^{1}H} NMR (125 MHz, C_6D_6, 26 °C): δ 163.7 (3-pz-*C*), 156.7 (*ipso*-Ar–C), 146.6 (5-pz-C), 132.5 (*C*F$_3$), 125.7 (*m*-Ar–C), 120.2 (*o*-Ar–C), 111.1 (*p*-Ar-C), 103.3 (4-pz-C), 32.2 (pz-*C*(CH$_3$)$_3$), 31.2 (pz-C(*C*H$_3$)$_3$), 13.4 (pz-*C*H$_3$), −3.4 (Ga(*C*H$_3$)$_3$) ppm. ^{171}Yb from ^{1}H–^{171}Yb HSQC (500.13 MHz, 87.52 MHz, C_6D_6, 26 °C): 582 ppm. IR Nujol (CsI, cm^{-1}): 3283 (vw), 3184 (vw), 2954 (vs, Nujol, C–H), 2923 (vs, Nujol, C–H), 2853 (vs, Nujol, C–H), 2725 (vw), 2565 (vw), 1607 (w), 1542 (m), 1462 (vs, Nujol), 1377 (vs, Nujol), 1352 (s), 1307 (vw), 1275 (vs), 1239 (vw), 1207 (vw), 1171 (vs), 1128 (s), 1065 (w), 1024 (w), 990 (w), 944 (w), 879 (vw), 864 (w), 845 (w), 786 (w), 767 (m), 726 (s), 703 (w), 683 (w), 644 (w), 541 (vw). Elemental analysis calcd (%) for $C_{35}H_{53}BF_6GaN_7Yb$ (939.44 g mol^{-1}): C 44.75, H 5.69, N 10.44; found C 45.81, H 6.36, N 9.19.

[(Tp^{tBu,Me})$_2$Yb$_2$I][NHAr^{iPr}(GaMe$_3$)$_2$] (8). To a solution of [Tp^{tBu,Me}Yb(NHAr^{iPr})(thf)] (50 mg, 0.059 mmol), contaminated with [(Tp^{tBu,Me})YbI], in 2 ml *n*-pentane a solution of GaMe$_3$ (13.6 mg, 0.118 mmol) in 2 ml *n*-pentane was added slowly and stirred at ambient temperature for 30 minutes. Then, all volatiles were removed under reduced pressure. The residual solids were dissolved in a small amount of *n*-pentane and stored at −40 °C. Due to bad crystallization behaviour only a connectivity structure could be obtained (see ESI†). No further analytics was performed of **8**.

[Tp^{tBu,Me}Yb(NHR)(Cl)]. In a standard procedure, to a solution of [Tp^{tBu,Me}Yb(NHR)(thf)$_2$] (R = Ar^{iPr}: 30 mg, 0.036 mmol; R = Ar^{CF3}: 30 mg, 0.031 mmol) in 5 ml THF a solution of C_2Cl_6 (R = Ar^{iPr} 8.4 mg, 0.036 mmol; R = Ar^{CF3} 7.3 mg, 0.031 mmol) in 2 ml THF was added dropwise and stirred for 2 h at ambient temperature. After removal of all volatiles under reduced pressure, the residual solids were extracted with *n*-hexane (3 × 1 ml). The volume of the combined phases was reduced under reduced pressure and the concentrated solution stored at +40 °C.

Tp^{tBu,Me}Yb(NHAr^{iPr})(Cl) (9a). The product was obtained as blue crystals in 77% yield. IR Nujol (CsI, cm^{-1}): 3175 (vw), 2954 (vs, Nujol, C–H), 2925 (vs, Nujol, C–H), 2854 (vs, Nujol, C–H), 2723 (vw), 2593 (vw), 1589 (vw), 1542 (m), 1416 (vs, Nujol), 1377 (vs, Nujol), 1367 (vs), 1351 (s), 1308 (w), 1263 (w), 1242 (w), 1171 (m), 1072 (w), 1070 (w), 1027 (w), 980 (w), 935 (vw), 889 (w), 794 (m), 766 (m), 742 (m), 724 (m), 681 (vw), 665 (vw), 636 (w), 567 (vw). Elemental analysis calcd (%) for $C_{36}H_{58}BClN_7Yb$ (808.22 g mol^{-1}): C 53.50, H 7.23, N 12.13; found C 53.57, H 7.31, N 11.78.

Tp^{tBu,Me}Yb(NHAr^{CF3})(Cl) (10a). The product was obtained as magenta crystals in 72% yield. IR Nujol (CsI, cm^{-1}): 3308 (vw), 3136 (vw), 2953 (vs, Nujol, C–H), 2924 (vs, Nujol, C–H), 2854 (vs, Nujol, C–H), 2727 (vw), 2565 (vw), 1605 (w), 1541 (m), 1462 (vs, Nujol), 1378 (vs, Nujol), 1369 (vs), 1356 (s), 1306 (vw), 1276 (vs), 1241 (w), 1195 (w), 1171 (s), 1126 (s), 1099 (w), 1063 (w), 1027 (w), 1014 (vw), 990 (w), 947 (w), 866 (w), 838 (w), 806 (w), 765 (m), 727 (m), 670 (w), 682 (w), 660 (vw), 643 (w), 595 (w). Elemental analysis calcd (%) for $C_{32}H_{44}BClF_6N_7Yb$ (860.06 g mol^{-1}): C 44.69, H 5.16, N 11.4; found C 44.75, H 6.36, N 11.1.

[Tp^{tBu,Me}Yb(NHR)(Br)]. In a standard procedure, to a solution of [Tp^{tBu,Me}Yb(NHR)(thf)$_2$] (R = Ar^{iPr}: 50 mg, 0.059 mmol; R = Ar^{CF3}: 50 mg, 0.052 mmol) in 5 ml THF a solution of $TeBr_4$ (R = Ar^{iPr} 6.6 mg, 0.015 mmol; R = Ar^{CF3} 5.8 mg, 0.013 mmol) in 2 ml THF was added dropwise and stirred for 2 h at ambient temperature. After removal of all volatiles under reduced pressure, the residual solids were extracted with *n*-hexane (3 × 1 ml). The volume of the combined phases was reduced under reduced pressure and the concentrated solution stored at +40 °C.

Tp^{tBu,Me}Yb(NHAr^{iPr})(Br) (9b). The product was obtained as turquoise crystals in 71% yield. IR Nujol (CsI, cm^{-1}): 3304 (vw), 3140 (vw), 2953 (vs, Nujol, C–H), 2923 (vs, Nujol, C–H), 2855 (vs, Nujol, C–H), 2725 (vw), 2569 (w), 1604 (m), 1539 (s), 1463 (vs, Nujol), 1378 (vs, Nujol), 1352 (vs), 1306 (w), 1275 (vs), 1259 (w), 1196 (m), 1169 (vs), 1126 (vs), 1099 (w), 1064 (m), 1027 (m), 990 (m), 948 (m), 866(w), 840 (w), 807 (m), 766 (s), 727 (s), 682 (m), 596 (w), 515 (vw). Elemental analysis calcd (%) for $C_{36}H_{58}BBrN_7Yb$ (852.68 g mol^{-1}): C 50.71, H 6.86, N 11.5; found C 50.33, H 6.88, N 11.51.

$Tp^{tBu,Me}Yb(NHAr^{CF3})(Br)$ (10b). The product was obtained as magenta crystals in 43% yield. IR Nujol (CsI, cm^{-1}): 3177 (vw), 2921 (vs, Nujol, C–H), 2856 (vs, Nujol, C–H), 2725 (vw), 2569 (w), 1587 (w), 1541 (s), 1461 (vs, Nujol), 1377 (vs, Nujol), 1350 (s), 1327 (w), 1310 (w), 1262 (m), 1242 (w), 1191 (m), 1172 (s), 1070 (m), 1060 (m), 1027 (m), 1012 (m), 983 (w), 930 (vw), 889 (w), 854 (w), 794 (s), 766 (s), 744 (s) 725 (m), 683 (vw), 662 (vw), 638 (w), 565 (vw). Elemental analysis calcd (%) for $C_{32}H_{44}BBrF_6N_7Yb$ (904.51 g mol^{-1}): C 42.49, H 4.90, N 10.84; found C 42.25, H 5.51, N 11.0.

$Tp^{tBu,Me}Yb(NHAr^{CF3})(N_2Ph_2)$ (11). To a solution (2 ml) of $\mathbf{3^{thf}}$ (30 mg, 0.031 mmol) in THF a solution of N_2Ph_2 (5.6 mg, 0.031 mmol) in 2 ml THF was added slowly and a colour change from orange to brown was observed. The solution was stirred for 30 minutes at ambient temperature. Then, all volatiles were removed under reduced pressure and the obtained residual solids were extracted with *n*-hexane (3 × 2 ml). The volume of the combined fractions was reduced under vacuum and stored at −40 °C. $Tp^{tBu,Me}Yb(NHAr^{CF3})(N_2Ph_2)$ was obtained as yellow-brownish needles in 84% (26 mg) yield. ^{1}H NMR (400 MHz, THF-d_8, 26 °C): δ 7.91 (d, 4 H, Ar–H_{ortho}), 7.50 (m, 6 H, Ar–$H_{meta/para}$), 6.59 (s, 2 H, NAr–H_{ortho}), 6.33 (s, 1 H, NAr–H_{para}), 5.88 (s, 3 H, pz-*H*), 3.99 (s, 1 H, N*H*), 2.38 (s, 9 H, pz-CH_3), 1.37 (s, 27 H, pz-C(CH_3)$_3$) ppm.

$Tp^{tBu,Me}Yb(pz^{tBu,Me})(OTf)$ (12). To a solution of $\mathbf{1^{thf}}$ (50 mg, 0.059 mmol) in 5 ml THF a solution of AgOTf (15.2 mg, 0.059 mmol) in 5 ml THF was added slowly. The reaction mixture was stirred for 60 minutes at ambient temperature. The formed silver metal was removed *via* filtration and all volatiles were removed from the filtrate under reduced pressure. The residual solids were dissolved in *n*-hexane (2 ml) and stored at −40 °C. The product was obtained in 35% (19 mg) yield. No further analytics was performed.

$Tp^{tBu,Me}{}_4Yb_5Cl_6$ (13). In a small-scale reaction, to compound **9** (29 mg, 0.036 mmol) dissolved in 3 ml toluene a solution of $AlMe_3$ in 3 ml toluene was added slowly and stirred for 30 minutes at ambient temperature. Afterwards, all volatiles were removed under reduced pressure and the residual solids were dissolved in a small amount of *n*-pentane. The solution was stored at −40 °C. Only a few crystals of bad quality could be obtained but a connectivity structure could be determined *via* XRD analysis (see ESI†). No further analytics was performed and no yield was determined.

X-Ray crystallography and crystal structure determinations

Crystals of $\mathbf{1^{thf}}$, $\mathbf{1^{thf,Sm}}$, $\mathbf{1^{thf,Eu}}$, $\mathbf{1^{py}}$, **1**, $\mathbf{3^{thf}}$, $\mathbf{4^{thf}}$, $\mathbf{1^{dmap}}$, $\mathbf{3^{dmap}}$, $\mathbf{4^{dmap}}$ and **5** were grown by standard techniques using saturated solutions of *n*-hexane at −40 °C. Crystals of **2** were obtained from a saturated diethyl ether solution at −40 °C. Crystals of **6**, **7**, **9a**, **10a**, **9b** and **10b** were grown from saturated *n*-hexane solutions at +40 °C. Crystals of **8** were grown from a *n*-pentane solution by cooling to −40 °C. Suitable crystals for X-ray structure analyses were selected inside a glovebox and coated with Parabar 10 312 (previously known as Paratone N, Hampton Research) and fixed on a microloop. X-Ray data were collected on a Bruker APEX III DUO instrument equipped with an IμS microfocus sealed tube and QUAZAR optics for MoK_α (λ = 0.71073 Å) radiation. The data collection strategy was determined using COSMO[40] employing ω and ϕ scans. Raw data were processed using APEX[41] and SAINT,[42] corrections for absorption effects were applied using SADABS.[43] The structures were solved by direct methods and refined against all data by full-matrix least-squares methods on F^2 using SHELXTL[44] and SHELXLE.[45] All graphics were produced employing CSD Mercury 4.1.0.[46] Disorder models are calculated using DSR,[47] a program included in SHELXLE, for refining disorder models. Further details regarding the refinement and crystallographic data are listed in Table S1† and in the CIF files. CCDC depositions 2248520–2248541† contain all the supplementary crystallographic data for this paper.

Conflicts of interest

There are no conflicts to declare.

References

1 A. A. Trifonov, M. N. Bochkarev, H. Schumann and J. Loebel, *Angew. Chem., Int. Ed. Engl.*, 1991, **30**, 1149–1151.
2 E. Lu, Y. Li and Y. Chen, *Chem. Commun.*, 2010, **46**, 4469–4471.
3 (*a*) G. R. Giesbrecht and J. C. Gordon, *Dalton Trans.*, 2004, 2387–2393; (*b*) O. T. Summerscales and J. C. Gordon, *RSC Adv.*, 2013, **3**, 6682–6692; (*c*) E. Lu, J. Chu and Y. Chen, *Acc. Chem. Res.*, 2018, **51**, 557–566; (*d*) Q. Zhu, J. Zhu and C. Zhu, *Tetrahedron Lett.*, 2018, **59**, 514–520; (*e*) D. Schädle and R. Anwander, *Chem. Soc. Rev.*, 2019, **48**, 5752–5805.
4 E. Lu, J. Chu, Y. Chen, M. V. Borzov and G. Li, *Chem. Commun.*, 2011, **47**, 743–745.
5 W. Rong, J. Cheng, Z. Mou, H. Xie and D. Cui, *Organometallics*, 2013, **32**, 5523–5529.
6 J. Chu, X. Han, C. E. Kefalidis, J. Zhou, L. Maron, X. Leng and Y. Chen, *J. Am. Chem. Soc.*, 2014, **136**, 10894–10897.
7 D. Schädle, M. Meermann-Zimmermann, C. Schädle, C. Maichle-Mössmer and R. Anwander, *Eur. J. Inorg. Chem.*, 2015, 1334–1339.
8 L. A. Solola, A. V. Zabula, W. L. Dorfner, B. C. Manor, P. J. Carroll and E. J. Schelter, *J. Am. Chem. Soc.*, 2017, **139**, 2435–2442.
9 E. A. Patrick, Y. Yang, W. E. Piers, L. Maron and B. S. Gelfand, *Chem. Commun.*, 2021, **57**, 8640–8643.
10 T. E. Rieser, R. Thim-Spöring, D. Schädle, P. Sirsch, R. Litlabø, K. W. Törnroos, C. Maichle-Mössmer and R. Anwander, *J. Am. Chem. Soc.*, 2022, **144**, 4102–4113.
11 H.-S. Chan, H.-W. Li and Z. Xie, *Chem. Commun.*, 2002, 652–653.
12 W. J. Evans, M. A. Ansari, J. W. Ziller and S. I. Khan, *Inorg. Chem.*, 1996, **35**, 5435–5444.

13 J. C. Gordon, G. R. Giesbrecht, D. L. Clark, P. J. Hay, D. W. Keogh, R. Poli, B. L. Scott and J. G. Watkin, *Organometallics*, 2002, **21**, 4726–4734.
14 L. A. Solola, A. V. Zabula, W. L. Dorfner, B. C. Manor, P. J. Carroll and E. J. Schelter, *J. Am. Chem. Soc.*, 2016, **138**, 6928–6931.
15 B. M. Wolf, C. Stuhl and R. Anwander, *Chem. Commun.*, 2018, **54**, 8826–8829.
16 B. M. Wolf, C. Stuhl, C. Maichle-Mössmer and R. Anwander, *Chem. – Eur. J.*, 2018, **24**, 15921–15929.
17 L. Hasinoff, J. Takats, X. W. Zhang, A. H. Bond and R. D. Rogers, *J. Am. Chem. Soc.*, 1994, **116**, 8833–8834.
18 T. D. Tilley, R. A. Andersen and A. Zalkin, *J. Am. Chem. Soc.*, 1982, **104**, 3725–3727.
19 M. M. Katzenmayer, B. M. Wolf, A. Mortis, C. Maichle-Mössmer and R. Anwander, *Chem. Commun.*, 2021, **57**, 243–246.
20 (*a*) X. Zhang, R. McDonald and J. Takats, *New J. Chem.*, 1995, **19**, 473–585; (*b*) K. Saliu, J. Takats and M. J. Ferguson, *Acta Crystallogr., Sect. E: Struct. Rep. Online*, 2009, **65**, m643–m644.
21 G. H. Maunder, A. Sella and D. A. Tocher, *J. Chem. Soc., Chem. Commun.*, 1994, 2689–2690.
22 R. Litlabø, K. Saliu, M. J. Ferguson, R. McDonald, J. Takats and R. Anwander, *Organometallics*, 2009, **28**, 6750–6754.
23 D. Schädle, M. Enders, C. Schädle, C. Maichle-Mössmer, K. W. Törnroos and R. Anwander, *New J. Chem.*, 2015, **39**, 7640–7648.
24 (*a*) N. Marques, A. Sella and J. Takats, *Chem. Rev.*, 2002, **102**, 2137–2159; (*b*) G. M. Ferrence and J. Takats, *J. Organomet. Chem.*, 2002, **647**, 84–93.
25 C. Apostolidis, A. Carvalho, A. Domingos, B. Kanellakopulos, R. Maier, N. Marques, A. P. d. Matos and J. Rebizant, *Polyhedron*, 1998, **18**, 263–272.
26 W. Yi, J. Zhang, Z. Chen and X. Zhou, *Inorg. Chem.*, 2012, **51**, 10631–10638.
27 (*a*) W. J. Evans, D. K. Drummond, L. R. Chamberlain, R. J. Doedens, S. G. Bott, H. Zhang and J. L. Atwood, *J. Am. Chem. Soc.*, 1988, **110**, 4983–4994; (*b*) Z. Hou, T.-A. Koizumi, M. Nishiura and Y. Wakatsuki, *Organometallics*, 2001, **20**, 3323–3328; (*c*) A. R. Willauer, A. M. Dabrowska, R. Scopelliti and M. Mazzanti, *Chem. Commun.*, 2020, **56**, 8936–8939.
28 C.-L. Pan, W. Chen, S. Su, Y.-S. Pan and J. Wang, *Dalton Trans.*, 2011, **40**, 7941–7945.
29 (*a*) A. Domingos, M. R. J. Elsegood, A. C. Hillier, G. Lin, S. Y. Liu, I. Lopes, N. Marques, G. H. Maunder, R. McDonald, A. Sella, J. W. Steed and J. Takats, *Inorg. Chem.*, 2002, **41**, 6761–6768; (*b*) F. A. Kunrath, O. L. Casagrande Jr., L. Toupet and J.-F. Carpentier, *Polyhedron*, 2004, **23**, 2437–2445.
30 S.-Y. Liu, G. H. Maunder, A. Sella, M. Stevenson and D. A. Tocher, *Inorg. Chem.*, 1996, **35**, 76–81.
31 J. M. Keates and G. A. Lawless, in *Advanced Applications of NMR to Organometallic Chemistry*, ed. M. Gielen, R. Willem and B. Wrackmeyer, Wiley, Chichester, U.K., 1996, ch. 12, pp. 357–370.
32 (*a*) A. G. Avent, M. A. Edelman, M. F. Lappert and G. A. Lawless, *J. Am. Chem. Soc.*, 1989, **111**, 3423–3425; (*b*) G. Heckmann and M. Niemeyer, *J. Am. Chem. Soc.*, 2000, **122**, 4227–4228.
33 For early examples on ^{171}Yb CP/MAS NMR spectroscopy, see: (*a*) X. Mao, X. Zhao, C. Ye and S. Wang, *Solid State Nucl. Magn. Reson.*, 1994, **3**, 107–110; (*b*) G. W. Rabe and A. Sebald, *Solid State Nucl. Magn. Reson.*, 1996, **6**, 197–200; (*c*) J. M. Keates, G. A. Lawless and M. P. Waugh, *Chem. Commun.*, 1996, 1627–1628; (*d*) M. Keates and G. A. Lawless, *Organometallics*, 1997, **16**, 2842–2846.
34 H.-M. Sommerfeldt, C. Meermann, M. G. Schrems, K. W. Törnroos, N. Å. Frøystein, R. J. Miller, E.-W. Scheidt, W. Scherer and R. Anwander, *Dalton Trans.*, 2008, 1899–1907.
35 S. P. Constantine, G. M. De Lima, P. B. Hitchcock, J. M. Keates and G. A. Lawless, *Chem. Commun.*, 1996, 2421–2422.
36 D. Schuhknecht, K.-N. Truong, T. P. Spaniol, L. Maron and J. Okuda, *Chem. Commun.*, 2018, **54**, 11280–11283.
37 X. W. Zhang, G. H. Maunder, S. Gießmann, R. MacDonald, M. J. Ferguson, A. H. Bond, R. D. Rogers, A. Sella and J. Takats, *Dalton Trans.*, 2011, **40**, 195–210.
38 S. Trofimenko, *Chem. Rev.*, 1993, **93**, 943–980.
39 G. R. Fulmer, A. J. M. Miller, N. H. Sherden, H. E. Gottlieb, A. Nudelman, B. M. Stoltz, J. E. Bercaw and K. I. Goldberg, *Organometallics*, 2010, **29**, 2176–2179.
40 *COSMO V., 1.61*, Bruker AXS Inc., Madison, WI, 2012.
41 (*a*) *APEX2 V. 2012.10_0*, Bruker AXS Inc., Madison, WI, 2012; (*b*) *APEX 3 V. 2019.11-0*, Bruker AXS Inc., Madison, WI, 2019.
42 *SAINT V., 8.40B*, Bruker AXS Inc., Madison, WI, 2019.
43 L. Krause, R. Herbst-Irmer, G. M. Sheldrick and D. Stalke, SADABS, *J. Appl. Crystallogr.*, 2015, **48**, 3–10.
44 (*a*) G. M. Sheldrick, SHELXTL, *Acta Crystallogr., Sect. A: Found. Adv.*, 2015, **71**, 3–8; (*b*) G. M. Sheldrick, SHELXL, *Acta Crystallogr., Sect. C: Struct. Chem.*, 2015, **71**, 3–8.
45 C. B. Hübschle, G. M. Sheldrick and B. Dittrich, SHELXLE, *J. Appl. Crystallogr.*, 2011, **44**, 1281–1284.
46 C. F. Macrae, I. J. Bruno, J. A. Chisholm, P. R. Edgington, P. McCabe, E. Pidcock, L. Rodriguez-Monge, R. Taylor, J. Van de Streek and P. A. Wood, *J. Appl. Crystallogr.*, 2008, **41**, 466–470.
47 D. Kratzert, J. J. Holstein and I. Krossing, *J. Appl. Crystallogr.*, 2015, **48**, 933–938.

Supporting Information

Potential precursors for terminal ytterbium(II) imide complexes bearing the tris(3-tert-butyl-5-methylpyrazolyl)hydroborato ligand

Markus M. Katzenmayer, Felix Kracht, Cäcilia Maichle-Mössmer and Reiner Anwander*

Institut für Anorganische Chemie, Eberhard Karls Universität Tübingen, Auf der Morgenstelle 18, 72076 Tübingen, Germany

E-mail for R.A.: reiner.anwander@uni-tuebingen.de.

Table of Contents

NMR Spectra S3

$Tp^{tBu,Me}Yb(NHAr^{iPr})(thf)$ (**1^{thf}**) S3

$Tp^{tBu,Me}Yb(NHAr^{iPr})$ (**1**) S4

$Tp^{tBu,Me}Yb(NHAr^{Me})$ (**2**) S7

$Tp^{tBu,Me}Yb(NHAr^{CF3})(thf)_2$ (**3^{thf}**) S7

$Tp^{tBu,Me}Yb(NHSiPh_3)(thf)$ (**4^{thf}**) S9

$Tp^{tBu,Me}Sm(NHAr^{iPr})(thf)$ (**$1^{thf,Sm}$**) S11

$Tp^{tBu,Me}Eu(NHAr^{iPr})(thf)$ (**$1^{thf,Eu}$**) S12

$Tp^{tBu,Me}Yb(NHAr^{iPr})(dmap)$ (**1^{dmap}**) S12

$Tp^{tBu,Me}Yb(NHAr^{CF3})(dmap)$ (**3^{dmap}**) S14

$Tp^{tBu,Me}Yb(NHSiPh_3)(dmap)$ (**4^{dmap}**) S16

$Tp^{tBu,Me}Yb(NHAr^{CF3})(AlMe_3)$ (**6**) S19

$Tp^{tBu,Me}Yb(NHAr^{CF3})(GaMe_3)$ (**7**) S20

$Tp^{tBu,Me}Yb(NHAr^{iPr})(Cl)$ (**9a**) S23

$Tp^{tBu,Me}Yb(NHAr^{iPr})(Br)$ (**9b**) S23

$(Tp^{tBu,Me})Yb(NHAr^{CF3})(Cl)$ (**10a**) S24

$Tp^{tBu,Me}Yb(NHAr^{CF3})(Br)$ (**10b**) S24

$Tp^{tBu,Me}Yb(NHAr^{CF3})(N_2Ph_2)$ (**11**) S25

Crystallographic Data S26

NMR Spectra

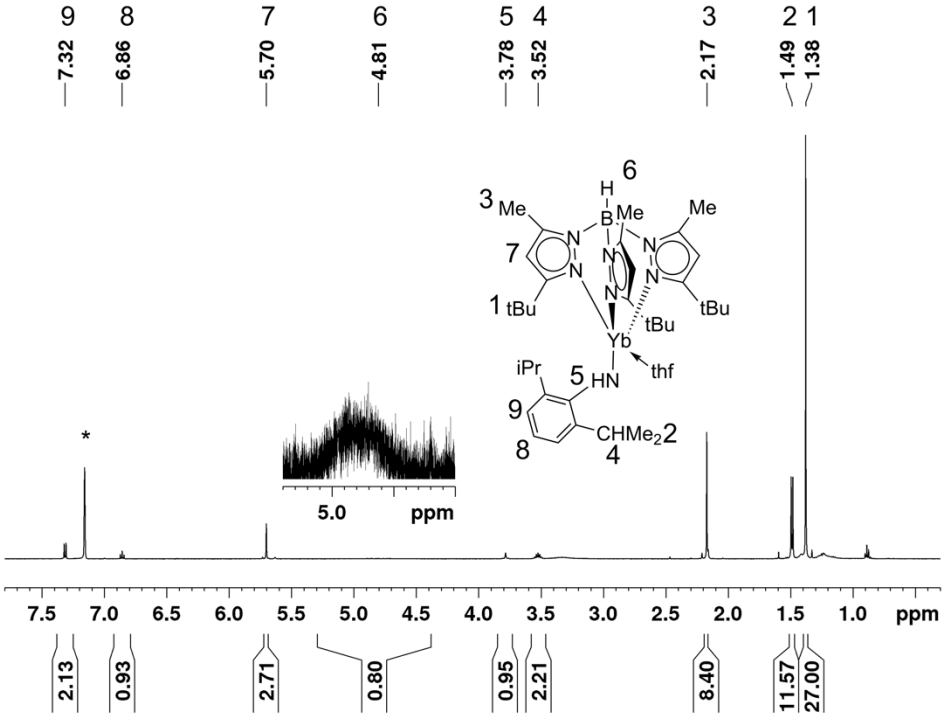

Figure S1 ^{1}H NMR spectrum (500 MHz, C_6D_6, 26 °C) of $Tp^{tBu,Me}Yb(NHAr^{iPr})(thf)$ (**1^{thf}**). Residual solvent signals are marked with *. Minor impurities are marked with #.

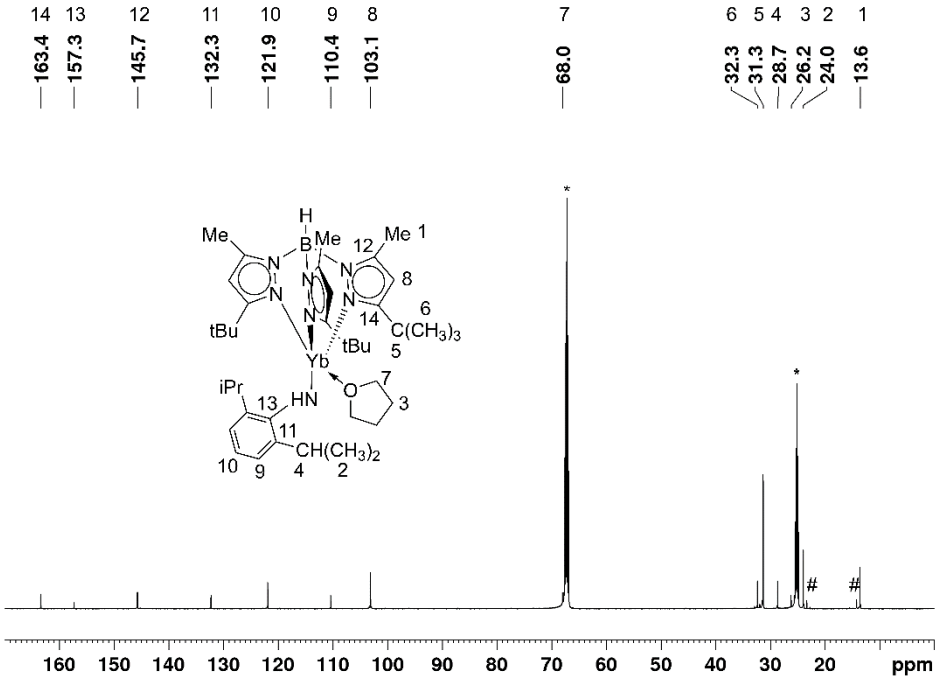

Figure S2 $^{13}C\{^{1}H\}$ NMR spectrum (125 MHz, [d8]thf, 26 °C) of $Tp^{tBu,Me}Yb(NHAr^{iPr})(thf)$ (**1^{thf}**). Residual solvent signals are marked with * impurities are marked with #.

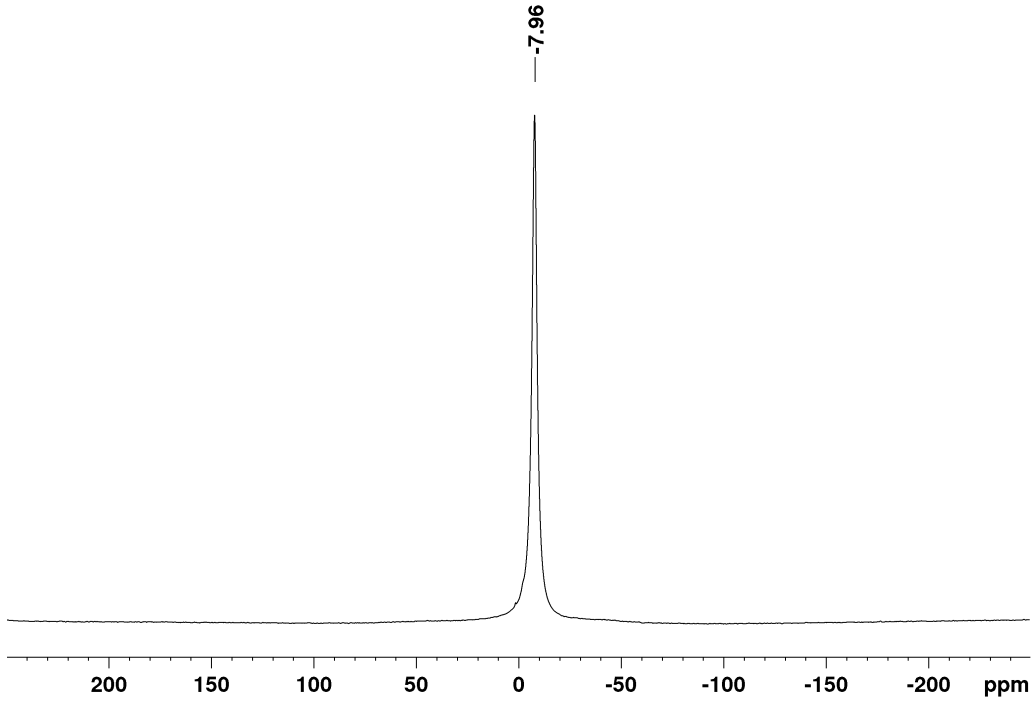

Figure S3 ^{11}B NMR spectrum (160 MHz) of $Tp^{tBu,Me}Yb(NHAr^{iPr})(thf)$ (**1^{thf}**) in C_6D_6 at 26 °C.

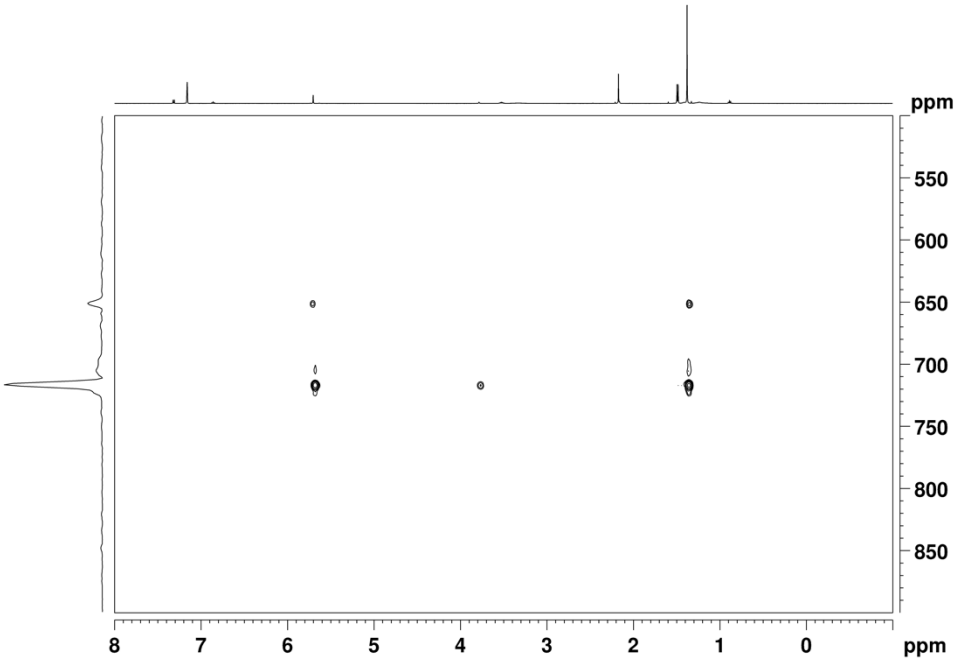

Figure S4 ^{1}H-^{171}Yb HSQC NMR spectrum (500 MHz, 87.52 MHz C_6D_6, 26 °C) of $Tp^{tBu,Me}Yb(NHAr^{iPr})(thf)$ (**1^{thf}**).

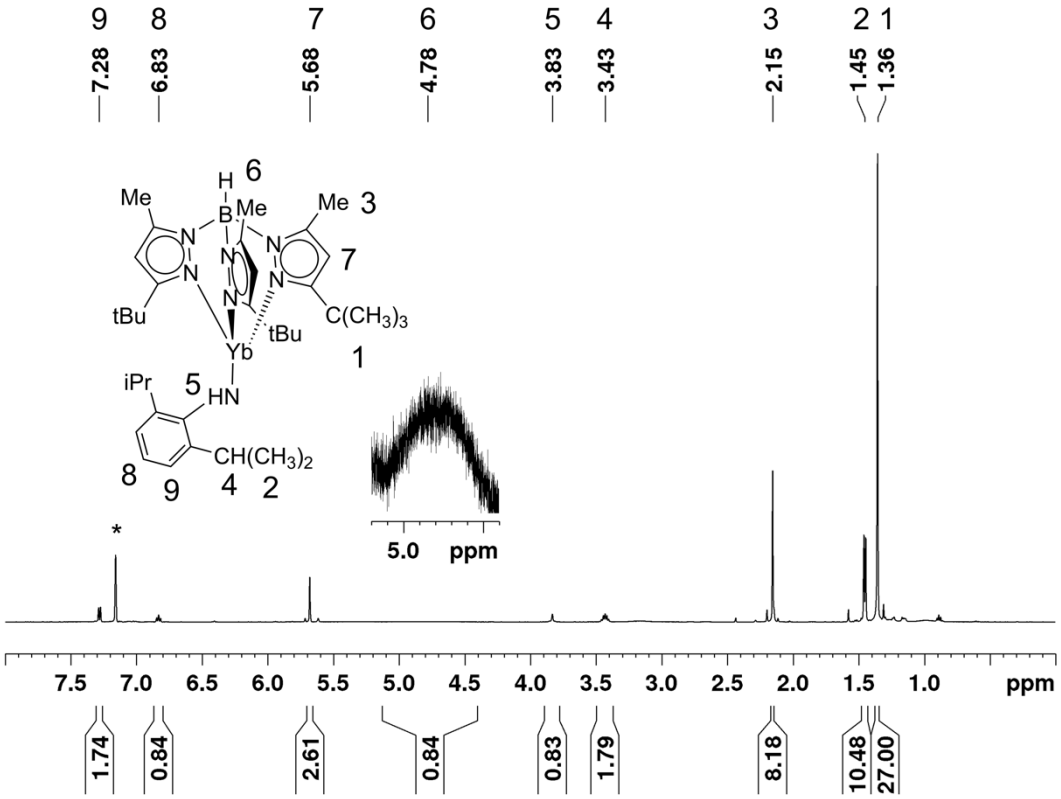

Figure S5 ^{1}H NMR spectrum (500 MHz, C_6D_6, 26 °C) of $Tp^{tBu,Me}Yb(NHAr^{iPr})$ (**1**). Residual solvent signals are marked with *.

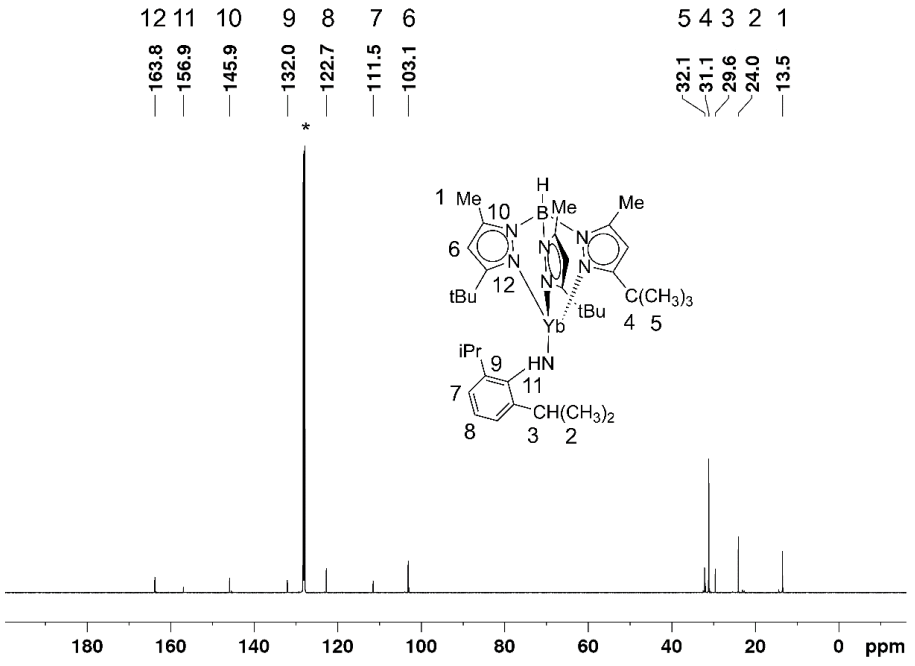

Figure S6 $^{13}C\{^{1}H\}$ NMR spectrum (125 MHz, C_6D_6, 26 °C) of $Tp^{tBu,Me}Yb(NHAr^{iPr})$ (**1**). Residual solvent signals are marked with *.

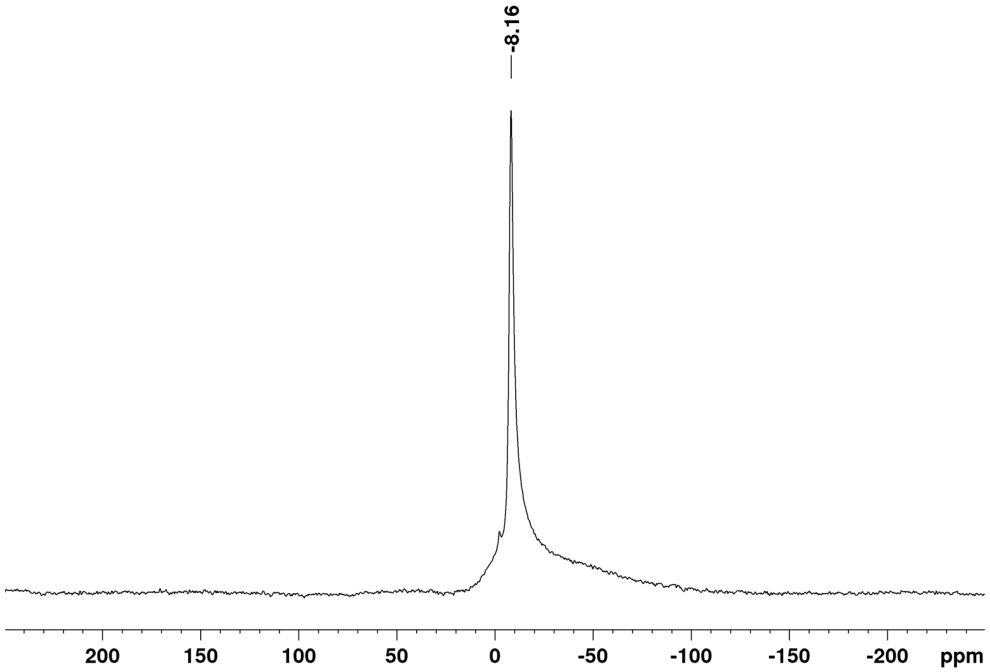

Figure S7 ^{11}B NMR spectrum (160 MHz) of a micro-scale reaction) of Tp^{tBu,Me}Yb(NHAr^{iPr}) (**1**) in C_6D_6 at 26 °C.

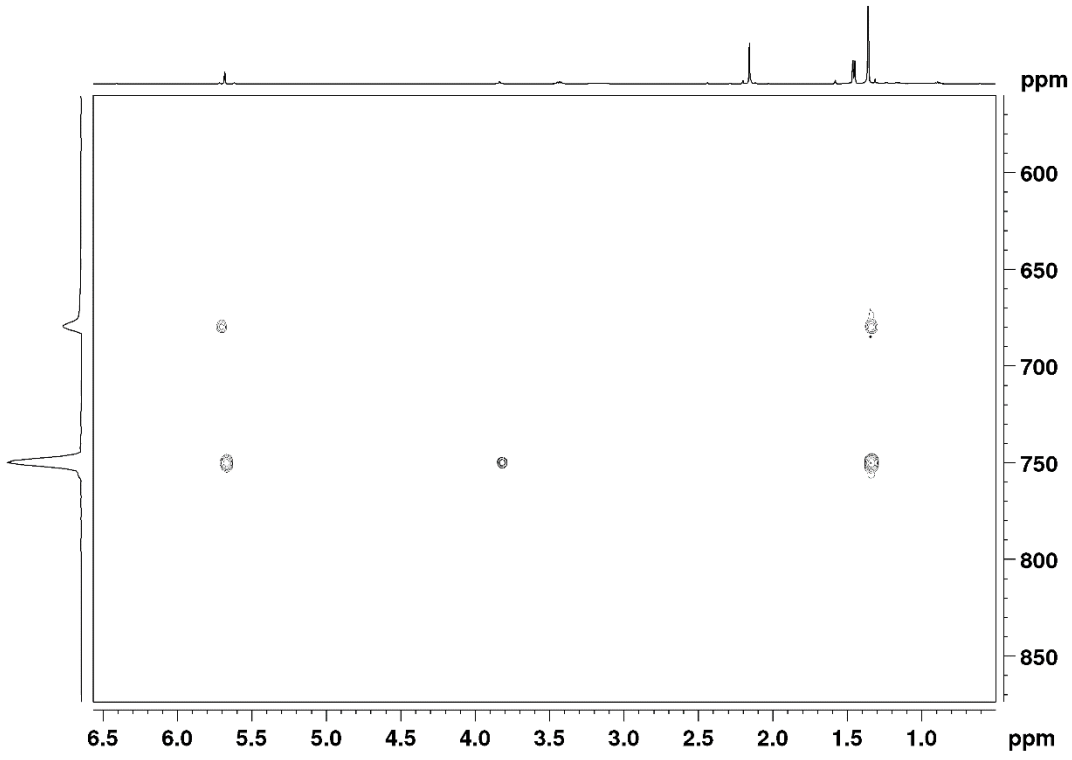

Figure S8 ^{1}H–^{171}Yb HSQC NMR spectrum (500 MHz, 87.52 MHz) of Tp^{tBu,Me}Yb(NHAr^{iPr}) (**1**) in C_6D_6 at 26 °C. Main product Tp^{tBu,Me}Yb(NHAr^{iPr}): signal at 750 ppm.

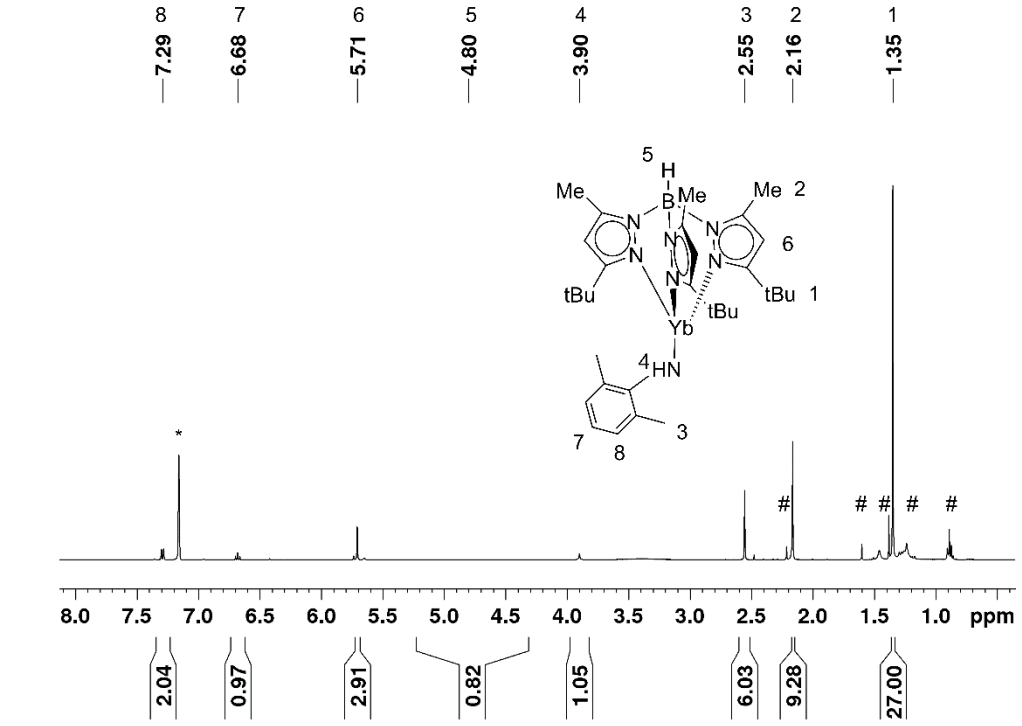

Figure S9 ^{1}H NMR spectrum (500 MHz, C_6D_6, 26 °C) of $Tp^{tBu,Me}Yb(NHAr^{Me})$ (**2**). Residual solvent signals are marked with *. Impurities are marked with #.

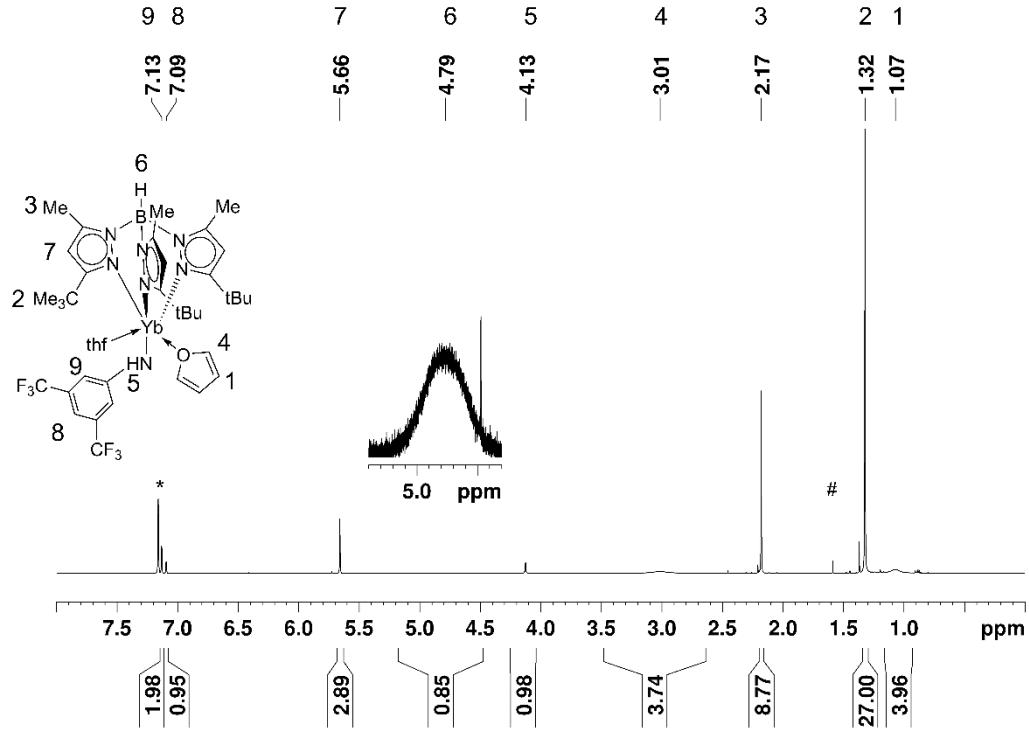

Figure S10 ^{1}H NMR spectrum (500 MHz, C_6D_6, 26 °C) of $Tp^{tBu,Me}Yb(NHAr^{CF3})(thf)_2$ (**3^{thf}**). Residual solvent signals are marked with *. Minor impurities are marked with #.

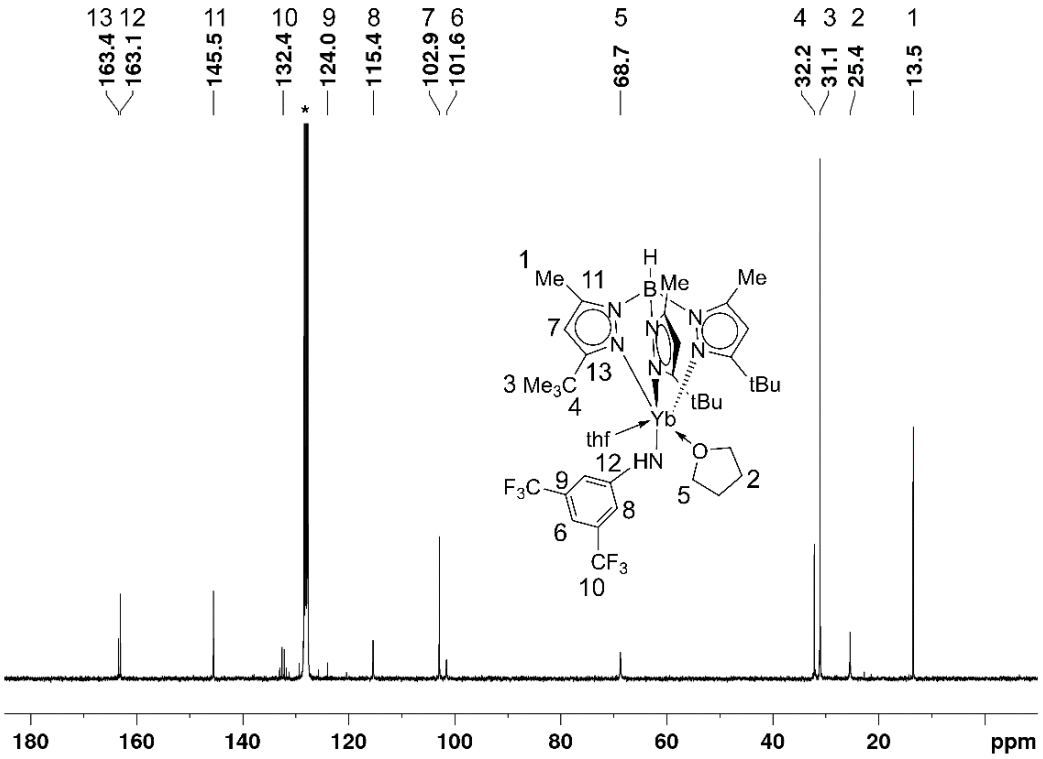

Figure S11 $^{13}C\{^{1}H\}$ NMR spectrum (125 MHz, C_6D_6, 26 °C) of $Tp^{tBu,Me}Yb(NHAr^{CF3})(thf)_2$ (**3^{thf}**). Residual solvent signals are marked with *.

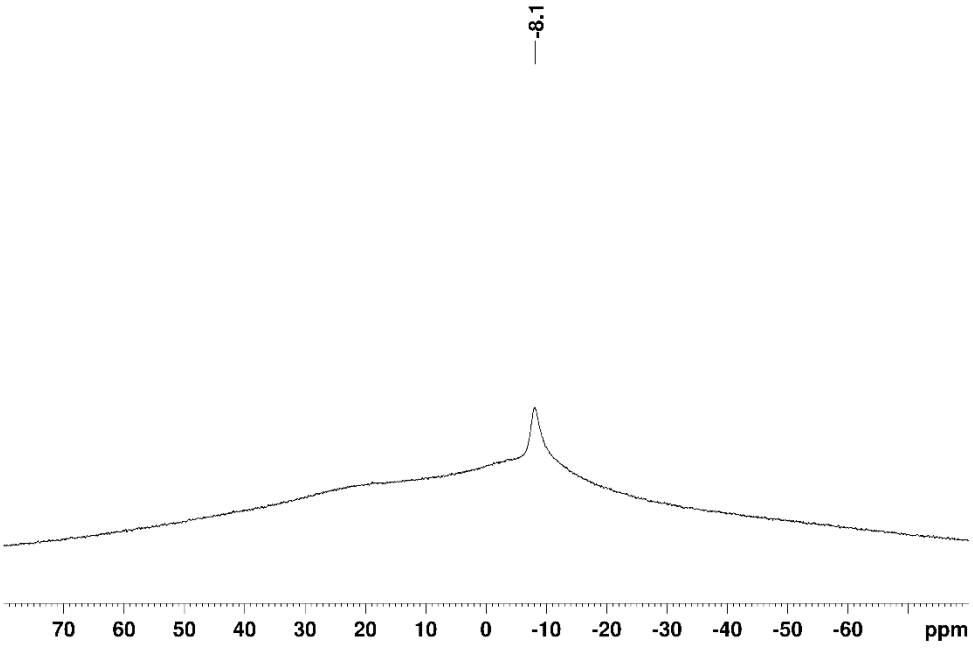

Figure S12 ^{11}B NMR spectrum (160 MHz, C_6D_6, 26 °C) of $Tp^{tBu,Me}Yb(NHAr^{CF3})(thf)_2$ (**3^{thf}**).

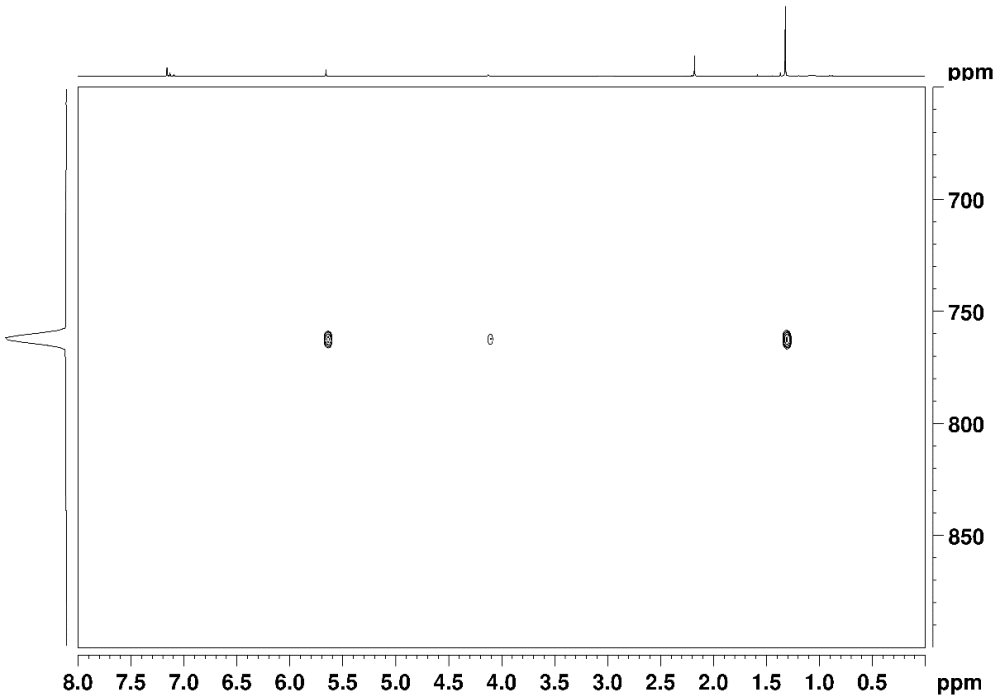

Figure S13 ^{1}H-^{171}Yb HSQC NMR spectrum (500 MHz, 87.52 MHz C_6D_6, 26 °C) of $Tp^{tBu,Me}Yb(NHAr^{CF3})(thf)_2$ (**3**^{thf}).

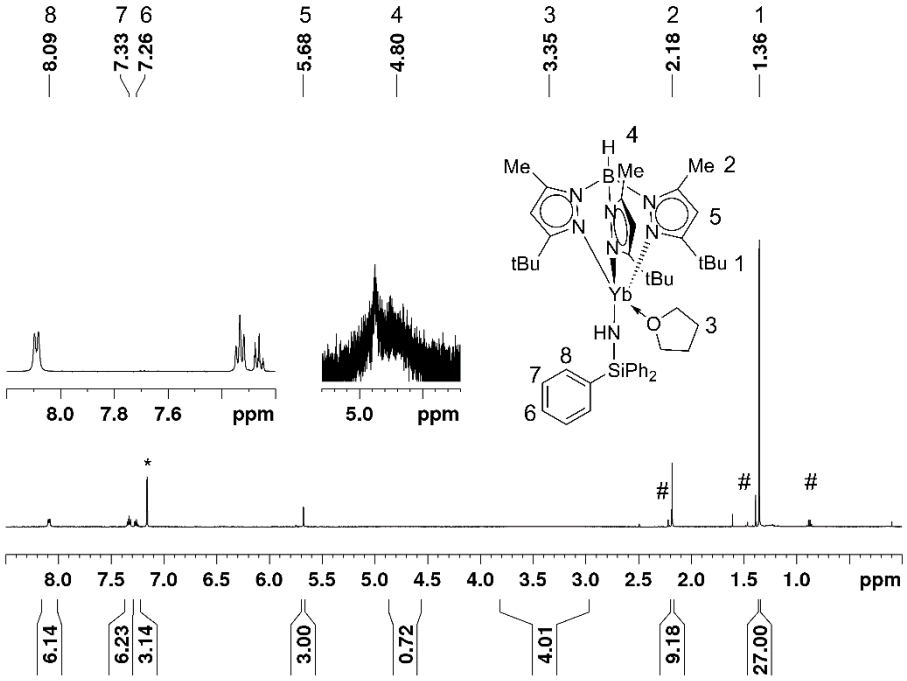

Figure S14 ^{1}H NMR spectrum (400 MHz, C_6D_6, 26 °C) of $Tp^{tBu,Me}Yb(NHSiPh_3)(thf)$ (**4**^{thf}). Residual solvent signals are marked with *, # marks minor impurities.

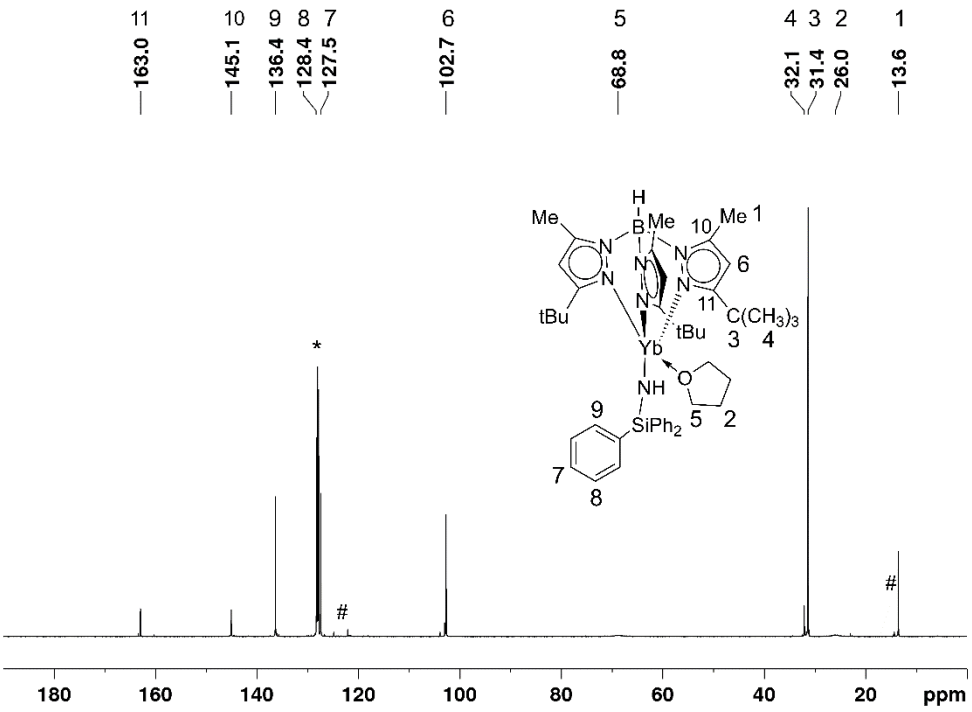

Figure S15 $^{13}C\{^{1}H\}$ UDEFT NMR spectrum (125 MHz, C_6D_6, 26 °C) of $Tp^{tBu,Me}Yb(NHSiPh_3)(thf)$ (**4**^{thf}). Residual solvent signals are marked with *, minor impurities are marked with #.

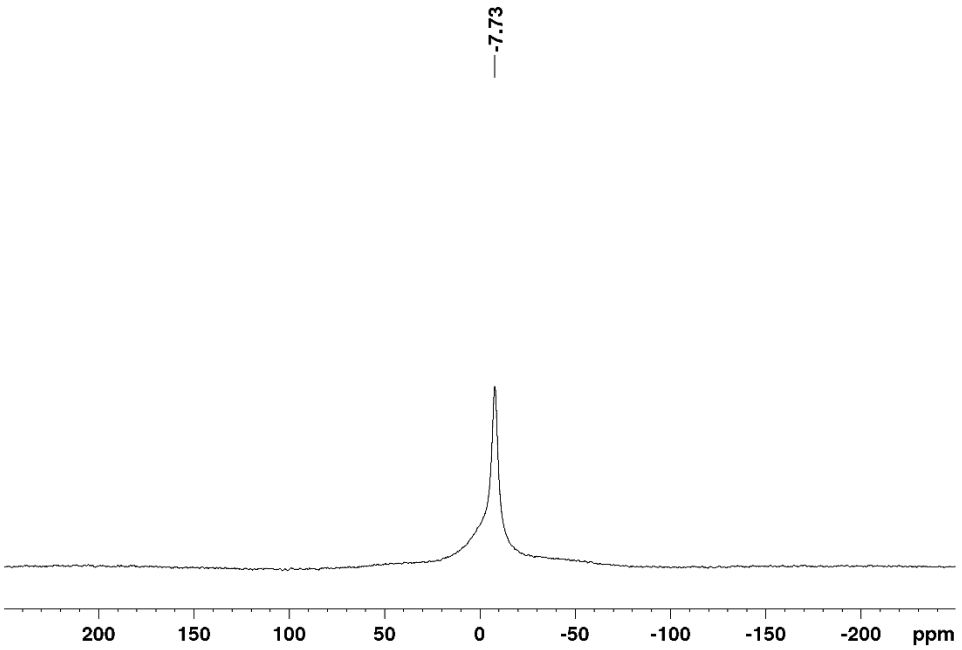

Figure S16 $^{11}B\{^{1}H\}$ NMR spectrum (160 MHz, C_6D_6, 26 °C) of $Tp^{tBu,Me}Yb(NHSiPh_3)(thf)$ (**4**^{thf}).

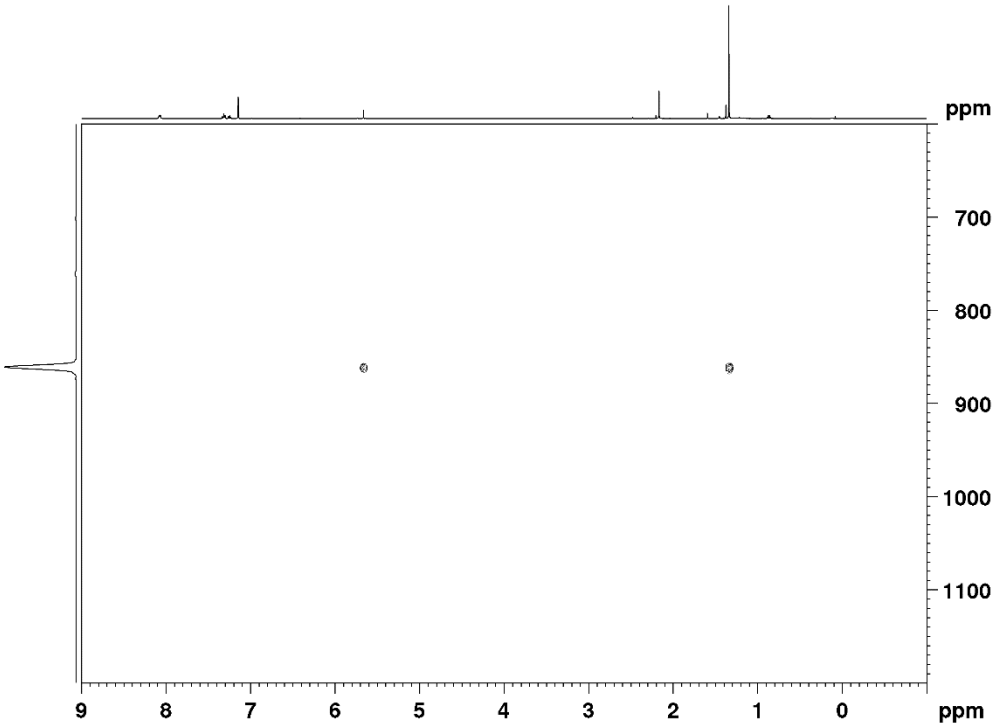

Figure S17 ^{1}H-^{171}Yb HSQC NMR spectrum (500 MHz,87.52 MHz C_6D_6, 26 °C) of $Tp^{tBu,Me}Yb(NHSiPh_3)(thf)$ (**4^{thf}**).

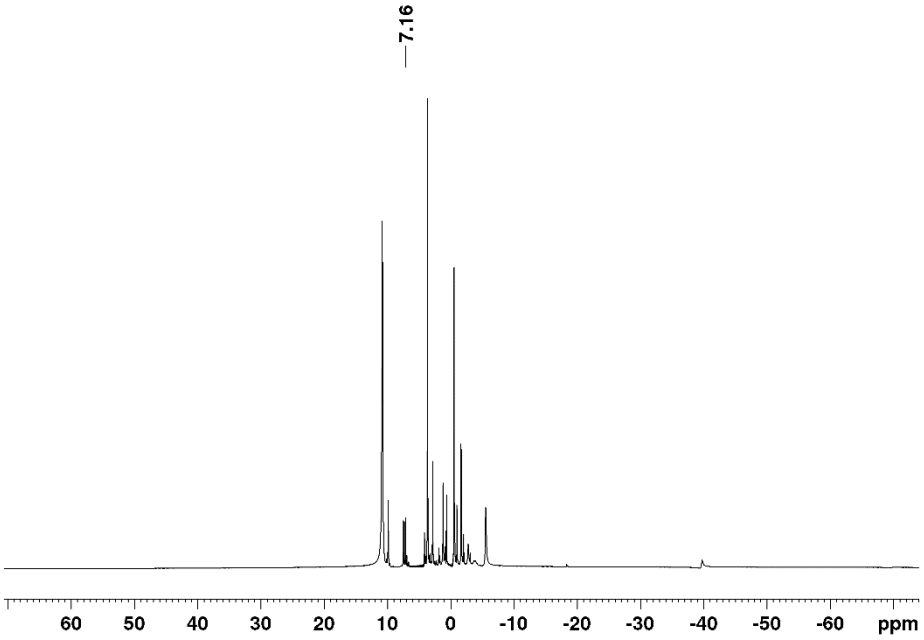

Figure S18 ^{1}H NMR spectrum (400 MHz, C_6D_6, 26 °C) of $Tp^{tBu,Me}Sm(NHAr^{iPr})(thf)$ (**1^{thf,Sm}**)

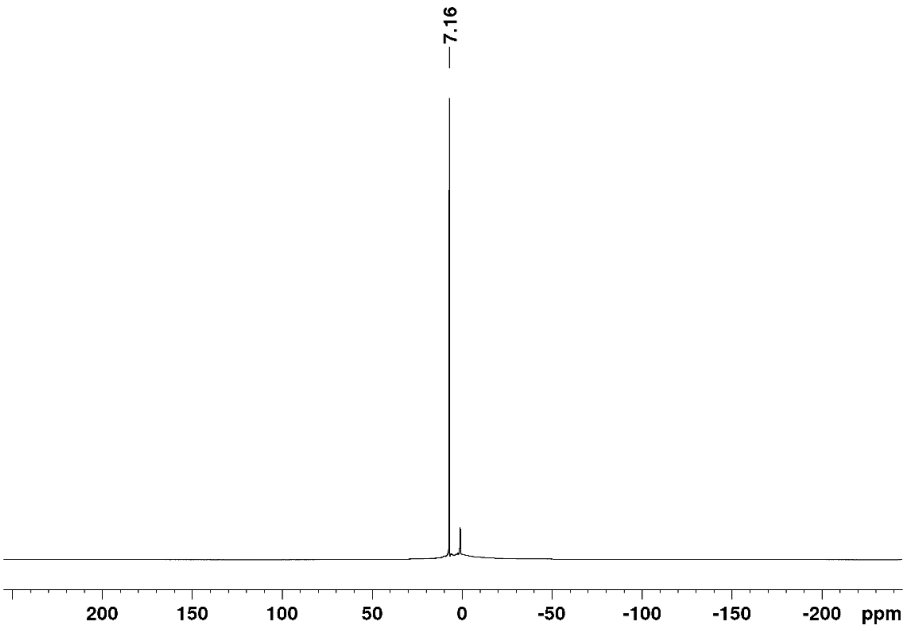

Figure S 19 ^{1}H NMR spectrum (400 MHz, C_6D_6, 26 °C) of $Tp^{tBu,Me}Eu(NHAr^{iPr})(thf)$ (**1^{thf,Eu}**).

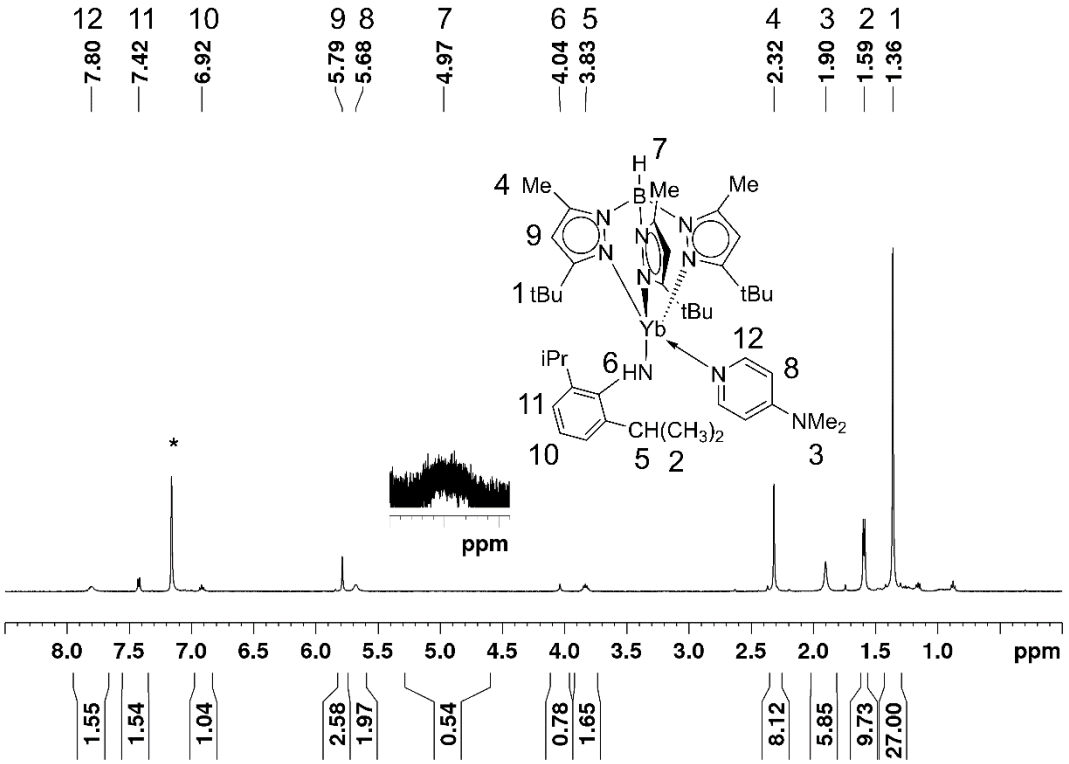

Figure S20 ^{1}H NMR spectrum (500 MHz, C_6D_6, 26 °C) of $Tp^{tBu,Me}Yb(NHAr^{iPr})(dmap)$ (**1^{dmap}**). Residual solvent signals are marked with *.

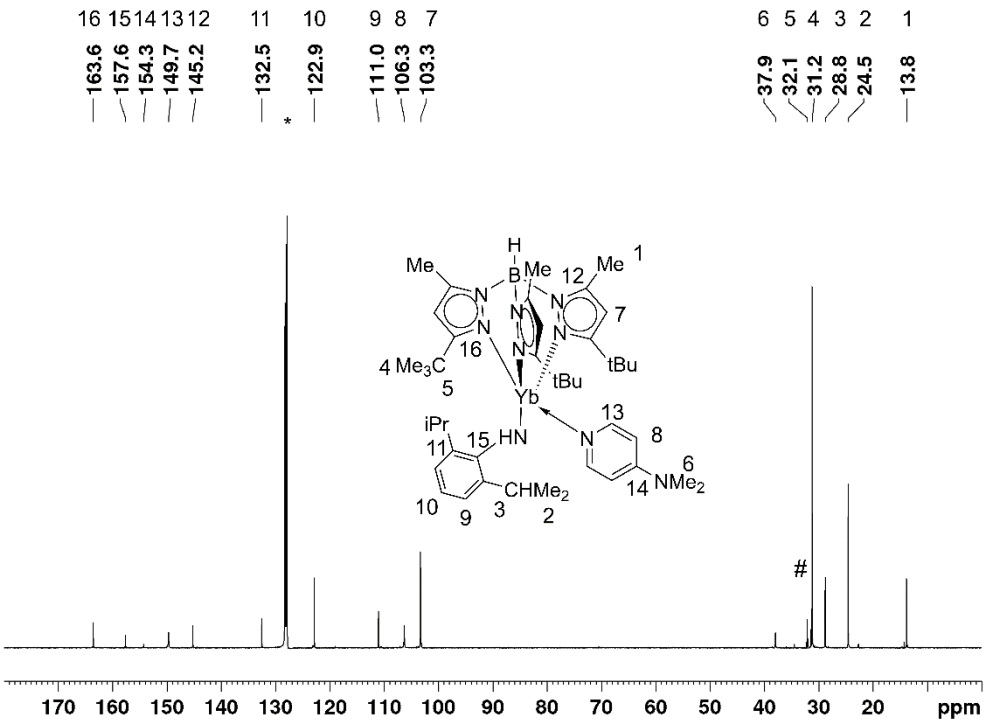

Figure S21 ^{13}C UDEFT NMR spectrum (125 MHz, C_6D_6, 26 °C) of $Tp^{tBu,Me}Yb(NHAr^{iPr})$(dmap) (**1^{dmap}**). Residual solvent signals are marked with *. Minor impurities are marked with #.

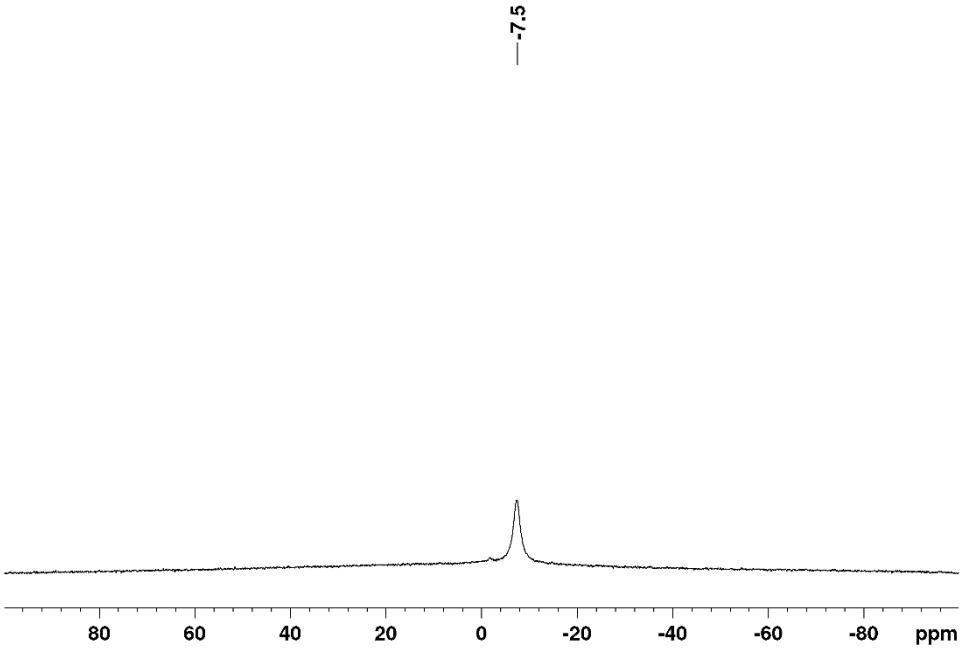

Figure S22 ^{11}B NMR spectrum (160 MHz, C_6D_6, 26 °C) of $Tp^{tBu,Me}Yb(NHAr^{iPr})$(dmap) (**1^{dmap}**).

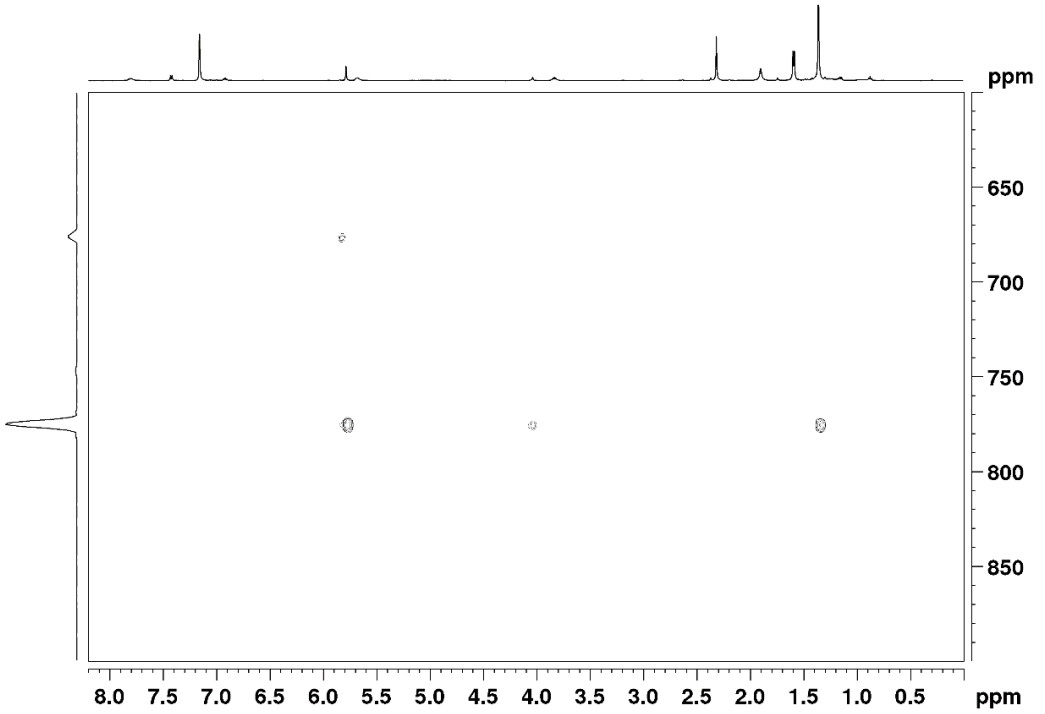

Figure S23 ^{1}H-^{171}Yb HSQC NMR spectrum (500 MHz, 87.52 MHz C_6D_6, 26 °C) of $Tp^{tBu,Me}Yb(NHAr^{iPr})$(dmap) (**1^{dmap}**). Product signal at 776 ppm.

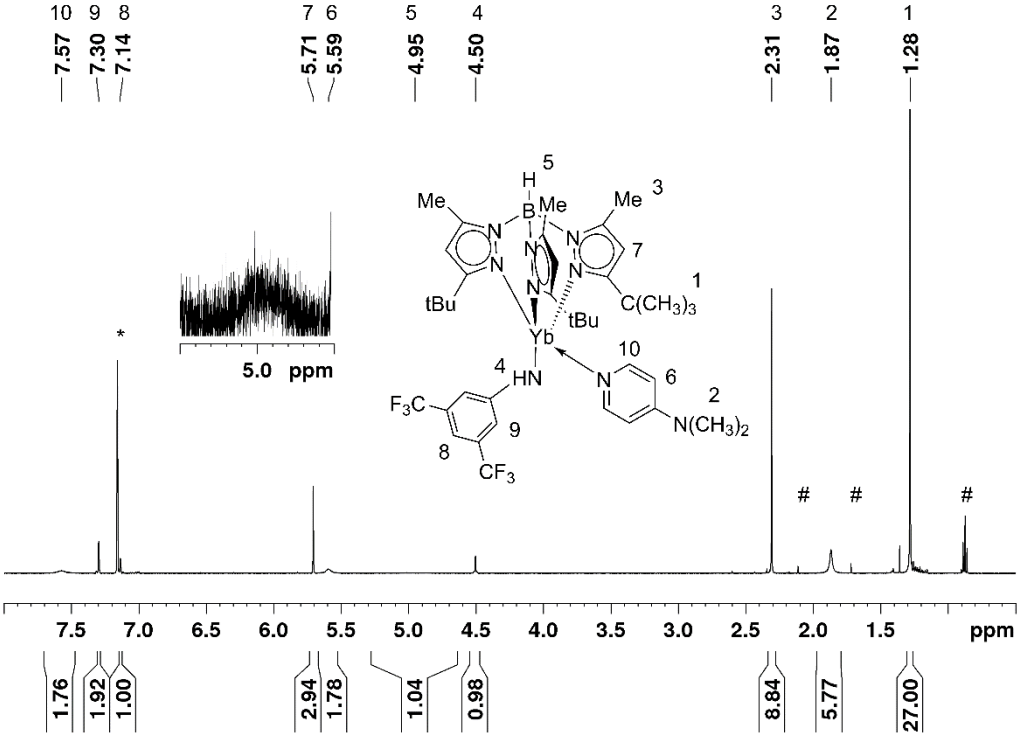

Figure S24 ^{1}H NMR spectrum (500 MHz, C_6D_6, 26 °C) of $Tp^{tBu,Me}Yb(NHAr^{CF3})$(dmap) (**3^{dmap}**). Residual solvent signals are marked with *.

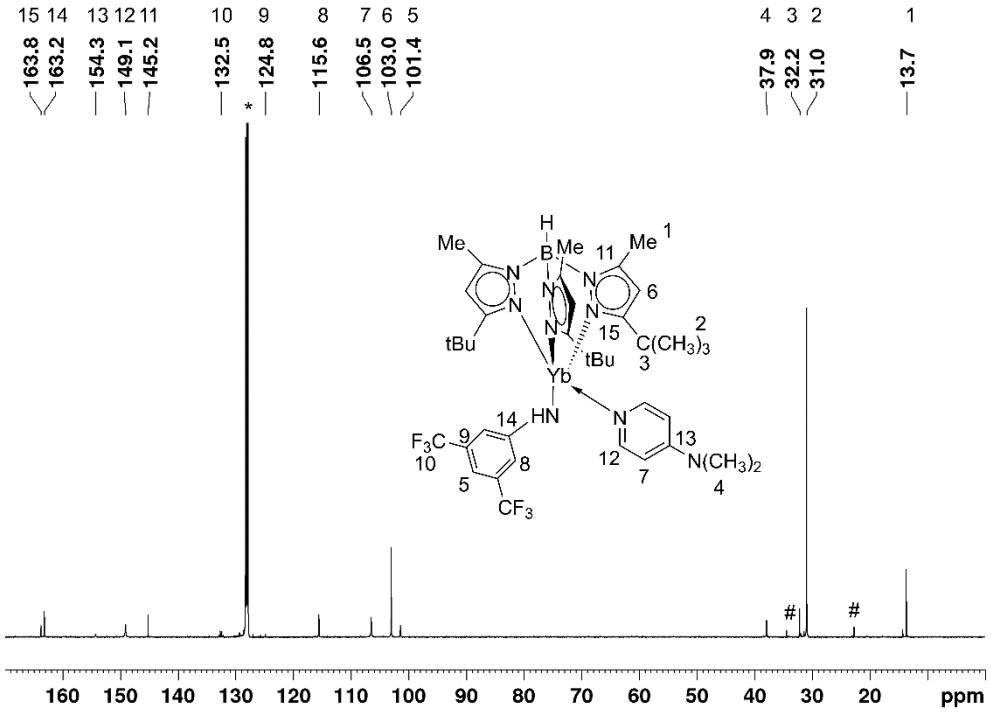

Figure S25 ^{13}C UDEFT NMR spectrum (125 MHz, C_6D_6, 26 °C) of $Tp^{tBu,Me}Yb(NHAr^{CF3})$(dmap) (**3^{dmap}**). Residual solvent signals are marked with *. Minor impurities are marked with #.

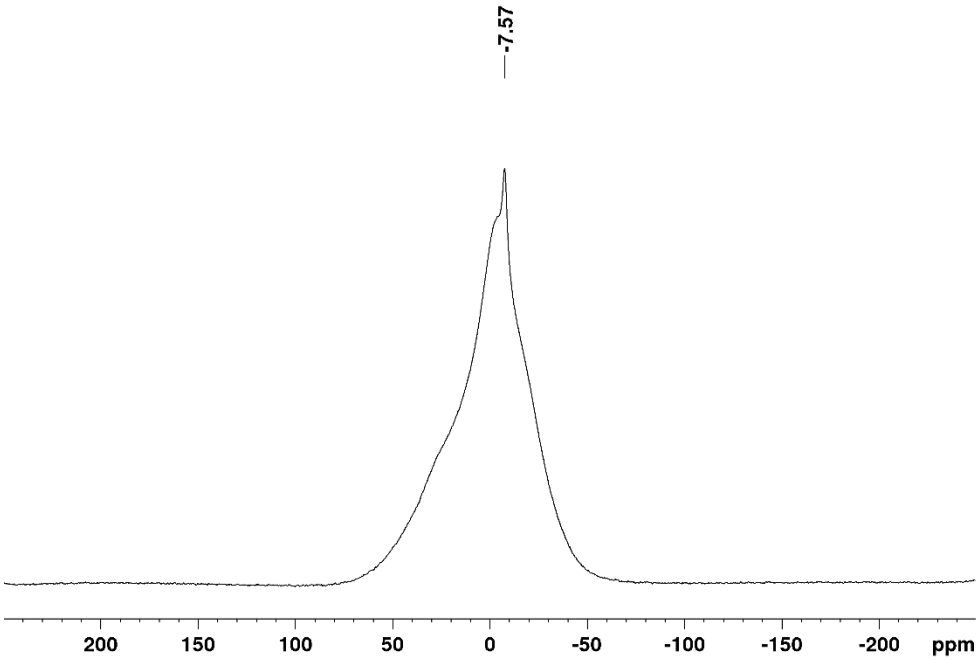

Figure S26 ^{11}B NMR spectrum (128 MHz, C_6D_6, 26 °C) of $Tp^{tBu,Me}Yb(NHAr^{CF3})$(dmap) (**3^{dmap}**).

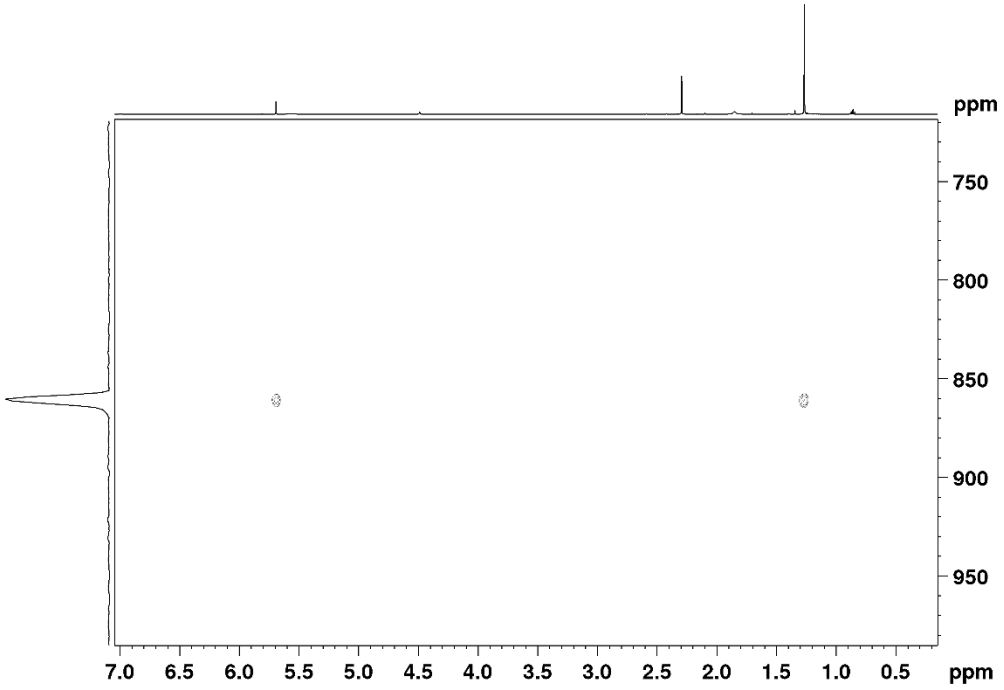

Figure S27 ^{1}H-^{171}Yb HSQC NMR spectrum (500 MHz, 87.52 MHz C_6D_6, 26 °C) of $Tp^{tBu,Me}Yb(NHAr^{CF3})(dmap)$ (**3^{dmap}**). Product signal at 862 ppm.

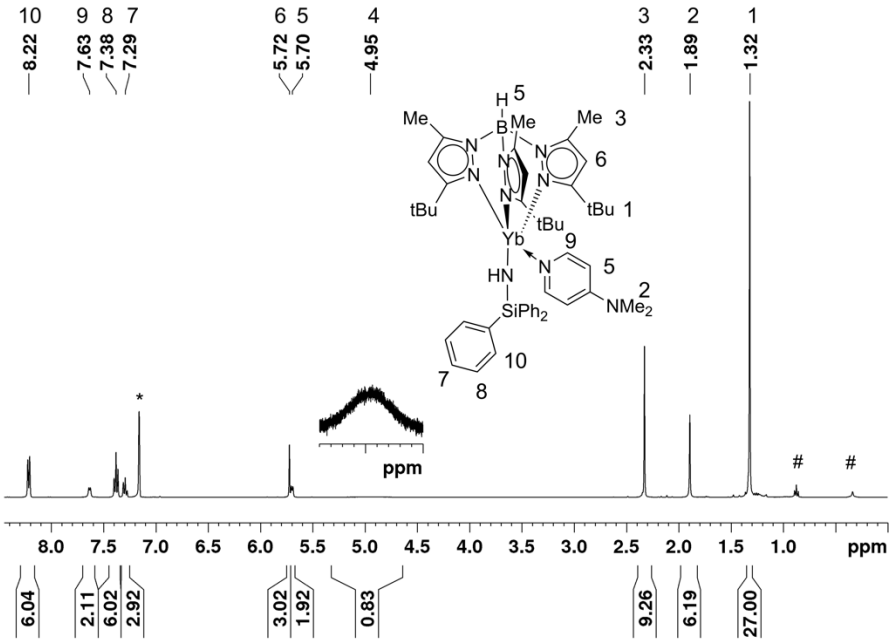

Figure S28 ^{1}H NMR spectrum (500 MHz, C_6D_6, 26 °C) of $Tp^{tBu,Me}Yb(NHSiPh_3)(dmap)$ (**4^{dmap}**). Residual solvent signals are marked with *, minor impurities are marked with #.

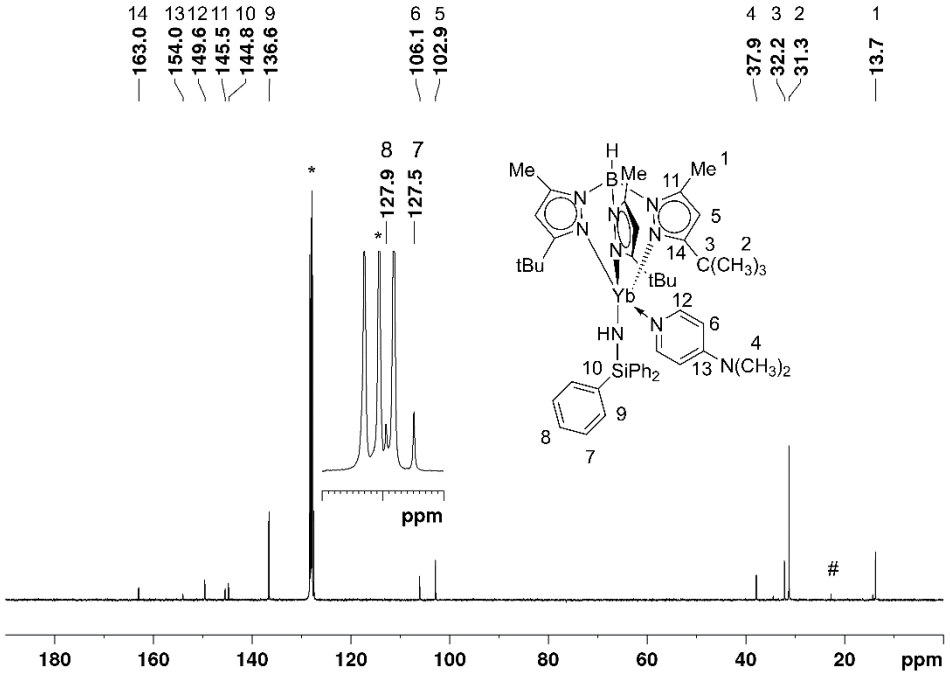

Figure S29 $^{13}C\{^{1}H\}$ UDEFT NMR spectrum (100 MHz, C_6D_6, 26 °C) of $Tp^{tBu,Me}Yb(NHSiPh_3)(dmap)$ (**4^{dmap}**). Residual solvent signals are marked with *, minor impurities are marked with #.

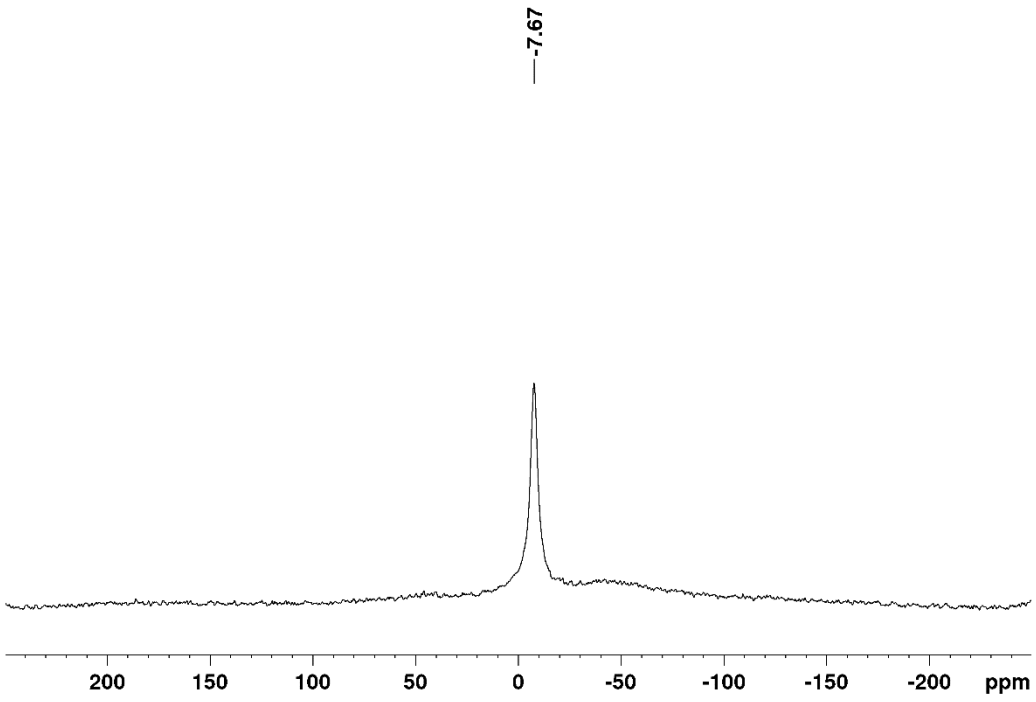

Figure S30 $^{11}B\{^{1}H\}$ NMR spectrum (96 MHz, C_6D_6, 26 °C) of $Tp^{tBu,Me}Yb(NHSiPh_3)(dmap)$ (**4^{dmap}**). Residual solvent signals are marked with *, minor impurities are marked with #.

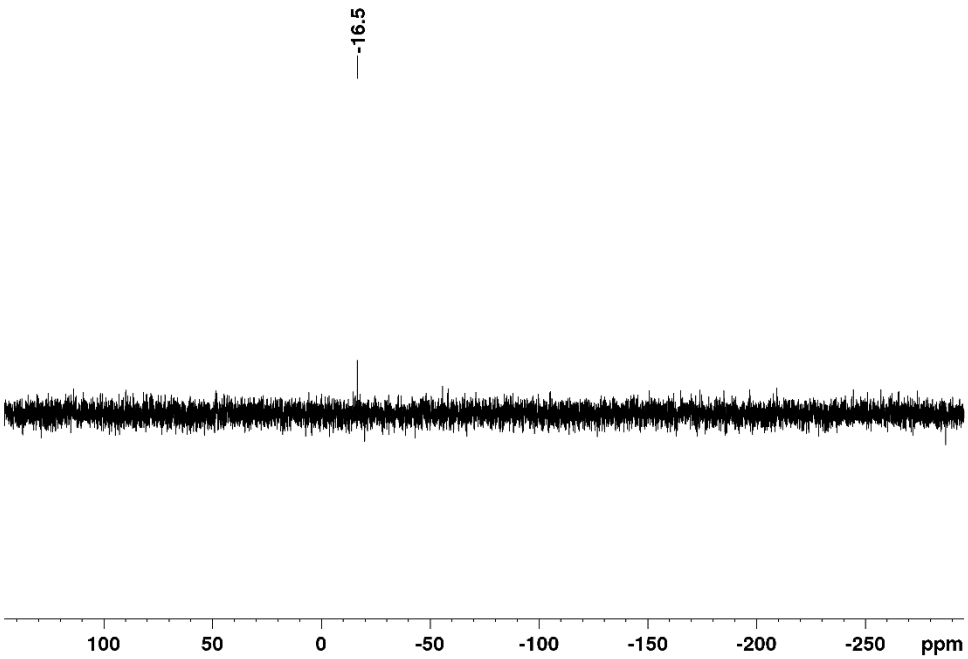

Figure S31 ^{29}Si DEPT45 NMR spectrum (60 MHz, C_6D_6, 26 °C) of $Tp^{tBu,Me}Yb(NHSiPh_3)(dmap)$ (**4^{dmap}**).

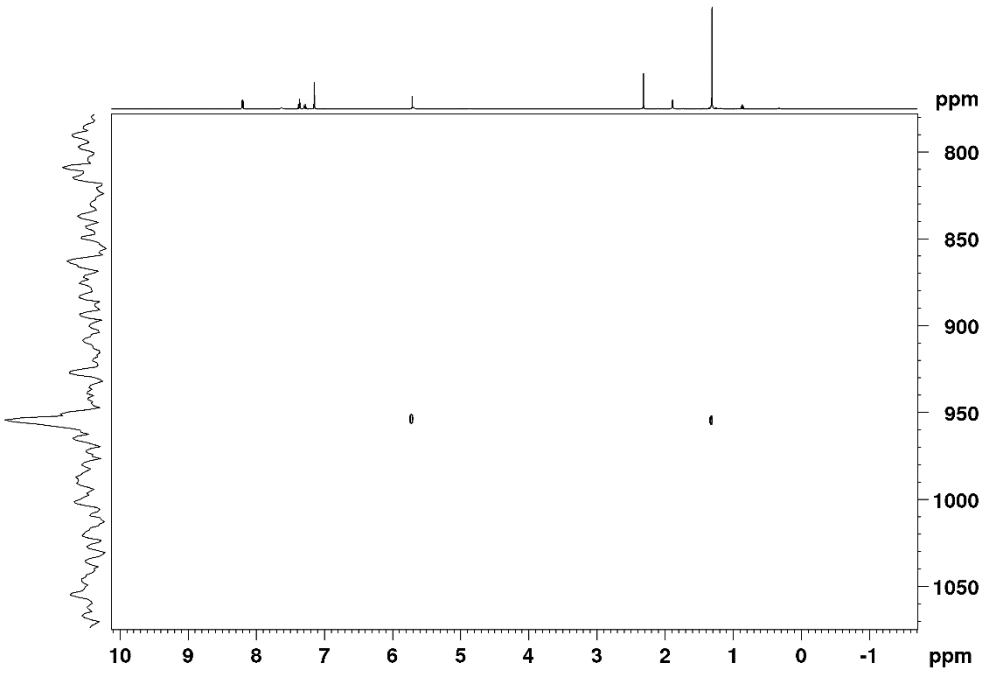

Figure S32 ^{1}H-^{171}Yb HSQC NMR spectrum (500 MHz, 87.52 MHz C_6D_6, 26 °C) of $Tp^{tBu,Me}Yb(NHSiPh_3)(dmap)$ (**4^{dmap}**). Product signal at 954 ppm

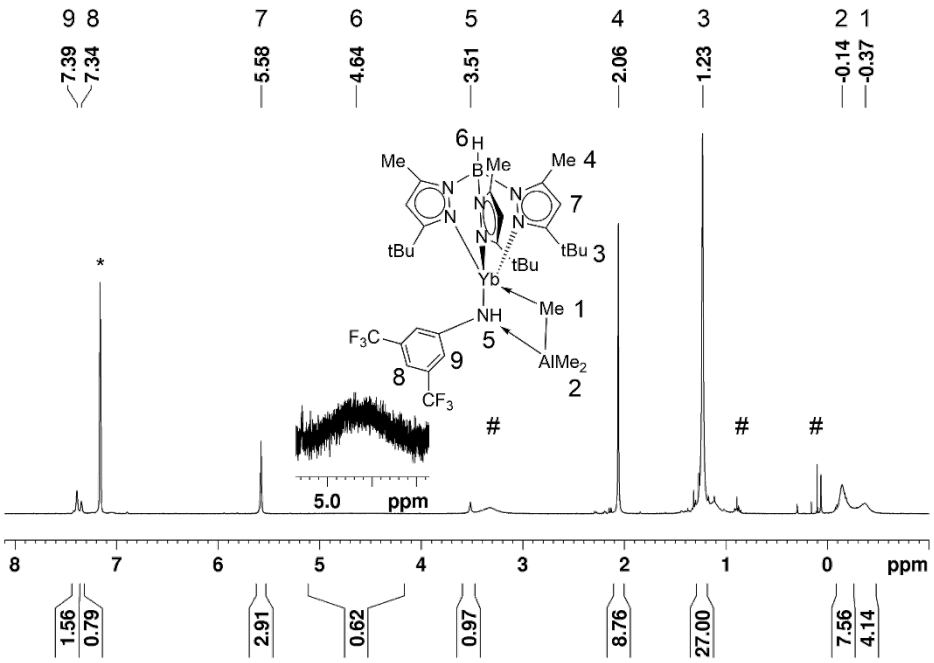

Figure S33 ^{1}H NMR spectrum (300 MHz, C_6D_6, 26 °C) of $Tp^{tBu,Me}Yb(NHAr^{CF3})(AlMe_3)$ (**6**).

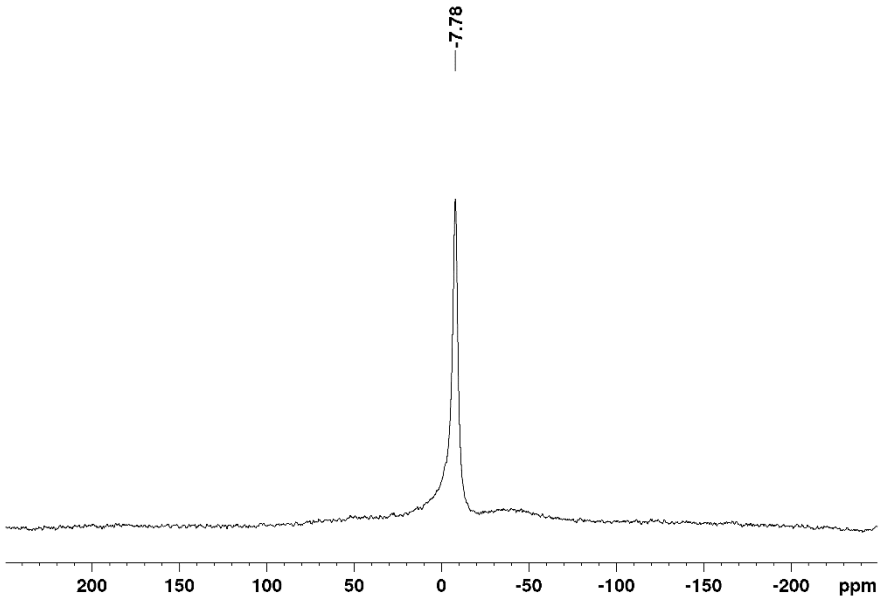

Figure S34 ^{11}B NMR spectrum (96 MHz, C_6D_6, 26 °C) of $Tp^{tBu,Me}Yb(NHAr^{CF3})(AlMe_3)$ (**6**).

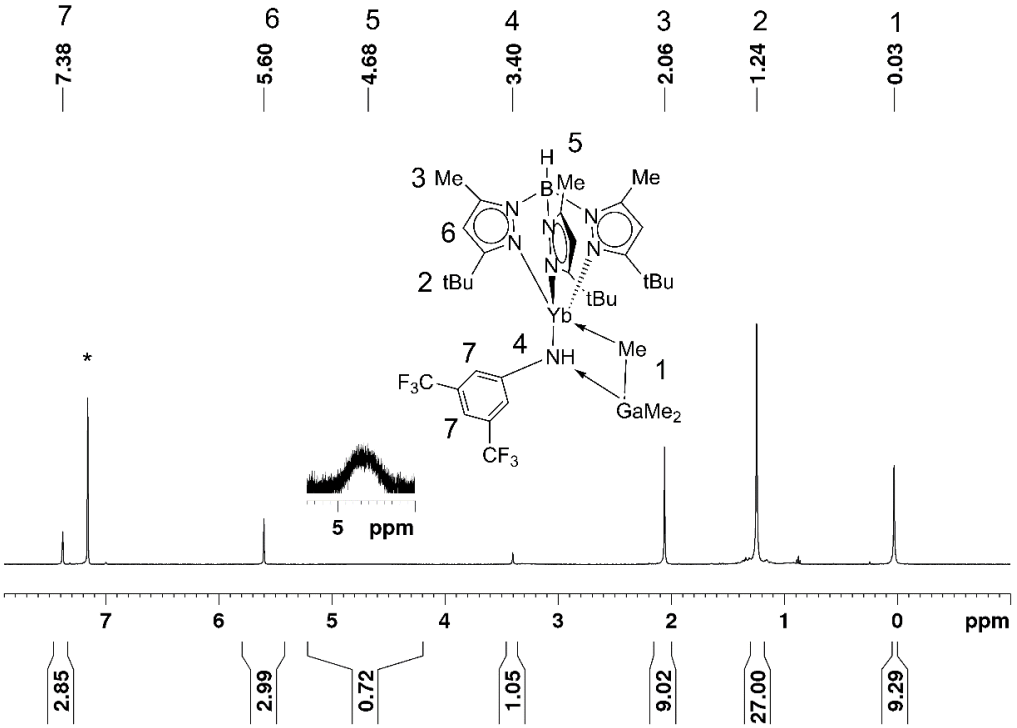

Figure S35 ^{1}H NMR spectrum (500 MHz, C_6D_6, 26 °C) of $Tp^{tBu,Me}Yb(NHAr^{CF3})(GaMe_3)$ (**7**).

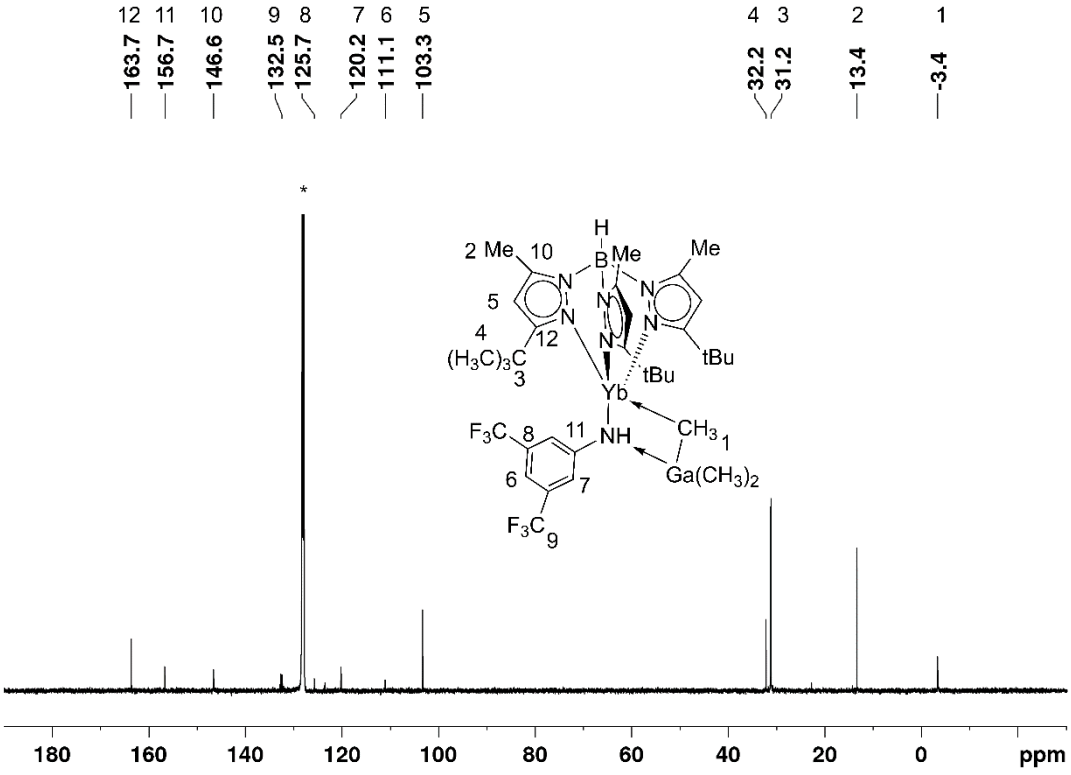

Figure S36 $^{13}C\{^{1}H\}$ NMR spectrum (125 MHz, C_6D_6, 26 °C) of $Tp^{tBu,Me}Yb(NHAr^{CF3})(GaMe_3)$ (**7**). Residual solvent signals are marked with *

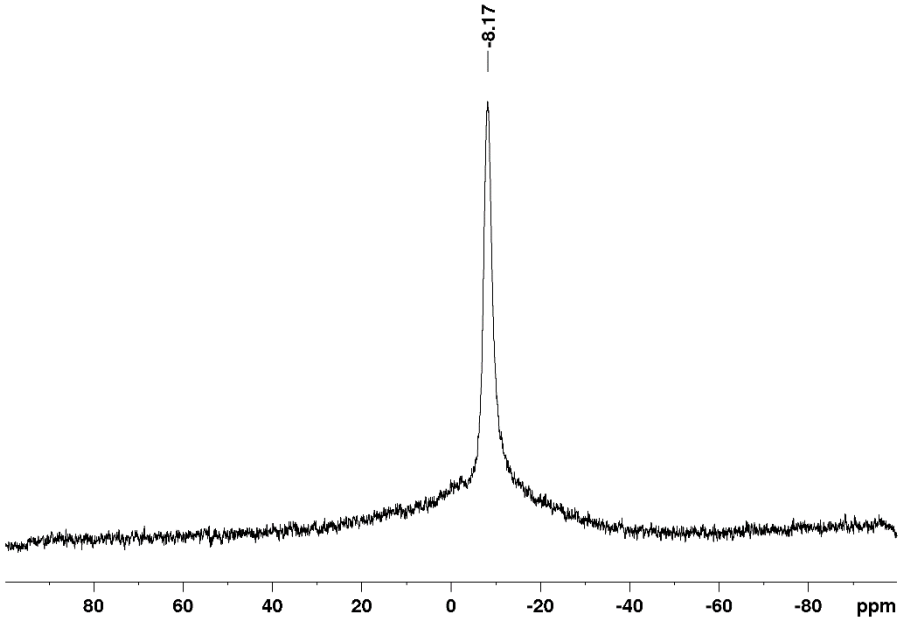

Figure S37 ^{11}B NMR spectrum (160 MHz, C_6D_6, 26 °C) of $Tp^{tBu,Me}Yb(NHAr^{CF3})(GaMe_3)$ (**7**).

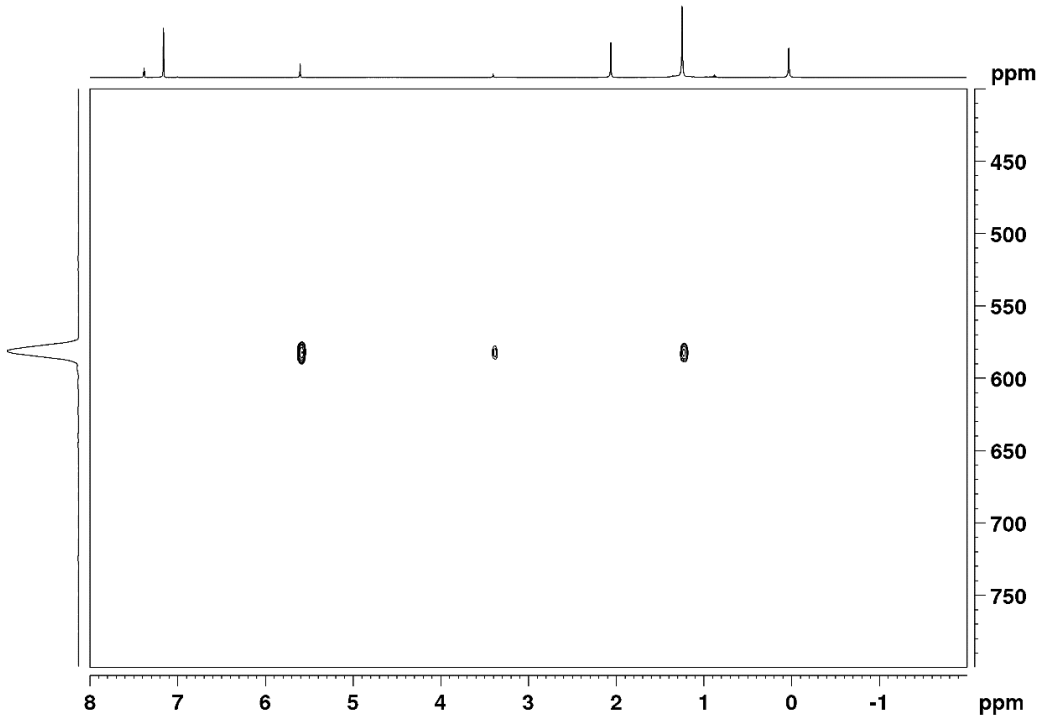

Figure S38 ^{1}H-^{171}Yb HSQC NMR spectrum (500 MHz, 87.52 MHz C_6D_6, 26 °C) of $Tp^{tBu,Me}Yb(NHAr^{CF3})(GaMe_3)$ (**7**). Product signal at 582 ppm.

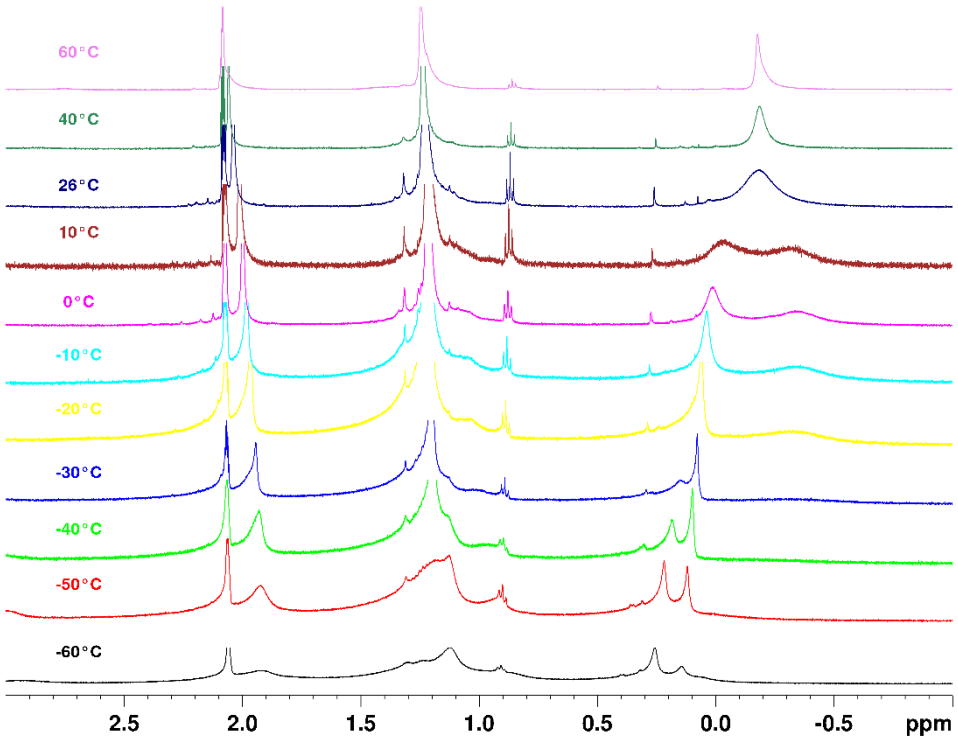

Figure S39 ^{1}H VT NMR spectra (500 MHz, toluene-d_8) of $Tp^{tBu,Me}Yb(NHAr^{CF3})(GaMe_3)$ (**7**). In the region of 0.5 to -0.5 ppm the signal splitting of the coordinated $Ga(CH_3)_3$ can be observed at low temperatures.

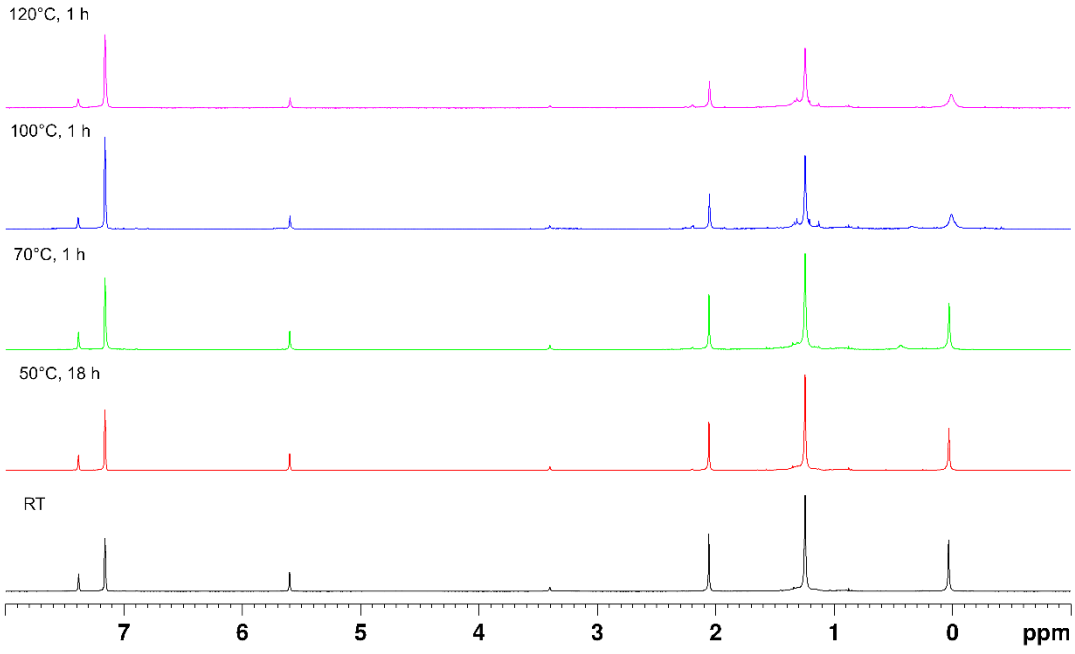

Figure S40 ^{1}H VT NMR spectra (500 MHz, C_6D_6) of $Tp^{tBu,Me}Yb(NHAr^{CF3})(GaMe_3)$ (**7**).

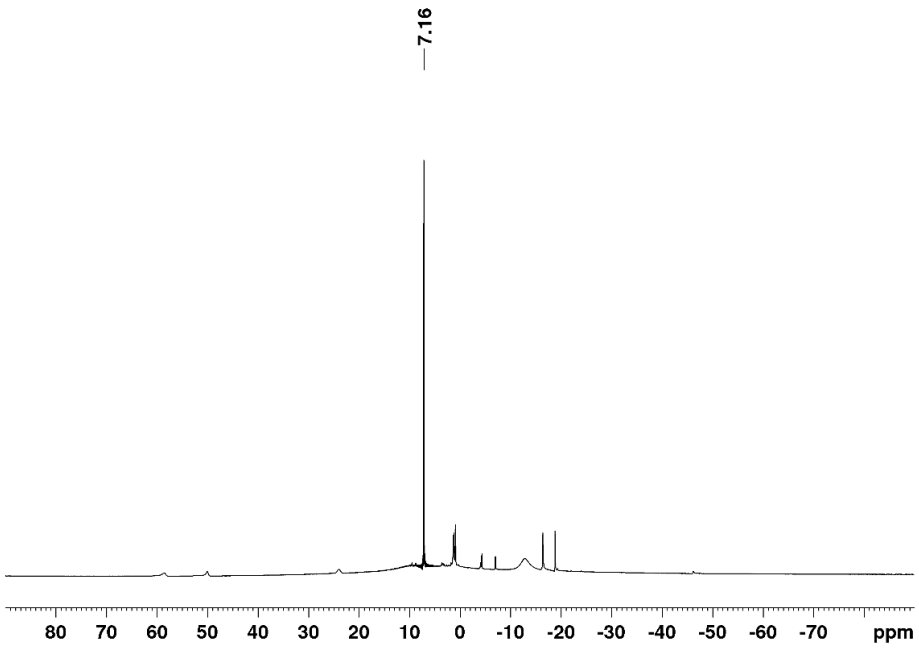

Figure S41 ^{1}H NMR spectrum (400 MHz, C_6D_6, 26 °C) of $Tp^{tBu,Me}Yb(NHAr^{iPr})(Cl)$ (**9a**).

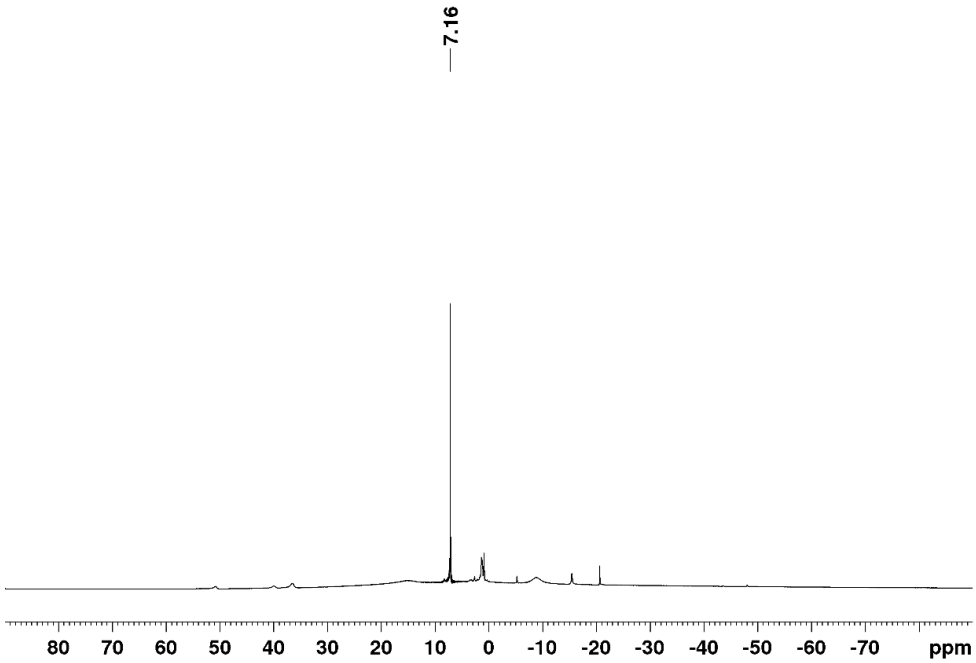

Figure S42 ^{1}H NMR spectrum (400 MHz, C_6D_6, 26 °C) of $Tp^{tBu,Me}Yb(NHAr^{iPr})(Br)$ (**9b**).

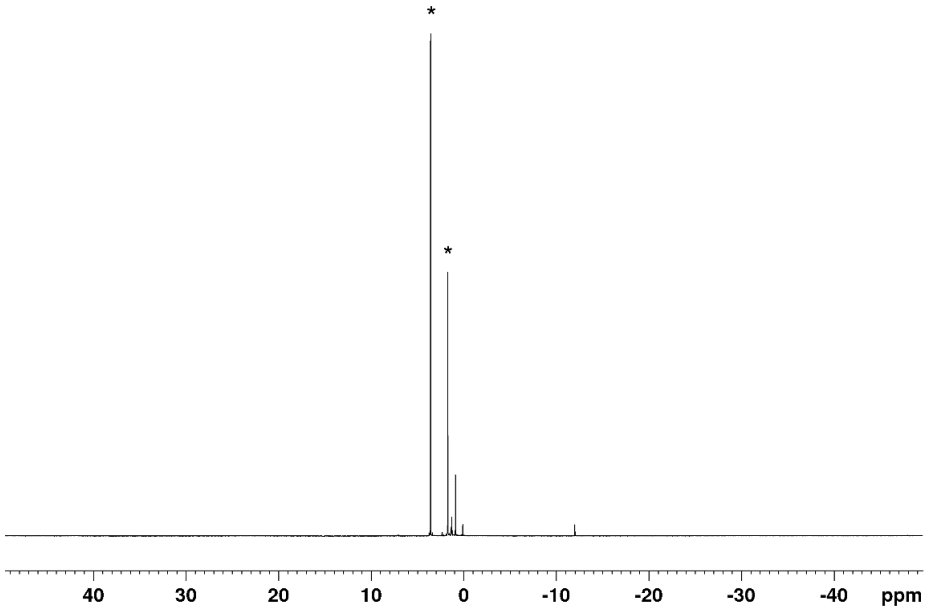

Figure S43 ^{1}H NMR spectrum (400 MHz, C_6D_6, 26 °C) of $Tp^{tBu,Me}Yb(NHAr^{CF3})(Cl)$ (**10a**).

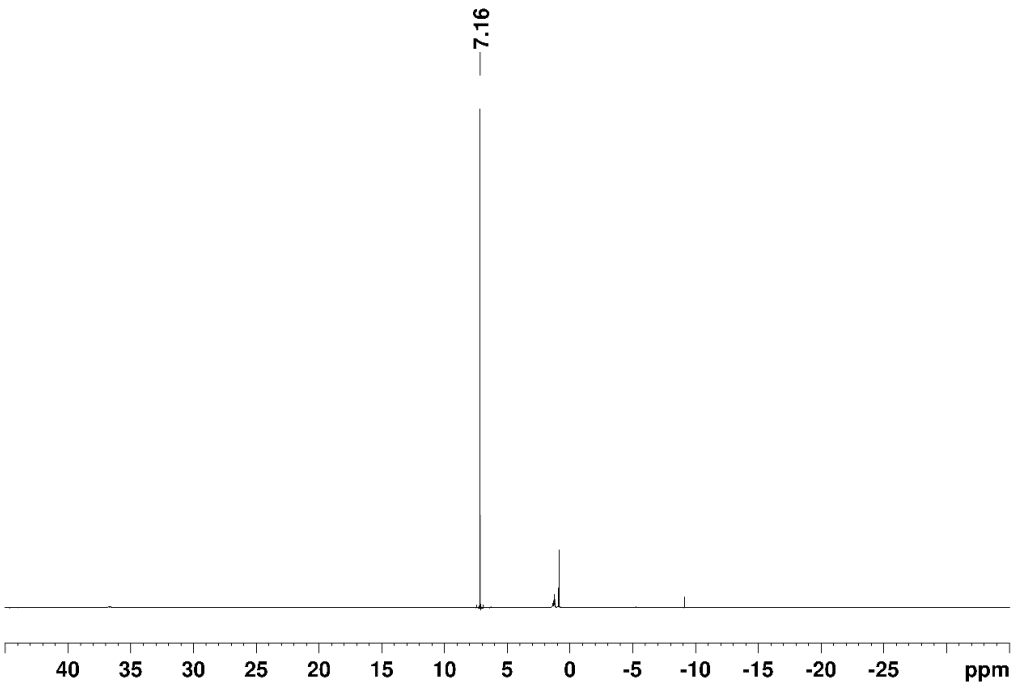

Figure S44 ^{1}H NMR spectrum (400 MHz, C_6D_6, 26 °C) of $Tp^{tBu,Me}Yb(NHAr^{CF3})(Br)$ (**10b**).

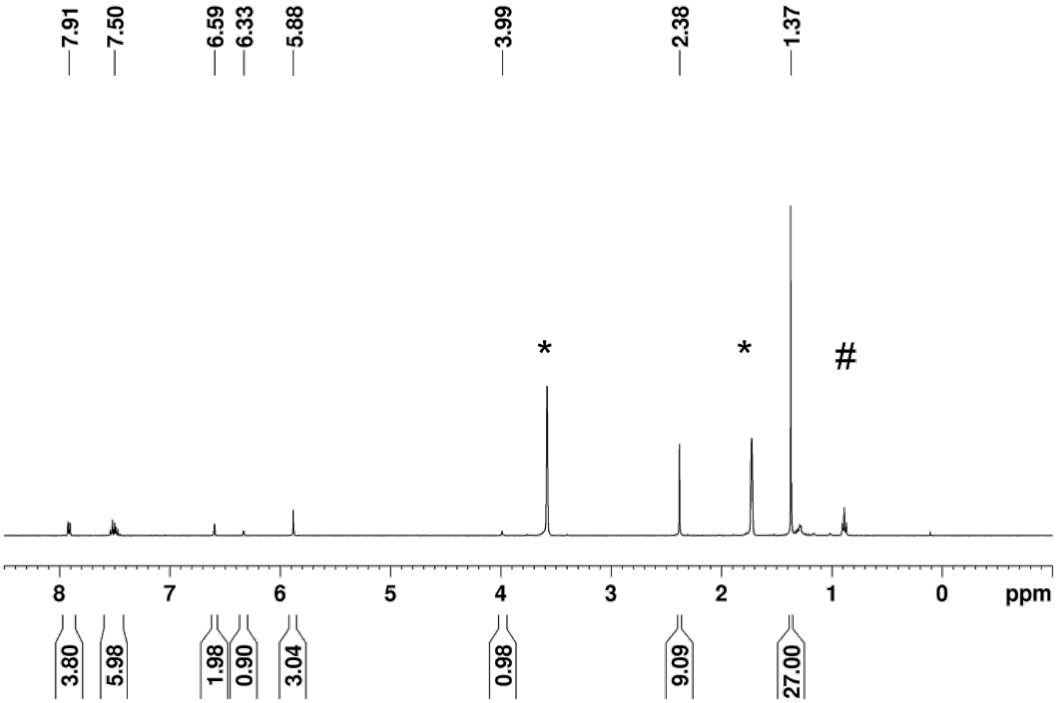

Figure S45 ^{1}H NMR spectrum (400 MHz, THF-*d*8, 26 °C) of $Tp^{tBu,Me}Yb(NHA^{CF3})(N_2Ph_2)$ (**11**). Residual solvent signals are marked with *. Minor impurities are marked with #.

Crystallographic Data

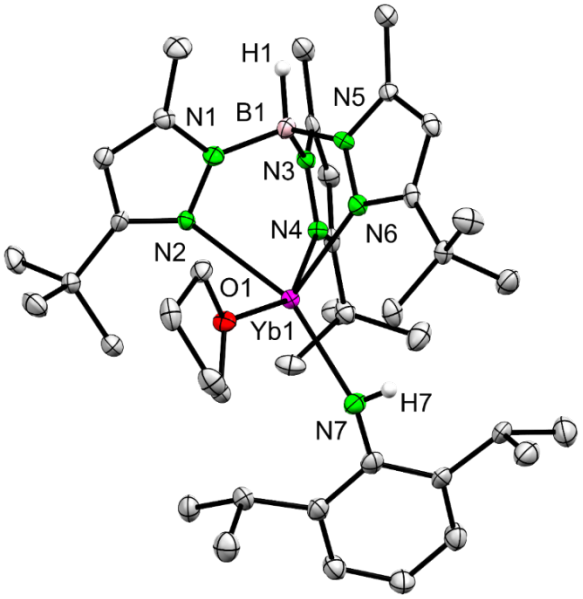

Figure S46 Crystal structure of $Tp^{tBu,Me}Yb(NHAr^{iPr})(thf)$ (**1**^{thf}). All atoms are represented by atomic displacement ellipsoids set at 50% probability. Hydrogen atoms, lattice solvent *n*-hexane and disorder in thf are omitted for clarity. Selected interatomic distances [Å] and angles [°]: Yb1 – N2 2.544(3), Yb1 – N4 2.487(3), Yb1 – N6 2.526(3), Yb1 – N7 2.353(4), Yb1 – O1 2.431(3), Yb1 – N7 – C25 147.8(3), Yb1 –N7 – H7 91(3), C25 – N7 – H7 110(3), N7 – Yb1 – O1 92.60(12).

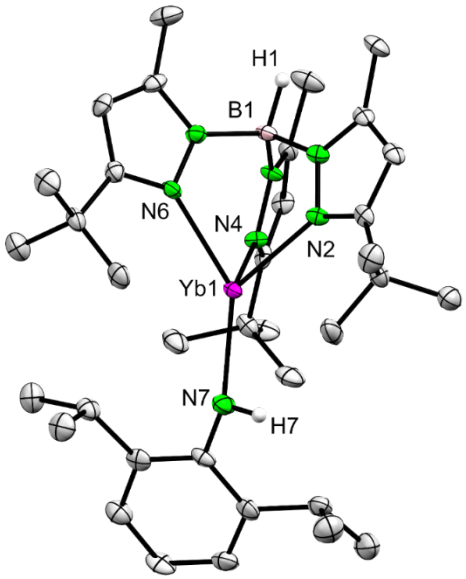

Figure S47 Crystal structure of $Tp^{tBu,Me}Yb(NHAr^{iPr})$ (**1**). All atoms are represented by atomic displacement ellipsoids set at 50% probability. Hydrogen atoms and disorder in thf are omitted for clarity. Selected interatomic distances [Å] and angles [°]: Yb1 – N2 2.428(4), Yb1 – N4 2.428(5), Yb1 – N6 2.425(4), Yb1 – N7 2.345(5), Yb1 – N7 – C25 139.1(4), Yb1 – N7 – H7 103(5), C25 – N7 – H7 105(5).

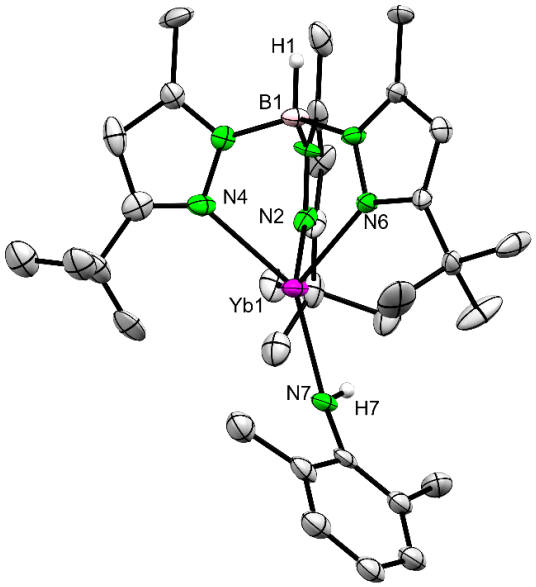

Figure S 48 Crystal structure of $Tp^{tBu,Me}Yb(NHAr^{Me})$ (**2**). All atoms are represented by atomic displacement ellipsoids set at 50% probability. Hydrogen atoms and disorder in *t*Bu groups as well as the amid substituent are omitted for clarity. Selected interatomic distances [Å] and angles [°], values marked with * were calculated with Platon: Yb1 – N2 2.40(2), Yb1 – N4 2.457(19), Yb1 – N6 2.410(4), Yb1 – N7/7A 2.30(3)/2.29(3), Yb1 – N7 – C25 150(2), Yb1 – N7A – C25A 153(2), Yb1 – N7 – H7 77(15), Yb1 – N7A – H7A 103*, C25 – N7 – H7 118(14), C25A – N7A – H7A 103*.

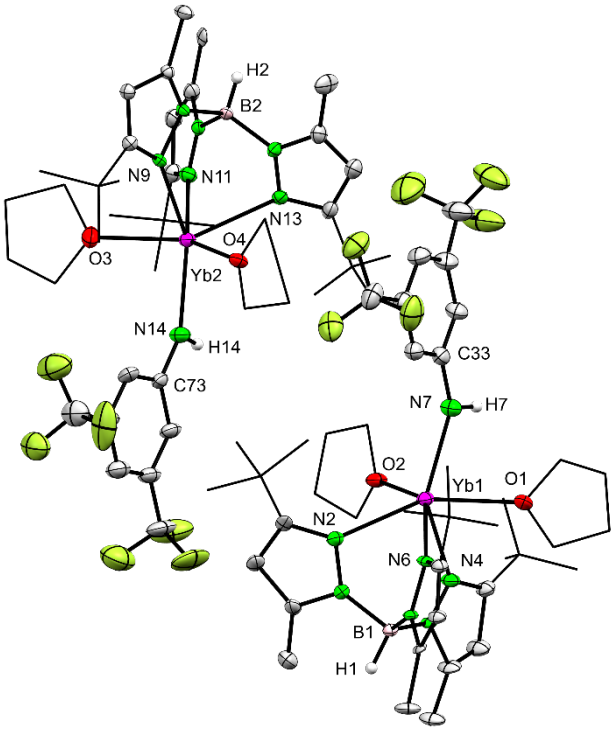

Figure S49 Crystal structure of $Tp^{tBu,Me}Yb(NHAr^{CF3})(thf)_2$ **(3^{thf})**. All atoms are represented by atomic displacement ellipsoids set at 50% probability. Hydrogen atoms, lattice solvent pentane and disorder in CF_3 groups are omitted for clarity. Selected interatomic distances [Å] and angles [°], values marked with * were calculated with Platon: Yb1 – N2 2.51(2), Yb1 – N4 2.55(2), Yb1 – N6 2.469(18), Yb1 – N7 2.411(12), Yb1 – N7 – C33 143.2(10), Yb1 – N7 – H7 108*, C33 – N7 – H7 108*, N7 – Yb1 – O1 78.4(5), N7 – Yb1 – O2 81.0(6), Yb2 – N9 2.599(19), Yb2 – N11 2.56(2), Yb2 – N13 2.60(2), Yb2 – N14 2.411(12), Yb2 – O3 2.50(2), Yb2 – O4 2.546(17), Yb2 – N14 – C73 145.4(10), Yb2 – N14 – H14 107*, C73 – N14 – H14 107*, N14 – Yb2 – O3 86.5(6), N14 – Yb2 – O4 83.8(5).

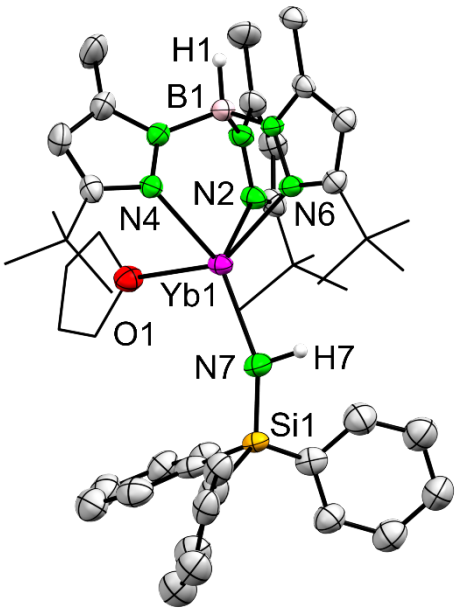

Figure S50 Crystal structure of $Tp^{tBu,Me}Yb(NHSiPh_3)(thf)$ (**4** ^{thf}). All atoms are represented by atomic displacement ellipsoids set at 50% probability. Hydrogen atoms and disorders in phenyl, *t*Bu substituents and thf are omitted for clarity. Selected interatomic distances [Å] and angles [°], values marked with * were calculated with Platon: Yb1 – N2 2.519(2), Yb1 – N4 2.473(2), Yb1 – N6 2.450(2), Yb1 – N7/7A 2.341(3)/2.287(10), Yb1 – O1 2.4472(19), Yb1 – N7 – Si1 154.0(2), Yb1 – N7A – Si1A 153.7(6), Yb1 – N7 – H7 94(2), Si1 – N7 – H7 111(2), Si1A – N7A – H7D 92(9).

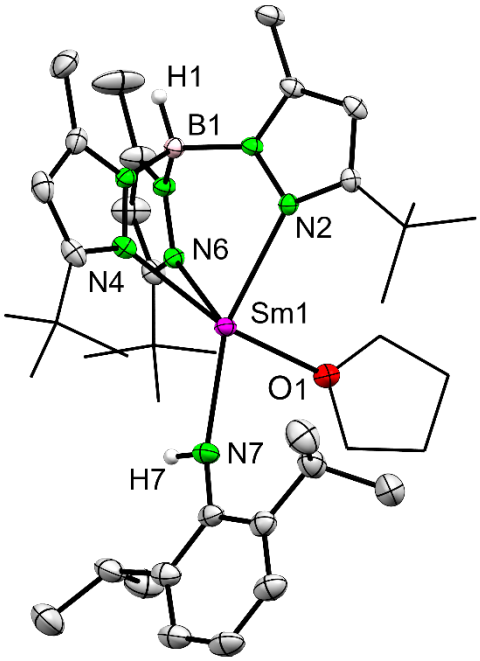

Figure S51 Crystal structure of $Tp^{tBu,Me}Sm(NHAr^{iPr})(thf)$ (**1**^{thf,Sm}). All atoms are represented by atomic displacement ellipsoids set at 50% probability. Hydrogen atoms and disorder in *t*Bu groups are omitted for clarity. Selected interatomic distances [Å] and angles [°], values marked with * were calculated with Platon: Sm1 – N2 2.6573(17), Sm1 – N4 2.632(2), Sm1 – N6 2.6184(17), Sm1 – N7 2.483(2), Sm1 – N7 – C25 157.46(17).

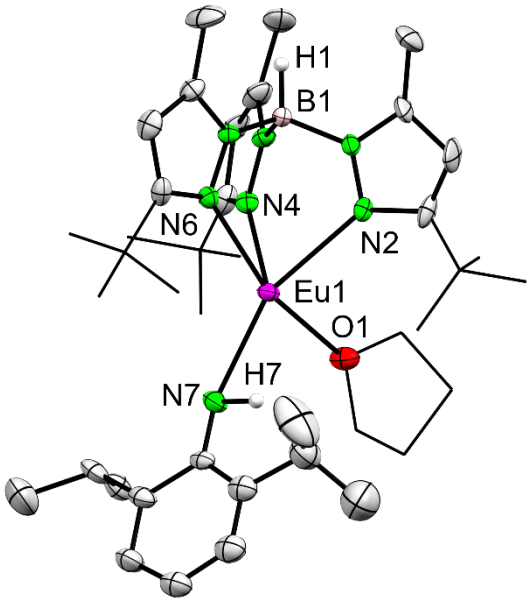

Figure S52 Crystal structure of Tp^{tBu,Me}Eu(NHAr^{iPr})(thf) (**1^{thf,Eu}**). All atoms are represented by atomic displacement ellipsoids set at 50% probability. Hydrogen atoms and disorder in *t*Bu groups as well as the amid substituent are omitted for clarity. Selected interatomic distances [Å] and angles [°]: Eu1 – N2 2.629(12), Eu1 – N4 2.616(12), Eu1 – N6 2.610(3), Eu1 – N7/7A 2.474(17)/2.48(3), Eu1 – N7 – C25 158.4(16), Eu1 – N7A – C25A 159(2).

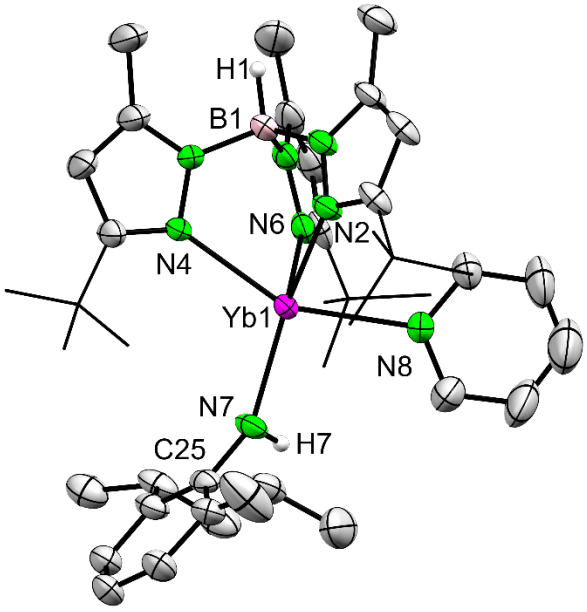

Figure S53 Crystal structure of Tp^{tBu,Me}Yb(NHAr^{iPr})(py) (**1^{py}**). All atoms are represented by atomic displacement ellipsoids set at 50% probability. Hydrogen atoms and disorders of the *i*Pr and one *t*Bu groups are omitted for clarity. Selected interatomic distances [Å] and angles [°]: Yb1 – N2 2.479(4), Yb1 – N4 2.508(4), Yb1 – N6 2.492(5), Yb1 – N7 2.358(4), Yb1 – N8 2.554(4), Yb1 – N7 – C30 147.6(3), Yb1 – N7 – H7 106.2, C30 – N7 – H7 106.2, N7 – Yb1 – N8 96.61(15).

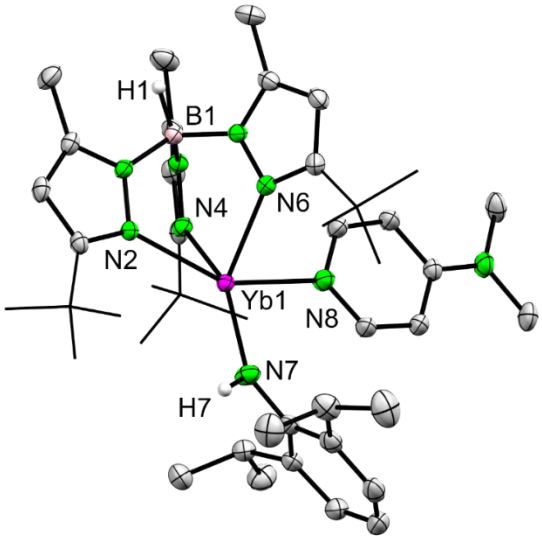

Figure S54 Crystal structure of $Tp^{tBu,Me}Yb(NHAr^{iPr})(dmap)$ (**1**^{dmap}). All atoms are represented by atomic displacement ellipsoids set at 50% probability. Hydrogen atoms and disorder in one *t*Bu are omitted for clarity. Selected interatomic distances [Å] and angles [°], values marked with * were calculated with Platon: Yb1 – N2 2.5105(14), Yb1 – N4 2.5294(15), Yb1 – N6 2.4535(15), Yb1 – N7 2.3443(16), Yb1 – N8 2.4896(15), Yb1 – N7 – C30 138.03(12), Yb1 – N7 – H7 125.0(13)*, C30 – N7 – H7 96.9(13)*, N7 – Yb1 – N8 97.46(5).

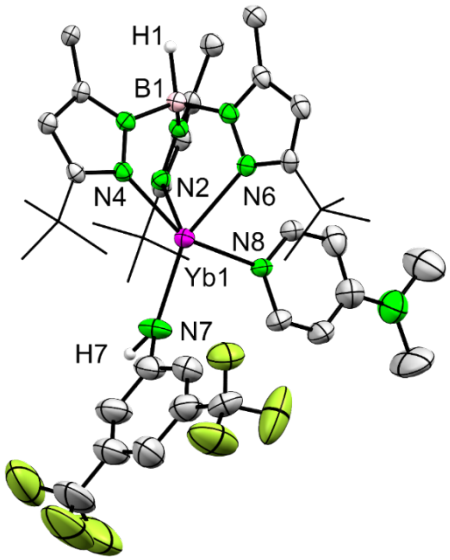

Figure S55 Crystal structure of $Tp^{tBu,Me}Yb(NHAr^{CF3})(dmap)$ (**3**^{dmap}). All atoms are represented by atomic displacement ellipsoids set at 50% probability. Hydrogen atoms and disorders of the CF_3 groups are omitted for clarity. Selected interatomic distances [Å] and angles [°], values marked with * were calculated with Platon: Yb1 – N2 2.461(5), Yb1 – N4 2.475(5), Yb1 – N6 2.484(5), Yb1 – N7 2.372(6), Yb1 – N8 2.486(5), Yb1 – N7 – C25 144.6(6), Yb1 – N7 – H7 84(8)*, N7 – Yb1 – N8 92.2(2).

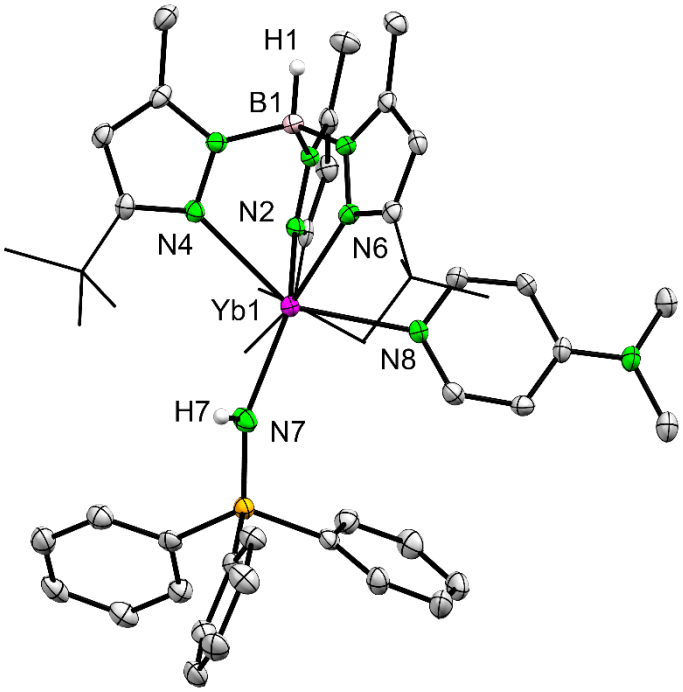

Figure S56 Crystal structure of$Tp^{tBu,Me}Yb(NHSiPh_3)(dmap)$ (**4**^{dmap}). All atoms are represented by atomic displacement ellipsoids set at 50% probability. Hydrogen atoms are omitted for clarity. Selected interatomic distances [Å] and angles [°]: Yb1 – N2 2.476(3), Yb1 – N4 2.566(3), Yb1 – N6 2.460(3), Yb1 – N7 2.337(3). Yb1 – N8 2.549(3), Yb1 – N7 – Si1 149.92(18), Yb1 – N7 – H7 107(4), Si1 – N7 – H7 103(4), N7 – Yb1 – N8 103.11(10).

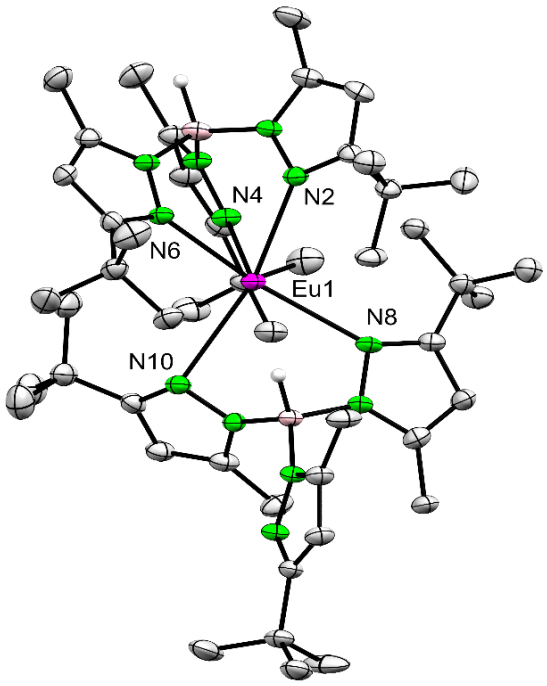

Figure S57 Crystal structure of $Eu(Tp^{tBu,Me})_2$ (**5**). All atoms are represented by atomic displacement ellipsoids set at 50% probability. Hydrogen atoms and disorders of the *i*Pr and one *t*Bu groups are omitted for clarity. Selected interatomic distances [Å] and angles [°]: Eu1 – N2 2.618(4), Eu1 – N4 2.600(4), Eu1 – N6 2.633(4), Eu1 – N8 2.718(4), Eu1 – N10 2.710(4), B2 – Eu1 3.130(5).

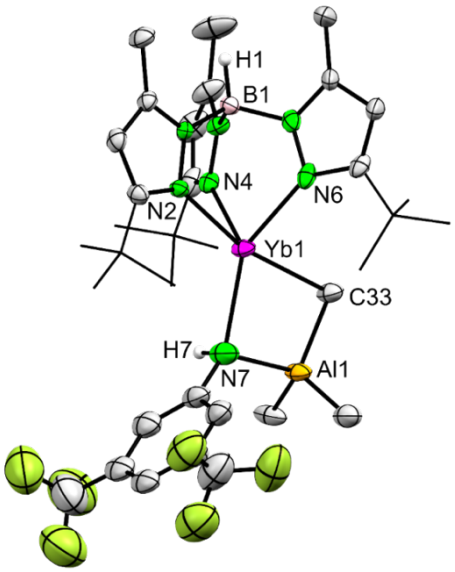

Figure S58 Crystal structure of $Tp^{tBu,Me}Yb(NHAr^{CF3})(AlMe_3)$ (**6**). All atoms are represented by atomic displacement ellipsoids set at 50% probability. Hydrogen atoms, disorders of CF3 and AlMe3 groups and one disorder of one pyrazole are omitted for clarity. Selected interatomic distances [Å] and angles [°]: Yb1 – N2 2.440(4), Yb1 – N4 2.422(4), Yb1 – N6 2.423(4), Yb1 – N7/N7A 2.510(9)/2.513(9), Yb1 – C33 2.810(6), Yb1 – Al1/Al1A 3.347(19)/3.43(2), Yb1 – N7/N7A – H7/H7AA 100.3/104.4, Yb1 – N7/N7A – C25/C25A, 136.0(10))/126.3(10), Yb1 – C33 – Al1/Al1A 85.4(6)/89.6(8), Yb1 – N7/N7A – Al1/Al1A 96.2(7)/98.4(9).

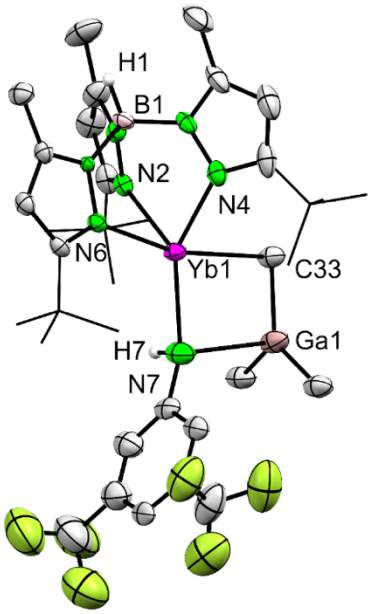

Figure S59 Crystal structure of $Tp^{tBu,Me}Yb(NHAr^{CF3})(GaMe_3)$ (**7**). All atoms are represented by atomic displacement ellipsoids set at 50% probability. Hydrogen atoms and disorders of the CF_3 and $GaMe_3$ groups are omitted for clarity. Selected interatomic distances [Å] and angles [°]: Yb1 – N2 2.431(6), Yb1 – N4 2.425(6), Yb1 – N6 2.440(5), Yb1 – N7/N7A 2.471(14)/2.477(12), Yb1 – C33 2.868(8), Yb1 – Ga1/Ga1A 3.382(8)/3.458(11), Yb1 – N7/N7A – H7/H7A 100.1/102.9, Yb1 – N7/N7A – C25/C25A, 140.0(13)/131.6(14), Yb1 – C33 – Ga1/Ga1A 84.6(4)/88.5(4), Yb1 – N7/N7A – Ga1/Ga1A 94.9(6)/97.8(6).

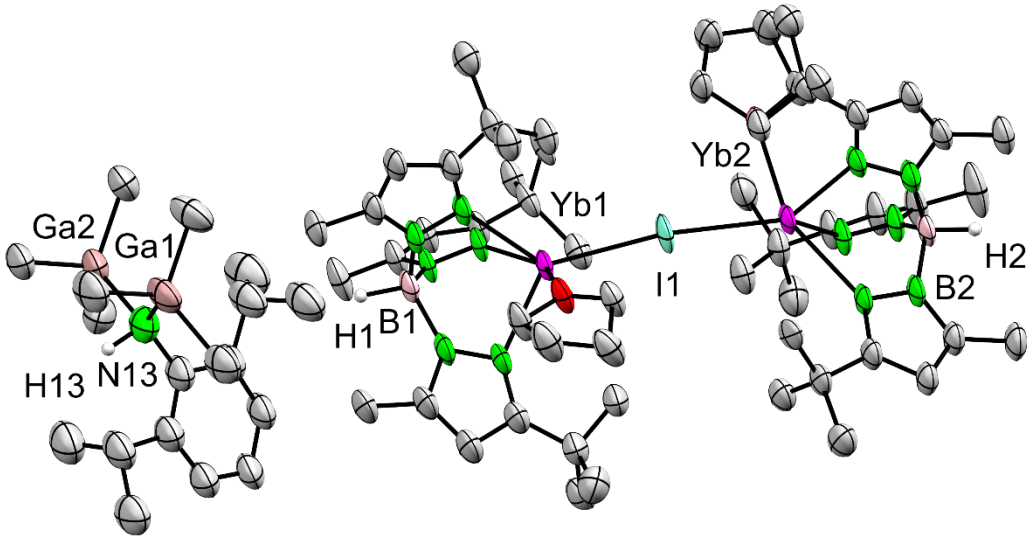

Figure S60 Crystal structure of $[(Tp^{tBu,Me})_2Yb_2I][NHAr^{iPr}(GaMe_3)_2]$ (**8**). Due to bad crystallization properties only a connectivity was obtained.

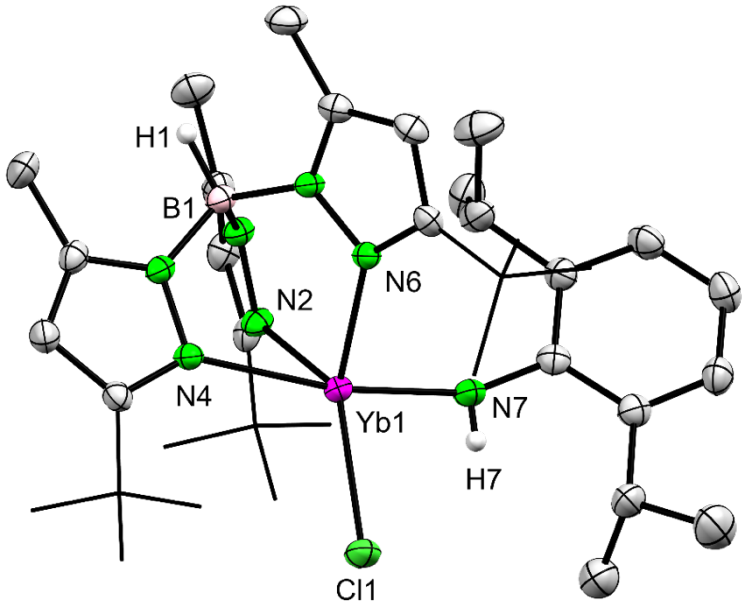

Figure S61 Crystal structure of $Tp^{tBu,Me}Yb(NHAr^{iPr})(Cl)$ (**9a**). All atoms are represented by atomic displacement ellipsoids set at 50 % probability. Hydrogen atoms and disorders of the CF_3 groups are omitted for clarity. Selected interatomic distances [Å] and angles [°]: Yb1 – N2 2.326(2), Yb1 – N4 2.476(2), Yb1 – N6 2.303(2), Yb1 – N7 2.160(2), Yb1 – Cl1 2.5152(11), Yb1 – N7 – C25 156.08(19), Cl1 – Yb1 – N7 87.23(7).

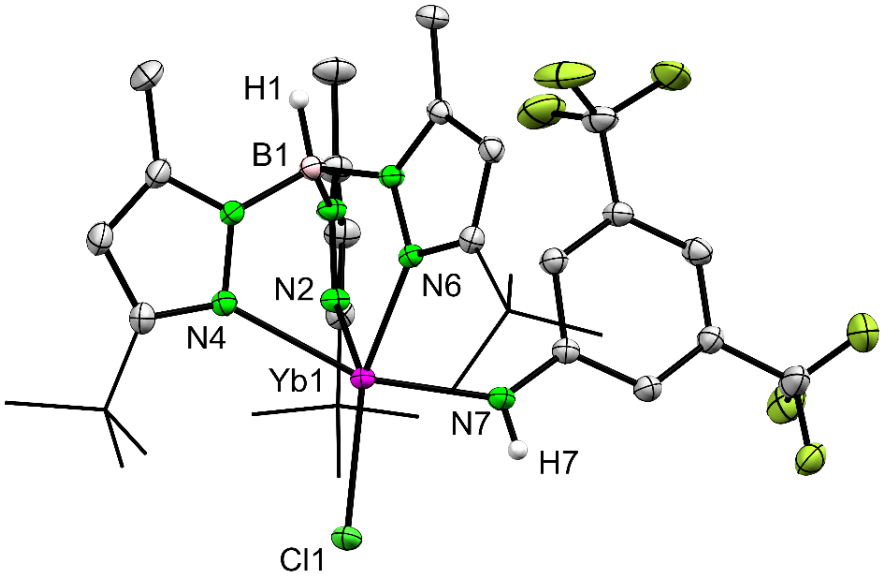

Figure S62 Crystal structure of $Tp^{tBu,Me}Yb(NHAr^{CF3})(Cl)$ (**10a**). All atoms are represented by atomic displacement ellipsoids set at 50% probability. Hydrogen atoms and disorders of the CF_3 groups are omitted for clarity. Selected interatomic distances [Å] and angles [°]: Yb1 – N2 2.3155(14), Yb1 – N4 2.4249(13), Yb1 – N6 2.3315(13), Yb1 – N7 2.2131(14), Yb1 – Cl1 2.5217(4), Yb1 – N7 – C25 137.42(11), Cl1 – Yb1 – N7 91.71(4).

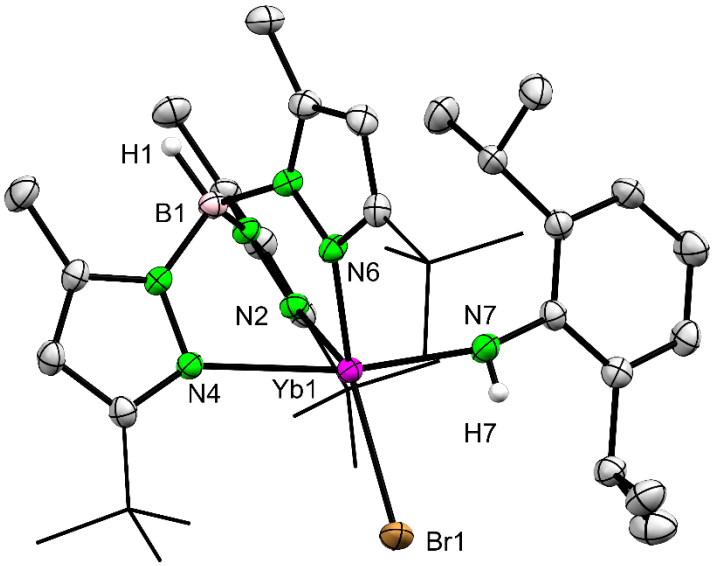

Figure S63 Crystal structure of $Tp^{tBu,Me}Yb(NHAr^{iPr})(Br)$ (**9b**). All atoms are represented by atomic displacement ellipsoids set at 50% probability. Hydrogen atoms are omitted for clarity. Selected interatomic distances [Å] and angles [°]: Yb1 – N2 2.331(2), Yb1 – N4 2.485(2), Yb1 – N6 2.305(2), Yb1 – N7 2.162(2), Yb1 – Br1 2.6947(13), Yb1 – N7 – C25 155.52(16), Br1 – Yb1 – N7 87.00(7).

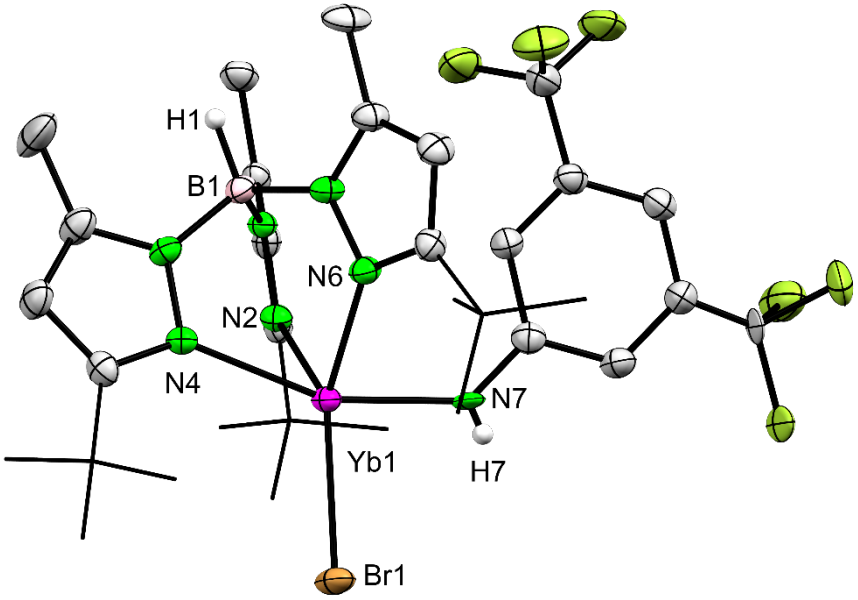

Figure S64 Crystal structure of $Tp^{tBu,Me}Yb(NHAr^{CF3})(Br)$ (**10b**). All atoms are represented by atomic displacement ellipsoids set at 50% probability. Hydrogen atoms and disorders of one CF_3 group are omitted for clarity. Selected interatomic distances [Å] and angles [°]: Yb1 – N2 2.419 (3), Yb1 – N4 2.321(3), Yb1 – N6 2.307(3), Yb1 – N7 2.253(3), Yb1 – Br1 2.6760(4), Yb1 – N7 – C25 136.6(2), Br1 – Yb1 – N7 91. 40(6).

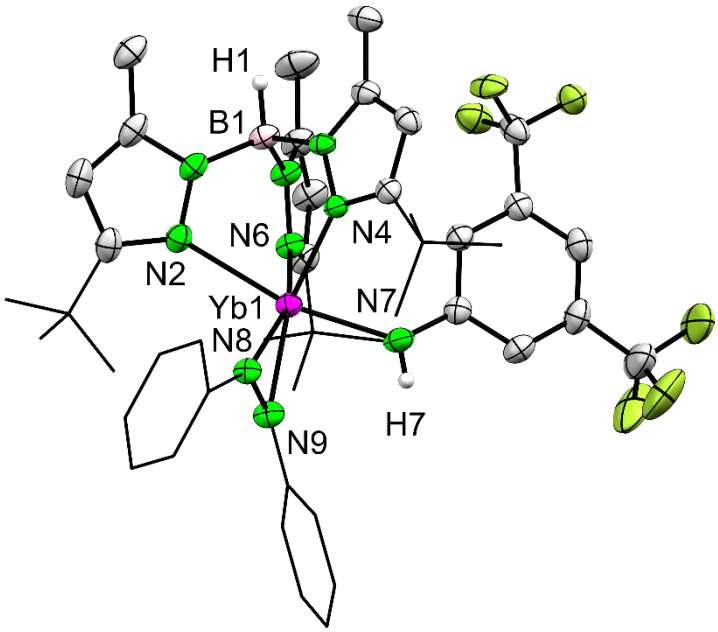

Figure S65 Crystal structure of $Tp^{tBu,Me}Yb(NHAr^{CF3})(N_2Ph_2)$ (**11**). All atoms are represented by atomic displacement ellipsoids set at 50% probability. Hydrogen atoms and disorders of the *i*Pr and one *t*Bu groups are omitted for clarity. Selected interatomic distances [Å] and angles [°]: Yb – N2 2.449(2), Yb1 – N4 2.378(2), Yb1 – N6 2.360(2), Yb1 – N7 2.233(3), Yb1 – N8 2.274(2), Yb1 – N9 2.229(2), Yb1 – N7 –C25 136.0(2), Yb1 – N7 – H7 115(3), N7 – Yb1 – N8 107.80(9), N7 – Yb1 – N9 86.78(10).

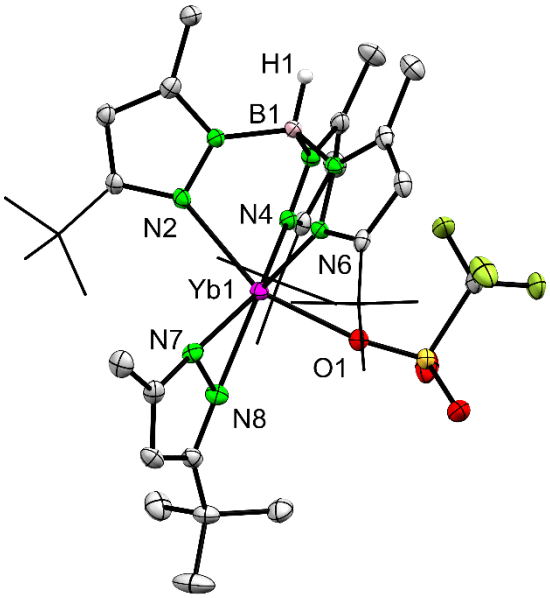

Figure S66 Crystal structure of $Tp^{tBu,Me}Yb(pz^{tBu,Me})(OTf)$ (**12**). All atoms are represented by atomic displacement ellipsoids set at 50% probability. Hydrogen atoms and disorders of the *i*Pr and one *t*Bu groups are omitted for clarity. Selected interatomic distances [Å] and angles [°]: Yb1 – N2 2.380(3), Yb1 – N4 2.345(3), Yb1 – N6 2.366(3), Yb1 – N7 2.272(3), Yb1 – N8 2.230(3), Yb1 – O1 2.216(3).

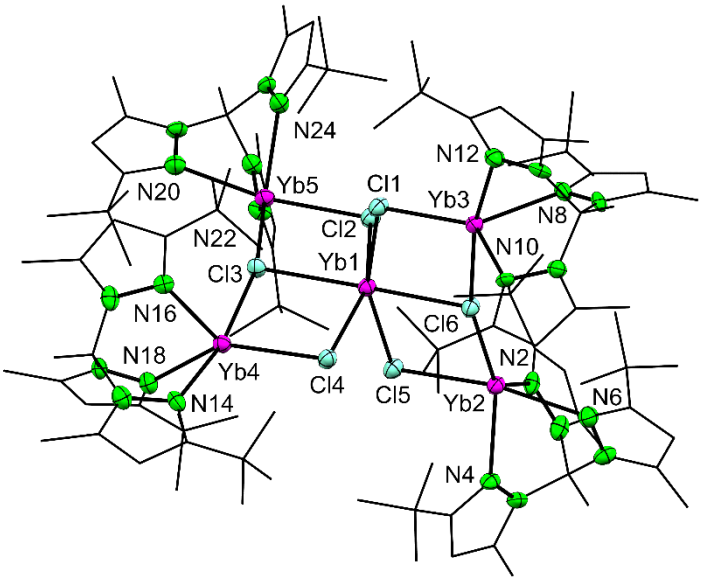

Figure S67 Crystal structure of $(Tp^{tBu,Me})_4Yb_6Cl_6$ (**13**). Due to bad crystallization properties only a connectivity was obtained.

Table **S1** Crystallographic data of compounds **1**^{thf}, **1** and **2**

Compound[a]	Tp^{tBu,Me}Yb(NHAr^{iPr})(thf) **1**^{thf}	Tp^{tBu,Me}Yb(NHAr^{iPr}) **1**	Tp^{tBu,Me}Yb(NHAr^{Me}) **2**
Molecular formula	$C_{43}H_{73}BN_7OYb$	$C_{36}H_{58}BN_7Yb$	$C_{32}H_{50}BN_7Yb$
CCDC No.	2248528	2248521	2248522
M [g/mol]	887.93	772.74	716.64
Temperature [K]	100(2)	100(2)	100(2)
Wavelength [Å]	0.71073	0.71073	0.71073
Crystal dimensions [mm]	0.156 x 0.134 x 0.090	0.246 x 0.134 x 0.072	0.460 x 0.094 x 0.065
Crystal description	orange needle	red needle	orange needle
Crystal system	Monoclinic	Monoclinic	Orthorhombic
Space group	C2/c	$P2_1/n$	$Pca2_1$
a [Å]	21.1160(14)	9.5488(4)	19.726(2)
b [Å]	13.3578(9)	23.9283(11)	10.5723(12)
c [Å]	32.769(2)	16.2362(7)	16.2311(19)
α [°]	90	90	90
β [°]	101.5050(10)	93.3820(10)	90
γ [°]	90	90	90
V [^{3}]	9057.2(11)	3384.9(7)	3384.9(7)
Z	8	4	4
ρ [mg/m^3]	1.302	1.386	1.406
μ [mm^{-1}]	2.104	2.559	2.794
F (000)	3704	1592	1464
θ range [°]	2.099 to 28.700	2.116 to 29.227	2.065 to 30.403
Indices	-28<=h<=28	-12<=h<=11	-26<=h<=28
	-18<=k<=18	-20<=k<=32	-13<=k<=15
	-44<=l<=43	-22<=l<=22	-23<=l<=23
Number of reflexes	91652	30426	33340
Unique reflexes	11676	9592	10155
R1[a]/wR2[b] (I < 2σ)	R1 = 0.0446, wR2 = 0.0984	R1 = 0.0512, wR2 = 0.1024	R1 = 0.0360, wR2 = 0.0756
R1[a]/wR2[a] (all)	R1 = 0.0542, wR2 = 0.1014	R1 = 0.0926, wR2 = 0.1196	R1 = 0.0580, wR2 = 0.0872
GOF [c]	1.256	1.001	1.024

[c]GOF = $[\Sigma w(F_0^2 - F_c^2)^2 / (n_0 - n_p)]^{1/2}$. [a]$R_1 = \Sigma(||F_0| - |F_c||) / \Sigma|F_0|$, $F_0 > 4\sigma(F_0)$. [b]$wR_2 = \{\Sigma[w(F_0^2 - F_c^2)^2 / \Sigma[w(F_0^2)^2]\}^{1/2}$.

Table **S1** continued Crystallographic data of compounds **3**^{thf}, **4**^{thf} and **1**^{thf,Sm}

Compound[a]	$Tp^{tBu,Me}Yb(NHAr^{CF3})(thf)_2$ **3**^{thf}	$Tp^{tBu,Me}Yb(NHSiPh_3)(thf)$ **4**^{thf}	$Tp^{tBu,Me}Sm(NHAr^{iPr})(thf)$ **1**^{thf,Sm}
Molecular formula	$C_{43}H_{67}BF_6N_7O_2Yb$	$C_{46}H_{64}BN_7OSiYb$	$C_{40}H_{66}BN_7OSm$
CCDC No.	2248537	2248530	2248529
M [g/mol]	1011.88	942.98	822.15
Temperature [K]	100(2)	100(2)	100(2)
Wavelength [Å]	0.71073	0.71073	0.71073
Crystal dimensions [mm]	0.244 x 0.062 x 0.049	0.226 x 0.225 x 0.205	0.193 x 0.140 x 0.117
Crystal description	red needle	red block	green block
Crystal system	Triclinic	Monoclinic	Monoclinic
Space group	P1	C2/c	$P2_1/c$
a [Å]	11.6419(9)	41.2689(13)	9.9313(5)
b [Å]	12.1357(10)	11.6943(4)	16.9639(8)
c [Å]	17.4345(14)	19.9784(7)	24.6920(12)
α [°]	100.123(3)	90	90
β [°]	107.912(3)	90.4350(10)	93.4090(10)
γ [°]	90.396(3)	90	90
V [^{3}]	2302.4(3)	9641.5(6)	4152.6(4)
Z	2	8	4
ρ [mg/m^3]	1.460	1.299	1.313
μ [mm^{-1}]	2.098	2.004	1.452
F (000)	1038	3888	1720
θ range [°]	1.249 to 26.505	1.810 to 28.308	2.043 to 30.519
Indices	-14<=h<=14	-54<=h<=43	-14<=h<=14
	-15<=k<=15	-15<=k<=15	-24<=k<=24
	-21<=l<=21	-26<=l<=26	-35<=l<=35
Number of reflexes	54467	64839	75787
Unique reflexes	18830	11912	12666
R1[a]/wR2[b] (I < 2σ)	R1 = 0.0526, wR2 = 0.1091	R1 = 0.0289, wR2 = 0.0649	R1 = 0.0328, wR2 = 0.0767
R1[a]/wR2[a] (all)	R1 = 0.0837, wR2 = 0.1253	R1 = 0.0369, wR2 = 0.0682	R1 = 0.0486, wR2 = 0.0851
GOF [c]	1.067	1.030	1.028

[c]$GOF = [\Sigma w(F_0^2 - F_c^2)^2 / (n_0 - n_p)]^{1/2}$. [a]$R_1 = \Sigma(||F_0| - |F_c||) / \Sigma|F_0|$, $F_0 > 4\sigma(F_0)$. [b]$wR_2 = \{\Sigma[w(F_0^2 - F_c^2)^2 / \Sigma[w(F_0^2)^2]\}^{1/2}$.

Table **S1** continued Crystallographic data of compounds $\mathbf{1}^{thf,Eu}$, $\mathbf{1}^{py}$ and $\mathbf{1}^{dmap}$

Compound[a]	$Tp^{tBu,Me}Eu(NHAr^{iPr})(thf)$ $\mathbf{1}^{thf,Eu}$	$Tp^{tBu,Me}Yb(NHAr^{iPr})(py)$ $\mathbf{1}^{py}$	$Tp^{tBu,Me}Yb(NHAr^{iPr})(dmap)$ $\mathbf{1}^{dmap}$
Molecular formula	$C_{40}H_{66}BEuN_7O$	$C_{41}H_{63}BN_8Yb$	$C_{43}H_{68}BN_9Yb$
CCDC No.	2248540	2248527	2248526
M [g/mol]	823.76	851.84	894.91
Temperature [K]	100(2)	100(2)	100(2)
Wavelength [Å]	0.71073	0.71073	0.71073
Crystal dimensions [mm]	0.190 x 0.088 x 0.033	0.253 x 0.057 x 0.044	0.400 x 0.179 x 0.146
Crystal description	yellow needle	black needle	red block
Crystal system	Monoclinic	Monoclinic	Monoclinic
Space group	$P2_1$	$P2_1/c$	$P2_1/n$
a [Å]	9.934(6)	11.854(7)	11.1230(7)
b [Å]	16.980(10)	21.460(14)	21.4324(13)
c [Å]	12.308(8)	19.117(11)	18.9230(11)
α [°]	90	90	90
β [°]	93.396(16)	96.938(10)	97.5190(10)
γ [°]	90	90	90
V [3]	2073(2)	4827(5)	4472.3(5)
Z	2	4	4
ρ [mg/m³]	1.320	1.172	1.329
μ [mm⁻¹]	1.551	1.970	2.130
F (000)	862	1760	1856
θ range [°]	1.657 to 30.507	1.731 to 27.102	2.171 to 30.534
Indices	-14<=h<=14	-15<=h<=13	-15<=h<=15
	-24<=k<=24	-27<=k<=27	-30<=k<=30
	-15<=l<=17	-21<=l<=24	-24<=l<=26
Number of reflexes	55048	51249	81723
Unique reflexes	12637	10647	13646
R1[a]/wR2[b] (I < 2σ)	R1 = 0.0305, wR2 = 0.0635	R1 = 0.0517, wR2 = 0.1168	R1 = 0.0238, wR2 = 0.0559
R1[a]/wR2[a] (all)	R1 = 0.0378, wR2 = 0.0675	R1 = 0.0818, wR2 = 0.1313	R1 = 0.0306, wR2 = 0.0586
GOF [c]	1.041	0.961	1.044

[c]GOF = $[\Sigma w(F_0^2 - F_c^2)^2 / (n_0 - n_p)]^{1/2}$. [a]$R_1 = \Sigma(||F_0| - |F_c||) / \Sigma|F_0|$, $F_0 > 4\sigma(F_0)$. [b]$wR_2 = \{\Sigma[w(F_0^2 - F_c^2)^2 / \Sigma[w(F_0^2)^2]\}^{1/2}$.

Table **S1** continued Crystallographic data of compounds **3**^{dmap}, **4**^{dmap} and **5**

Compound[a]	$Tp^{tBu,Me}Yb(NHAr^{CF3})(dmap)$ **3**^{dmap}	$Tp^{tBu,Me}Yb(NHSiPh_3)(dmap)$ **4**^{dmap}	$Eu(Tp^{tBu,Me})_2$ **5**
Molecular formula	$C_{39}H_{54}BF_6N_9Yb$	$C_{63}H_{82}BN_9SiYb$	$C_{48}H_{80}B_2EuN_{12}\cdot 1/2C_5H_{12}$
CCDC No.	2248541	2248531	2248536
M [g/mol]	946.76	1177.31	1034.89
Temperature [K]	100(2)	100(2)	100(2)
Wavelength [Å]	0.71073	0.71073	0.71073
Crystal dimensions [mm]	0.113 x 0.062 x 0.039	0.402 x 0.079 x 0.065	0.321 x 0.129 x 0.047
Crystal description	orange plate	yellow block	yellow block
Crystal system	Triclinic	Monoclinic	Monoclinic
Space group	$P\bar{1}$	$P2_1/c$	$P2_1/n$
a [Å]	12.013(10)	11.3413(10)	12.110(9)
b [Å]	12.377(10)	19.1966(18)	25.76(2)
c [Å]	16.032(14)	27.315(3)	17.757(12)
α [°]	85.204(12)	90	90
β [°]	87.406(10)	90.707(2)	92.761(12)
γ [°]	64.265(12)	90	90
V [³]	2140(3)	5946.4(9)	5534(7)
Z	2	8	4
ρ [mg/m³]	1.470	1.315	1.242
μ [mm^{-1}]	2.250	1.639	1.177
F (000)	960	2448	2184
θ range [°]	1.275 to 28.517	1.297 to 26.418	1.394 to 28.386
Indices	-16<=h<=16	-14<=h<=14	-16<=h<=16
	-16<=k<=16	-23<=k<=24	-34<=k<=34
	-21<=l<=21	-33<=l<=34	-23<=l<=23
Number of reflexes	81932	73316	82682
Unique reflexes	10733	12169	13753
R1[a]/wR2[b] (I < 2σ)	R1 = 0.0531, wR2 = 0.1264	R1 = 0.0360, wR2 = 0.0753	R1 = 0.0511, wR2 = 0.1076
R1[a]/wR2[a] (all)	R1 = 0.0799, wR2 = 0.1439	R1 = 0.0583, wR2 = 0.0846	R1 = 0.0972, wR2 = 0.1274
GOF [c]	1.016	1.007	1.011

[c]$GOF = [\Sigma w(F_0^2 - F_c^2)^2 / (n_0 - n_p)]^{1/2}$. [a]$R_1 = \Sigma(||F_0| - |F_c||) / \Sigma|F_0|$, $F_0 > 4\sigma(F_0)$. [b]$wR_2 = \{\Sigma[w(F_0^2 - F_c^2)^2 / \Sigma[w(F_0^2)^2]\}^{1/2}$.

Table **S1** continued Crystallographic data of compounds **6**, **7** and **8**

Compound[a]	$Tp^{tBu,Me}Yb(NHAr^{CF3})(AlMe_3)$ **6**	$Tp^{tBu,Me}Yb(NHAr^{CF3})(GaMe_3)$ **7**	$[(Tp^{tBu,Me})_2Yb_2I][NHAr^{iPr}(GaMe_3)_2]$ **8***
Molecular formula	$C_{35}H_{53}AlBF_6N_7Yb$	$C_{35}H_{53}GaBF_6N_7Yb$	$C_{95}H_{156}B_2Ga_2IN_{13}O_2Yb$
CCDC No.	2248523	2248525	2248534
M [g/mol]	896.67	939.41	2146.36
Temperature [K]	100(2)	100(2)	100(2)
Wavelength [Å]	0.71073	0.71073	0.71073
Crystal dimensions [mm]	0.142 x 0.139 x 0.098	0.198 x 0.123 x 0.057	0.248 x 0.058 x 0.037
Crystal description	Yellow needle	Yellow needle	yellow needle
Crystal system	Monoclinic	Monoclinic	Monoclinic
Space group	$P2_1/c$	$P2_1/c$	$P2_1/c$
a [Å]	9.6523(8)	9.6012(8)	17.520(15)
b [Å]	17.0921(15)	17.1131(14)	30.61(3)
c [Å]	25.098(2)	25.200(2)	19.717(18)
α [°]	90	90	90
β [°]	90.5840(10)	90.868(3)	103.34(3)
γ [°]	90	90	90
V [³]	4140.4(6)	4140.0(6)	10291(16)
Z	4	4	4
ρ [mg/m³]	1.438	1.507	1.385
μ [mm⁻¹]	2.340	2.955	2.669
F (000)	1816	1888	4392
θ range [°]	1.623 to 26.369	1.438 to 28.474	1.194 to 27.679
Indices	-12<=h<=12	-12<=h<=10	-22<=h<=22
	-21<=k<=21	-22<=k<=22	-35<=k<=35
	-31<=l<=31	-33<=l<=32	-20<=l<=20
Number of reflexes	55710	73872	124709
Unique reflexes	8434	10363	17261
R1[a]/wR2[b] (I < 2σ)	R1 = 0.0443, wR2 = 0.0997	R1 = 0.0656, wR2 = 0.1500	R1 = 0.0806, wR2 = 0.1817
R1[a]/wR2[a] (all)	R1 = 0.0608, wR2 = 0.1096	R1 = 0.0981, wR2 = 0.1674	R1 = 0.1963, wR2 = 0.2386
GOF [c]	1.035	1.055	1.008

[c]$GOF = [\Sigma w(F_o^2 - F_c^2)^2 / (n_o - n_p)]^{1/2}$. [a]$R_1 = \Sigma(||F_o| - |F_c||) / \Sigma|F_o|$, $F_o > 4\sigma(F_o)$. [b]$wR_2 = \{\Sigma[w(F_o^2 - F_c^2)^2 / \Sigma[w(F_o^2)^2]\}^{1/2}$; * only connectivity obtained.

Table **S1** continued Crystallographic data of compounds **9a**, **10a** and **9b**

Compound[a]	$Tp^{tBu,Me}Yb(NHAr^{iPr})(Cl)$ **9a**	$Tp^{tBu,Me}Yb(NHAr^{CF3})(Cl)$ **10a**	$Tp^{tBu,Me}Yb(NHAr^{iPr})(Br)$ **9b**
Molecular formula	$C_{36}H_{58}BClN_7Yb$	$C_{32}H_{44}BClF_6N_7Yb$	$C_{36}H_{58}BBrN_7Yb$
CCDC No.	2248524	2248533	2248532
M [g/mol]	808.19	860.04	852.65
Temperature [K]	100(2)	100(2)	100(2)
Wavelength [Å]	0.71073	0.71073	0.71073
Crystal dimensions [mm]	0.119 x 0.113 x 0.094	0.154 x 0.128 x 0.125	0.179 x 0.119 x 0.105
Crystal description	intense blue needle	purple needle	turquoise needle
Crystal system	Monoclinic	Monoclinic	Monoclinic
Space group	$P2_1/c$	$P2_1/n$	$P2_1/c$
a [Å]	11.645(6)	11.6245(3)	11.675(8)
b [Å]	18.016(10)	16.0723(4)	18.213(13)
c [Å]	18.923(10)	20.2693(5)	18.789(13)
α [°]	90	90	90
β [°]	98.925(10)	104.3460(10)	98.165(19)
γ [°]	90	90	90
V [3]	3922(4)	3668.87(16)	3955(5)
Z	4	4	4
ρ [mg/m³]	1.369	1.557	1.432
μ [mm⁻¹]	2.486	2.685	3.408
F (000)	1660	1724	1732
θ range [°]	1.570 to 28.336	1.637 to 30.539	1.565 to 30.544
Indices	-15<=h<=15	-16<=h<=15	-16<=h<=16
	-24<=k<=24	-22<=k<=22	-26<=k<=26
	-25<=l<=25	-28<=l<=24	-26<=l<=26
Number of reflexes	61775	79290	202113
Unique reflexes	9777	11225	12111
R1[a]/wR2[b] (I < 2σ)	R1 = 0.0257, wR2 = 0.0536	R1 = 0.0201, wR2 = 0.0473	R1 = 0.0257, wR2 = 0.0570
R1[a]/wR2[a] (all)	R1 = 0.0360, wR2 = 0.0580	R1 = 0.0236, wR2 = 0.0490	R1 = 0.0345, wR2 = 0.0612
GOF [c]	1.022	1.048	1.069

[c]$GOF = [\Sigma w(F_0^2 - F_c^2)^2 / (n_0 - n_p)]^{1/2}$. [a]$R_1 = \Sigma(||F_0| - |F_c||) / \Sigma|F_0|$, $F_0 > 4\sigma(F_0)$. [b]$wR_2 = \{\Sigma[w(F_0^2 - F_c^2)^2 / \Sigma[w(F_0^2)^2]\}^{1/2}$.

Table **S1** continued Crystallographic data of compounds **10b**, **11** and **12**

Compound[a]	$Tp^{tBu,Me}Yb(NHAr^{CF3})(Br)$ **10b**	$Tp^{tBu,Me}Yb(NHAr^{CF3})(N_2Ph_2)$ **11**	$Tp^{tBu,Me}Yb(pz^{tBu,Me})(OTf)$ **12**
Molecular formula	$C_{32}H_{44}BBrF_6N_7Yb$	$C_{44}H_{54}BF_6N_9Yb$	$C_{33}H_{53}BF_3N_8O_3SYb$
CCDC No.	2248539	2248535	2248520
M [g/mol]	904.50	1006.81	882.74
Temperature [K]	100(2)	100(2)	100(2)
Wavelength [Å]	0.71073	0.71073	0.710703
Crystal dimensions [mm]	0.142 x 0.120 x 0.116	0.251 x 0.091 x 0.089	2.461
Crystal description	deep blue needle	yellow needle	light green plate
Crystal system	Monoclinic	Triclinic	Triclinic
Space group	$P2_1/n$	$P\bar{1}$	$P\bar{1}$
a [Å]	11.7019(11)	10.2802(4)	10.572(12)
b [Å]	16.1670(15)	12.5250(5)	11.769(13)
c [Å]	20.2544(19)	18.7909(8)	17.94(2)
α [°]	90	94.0850(10)	87.201(18)
β [°]	104.1270(10)	94.0530(10)	83.321(18)
γ [°]	90	111.3230(10)	63.69(3)
V [³]	3715.9(6)	2235.98(16)	1988(4)
Z	4	2	2
ρ [mg/m³]	1.617	1.495	1.475
μ [mm^{-1}]	3.654	2.158	2.461
F (000)	1796	1020	898
θ range [°]	1.631 to 27.102	1.755 to 28.310	1.143 to 26.341
Indices	-15<=h<=15	-13<=h<=13	-13<=h<=13
	-20<=k<=20	-16<=k<=16	-14<=k<=14
	-25<=l<=25	-25<=l<=25	0<=l<=22
Number of reflexes	53047	52910	8088
Unique reflexes	8187	11115	8088
R1[a]/wR2[b] (I < 2σ)	R1 = 0.0283, wR2 = 0.0559	R1 = 0.0319, wR2 = 0.0709	R1 = 0.0261, wR2 = 0.0587
R1[a]/wR2[a] (all)	R1 = 0.0459, wR2 = 0.0622	R1 = 0.0410, wR2 = 0.0749	R1 = 0.0296, wR2 = 0.0604
GOF [c]	1.029	1.038	1.069

[c]$GOF = [\Sigma w(F_0^2 - F_c^2)^2 / (n_0 - n_p)]^{1/2}$. [a]$R_1 = \Sigma(||F_0| - |F_c||) / \Sigma|F_0|, F_0 > 4\sigma(F_0)$. [b]$wR_2 = \{\Sigma[w(F_0^2 - F_c^2)^2 / \Sigma[w(F_0^2)^2]\}^{1/2}$.

Table **S1** continued Crystallographic data of compound **13**

Compound[a]	$(Tp^{tBu,Me})_4Yb_5Cl_6$ **13***
Molecular formula	$C_{108}H_{188}B_4Cl_4N_{24}Yb_5$
CCDC No.	2248538
M [g/mol]	2943.95
Temperature [K]	97(2)
Wavelength [Å]	0.71073
Crystal dimensions [mm]	0.136 x 0.056 x 0.047
Crystal description	green-yellow plate
Crystal system	Monoclinic
Space group	C2/c
a [Å]	46.844(2)
b [Å]	19.2663(8)
c [Å]	28.8401(13)
α [°]	90
β [°]	96.973(2)
γ [°]	90
V [^{3}]	25836.1(19)
Z	8
ρ [mg/m^3]	1.514
μ [mm^{-1}]	3.760
F (000)	11808
θ range [°]	1.144 to 26.404
Indices	-58<=h<=58
	-24<=k<=24
	-36<=l<=36
Number of reflexes	256180
Unique reflexes	26462
R1[a]/wR2[b] (I < 2σ)	R1 = 0.0537, wR2 = 0.0875
R1[a]/wR2[a] (all)	R1 = 0.1168, wR2 = 0.1428
GOF [c]	0.999

[c]GOF = $[\Sigma w(F_0^2 - F_c^2)^2 / (n_0 - n_p)]^{1/2}$. [a]$R_1 = \Sigma(||F_0| - |F_c||) / \Sigma|F_0|$, $F_0 > 4\sigma(F_0)$. [b]$wR_2 = \{\Sigma[w(F_0^2 - F_c^2)^2 / \Sigma[w(F_0^2)^2]\}^{1/2}$; * only connectivity obtained.

F

Appendix

Appendix

Structurally characterized complexes

On the following pages all X-ray structurally characterized compounds which are not included in publications or manuscripts are summarized.

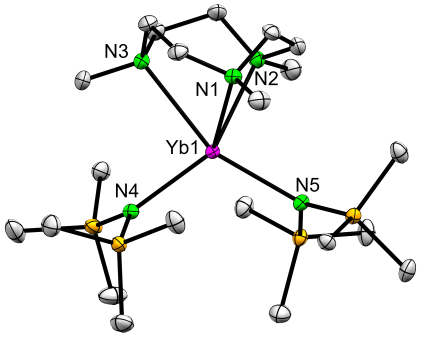

$[(Me_3TACN)Yb\{N(SiMe_3)_2\}_2]$; MK197

Additional analysis: ^{1}H NMR

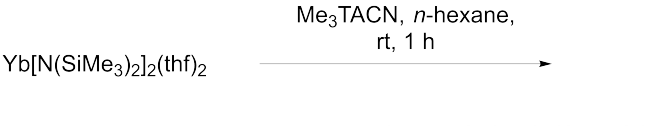

Monoclinic $P2_{1/C}$

$a = 9.171(6)$ Å	$\alpha = 90°$
$b = 16.922(11)$ Å	$\beta = 101.31(3)°$
$c = 20.92(3)$ Å	$\gamma = 90°$
$V = 3184(6)$ Å^3	=

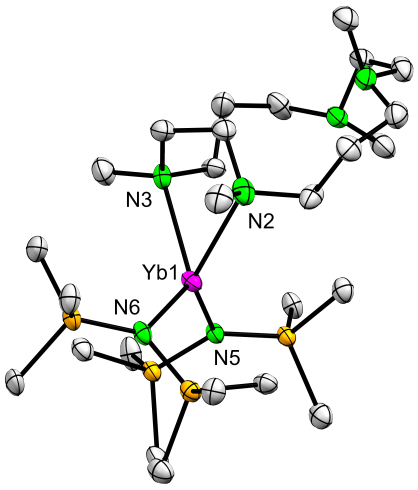

$[(Me_4cyclam)Yb\{N(SiMe_3)_2\}_2]$; MK190

Additional analysis: ^{1}H NMR

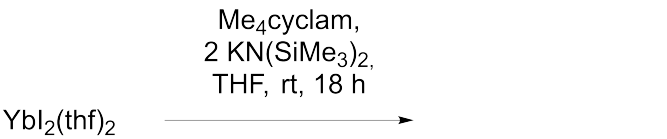

Triclinic P-1

a = 8.6675(7) Å	$\alpha = 92.923(2)°$
b = 11.4294(9) Å	$\beta = 96.440(2)°$
c = 19.4168(14) Å	$\gamma = 96.440(2)°$
V = 1878.3(3) Å^3	=

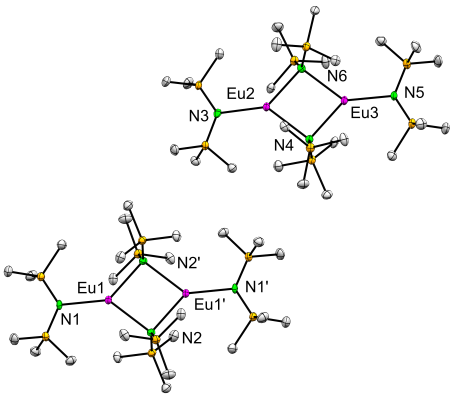

$EuI_2(thf)_2$ —(1) 1.95 KCH_2Ph, thf, rt, 1h; (2) exc. $HN(SiMe_3)_2$, *n*-hexane, rt, 2 h→ $[Eu\{N(SiMe_3)_2\}_2]_2$

$[Eu\{N(SiMe_3)_2\}_2]_2$; MK129

Additional analyses: -

Triclinic P-1

a = 9.6275(5) Å	α = 101.8650(10)°
b = 12.2797(6) Å	β = 95.6710(10)°
c = 28.6888(14) Å	γ = 96.4170(10)°
V = 3272.4(3) Å^3	=

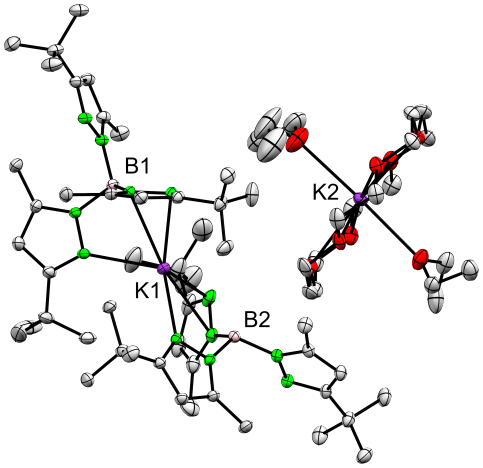

$[Tp^{tBu,Me}Yb(NHAr^{iPr})(thf)]$ —KCH_2Ph, 18-crown-6, THF-*d8*, 30 min, rt→ $[K(Tp^{tBu,Me})_2]$ $[K(18\text{-crown-6})]*2Et_2O$

$[K(Tp^{tBu,Me})_2][K(18\text{-crown-6})\cdot 2\ Et_2O$;

MK164

Additional analyses: -

Triclinic P-1

a = 15.744(6) Å	α = 71.911(9)°
b = 16.392(6) Å	β = 74.944(6)°
c = 18.168(7) Å	γ = 73.817(8)°
V = 4202(3) Å^3	=

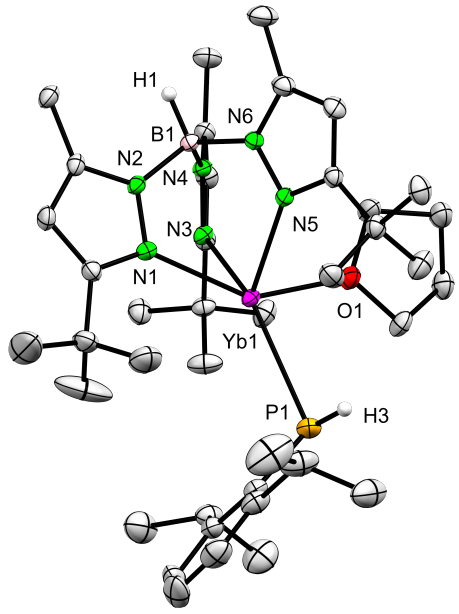

$[Tp^{tBu,Me}Yb(PHAr^{iPr})(thf)]$; MK193

Additional analyses: ^{1}H, ^{11}B, ^{31}P NMR, elemental analysis

$[Tp^{tBu,Me}YbN(SiMe_3)_2]$ —(PH_2Ar^{iPr}, THF, 60 min, rt)→ $[Tp^{tBu,Me}Yb(PHAr^{iPr})(thf)]$

Monoclinic $P2_{1/n}$

a =	12.8399(7) Å	α =	90°
b =	20.4283(12) Å	β =	110.9680(10)°
c =	17.9204(10) Å	γ =	90°
V =	4389.2(4) Å^3		